School of Electrical Engineering, Computing, and Mathematical Sciences

High Resolution Direction of Arrival Estimation with Switched Active Switched Parasitic Antenna Arrays

RABAH ABDULJABBAR JASEM

This thesis is presented for the Degree of

Doctor of Philosophy

of

Curtin University

July 2020

Declaration

To the best of my knowledge and belief this thesis contains no material previously published by any other person except where due acknowledgment has been made.

This thesis contains no material which has been accepted for the award of any other degree or diploma in any university.

Signature: …………………………………………….

01/07/2020
Date: ………………………...

"In the name of Allah,

the most gracious,

the most Merciful"

To the memory of my parents

To my beloved family

ABSTRACT

A Switched Active Switched Parasitic Antenna (SASPA) array consists of a number of antenna elements, e.g., dipoles, arranged in a specific geometry, and where, through PIN diodes, the antenna elements can be individually switched into an active state or into a parasitic state. In the case of a receiving SASPA array, the antenna elements are each terminated by a load (active state) or its terminals may be short-circuited via a PIN diode (parasitic state). Because of the fast switching speed of PIN diodes, a single snapshot of the receiving SASPA array can be formed from a number of sub-snapshots, where in each sub-snapshot, one of the elements is made active while the remaining elements are made parasitic, and the voltage across the load of the active element measured. In the next sub-snapshot, a different element is made active while the formerly active element is switched to the parasitic state and the remaining elements stay parasitic. The aforesaid mode of operation differs significantly from conventional all-active receiving arrays where the antenna elements are all active and the voltages across their loads measured simultaneously in one snapshot.

Despite not being studied extensively, SASPA arrays offer multiple advantages over all-active antenna arrays. These include directivity, compactness, and less requirements on the electronic circuitry. SASPA arrays depend on the strong mutual coupling between the antenna elements for their basis of operation. This complicates their analyses relative to the analyses of all-active arrays whose mutual coupling can often be deemed negligible.

A difficulty with the mutual coupling models that are available in the literature is that they are not suitable for SASPA arrays. In particular, terms in the mutual coupling matrix involving parasitic antenna elements are singular. To overcome this, a new mutual coupling model, called Coupled Voltage to Uncoupled Current (CVUC), is

proposed in this thesis. This model is derived from first principles, that is, from electromagnetic field theory.

In this thesis, two data models applicable to the direction-finding application of SASPA arrays are investigated. The first model assumes background noise in the transmission media is the dominant noise. Accordingly, the noise measured at the terminal of the active receiving antenna element is composed of the noise sensed by that element, plus the noise coupled from the other antenna elements. A direction-of-arrival (DOA) estimation algorithm making use of this coupled-signals-coupled-noise model is derived in this thesis. The proposed DOA estimation algorithm is based on the well-known MUSIC algorithm.

The second data model assumes that the noise measured at the active antenna element is dominated by that element's self-noise, and this noise term is independent of the other elements' self-noise. By exploiting the properties of this coupled-signals-uncoupled-noise model in a uniform linear array, a more accurate MUSIC-based DOA algorithm is derived in this thesis. The new algorithm is also computationally more efficient for simulation studies and on-line DOA estimation.

In practice, as a result of, for example manufacturing tolerances, the actual mutual coupling matrix may differ from that predicted by theory. Accordingly, a new method for determining the mutual coupling matrix of SASPA arrays from measurements is presented in this thesis. This method is based on finding the null space of a rank deficient matrix.

Finally, simulation studies were conducted to verify the various methods developed in this thesis. It is shown that SASPA arrays can provide significant improvements in DOA estimation accuracy over all-active antenna arrays of similar size.

Acknowledgments

First, I would like to present my sincere thanks to Allah Almighty for giving me the ability to do this work. I mean by ability is all the requirements that I needed to make this dissertation possible such as my physical ability (thinking, seeing, writing, reading and else), financial support, opportunity to obtaining this study, and lastly meeting the nice, kind and helpful people at Curtin University.

Also, I would like to express my deepest thanks to my supervisor, Dr. Yee-Hong Leung for his scientific, technical, and social support and for the long time we spent together (when I was doing my work in Perth and then after in my country, Iraq) for discussing the subjects of this thesis. His valuable and comprehensive knowledge notes and remarks have guided me for having the straightforward track of the main aim of this work. Also, I would like to thank him for providing me some of valuable and up-to-date references that help me to have a comprehensive view about this work.

My sincere thanks with respect are also dedicated to Julie Craig, Raquel Iliano and Ian Tsen at ISSU/Curtin International. I will never forget their assistance and support when I was facing several problems in my study. I am truly grateful towards Curtin University for providing me financial support and for appreciating my critical situations due to the circumstances that Iraqi students have met during their study in Australia.

Finally, my gratefulness goes to my wife, and to my sisters and their husbands who were supporting me all the time of doing this work. My faithful thanks are dedicated to all my colleagues at Al-Dour Technical Institute who guaranteed and supported my study.

Table of Contents

Mathematical Notations and Symbols

Notations and Symbols	**Description**
$\mathbf{A}$	Matrix notation
$\mathbf{x}$	Column vector
$\mathbf{A}^T$	Matrix transpose
$\mathbf{x}^T$	Row vector
$\mathbf{A}^H$	Matrix conjugate transpose
$\mathbf{x}^H$	Vector conjugate transpose
$\mathbf{A}^*$	Matrix conjugate
$\mathbf{x}^*$	Vector conjugate
$\mathrm{rank}(\mathbf{A})$	Rank of a matrix
$\mathbf{A}^{-1}$	Inverse of a square matrix
$\mathbf{A}^{\dagger}$	Moore-Penrose pseudo inverse of a matrix
$[\mathbf{A}]_{ij}$	Element of a matrix at the ith row j^{th} column
$\dim(\mathbf{V})$	Dimension of the subspace $\mathbf{V}$
$\mathrm{diag}(\mathbf{a})$	Diagonal matrix with the elements of $\mathbf{a}$ along the main diagonal
$\mathrm{vec}(\mathbf{A})$	Vectorization operator
$\lVert \cdot \rVert_p$	p-norm of a matrix or vector
$\mathrm{Re}(\mathbf{A})$	Real part of a complex matrix
$\mathrm{Im}(\mathbf{A})$	Imaginary part of a complex matrix

Notations and Symbols	Description
$\mathbf{I}_N$	$N \times N$ identity matrix
$\mathbf{J}_N$	$N \times N$ exchange matrix
$\mathbf{0}_{N \times M}$	$N \times M$ zero matrix
$\mathbf{1}_{N \times M}$	$N \times M$ matrix of all ones
j	$\sqrt{-1}$
$\mathbb{C}^{N \times M}$	The set of $N \times M$ complex matrices
$\mathbb{R}^{N \times M}$	The set of $N \times M$ real matrices
$\otimes$	Kronecker product
$\odot$	Hadamard matrix product
$\mathcal{R}(\mathbf{A})$	Range space or column space of the matrix $\mathbf{A}$
$\mathcal{N}(\mathbf{A})$	Null space of the matrix $\mathbf{A}$
$\text{sinc}(x)$	The "*sinc*" function $\text{sinc}(x) = \dfrac{\sin \pi x}{\pi x}$
$\lambda = c/f$	Wavelength of a signal where c is the speed of light in free space and f is the signal frequency
Λ_i	ith eigenvalue of a matrix
$\sim$	is distributed as
$N(\mu, \Sigma)$	Normal distribution with mean μ and covariance Σ
$\mathbb{E}\{\cdot\}$	Statistical expectation

Acronyms

Acronyms	Description
1D	One dimensional
2D	Two dimensional
3D	Three dimensional
AA	Antenna array with all elements active (loaded by a load)
AF	Array Factor
AIC	Akaike's Information Criteria
AWGN	Additive White Gaussian Noise
BS	Beam Space
CSCN	Coupled-Signals-Coupled-Noise
CSUN	Coupled-Signals-Uncoupled-Noise
CVUC	Coupled-Voltages-Uncoupled-Currents
DF	Direction finding
DFT	Discrete Fourier Transform
DML	Deterministic Maximum Likelihood
DOA	Direction of Arrival
EMF	Electro-Magnetic Force
EVD	Eigen Value Decomposition
ESPRIT	Estimation of Signal Parameters via Rotational Invariance Technique
FASPA	Fixed Active Switched Parasitic Antenna

Acronyms	Description
LS	Least Square method
MCM	Mutual Coupling Matrix
MDL	Minimum Description Length
MUSIC	Multiple Signal Classification
MOM	Method of Moments
OCV	Open Circuit Voltage
PIN	Positive-Intrinsic-Negative diode
pd	Positive definite
RMIM	Receiving Mutual Impedance Method
RMSE	Root Mean Square Error
SASPA	Switched Active Switched Parasitic Antenna
SML	Stochastic Maximum Likelihood
SNR	Signal to Noise Ratio
SOI	Signal of Interest
SPA	Switched Parasitic Antenna
SPDT	Single Pole Double Threw
SPST	Single Pole Single Threw
SSF	Signal Subspace Fitting
UCA	Uniform Circular Array
ULA	Uniform Linear Array

Chapter 1

INTRODUCTION

1.1　Compact Antenna Arrays

With the rise of mobile communication devices with increasing capabilities and the growing deployment of Internet of Things (IOT) devices, there is now a strong demand for radio technologies that can be fitted into physically small spaces. In this thesis, the capabilities of a type of compact radio antennae, called Switched Active Switched Parasitic Antenna (SASPA) array, are investigated.

An antenna array [1]–[11] is comprised of a number of *antenna elements* placed in strategic distinct locations in space and working together as a single antenna. The antenna elements are often simple and identical devices such as a dipole. Common array configurations include the Uniform Linear Array (ULA) where the antenna elements are uniformly spaced along a line; the Uniform Circular Array (UCA) where the antenna elements are uniformly spaced around a circle; the concentric ring array which consists of a number of concentric UCAs each with a different radius; the planar grid antenna array (GAA) where the antenna elements are placed at the vertices of a rectangular grid; and the conformal array where the placement of the antenna elements conforms to the contour or shape of the body on which the array is mounted.

Antenna arrays can be *transmitting* or *receiving*. This thesis considers the SASPA array when operated as a receiving array. In a receiving antenna array, the antenna elements, or sensors, sample in space the wavefield of a propagating signal which may be acoustic, seismic, electromagnetic, or cosmic in nature, and converts the field energy sensed to electrical energy. Based on the measurements collected from the array of sensors, various attributes of the propagating signal are then extracted through suitable *array signal processing* algorithms.

1.2   Array Signal Processing

An early application of sensor arrays was in France during World War I where microphone arrays were deployed to enable the early detection of approaching enemy aircrafts [7]. The array signal processing technique implemented then was rudimentary. The outputs of the microphones were simply summed electronically to form, effectively, a highly directional microphone. A human operator then listens to output of this super-directional microphone and decides on the presence or otherwise of approaching aircrafts. It was not till the 1960s, with the advancement of digital computer technology and numerical methods, that array signal processing started to blossom as an area of active research. This growth is stimulated by the ability of computers to perform complex numerical operations, such as those in array signal processing algorithms, rapidly and autonomously. The estimation of the various parameters of the propagating signals received by an antenna array, and the enhancement of the signal of interest, attracted the attention of many researchers, scientists and engineers.

The field of array signal processing is diverse. It can be classified in many ways. Firstly, there is the obvious classification into *time-domain* or *frequency-domain* methods. A less obvious classification is that array signal processing can take place in either *element-space* or *beam-space*. In element-space methods, the signal outputs from the antenna elements are fed directly into the array signal processing algorithm; while in beam-space methods, the signal outputs are first combined to form a number of different beampatterns where each beampattern gives the response of the array as a function of directions in space, and the outputs of these beams are then fed into the array signal processing algorithm.

Next, there is *broadband* and *narrowband* array signal processing. In broadband array signal processing, the bandwidth of the information-carrying signal is "broad" with respect to the carrier frequency of the propagating signal. Seismic arrays and

sonar and microphone arrays are typical examples of broadband arrays.

In contrast, in narrowband array signal processing, the bandwidth of the information-carrying signal is "narrow" with respect to the carrier frequency of the propagating signal. Examples of narrowband arrays are seen typically in radar and radio systems.

Yet another classification of array signal processing relates to the location of the signal sources. In *nearfield* array signal processing, the sources are located close to the array and the wavefronts of these sources are cylindrical or spherical as they travel across the array. In *farfield* array signal processing, the sources are located far from the array such that their wavefronts can be approximated as plane-waves arriving at the array. Most of the published research on array signal processing assumed the plane-wave model since this will lead to algorithms that are simpler to derive, implement and analyse. In this thesis, the farfield model is adopted.

In the above discussion on nearfield and farfield array signal processing, an implicit assumption is that the signal sources are *point* sources. Research on *distributed* sources have also been reported [12] but the algorithms developed and analysed are very much scenario dependent and cannot be transferred readily to other applications. As with the farfield assumption, the point source assumption is convenient as it will lead also to algorithms that are straightforward to implement and can be applied to many array signal processing applications. In this thesis, all signal sources are assumed to be point sources.

Finally, array signal processing can be classified in terms of the signal processing objectives. In *beamforming*, which includes conventional beamforming, optimum beamforming, and adaptive beamforming, the objective is to enhance the reception of a signal arriving from a certain direction while suppressing noise and the influence of interfering signals arriving from other directions. Implicit to this class of array signal processing algorithms is the ability to steer, electronically, the main beam of the

array[1] to different directions.

In *parameter estimation,* the objective is to estimate, as accurately as possible, the parameters of the signal of interest. A parameter that has attracted much interest is the Direction of Arrival (DOA) of the signals received by the array. Various researchers have proposed and studied algorithms that can perform DOA estimation with high-resolution. These algorithms are based on the idea that the received signals experience a time delay as they move across the array from sensor to sensor.

DOA algorithms can be classified further into *parametric* and *non-parametric* methods according to the cost function of the algorithm [8]. In parametric methods such as Deterministic Maximum Likelihood and Stochastic Maximum Likelihood, all parameters are estimated simultaneously. These methods require an accurate statistical structure or data model that captures all the characteristics of the variables to be estimated. Sometimes constraint conditions are also imposed to avoid trivial solutions. A drawback of these algorithms is that they require high computations and accordingly are less prevalent although they are statistically more accurate in estimation. In contrast, the non-parametric methods estimate only one specific parameter, e.g. the DOAs, by making use of spectral-based techniques to analyse the measurements provided by the antenna elements of the arrays. For narrowband arrays, the most effective and popular DOA algorithms are the Multiple Signal Classification (MUSIC) algorithm [13] and the Estimation of Signal Parameters via Rotational Invariance Technique (ESPRIT) algorithm [14]. In these two algorithms, the covariance matrix of the measurements is first eigen decomposed into a signal subspace and a noise subspace. The MUSIC algorithm locates the DOAs by finding the angles at which its search vector is orthogonal to the noise subspace; while the ESPRIT algorithm looks for an invariant rotation matrix between the two signal subspaces generated from splitting the antenna array into two subarrays. The DOA information is contained in this rotation matrix.

---

[1] That is, the main beam of the receiving beampattern.

In this thesis, the focus is on the derivation and study of DOA estimation algorithms for a special type of narrowband arrays for radio applications – the Switched Active Switched Parasitic Antenna array.

1.3   Switched Active Switched Parasitic Antenna (SASPA) Arrays

An assumption often made in the study of narrowband array signal processing is that the antenna elements are spaced far enough apart[2] so that mutual coupling between the elements can be ignored. However, for compact arrays, the subject of this thesis, the antenna elements are, by design, spaced closely. Mutual coupling cannot, therefore, be ignored. Indeed, it is mutual coupling that lends compact arrays their particular characteristics.

An example of an antenna array that exploits mutual coupling for its success is the Yagi-Uda antenna, which is used commonly for TV signal reception. In this array, one element is used to intercept the electromagnetic waves of the broadcast signal and the other elements (the parasites) act as reflectors and directors. The Yagi-Uda antenna can be regarded as a Fixed Active Fixed Parasitic Antenna (FAFPA) array.

Transmitting, as opposed to receiving, switched parasitic antenna (SPA) arrays were studied by Thiel and Smith in [15]. In a transmitting Fixed Active Switched Parasitic Antenna (FASPA) array, only one antenna element acts as the active element, i.e. is driven by the radio source, and the remaining antenna elements can be either enabled as parasitic elements by short circuiting their terminals via a PIN diode or disabled if their associated PIN diode is not forward biased. That is to say, the parasitic elements can be *switched* ON or OFF. Thus, by controlling the bias of the PIN diodes of the antenna elements close to the active element, the radiation pattern of the array can be controlled electronically due to the induced currents in the enabled parasites.

Thiel and Smith [15] also studied the transmitting Switched Active Switched

---

[2] But not too far apart, for otherwise, the array will suffer from spatial aliasing.

Parasitic Antenna (SASPA) array. In this array, all antenna elements are in the parasitic state (their terminals are short-circuited) except for one antenna element which is active (its terminals connected to the load). At another point in time, through PIN diodes, the active antenna element is switched to the parasitic state while a formerly parasitic antenna element is switched to take over as the active element. Thiel and Smith [15] explored the advantages of implementing FASPA and SASPA arrays as transmitting antenna arrays in cellular communications. It is shown that arrays with dipole or patch antennas can provide flexibility in steering the array radiation pattern with a very low value of the scattering parameter S_{11} at resonance (as low as -30 dB for some SASPA configurations). Compared to the conventional all-active antenna arrays, SPA arrays offer the following advantages:

1. Self-beamforming array;
2. Flexible and easy in steering the radiation pattern;
3. Less power consumption;
4. Less electronic circuitry is needed;
5. Compact in size.

In the case of *receiving* FASPA or SASPA arrays, the output terminals of the active element are terminated by a load impedance and the voltage across this impedance is sensed. The remaining antenna elements are either enabled as parasitic elements by shorting their output terminals via forward-biased PIN diodes (as in FASPA and SASPA) or disabled by not putting their PIN diodes in forward bias thereby effectively disconnecting these array elements from the array (as in FASPA).

As discussed, arrays with parasitic elements such as the FASPA and the SASPA array depend on the mutual coupling interaction between their antenna elements for them to operate, for example, as direction funding arrays. On the other hand, it is well known that mutual coupling has an adverse effect on the performance of all-active receiving antenna arrays when they are operated as direction finders. Svantesson investigated in [16][17] the possibility of using switched parasitic

antenna arrays as DOA estimators. He considered a UCA-FASPA array with an active element located at the centre of the UCA and the parasitic elements distributed equally spaced on the circumference of the UCA. However, mutual coupling was not studied for this geometry because the signal model that expressed the measurements was based on the switched radiation patterns generated as a result of successively switching the parasites between ON and OFF states. In other words, Svantesson studied direction finding in beamspace. In this thesis, DOA estimation in element space with SASPA arrays is investigated.

1.4   Goals of this Thesis

In this dissertation, the benefits and enhancement that are achieved when SASPA arrays are used as direction finding (DF) arrays will be investigated. It is assumed the elements of the SASPA array are half-wave dipole antennas and they are located in an isotropic and homogenous transmission medium. Also, the mutual coupling between the elements is not DOA dependent. The improvements in DOA estimation over the all-active array, when used in conjunction with the conventional DOA algorithms, may be expressed through the following aspects:

First Goal:

As mentioned above, mutual coupling governs the performance of SASPA arrays. Therefore, it is important to have an accurate model that describes this phenomenon. In the literature, different models have been postulated to describe the mutual coupling effect. However, because these models were derived from different viewpoints such as circuit theory or electromagnetic theory, there is some controversy regarding the "correct" model. In any event, none of these models can be applied to an SASPA array since the mutual coupling matrices of these models apply only to all-active arrays whose elements are all terminated by a load impedance (of the same value) while the parasitic elements of an SASPA array has zero load

impedance.

A new model, called *Coupled-Voltage-Uncoupled-Current* (CVUC), is derived in this thesis. The model is applicable to antenna arrays in general and to SASPA arrays in particular. The derivation is based on electromagnetic theory and the resultant model is represented by a Thévenin equivalent circuit.

Second Goal:

Having derived a suitable mutual coupling model, and assuming there is prior knowledge of the parameters of this model, couple-free measurements can be extracted from the coupled measurements obtained from an SASPA array by applying the decoupling matrix (the pseudo-inverse of the mutual coupling matrix) to the coupled measurements of a session or *snapshot*. This procedure is appropriate if the noise measured is also affected by the same mutual coupling effect as the received signals. In other words, the data model applicable to this signal scenario is the *coupled-signals-coupled-noise* model.

Suppose the SASPA array has N antenna elements, and a snapshot of the wavefield of the propagating signals is obtained by making N sub-snapshots where in each sub-snapshot, a different element of the array is switched to the active state. It is assumed, relative to the signal bandwidth, that the time taken to collect the N sub-snapshots of a snapshot can be neglected because of the very short switching time of the PIN diodes. In other words, the sub-snapshots can be assumed to be made simultaneously (If the time between sub-snapshots in one snapshot is not neglected, a time allingment scenario can be applied on the measurement). In this approach, the N measurements of coupled voltages are mapped to $N \times N$ measurements of uncoupled currents. This will produce N similar steering matrices. Summing up these steering matrices will result in a steering matrix that is similar to the steering matrix of the all-active array with omnidirectional elements but multiplied by the factor of N. This advantage will contribute to reducetion in the distance measure between the

steering matrix and the estimated signal subspace. The scaled steering matrix, together with the estimated noise or signal subspace, can result in superior performance in direction finding when used in the cost function of the MUSIC algorithm, despite the spacing between the elements being much less than $\lambda/2$ (as small as 0.15λ).

In the case where noise is not affected by mutual coupling, that is, they are mainly self-noise from the antenna elements, then the relevant data model of the SASPA array is the *coupled-signals-uncoupled-noise* model. This model will result in a steering matrix that is the product between a real-valued DOA dependent matrix and a matrix that is in half size of the actual mutual coupling matrix. The real-valued matrix is formed due to the unitary characteristic of the SASPA array structure, while the Toeplitz structure of mutual coupling permits one to represent this effect by the halved size mutual coupling matrix. Again, superior performance in direction finding relative to an all-active antenna arrays can be obtained. The reason for this can be attributed to the fact that only real-valued variables rather than complex variables are processed, as a consequence of which the computational effort to perform spectral analysis is reduced significantly leading to a numerically more accurate determination of the subspaces. Also, the round-off errors accumulated due to processing less components of the mutual coupling matrix will be reduced.

Third Goal:

If the mutual coupling is not known prior to the processing of the measurements, then it must be found first. One approach is to inundate the array with a known test signal. The mutual coupling matrix is then determined from the measurements. In the case of a SASPA array operating under the assumption of coupled-signals-uncoupled-noise model, this process reduces to the determination of a mutual coupling vector because of the symmetrical Toeplitz structure of the SASPA array's mutual coupling matrix. The mutual coupling vector is found from the null space of

the matrix formed from the product between the orthogonal projection on the estimated noise subspace and the real-valued matrix mentioned above. This step makes use of the one-to-one correspondence between that null space and the mutual coupling vector. The estimated mutual coupling matrix is then introduced into the cost function of the MUSIC algorithm to achieve high resolution DOA estimation.

If the array's applicable data model is the coupled-signals-coupled-noise model, then the above procedure can still be used. This requires the test signal impinging on the SASPA array to have a high enough signal to noise ratio (SNR) such that it dominates the ambient or background noise picked up by the antenna elements.

1.5   Thesis Outline

This thesis is devoted to study the performance of SASPA arrays and their improvements as DF arrays in conjunction with the MUSIC algorithm. The following Chapters give the framework of this thesis:

- **Chapter 2** is devoted to explaining the concept of mutual coupling between the elements of an antenna array since SASPA arrays depend on this unavoidable phenomenon. A literature review on the available mutual coupling models will be conducted. In addition, a new model, called the Coupled Voltages to Uncoupled Currents (CVUC) model, will be proposed in this chapter. Although this model is derived for all-active receiving antenna arrays, it is also applicable to SASPA arrays. The model is derived from the principle of electromagnetic theory and is represented by a Thévenin equivalent circuit. To establish the aforementioned work in this chapter, some important characteristics of half-wave dipole antenna, which is the antenna type used in this dissertation, will be first explored. These parameters include current distribution on the antenna, radiation pattern of a transmitting antenna, induced voltage of a receiving antenna, and self and mutual impedances.

- **Chapter 3** is dedicated to illustrating in detail the idea of Switched Parasitic Antenna (SPA) and Switched Active Switched Parasitic Antenna (SASPA) arrays. An SPA array consists of N elements in which one element is always in the active state (connected to the radio source if the array is transmitting or to a load if the array is receiving), and the other elements are in the parasitic state by short circuiting their terminals. An SASPA array consists of N elements in which each element can be switched between the active and parasitic states. An RF switch, such as PIN diode, can be used to implement the required fast switching action. The formulae for the switched far field radiation patterns and the related formulae for the currents induced on the elements in transmitting SASPA arrays will be studied. The mutual coupling phenomenon in transmitting SASPA arrays will also be investigated. Several examples showing the directive and switched radiation patterns for ULA-SASPA and UCA-SASPA arrays will be provided to demonstrate the self-beamforming and self-steering abilities of these arrays. The induced voltages and the mutual coupling in SASPA arrays acting in receive mode will also be shown. The validity and appropriateness of the proposed CVUC as a model that represents the mutual coupling in receiving SASPA arrays will be highlighted via an example of a simple SASPA array. Therefore, the work and the analysis in this chapter provide a basis to examine and evaluate the performance of SASPA arrays as DF arrays and the advantages that can be achieved from using such antenna arrays.

- **Chapter 4** gives a review of the well-known DOA algorithms: MUSIC. The capability and improvements obtained from using SASPA arrays in conjunction with this algorithm will be examined in the following Chapters. The MUSIC algorithm is based on the spectral decomposition of the covariance matrix of the array measurements. Therefore, an accurate data model should be considered first to reflect the response of array elements to the received signals. Two data models are considered in this Chapter. The first model assumes mutual coupling affects

both the elements' response and the measured noise. The second model assumes that noise is due mainly to the antenna elements' self-noise and is not affected by mutual coupling. These two data models will be applied to SASPA arrays in the next two Chapters to study the enhancement on DOA estimation. Also, the effectiveness of the CVUC model in conjunction with MUSIC algorithm will be shown in this Chapter by several simulations.

- **Chapter 5** considers the performance of ULA-SASPA and UCA-SASPA as direction finding arrays when background noise picked up by the parasitic array elements is coupled to the active element. Assuming that mutual coupling is known, compensating for this phenomenon will result in a system of N^2 sub-snapshot couple-free measurements from N snapshot measurements. Averaging the measurements will result in a covariance matrix whose noise component is reduced by the number of the elements N. As a consequence, the signal subspace obtained from the eigendecomposition of the covariance matrix of the measurements will be better fitted to the steering matrix of the underlying DOA; and a superior high-resolution DOA estimation over the all-active antenna arrays will be achieved even in small size aperture arrays. DOA simulations in conjunction with the MUSIC algorithm for different scenarios of received signals and SASPA arrays are implemented to confirm the advantages of this method. The RMSE criterion is also examined from which it is found that this criterion is almost unchanged over a wide range of SNR. This reinforces the beneficial outcome of this method.

- **Chapter 6** assumes that the measured noise is not affected by mutual coupling. That is, the measured noise is due mainly to the active element's self-noise. A rearrangement of the data model for a ULA-SASPA array will result in a steering matrix that is the product of two matrices. The first matrix is DOA dependent, and its entries are real values, while the second matrix is complex and represents mutual coupling but with reduced size than the actual mutual coupling matrix. As

a result of the numerically simpler structure of the steering matrix, a reduction in the computational load when simulating the ULA-SASPA array can be obtained. It can also reduce the computational load if DOA estimation is required to be performed on-line. Another advantage of the new data model is that it allows the ULA-SASPA array to outperform its all-active ULA counterpart in DOA estimation. Several simulations for signals that are received from different directions and impinging on small aperture arrays are conducted to show the effectiveness of this method. Another simulation study was conducted to determine the RMSE of the estimated DOAs as a function of the signal's SNR.

- The mutual coupling parameters of an array can vary with time due to changing environmental factors. The actual mutual coupling parameters may also differ from the theoretical values due to manufacturing tolerances. **Chapter 7** investigates the viability of estimating the on-line mutual coupling parameters of a ULA-SASPA direction funding array. The proposed method relies on impinging the array with a test signal, then estimating the mutual coupling vector from the null space of the rank deficient matrix formed from pre-multiplying the real-valued matrix mentioned in Chapter 6 by the orthogonal projection matrix with range space spanned by the estimated noise subspace. The proposed method is much simpler than the methods available in the literature and requires only a small amount of computations. The feasibility of the method will be demonstrated and verified through simulations.

- **Chapter 8** concludes the whole work of this thesis and gives some suggestions on potential future work on SASPA arrays.

Chapter 2

MUTUAL COUPLING IN ANTENNA ARRAYS

2.1   Introduction

This thesis investigates the ability of an SASPA array to estimate the DOA of the received signals in conjunction with the MUSIC algorithm. Thus, to start with, some of important characteristics of a single antenna and antenna arrays should be studied. Among these characteristics is the inevitable *mutual coupling*. Therefore, in this chapter, the concepts of this phenomenon will be reviewed in light of the analysis found in the literature. However, the available models, which might appropriately express mutual coupling in all-active antenna arrays, cannot be applied to SASPA arrays. As a result, a new model called *Coupled Voltage to Uncoupled Currents* (CVUC) is proposed first for all-active antenna arrays, and then updated to match SASPA arrays in the next chapter.

Note that in this chapter, the mathematical notations and symbols used were chosen to conform with those commonly found in the literature on electromagnetics. Thus, for example, $\vec{E}$ is the electric field vector, E is its amplitude, E_θ is the amplitude of $\vec{E}$ in the θ direction, $\vec{\theta}$ is the unit vector in the direction θ, and $\vec{a} \times \vec{b}$ and $\vec{a} \cdot \vec{b}$ denote, respectively, the cross- and dot-product of the vectors $\vec{a}$ and $\vec{b}$.

2.2   Single Antenna Element

An antenna is a device that converts electrical alternating current to electromagnetic waves and vice versa. In the first case it is called a transmitter while when it converts the intercepted electromagnetic waves to electrical current it is called a receiver. Antenna can be found in different shapes such as wire antenna, slot antenna, microstrip antenna, etc. [18]. Antenna can act alone as a single element or together with other antenna elements in an array. The shape or geometry of an array is

designed to provide certain characteristics which may serve a specific requirement in a communication system.

2.2.1 Antenna Parameters

In this section, some of the important and useful antenna parameters for this work will be explored. To be specific, the half-wave dipole antenna which is a type of wire antenna will be considered as the members of an SASPA array. Figure 2.1 depicts this antenna in the Cartesian and polar coordinates. As Figure 2.1 shows, the antenna is assumed to be centred at the origin in free space and lying along the z-axis. The antenna is assumed to be made from a perfect conducting material. This means that the electric field on its surface is zero [18]. The length of this antenna is $l = \lambda/2$ where $\lambda = c/f$ in meters is the wave length of the operating frequency f and c is the speed of light in vacuum. Thus, this antenna resonates at that frequency and accordingly is called half-wave dipole antenna [18].
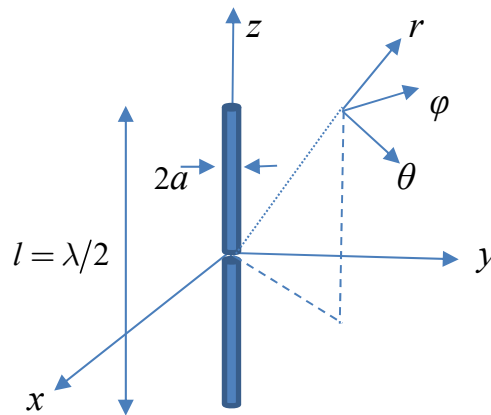
Figure 2.1: Dipole antenna in Cartesian and polar coordinates.

It is assumed that the dipole is very thin, i.e. $a \ll \lambda$, where a is the radius, so that its length should be exactly half the wavelength of the resonance frequency [18]. Furthermore, the surface currents that are induced due to the incident waves can be ignored. Usually, this antenna is fed, when acting as a transmitter, or loaded, when receiving a signal, at the centre where its current distribution is maximum. Using such an antenna type allows an accurate study with less complication [19] in

conjunction with practical considerations.

2.2.1.1 The Radiation Intensity Pattern

The most important parameter that is to be found first for a given antenna is the spatial distribution of the energy emitted from that antenna, i.e. its radiation intensity pattern. This parameter is defined in the far-field region. It is derived from the antenna radiation pattern [18][20]. The shape of that pattern is determined mainly by the distribution of the antenna current. For a very thin dipole antenna, the current is assumed to have sinusoidal distribution [18]-[20], i.e. for $x' = y' = z' = 0$, the current is:

$$\vec{I}(x' = y' = z' = 0) = \bar{z} I_m \sin\left[k\left(\frac{l}{2} - |z'|\right)\right], \quad -l/2 \le z' \le l/2 \tag{2.1}$$

where I_m is the current amplitude, $k = 2\pi/\lambda = \omega\sqrt{\mu\varepsilon}$ is the wave number, and μ and ε are the permeability and permittivity of the medium respectively. Since (2.1) gives zero values at $z = \pm l/2$, it is considered to be a good approximation of the practical situation [18][19]. This means the maximum current occurs at the feed point which is at the centre in Figure 2.1. This is justified as long as the dipole is very thin and the feed gap is very small in size. The electric far field produced by the current in (2.1) for a dipole antenna with arbitrary finite length is expressed in (2.2). It can be derived from the magnetic potential vector which can be found in many antenna reference books such as in [18]-[20].

$$\vec{E}(r,\theta,\phi) = \vec{E}_\theta = \vec{\theta}\, j\eta \frac{I_m e^{-jkr}}{2\pi r}\left[\frac{\cos\left(\frac{kl}{2}\cos\theta\right) - \cos\left(\frac{kl}{2}\right)}{\sin\theta}\right] \tag{2.2}$$

where $\eta = \sqrt{\mu/\varepsilon}$ is the intrinsic impedance and r is the distance between the centre of the antenna and the observation point. It is clear from (2.2) that the magnitude of the electric far field depends significantly on the dipole length and the elevation angle θ, the angle made between the z-axis and the line connecting the centre of the

dipole to the observation point. The factor e^{-jkr} is the spatial phase shift with the term r/λ analogous to the time shift term t/T in time varying signals. For a half-wave dipole antenna, (2.2) becomes:

$$\vec{E}_\theta = \vec{\theta}\, j\eta \frac{I_m e^{-jkr}}{2\pi r} \left[\frac{\cos\left(\frac{\pi}{2}\cos\theta\right)}{\sin\theta} \right] \qquad (2.3)$$

The Poynting vector is defined as the instantaneous power per unit area radiated from an antenna and is the cross product between the instantaneous electric field $\dot{E}$ and instantaneous magnetic field $\dot{H}$ produced by the alternating current on the antenna [18][20][22]:

$$\dot{P} = \dot{E} \times \dot{H} \qquad (2.4)$$

The average of this power is [18][20][21]:

$$\vec{W}_{\mathrm{av}} = \frac{1}{2}\mathrm{Re}\left[\vec{E}_\theta \times \vec{H}_\phi^*\right] = \frac{1}{2}\mathrm{Re}\left[\vec{E}_\theta \times \vec{\phi}\,\frac{E_\theta^*}{\eta}\right] = \vec{r}\,\frac{1}{2\eta}\left|E_\theta^2\right|$$

$$= \vec{r}\eta \frac{|I_m|^2}{8\pi^2 r^2}\left[\frac{\cos\left(\frac{kl}{2}\cos\theta\right) - \cos\left(\frac{kl}{2}\right)}{\sin\theta}\right]^2 \qquad (2.5)$$

The radiation intensity U is the average power times the distance squared measured from the centre of the antenna to the observation point [18][20][22]:

$$U = r^2 W_{\mathrm{av}} = \eta\frac{|I_m|^2}{8\pi^2}\left[\frac{\cos\left(\frac{kl}{2}\cos\theta\right) - \cos\left(\frac{kl}{2}\right)}{\sin\theta}\right]^2 \qquad (2.6)$$

Figure 2.2 shows a polar diagram for the normalized radiation intensity for a dipole with sinusoidal current distribution and for different lengths [18]. As (2.6) reveals, the maximum radiation from a half-wave dipole antenna is at $\theta = \pi/2$ and this coincides with the fact that maximum radiation occurs where the current is

maximum. In addition, it is obvious that this type of antenna is omni-directional as it is clear from the 3D polar plot for the radiation intensity in Figure 2.3, i.e. the locus of the radiation intensity in the *H*-plane is a circle. For dipoles having lengths more than half wavelength, more than one main lobe will appear in their radiation pattern. This results in nulls in certain directions and complicates the directivity of the antenna. Accordingly, the analysis in this work assumes that the antennas are half wave dipoles. Also, it is assumed that signals are incident on the antenna in the azimuth plane where maximum radiation occurs and is independent of elevation angle. It is worth mentioning that the radiation pattern is mainly determined by the antenna current and not by its applied voltage [19]. This fact is crucial in analysing the SASPA array since parasitic elements will conduct short circuit current when intercepting a signal while its terminal voltage is zero. In other words, the currents in the active and parasitic elements all contribute to the overall response of the array to that signal.
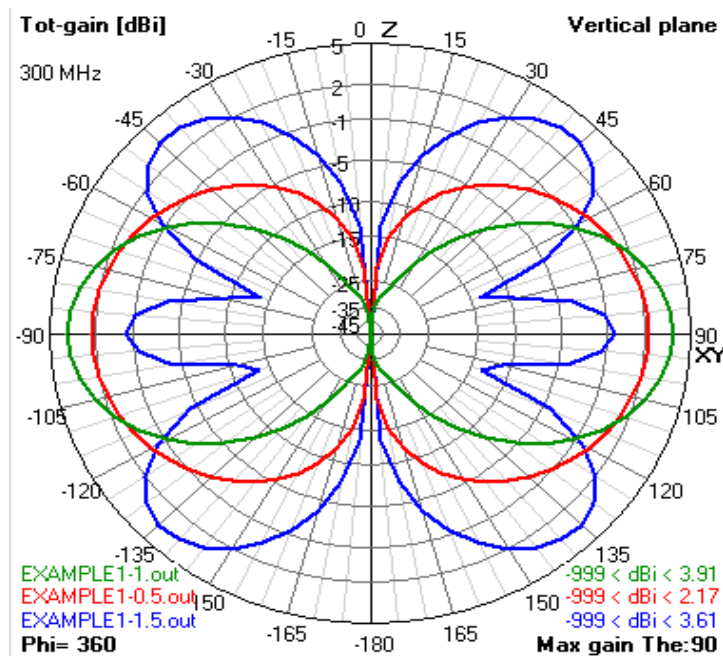

Figure 2.2[3]: Radiation intensity for the dipole antenna of Figure 2.1.

---

[3] The software 4NEC2 is used for plotting figures 2.2. The official web site for 4NEC2 is:
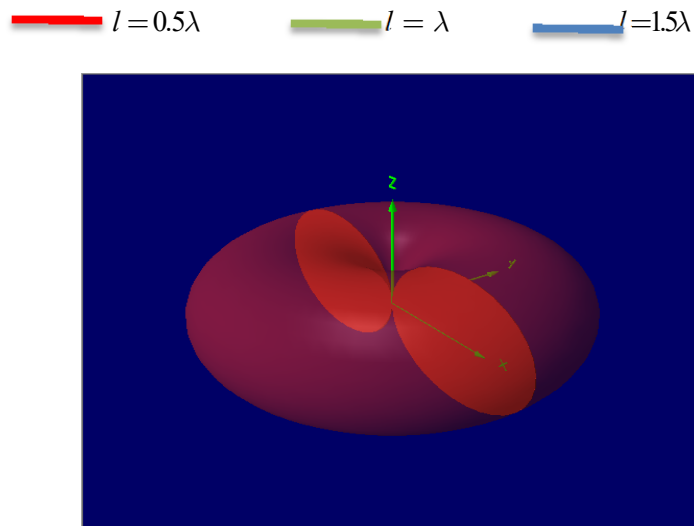https://www.qsl.net/4nec2/

Figure 2.3[4]: 3-D radiation intensity for a half wave dipole antenna in free space.

2.2.1.2 Antenna Self-Impedance and Equivalent Circuits

Electrical engineers usually model telecommunication devices in terms of distributed or lumped components. This helps them to have good approaches to the characteristics of these devices and accurate analysis of the response or transfer function of these devices to certain inputs. For example, the uniform transmission line with characteristic impedance Z_o when analysed is replaced by a cascade of R-L-C networks per unit length that gives almost accurate mathematical formulae to express Z_o in terms of voltages and currents over the whole length of the transmission line. Thus, those formulae will be functions of frequency and as well as distance along the transmission line. Similarly, the isolated antenna can be replaced by a complex impedance called self-impedance which is a function of the operating frequency and the antenna shape. Therefore, the calculation of Z_o requires derivations of typical expressions for the current and voltage developed on the antenna taking into consideration parameters such as length, diameter, area of the gap across which the supply or the load is connected (e.g. in the case of dipole

---

[4] The software 4NEC2 is used for plotting figures 2.3. The official web site for 4NEC2 is:
https://www.qsl.net/4nec2/

antennas), and some boundary conditions.

There are several different approaches to modelling the self-impedance and mutual impedance for dipole antennas, which will be explained in later sections. Derivation of the self-impedance models is based mainly on the current distribution on the antenna especially when their diameters are finite, and the sinusoidal current distribution is no longer valid as well [18]-[20]. In addition to the current distribution, estimating the mutual coupling impedance relies on other parameters such as the type of array elements, the element's relative location, 3-D figures of element radiation patterns, the hybrid network supplying the elements, etc [23]. The most prevalent methods are the induced electro motive force (EMF), the method of moments (MOM), Hallen's integral equation and Pocklington's integral-differential equation [18][19][23]. The analysis in these approaches starts from the solutions for either the magnetic or electric vector potential of Maxwell's equations with the constraint that the electric field component parallel to the dipole vanishes. In this work, because straight wire-based antenna arrays will be investigated as DOA estimators, the radius of the dipole in these arrays is assumed to be very thin, hence the current distribution will be sinusoidal, and the dipole is assumed to resonate, i.e. with a length equals half the wavelength of the operating frequency. The induced EMF approach turns out to be good approach. In addition, the induced EMF method affords closed form solutions for such arrays [23]. However, Hallen's integral equation will also be used since this approach provides a better view for the short circuit current which is induced on a receiving dipole acting as a parasitic element [19].

Induced Voltage of a Receiving Antenna

If a dipole intercepts an incident EM wave, an open circuit voltage V_{ind} will be induced at its unloaded terminals while a current will be delivered to the load connected across the antenna terminals, see Figure 2.4.
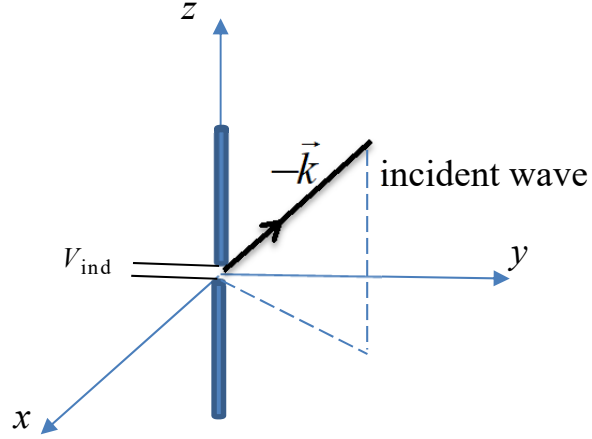
Figure 2.4: EM wave incident on a dipole antenna.

Here, $\vec{k} = 2\pi/\lambda$ is the wave number of the incident EM wave. In this model, it is assumed that the wave is narrowband, travelling in homogenous and isotropic medium and emanating from a source that is located very far from the centre of the antenna so that what the antenna receives is a plane wave, i.e., all points on the wavefront have the same phase shift. In addition, the electric field component of the wave is perpendicular to the propagation direction, i.e., it is vertically polarized [8][18][19][24]. This plane-wave propagation model lets one to write the expression for the tangential component of the received electric field as follows [19][24]:

$$\vec{E}^{inc}(z') = E_o e^{-j(-\mathbf{k})\cdot\mathbf{z}} = E_o e^{jkz'\cos\theta} \tag{2.7}$$

where E_o is the strength of the electric field at the antenna surface. Because of the narrowband assumption, the elevation dependence is only a phase shift. Also, because the dipole is assumed to be very thin, (2.7) is an azimuth independent function, and cylindrical waves have also not been considered in it. The induced voltage V_{ind} can be derived from the formula [18][24]:

$$V_{ind} = -\frac{1}{I_i}\int_{-l/2}^{l/2}\vec{E}^{inc}(z')\cdot\vec{I}(z')\,dz' \tag{2.8}$$

where I_i is the current at the antenna terminals. Inserting $\vec{E}^{inc}(z')$ from (2.7) and $\vec{I}$ from (2.1) into (2.8) and evaluating the integral yields [18][19][20][24]:

$$V_{\text{ind}} = \frac{\lambda E_o}{\pi \sin\left(\frac{kl}{2}\right)} \left| \frac{\cos\left(\frac{kl}{2}\cos\theta\right) - \cos\left(\frac{kl}{2}\right)}{\sin\theta} \right| \tag{2.9}$$

Note that the induced voltage of an open circuited receiving dipole antenna has the same elevation dependence as in (2.2) which is for the electric field of a transmitting antenna in the far field. This proves that antennas obey the phenomenon called "Reciprocity". This means that antennas possess identical characteristics when acting as a transmitter or a receiver [18][20][21]. The principle of antenna reciprocity assumes that for two antennas located far away from each other the voltage induced on one of them due to the radiation from the second one which is current driven is the same as the voltage induced on the second one by the radiation of the first one if it is current driven [18][21]. The EMF models in (2.8) is a consequence of this phenomenon.

In [19], the approach of Hallen's equation for a receiving antenna has been used to derive formulae for the induced voltage and short circuit current in the case of open circuited and short-circuited receiving dipole respectively. The respective formulae are as follows:

$$V_{oc} = \frac{2E_o}{k\sin\left(\frac{kl}{2}\right)} \frac{\cos\left(\frac{kl}{2}\right) - \cos\left(\frac{kl}{2}\cos\theta\right)}{\sin\theta} \tag{2.10}$$

$$I_{sc} = I(0) = \frac{2E_o}{Bk\cos\left(\frac{kl}{2}\right)} \frac{\cos\left(\frac{kl}{2}\right) - \cos\left(\frac{kl}{2}\cos\theta\right)}{\sin\theta} \tag{2.11}$$

where $B = B(z)$ is a slowly varying function with respect to z and hence is considered a constant (see [19] Section 22.3). Notice the resemblances in the elevation dependence for open circuited induced voltage that is derived using both methods: EMF and Hallen's equation.

Antenna Self Impedance

The self-impedance Z_s of an isolated dipole antenna located in free space can be written as:

$$Z_s = R_s + jX_s \tag{2.12}$$

where $R_s = R_r + R_l$ is the sum of the radiation resistance R_r and the material loss resistance R_l. In (2.9), the voltage developed at the terminal of a receiving dipole antenna is found. If this voltage is defined in terms of the maximum current and then divided by that current, the self-impedance of the dipole referred to the maximum current can be calculated [18][21], i.e.

$$Z_{S_m} = -\frac{1}{I_m^2} \int_{-l/2}^{l/2} E(z') I_z(z') dz' \tag{2.13}$$

Plugging (2.1) and (2.7) into (2.13) and evaluating the integral, the real and imaginary part of self-impedance, after a lengthy derivation [18], are given by [20][21][24]:

$$R_s = \frac{\eta}{2\pi}\left\{C + \ln(kl) - \alpha_i(kl) + 0.5\sin(kl)[\beta_i(2kl) - 2\beta_i(kl)] \right. $$
$$\left. + 0.5\cos(kl)[C + \ln(kl/2) + \alpha_i(2kl) - 2\alpha_i(kl)]\right\} \tag{2.14}$$

$$X_s = \frac{\eta}{4\pi}\left\{2\beta_i(kl) + \cos(kl)[2\beta_i(kl) - \beta_i(2kl)] \right. $$
$$\left. - \sin(kl)\left[2\alpha_i(kl) - \alpha_i(2kl) - \alpha_i\left(2ka^2/l\right)\right]\right\} \tag{2.15}$$

where $C = 0.5772$ is Euler's constant, and $\alpha_i(x)$ and $\beta_i(x)$ are the cosine and sine integral of x respectively [18]:

$$\alpha_i(x) = \int_{\infty}^{x} \frac{\cos y}{y} dy \tag{2.16}$$

$$\beta_i(x) = \int_{0}^{x} \frac{\sin y}{y} dy \tag{2.17}$$

While the real and imaginary parts of the self-impedance in (2.14) and (2.15) respectively depend mainly on the dipole length, the latter is also a function of the

diameter as well. Accordingly, the imaginary part of the antenna power vanishes at far distances and the only component that contributes to energy emission from the antenna is the real part of its power [18][20]. The self-impedance components given in (2.14) and (2.15) are referred to the maximum current. In case that the maximum current does not occur at the driving point terminals, i.e. at points other than the antenna terminals, the self-impedance may be referred to its maximum value via the relationship:

$$Z_s = \frac{I_m}{I_s} Z_m \tag{2.18}$$

While the above analysis for deriving the formula for self-impedance uses the induced EMF method, another expression to the self-impedance can be found from the solutions of Hallen's integral equation by dividing the open circuit voltage in (2.10) by the short circuit current in (2.11):

$$Z_s = -\frac{V_{oc}}{I_{sc}} = -B \cot(kl/2) \tag{2.19}$$

The self-impedance parts in (2.14) and (2.15) may be more precise than the one in (2.19) due to the required boundary conditions and approximations that have been made in the Hallen's approach.

Antenna Equivalent Circuits

Having been calculated, the self-impedance of an antenna can be used to represent a transmit or receive antenna in a Thévenin's and Norton's equivalent circuits, see Figures 2.5. Note that Z_s for a transmit antenna is the same as for a receive antenna according to the reciprocity theorem [18][20][24][25]. In Figure 2.5d, the self-impedance Z_s contributes to the retransmission of EM wave from the receiving antenna and accordingly this means that the power dissipated in each of the equivalent circuits should be equal to the reradiated and scattered power [20][25][26] especially in the case of an antenna in free space [27]. The total scattered and

retransmitted power can be calculated from [28]:

$$P_s = \frac{1}{240\pi} \int_0^{2\pi} \int_0^{\pi} \left| E^{sca}(\theta,\phi) \right|^2 \sin\theta \, d\theta \, d\phi \qquad (2.20)$$

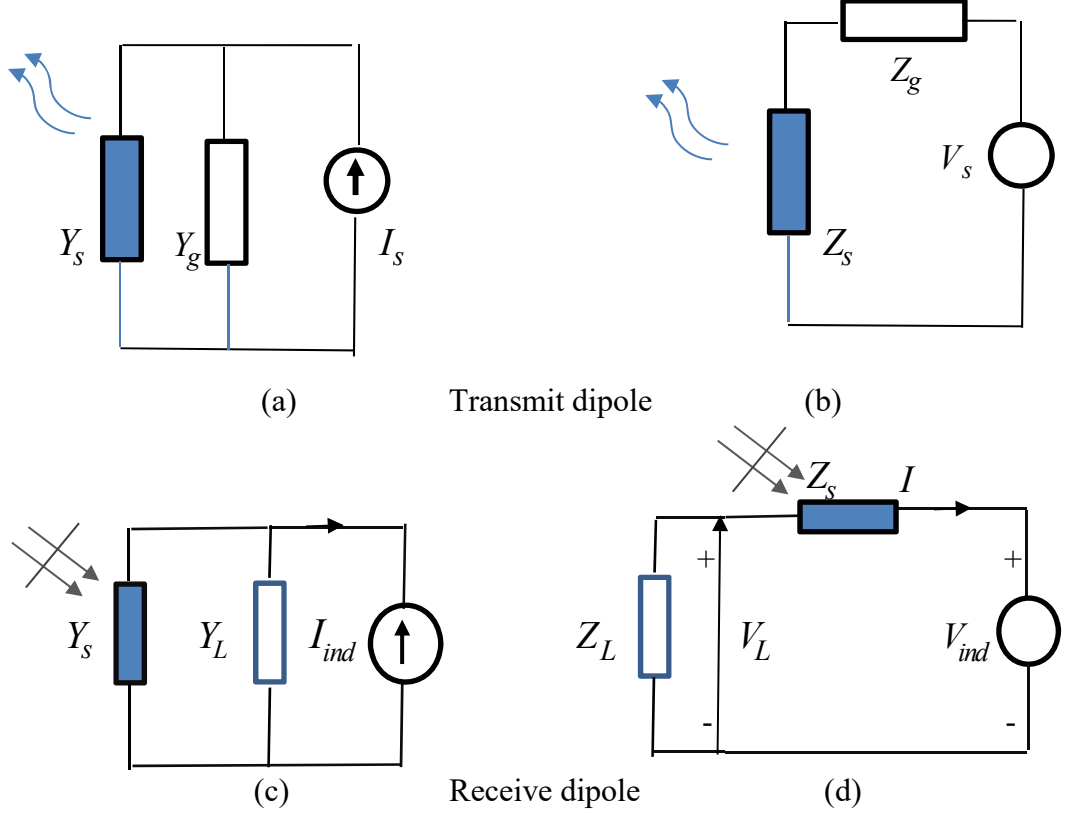(a) Transmit dipole (b)

(c) Receive dipole (d)

Figure 2.5: Thévenin and Norton equivalent circuits for a dipole. (a) and (c) Norton equivalent circuits; (b) and (d) Thévenin equivalent circuits.

where $E^{sca}(\theta,\phi)$ is the total scattered field and where [29]:

$$E_z^{inc}(\rho = a, \theta, \phi) + E_z^{sca}(\rho = a, \theta, \phi) = \begin{cases} E_z^{gap}, & |z - z'| < \Delta_g \\ 0, & |z - z'| > \Delta_g \end{cases} \qquad (2.21)$$

where E_z^{gap} is the electric field across the gap Δ_g where a load or a source can be attached to the dipole. Obviously, the scattered field will equal approximately to the incident field for a short-circuited dipole and this asserts that a parasitic antenna acts as a reflector. In the literature, the circuits in Figures 2.5c and 2.5d are found to be good approximations as equivalent electric networks to the receive antenna [25][30][31]. However, Collin in [32] argues that equality between the absorbed power of a receiving antenna and the scattered power is valid only in the case of a

dipole antenna that is loaded with a matched load. Accordingly, the circuits of Figure 2.5 may not be valid for calculating the total scattered power for non-matched loads. It has been proved in [32], as a confirmation for this argument, that the power consumed by the load of a receiving antenna using Thévenin equivalent circuit is different from the load power calculated using Norton equivalent circuit. Love [33] has suggested 'A constant-power generating circuit for a receiving antenna'. In this circuit, the Thévenin and Norton equivalent circuits have been used together in one circuit to represent a receiving antenna. Thus, the absorbed power and the scattered or reradiated power will be referred to the total constant power resulting from the product of the induced voltage source V_{ind} shown in the Thévenin circuit (Figure 2.5d) and by the current source I_{ind} of the Norton circuit (Figure 2.5c). In addition, this model shows that the power delivered to a matched load will be maximum and the scattered power will be minimum. In this thesis, the argument of the circuits in Figure 2.5 being accurate for a matched load will be taken into consideration since it has been agreed in the above discussion that an antenna loaded by a matched load will be 50% efficient. In addition, it is clear from (2.20) that scattered power will be small for arrays with small aperture which is the case in SASPA arrays.

2.3   Antenna Arrays

Antenna arrays have been used since the early days of electrical wireless communications. Despite possessing more complicated characteristics than the single-element antenna, antenna arrays provide several advantages over a single antenna such as increased gain, directivity, etc. Recently, antenna arrays that are called "smart antenna" have been used to perform many tasks that could not be achieved by a single element. Beamforming, direction finding are some examples of those tasks that are crucial in communication systems aiming to deliver more throughput to users in dense areas. However, the main price paid for having these advantages when using antenna arrays is the adverse effect of the mutual coupling

effect between the array members especially when the spacing between them is small ($\leq \lambda/2$). This phenomenon will be discussed in detail in Section 2.5. In this thesis, two types of antenna arrays most commonly used as DF arrays will be considered: The Uniform Linear Array (ULA), and the Uniform Circular Array (UCA).

2.3.1 Uniform Linear Array (ULA)

This geometry is the simplest one in which the antenna elements are located along a straight line with a uniform inter-element spacing d. Figure 2.6a depicts a ULA in which identical dipole antennas are used and is assumed to be in free space. Each element in this array is oriented parallel to the z-axis with its centre located on the x-axis. This arrangement is also called the "side by side" array [18][20]. The edge (or end) of a ULA may present a cut in the overall current distribution, hence lacking symmetry. For large ULAs, it is assumed that mutual coupling between array elements that are far apart is very small and can be ignored, hence their mutual coupling matrix is banded [24]. However, this is not the case for ULA-SASPA arrays since the operation of this type of antenna arrays depend intimately on the presence of mutual coupling. The steering matrix of ULA arrays, which gives the response of the array elements to the received signals, has a Vandermonde structure [8]. However, the main drawbacks of ULAs when acting as DF arrays are ambiguity, i.e., they cannot distinguish signals arriving from $\pm\phi$ for a given θ, and asymmetry in their beam patterns.

2.3.2 Uniform Circular Array (UCA)

If a symmetrical antenna array is required, the ULA is not the right choice. The UCA could be a good selection instead [18], see Figure 2.6b. In this geometry, the antenna elements are distributed over the circumference of a circle in a certain plane, say the x-y plane, with a radius R and oriented parallel to the z-axis. This geometry has azimuth symmetry; therefore, the azimuth plane can be scanned by the same switched radiation pattern if the array consists of identical elements with uniform

spacing. Accordingly, UCA provides more DOA resolution over the ULA as will be seen later. In addition, 2D DOA estimation can be performed with UCA arrays. Also, UCA does not suffer from ambiguity and has no edge effect. Therefore, it may effectively line up with the requirements of adaptive smart antenna arrays [18].
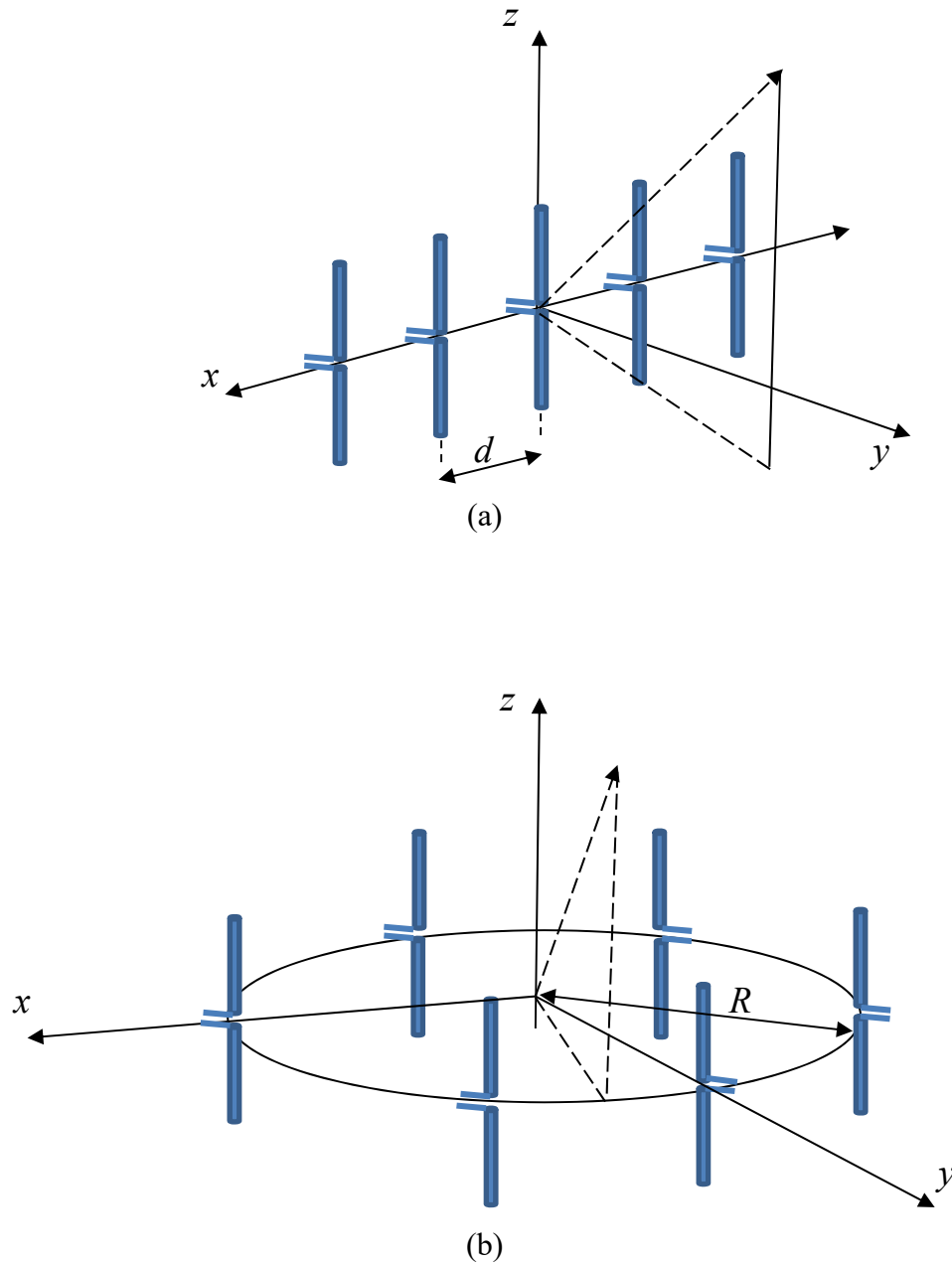

(a)

(b)

Figure 2.6: Two types of antenna arrays. (a) ULA; (b) UCA.

2.4   Mutual Coupling and Mutual Impedance

Mutual coupling is the phenomenon of exchanging power between neighbouring antenna elements. The electromagnetic characteristic of a single element, such as the radiation pattern, induced voltage, and terminal input impedance will be influenced and contaminated when another antenna is in its proximity. In the literature, most authors argued that the phenomenon of mutual coupling between array elements has an adverse effect on the performance of antenna arrays when acting as direction finding (DF) arrays [23][24]. This is due to contaminating the measurements of the array by the coupled voltages or currents from the neighbour antenna elements [23]. Consequently, DOA algorithms performance will undergo degradation because the actual intelligence related to the received signals becomes embedded into the measurements. Therefore, the model that correctly and precisely interprets the mutual coupling should be investigated to establish further step towards compensating such effect.

Mutual coupling depends on various parameters such as the antenna type, the number of antenna elements in the array, the spacing between the elements, the element position, the element alignment, the DOA of the signal impinging on the array, and the hardware used to process the measurements [18][23]. Expressing this characteristic of energy exchange between the array elements has been viewed in different perspectives, see [18][23][34][35]. These views are based mainly on interpreting the mechanism of spatial exchange of power between the elements of the array and interpreting this exchange by equivalent electrical circuits. Therefore, different approaches such as induced EMF and MoM have been used to calculate the mutual impedance between two wire antennas. The overall model for mutual coupling in an array takes the form of a matrix. This matrix may have special structure depending on the geometry of the array. For example, ULA is symmetric when rotated around the axis which is perpendicular to the array's axis, therefore its

mutual coupling matrix is a symmetric complex Toeplitz. Likewise, the UCA has a circulant mutual coupling matrix.

In DOA estimation, the simplest method to compensate for mutual coupling is by applying the inverse of the mutual coupling matrix to the measurements as in [17][24][36]-[38] assuming noise is not affected by mutual coupling. This means that prior knowledge of mutual coupling is assumed to be already available. However, because of various environmental or manufacturing factors, the actual mutual coupling may be change over time. Therefore, to compensate for mutual coupling in an antenna array by applying the inverse of this effect is not reliable for counteracting the coupled measurement in high resolution DOA estimation. In the literature, methods such as in [39] have been proposed to eliminate the requirement for having prior knowledge about the underlying mutual coupling.

2.4.1 Mutual Impedance

To start defining mutual coupling in antenna arrays, the mutual impedance between two elements must first be analysed. King [40] has derived analytical formulae for the mutual impedance between two wire antennas with any length and located in a side-by-side configuration. Kraus [20] has also derived similar expressions for the aforementioned configuration and both of their methods are based on the induced EMF method. Let the mutual impedance between two identical elements p and q located in a side-by-side configuration be:

$$Z_{pq} = \frac{V_{pq}}{I_q} \qquad (2.22)$$

where V_{pq} is the open-circuited voltage induced at the feed point of element p due to the current in element q and I_q is the current at the feed point of element q. According to the induced EMF method, V_{pq} can be written as [18] [20]:

$$V_{pq} = -\frac{1}{I_p} \int\limits_{-l/2}^{l/2} E_{z_{pq}}(z') I_p(z') dz' \qquad (2.23)$$

Hence,

$$Z_{pq} = -\frac{1}{I_q I_p} \int\limits_{-l/2}^{l/2} E_{z_{pq}}(z') I_p(z') dz' \tag{2.24}$$

Here, $E_{z_{pq}}(z')$ is the z-component of the radiated field from element q and parallel to the axis of element p and is given by [18][19]:

$$E_{z_{pq}}(z') = -\frac{j\eta I_{m_q}}{4\pi} \left(\frac{e^{-jkR_1}}{R_1} + \frac{e^{-jkR_2}}{R_2} - 2\cos\left(\frac{kl}{2}\right) \frac{e^{-jkR_o}}{R_o} \right) \tag{2.25}$$

I_{m_q} is the maximum current of element q and R_1, R_2 and R_o are as follows [18]-[20], see Figure 2.7:

$$R_o = \sqrt{d^2 + (z+h)^2} \tag{2.26}$$

$$R_1 = \sqrt{d^2 + \left(z + h - \left(\frac{l_q}{2}\right)\right)^2} \tag{2.27}$$

$$R_2 = \sqrt{d^2 + \left(z + h + \left(\frac{l_q}{2}\right)\right)^2} \tag{2.28}$$

Plugging (2.25) and (2.1) as the current distribution for $I_p(z')$ into (2.24) and after some lengthy derivations (see [18][20]), the real and imaginary parts of the mutual impedance between identical very thin half-wave dipole antennas p and q in an array with N identical elements located side by side in free space is given by [24]:

$$R_{pq} = \frac{\eta}{4\pi} [2\alpha_i(u_o) - \alpha_i(u_1) - \alpha_i(u_2)] \tag{2.29}$$

$$X_{pq} = \frac{\eta}{4\pi} [2\beta_i(u_o) - \beta_i(u_1) - \beta_i(u_2)] \tag{2.30}$$

where α_i and β_i are defined previously in (2.16) and (2.17) respectively while their arguments are defined as:

$$u_o = kd \tag{2.31}$$

$$u_1 = k\left(\sqrt{d^2 + l_q^2} + l_q\right) \tag{2.32}$$

31

$$u_2 = k\left(\sqrt{d^2 + l_q^2} - l_q\right) \tag{2.33}$$

Figure 2.8 shows the variation of R_{pq} and X_{pq} as a function of the spacing d/λ. It is clear from (2.29) and (2.30) that the mutual impedance depends mainly on the inter-element spacing and the antenna length. Thus, for two very close elements, the coupling is strong and cannot be ignored. When $d = 0$, the mutual impedance has a value of $(73 + j42.5)$ which is the same value as the self-impedance.
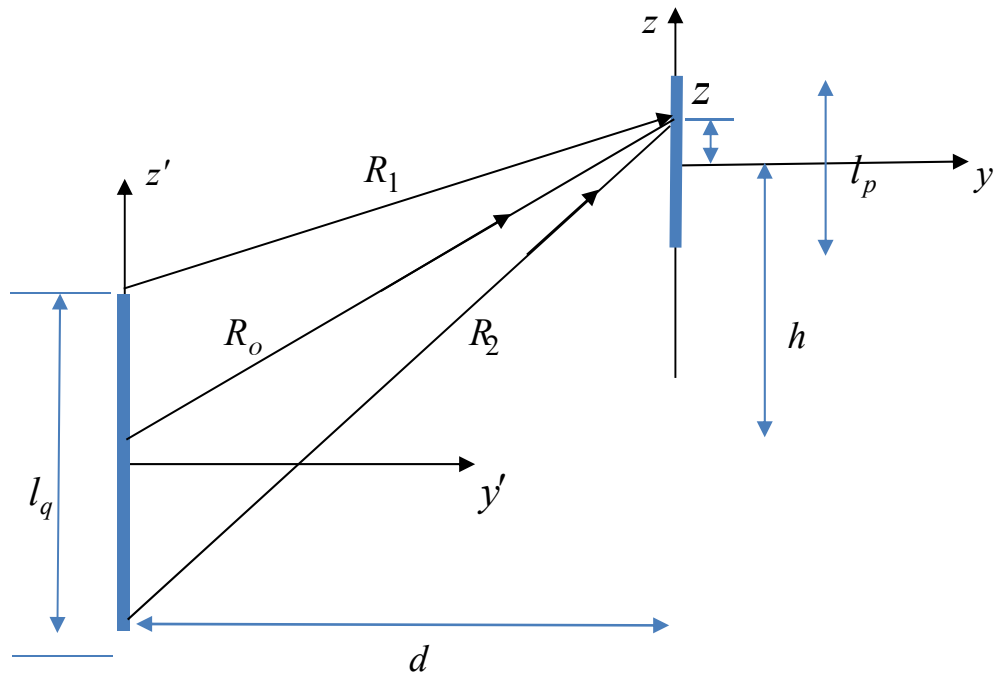

Figure 2.7: Two dipoles in side-by-side configuration.

It is worthwhile mentioning here the analysis presented in the literature such as in [18][19][21] for calculating the driving point impedance for a simple transmitting array consisting of two antennas. Starting with the following system of equations:

$$V_1 = I_1 Z_{11} + I_2 Z_{12} \tag{2.34}$$

$$V_2 = I_2 Z_{22} + I_1 Z_{21} \tag{2.35}$$

one gets, after dividing the first equation by I_1 and the second equation by I_2:

$$\frac{V_1}{I_1} = Z_{1d} = Z_{11} + \frac{I_2}{I_1} Z_{12} \tag{2.36}$$

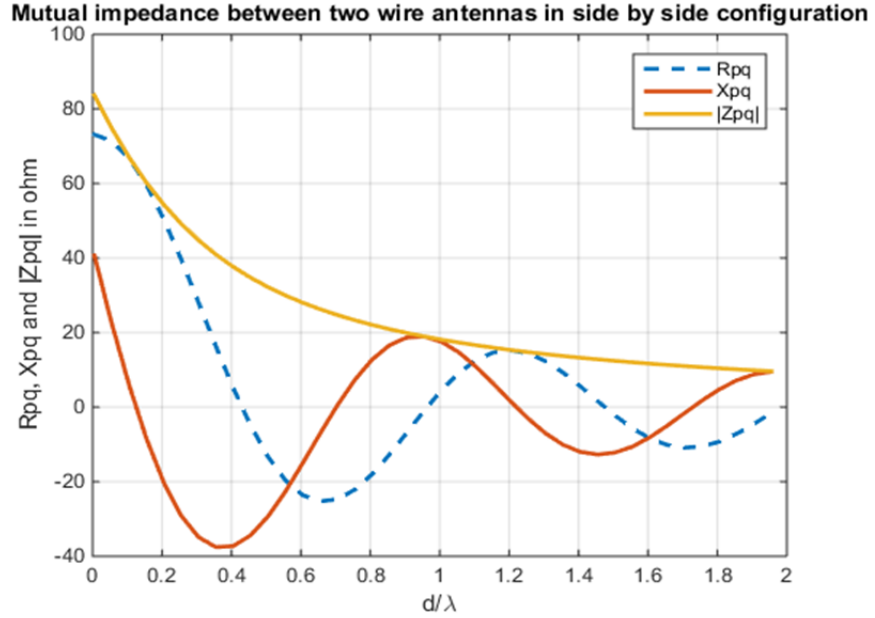$$\frac{V_2}{I_2} = Z_{2d} = Z_{22} + \frac{I_1}{I_2} Z_{21} \tag{2.37}$$

Figure 2.8: Variation of R_{pq} and X_{pq} versus inter-element spacing d/λ for two very thin half-wave dipoles located in side by side configuration.

I_1 and I_2 are actually the uncoupled currents in antennas #1 and #2, while V_1 and V_2 are the terminal voltages of antennas #1 and #2 respectively. Thus, dividing V_1 by I_1 or V_2 by I_2 does not give the true driving point impedance of each element in the array. In the next section, the relationship between the coupled voltages and currents induced on each element in a receiving array will be analysed. The aim is to derive mutual coupling models that give a closer view on the energy exchange between the array elements.

2.4.2   Mutual Coupling Models for Receiving Antenna Arrays

The aim of using antenna arrays is to provide observations or measurements from which information about the DOA and other parameters of the received signals can be estimated. For DOA estimation, this can be achieved after finding the correlation

between the measurements of the response of the array elements to the received signals. These responses are measured multiple times to give a statistically more accurate estimate of the parameters after processing the correlated observations using suitable signal processing algorithms. Obviously, this cannot be done by a single antenna. In the next chapters, it will be shown that the responses of the array elements are different from each other by the phase shift $e^{-j\vec{\mathbf{k}}\cdot\vec{\mathbf{r}}_n}$ due to the time delay the received signal experiences when travelling across the array. However, the measurements, i.e., the load or terminal voltages of the array elements, include the mutual coupling effect between the array elements in addition to their response to the received signals. If each element in the array is loaded by the same load (usually chosen to be the complex conjugate of the antenna input impedance to attain maximum power transfer), the load voltage will be related to the induced voltage through the relationship:

$$\mathbf{v}_L = \mathbf{C}\mathbf{v}_{ind} \tag{2.38}$$

where $\mathbf{v}_L \in \mathbb{C}^{N\times 1}$ is the vector of the load voltages at the element terminals and $\mathbf{v}_{ind} \in \mathbb{C}^{N\times 1}$ is the vector of the stand-alone induced voltages, i.e. the uncoupled load voltages. The square matrix $\mathbf{C} \in \mathbb{C}^{N\times N}$, which is called the Mutual Coupling Matrix (MCM), is based on self and mutual impedances [23][24]. It has a Toeplitz structure for ULA [24] and circulant structure for UCA [23]. Obviously, the size of the MCM becomes larger as the number of elements in the array increases. This may lead to larger errors in signal processing algorithms that involve decoupling the measurements because of their need to calculate the inverse of the MCM. However, since $|Z_{pq}| \to 0$ for large spacing d/λ, see Figure 2.8, the MCM could have a banded structure, i.e. with zero entries on the sub-diagonals that are far from the main diagonal. In SASPA arrays this may not be valid since in the structure of SASPA, it is imperative that the elements should be close to each other. In the literature, different interpretations have been applied on the MCM in order that an accurate decoupling scheme could be devised to remove the adverse effect of mutual

coupling on the performance of DOA algorithms. However, this has led to disagreements resulting from using different views such as microwave circuit theory or electromagnetic field analysis when interpreting the interaction between the elements in an antenna array. While some authors argue that because of reciprocity, the mutual coupling effect is the same for receiving and for transmitting arrays [23] [25][37], others have defined two separate models for transmitting and receiving antenna arrays [41]-[43]. The two most well-known models for modelling mutual coupling in receiving antenna arrays are in [37] and in [43]-[47]. In [37], Gupta and Ksienski viewed an N-element receiving antenna array as a linear bilateral $N+1$ port network, where the extra port which represents the received signal is modelled as an external power supply the network and having an internal impedance. By imposing the condition that the open circuit voltage at the terminal of each array element is due to the power supply (the incoming signal) alone, the relationship between the open circuited voltages and the load voltages will be:

$$
\begin{bmatrix} v_{o1} \\ v_{o2} \\ . \\ . \\ . \\ v_{oN} \end{bmatrix} = \begin{bmatrix} 1+\dfrac{Z_{11}}{Z_L} & \dfrac{Z_{12}}{Z_L} & . & . & \dfrac{Z_{1N}}{Z_L} \\ \dfrac{Z_{21}}{Z_L} & 1+\dfrac{Z_{22}}{Z_L} & . & . & \dfrac{Z_{2N}}{Z_L} \\ . & . & . & . & . \\ . & . & . & . & . \\ \dfrac{Z_{N1}}{Z_L} & \dfrac{Z_{N2}}{Z_L} & . & . & 1+\dfrac{Z_{NN}}{Z_L} \end{bmatrix} \begin{bmatrix} v_{L1} \\ v_{L2} \\ . \\ . \\ . \\ v_{LN} \end{bmatrix}
$$

or (2.39)

$$ \mathbf{v}_o = \mathbf{F}_{\mathrm{OCV}} \, \mathbf{v}_L $$

Thus, for this MCM model, the open circuit voltages represent the couple free voltages. This MCM model is called the Open-Circuit Voltage (OCV) method [46][48]. Note that $\mathbf{F}_{\mathrm{OCV}} \in \mathbb{C}^{N \times N}$ in (2.39) is equivalent to $\mathbf{C}^{-1}$ in (2.38). Also, $\mathbf{F}_{\mathrm{OCV}}$ is angle independent [23][36]. Z_{pp} and Z_{pq} in $\mathbf{F}_{\mathrm{OCV}}$ are the conventional self and mutual impedances given by (2.14) and (2.15), and (2.29) and (2.30) respectively [23][46]. The OCV has the interpretation of adaptive receiving arrays in view of

microwave circuits analysis in which the network port is the only source of excitation. However, the actual induced voltage across the antenna terminal is the result of integrating the antenna current over the antenna surface [48]. Therefore, the open circuit voltages are not the exact uncoupled voltages induced by the incoming signals [41]. Furthermore, OCV assumes that no radiation occurs from an antenna with open circuited terminal [45]. Thus, using the inverse of OCV results only in a partial elimination of mutual coupling [49]. However, OCV, which is based on microwave circuit theory, was found to be a good approximation [41], especially when the array is built up of half-wave dipoles since the current in an open circuited dipole can be neglected [36]. Accordingly, it has been used in different DOA estimations studies such as in [24][50].

In [43]-[47], a different MCM model was postulated and is called the Receiving Mutual Impedance Method (RMIM). In this model, the voltage measurement at the antenna terminals in a receiving array is related to the couple-free terminal voltages due to the received signals only through the following relationship:

$$
\begin{bmatrix} u_1 \\ u_2 \\ \cdot \\ \cdot \\ \cdot \\ \cdot \\ u_N \end{bmatrix} = \begin{bmatrix} 1 & \dfrac{-Z^{1,2}}{Z_L} & \cdot & \cdot & \dfrac{-Z^{1,N}}{Z_L} \\ \dfrac{-Z^{2,1}}{Z_L} & 1 & \cdot & \cdot & \dfrac{-Z^{2,N}}{Z_L} \\ \cdot & \cdot & \cdot & \cdot & \cdot \\ \cdot & \cdot & \cdot & \cdot & \cdot \\ \dfrac{-Z^{N,1}}{Z_L} & \dfrac{-Z^{N,2}}{Z_L} & \cdot & \cdot & 1 \end{bmatrix} \begin{bmatrix} v_{L1} \\ v_{L2} \\ \cdot \\ \cdot \\ \cdot \\ \cdot \\ v_{LN} \end{bmatrix}
$$

or   (2.40)

$$\mathbf{u} = \mathbf{F}_{\text{RMIM}} \, \mathbf{v}_L$$

where $\mathbf{u} \in \mathbb{C}^{N \times 1}$ is the vector of load voltages (terminal voltages) due to the incoming signal alone, i.e. the couple free voltages, and $Z^{p,q}$ is the receiving mutual impedance between elements p and q as defined in [44][46]. While OCV assumes the open circuit voltages are the uncoupled voltages, RMIM considers the couple free

voltages as the closed-circuit voltages [45][46]. Note that RMIM needs no prior knowledge about the self-impedances. Also, in this method, $Z^{p,q}$ has been calculated experimentally based on the scattered powers from the array elements [44][46]. However, the calculation is implemented using hardware necessary for the measurement of scattered power in an array consisting only two monopoles regardless of the incident angle of the test signal [44][46]. Accordingly, such a method may need more hardware and computations for large arrays or arrays consisting of another type of antenna. Also, the experimental results for calculating the receiving mutual impedance reveal that the mutual coupling between two dipole antennas almost vanishes for $d/\lambda > 1$. Accordingly, this method might not be useful for such inter-element spacings in large arrays [44, Figure 2]. Yamada *et al.* [41] have used in their suggested MCM another mutual impedance that represents the mutual coupling due to the scattered or reradiated power in addition to the conventional mutual coupling of a transmitting array. However, this MCM requires N^2 simultaneous equations to be solved. Also, the method to calculate the mutual impedance due to the scattered power has not been defined.

In this work, a new approach will be explored for modelling the coupling matrix **C** of (2.38) in conventional receiving antenna arrays, i.e. arrays with all-active elements and to SASPA arrays as a special case. This approach is based on electromagnetic theory in conjunction with circuit theory but in terms of the uncoupled or stand-alone values of currents rather than voltages.

2.4.3 The Coupled Voltages-Uncoupled Currents (CVUC) Model

The proposed MCM model relates the couple-free or stand-alone currents that are induced on each element in a receiving antenna array due to the received signals only to the coupled voltages that are measured at the element's terminal (load voltage). By coupled voltage it is meant the voltage induced at the element's terminal due to the received signal and contaminated by the energy exchanged between the array

elements. The CVUC model is derived from electromagnetic theory and is characterized by a Thévenin equivalent circuit or Norton equivalent circuit. As a result, an efficient view of the mechanism of mutual coupling, which will be interpreted in terms of an electrical network, will be achieved. Moreover, this model matches SASPA arrays as it will be shown in the next chapter. Based on Thévenin equivalent circuit, any antenna in a receiving array can be substituted by the circuit shown in Figure 2.9a [24][25][30][51] and assuming the dependent voltage sources which account for the mutual coupling effect have zero internal impedance [21]. Thus, the load voltage of the element p in an N-element receiving antenna array can be written as:

$$v_{Lp} = u_p - i_p Z_{pp} + i_1 Z_{p1} + \cdots + i_q Z_{pq} + \cdots + i_N Z_{pN} \tag{2.41}$$

Despite being regarded as controversial by many authors, the validity of using a Thévenin equivalent circuit to model a receiving antenna array may be verified through the application of the concept of induced EMF theory to (2.41). It is assumed throughout this proof that the array is in the first stage of exchanging energy between the elements since a series of this exchange yields the coupled currents. The induced voltage at the terminal of a receiving dipole antenna p intercepting a signal can be calculated from (2.8) and is rewritten below:

$$u_p = -\frac{1}{I_p} \int_{-l/2}^{l/2} E_z(z') I_z(z') \, dz' \tag{2.42}$$

The system in (2.41) can be formulated in another way starting with considering the superposition of the Magnetic Vector Potential $\vec{A}$ of a receiving antenna in an array as follows [19] [52]:

$$A_{z,p}(z) = A_{z,p}^{(gap)}(z) + A_{z,p}^{(sca)}(z) + \sum_{\substack{q=1 \\ q \neq p}}^{N} A_{z,pq}^{(sca)}(z) \tag{2.43}$$

where $A_{z,p}(z)$ is the total z-component of $\vec{A}$ on the antenna surface, $A_{z,p}^{(gap)}(z)$ is the z-component of $\vec{A}$ across the gap of element p, $A_{z,p}^{(sca)}(z)$ is the z-component of

the scattered $\vec{A}$ by element p, and $A_{z,pq}^{(sca)}(z)$ is the z-component of the scattered $\vec{A}$ by element q on the surface of element p. Multiplying both sides of (2.43) by $2jc$, where c is the speed of light and applying the operator $\left(\partial_z^2 + k^2\right)$ gives [19]:

$$\left(\partial_z^2 + k^2\right)\left(2jcA_{z,p}(z)\right)$$
$$= \left(\partial_z^2 + k^2\right)\left(2jcA_{z,p}(z)\right)\left(2jc\left[A_{z,p}^{(gap)}(z) + A_{z,p}^{(sca)}(z) + \sum_{\substack{q=1 \\ q \neq p}}^{N} A_{z,pq}^{(sca)}(z)\right]\right) \quad (2.44)$$

$$\therefore \quad 2kE_{z,p}^{inc}(z) = -2kv_{L,p}\delta(z) + 2kE_{z,p}^{sca}(z) - 2k\sum_{\substack{q=1 \\ q \neq p}}^{N} E_{z,pq}^{sca}(z) \quad (2.45)$$

where $E_{z,p}^{inc}(z)$ is the z-component of the electric field of the incident wave and $E_{z,p}^{sca}(z)$ is the z-component of the scattered electric field by element p. To obtain (2.45), the following relationship has been used [19]:

$$v_p(z) = 2jcA_{z,p}(z) \quad (2.46)$$

where $v_p(z)$ (in volts) is a scaled version of $A_{z,p}(z)$. This results in a scaled value of the electric field when $\left(\partial_z^2 + k^2\right)$ is applied to it [19, pp. 1176], i.e.:

$$\left(\partial_z^2 + k^2\right)v_p(z) = \left(\partial_z^2 + k^2\right)2jcA_{z,p}(z) = 2kE_{z,p}^{inc}(z) \quad (2.47)$$

The antenna elements are assumed to be good conductors. Therefore, the tangential electric field on the surface of a dipole should be zero except at the gap [29], i.e.:

$$E_{z,p}^{inc}(z) + E_{z,p}^{sca}(z) = \begin{cases} E_{z,p}^{gap} & |z - z_{g,p}| < \dfrac{\Delta_{g,p}}{2} \\ 0 & |z - z_{g,p}| > \dfrac{\Delta_{g,p}}{2} \end{cases} \quad (2.48)$$

where $E_{z,p}^{gap}$ is the z component of the electric field developed at the gap of element p and $E_{z,pq}^{sca}(z)$ is the z-component of the scattered electric field by element q on the surface of element p. Furthermore, the delta gap source model assumes that the incident electric field $E_{z,p}^{inc}(z)$ at the gap is constant and equals $v_{s,p}/\Delta_{g,p}$, where $v_{s,p}$ is the excitation voltage at the feed gap of element p [18]. Note that in [19],

$E_{z,p}^{inc}(z)$ is expressed in another way as $E_{z,p}^{inc}(z) = v_{s,p}\delta(z)$, where $\delta(z)$ is the delta function. In [29], the load voltage of a loaded dipole is defined as:

$$E_{z,p}^{gap} = -\frac{v_{L,p}}{\Delta_{g,p}} = \frac{I_{L,p}Z_{L,p}}{\Delta_{g,p}} \tag{2.49}$$

Therefore, the electric field at the gap of a loaded dipole receiving one signal can be written as:

$$E_{z,p}^{gap}(z) = v_{L,p}\delta(z) \tag{2.50}$$

Finally, (2.45) becomes:

$$v_{L,p}\delta(z) = -E_{z,p}^{inc}(z) + E_{z,p}^{sca}(z) - \sum_{\substack{q=1\\q\neq p}}^{N} E_{z,pq}^{sca}(z) \tag{2.51}$$

Substituting (2.24) and (2.42) into the RHS of (2.41) yields:

$$-\frac{1}{I_p}\int_{-l/2}^{l/2} E_{p_z}^{inc}(z)I_{p_z}(z)dz + \frac{I_p}{I_p^2}\int_{-l/2}^{l/2} E_{p_z}^{sca}(z)I_{p_z}(z)dz$$

$$-\sum_{\substack{q=1\\q\neq p}}^{N-1}\int_{-l/2}^{l/2} \frac{I_q}{I_p I_q} E_{pq_z}^{sca}(z)I_{p_z}(z)dz$$

or

$$-\frac{1}{I_p}\int_{-l/2}^{l/2}\left\{ E_{p_z}^{inc}(z) - E_{p_z}^{sca}(z) + \sum_{\substack{q=1\\q\neq p}}^{N-1} E_{pq_z}^{sca}(z)\right\}I_{p_z}(z)dz \tag{2.52}$$

Substituting the term between the brackets in (2.52) by $v_{L,p}\delta(z)$ as in (2.51) yields:

$$\frac{1}{I_p}\int_{-l/2}^{l/2} v_{L,p}\delta(z)I_{p_z}(z)dz = \frac{1}{I_p}v_{L,p}I_p = v_{L,p}$$

Thus, the RHS of (2.41) equals $v_{L,p}$. Note that I_p and I_q are the uncoupled currents of elements p and q respectively at $z = 0$. Thus, validation of (2.41) has been proved for the contribution of the uncoupled currents of the elements into $v_{L,p}$,

i.e., the terminal load voltage developed at the first instant of receiving the incident signal. Once the elements begin to exchange the energy, the element currents become coupled currents i_n, $n = 1, 2, \ldots, N$, which can be inserted into (2.41) instead of the uncoupled currents to include the contribution of them into the load voltage $v_{L,p}$.
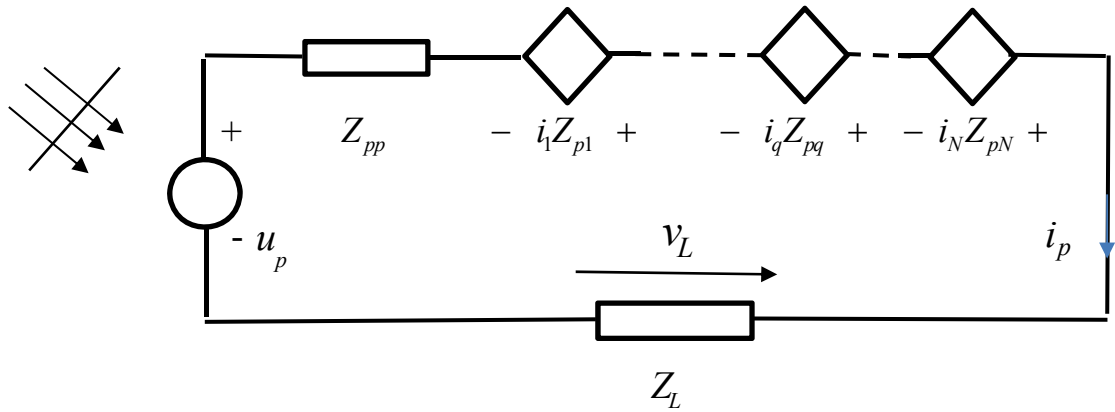
(a) Thévenin's equivalent circuit
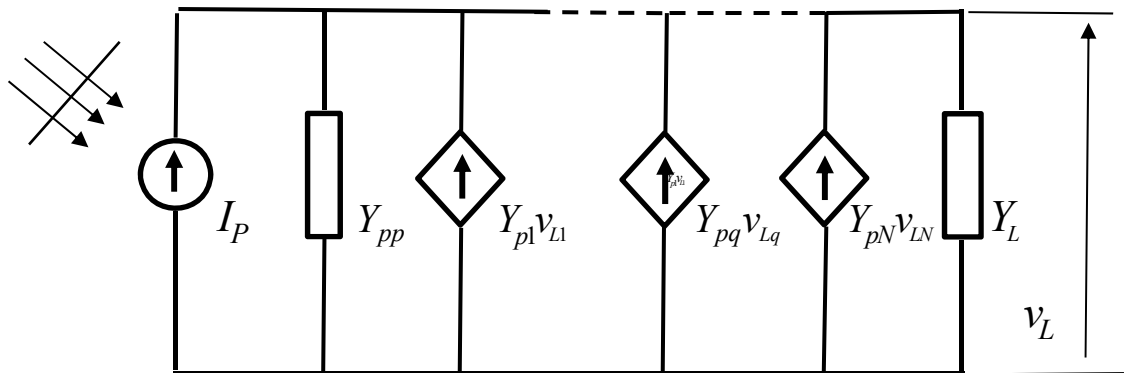
(b) Norton's equivalent circuit

Figure 2.9: Thévenin and Norton equivalent circuits of a dipole in an antenna array.

Similarly, the above analysis can be applied to all the other elements in the array to give the following system of equations that expresses the terminal voltages of an all-active receiving antenna array:

$$v_{L,1} = u_1 - i_1 Z_{11} + i_2 Z_{12} + \cdots + i_q Z_{1q} + \cdots + i_N Z_{1N}$$

$$v_{L,2} = u_2 - i_2 Z_{22} + i_1 Z_{21} + \cdots + i_q Z_{2q} + \cdots + i_N Z_{2N}$$

$$\vdots$$

$$v_{L,N} = u_N - i_N Z_{NN} + i_1 Z_{N1} + \cdots + i_q Z_{Nq} + \cdots + i_{N-1} Z_{NN-1}$$

(2.53)

The uncoupled voltage u_p can be substituted by $u_p = I_p \left(Z_{pp} + Z_{L,p} \right)$, where I_p is the uncoupled current of element p and $Z_{L.p}$ is its load impedance. Also, $v_{L,p}$ can be substituted by $v_{L,p} = i_p Z_{L,p}$. After some rearrangements, the system in (2.53) can be rewritten in matrix-vector form to finally give the CVUC model as:

$$\mathbf{v_L} = \left(\mathbf{D} + \mathbf{S T^{-1}} \right) \mathbf{I}$$

(2.54)

where $\mathbf{v_L} = \begin{bmatrix} v_{L,1} & v_{L,2} & \cdots & v_{L,N} \end{bmatrix}^T$ is the vector of coupled voltages which are measured at the terminals of the array elements and $\mathbf{I} = \begin{bmatrix} I_1 & I_2 & \cdots & I_N \end{bmatrix}^T$ is the vector of uncoupled currents at the terminals of the array elements. The structure of the matrices $\mathbf{D}$, $\mathbf{S}$, and $\mathbf{T}$ are as follows:

$$\mathbf{D} = \begin{bmatrix} Z_{11} + Z_{L,1} & 0 & \cdots & 0 \\ 0 & Z_{22} + Z_{L,2} & \cdots & 0 \\ \vdots & \vdots & \ddots & \vdots \\ 0 & 0 & \cdots & Z_{NN} + Z_{L,N} \end{bmatrix}$$

$$\mathbf{S} = \begin{bmatrix} -Z_{11} & Z_{12} & \cdots & Z_{1N} \\ Z_{21} & -Z_{22} & \cdots & Z_{2N} \\ \vdots & \vdots & \ddots & \vdots \\ Z_{N1} & Z_{N2} & \cdots & -Z_{NN} \end{bmatrix}$$

$$\mathbf{T} = \begin{bmatrix} 1 & \dfrac{-Z_{12}}{Z_{11} + Z_{L,1}} & \cdots & \dfrac{-Z_{1N}}{Z_{11} + Z_{L,1}} \\ \dfrac{-Z_{21}}{Z_{22} + Z_{L,2}} & 1 & \cdots & \dfrac{-Z_{2N}}{Z_{22} + Z_{L,2}} \\ \vdots & \vdots & \ddots & \vdots \\ \dfrac{-Z_{N1}}{Z_{NN} + Z_{L,N}} & \dfrac{-Z_{N2}}{Z_{NN} + Z_{L,N}} & \cdots & 1 \end{bmatrix}$$

Notice that the CVUC model overcomes the singularity case that might arise in OCV and RMIM for short-circuited antenna, i.e. when $Z_{L,p} = 0$. Note also that the CVUC mutual coupling model can be applied to any array geometry such as Uniform Linear Array (ULA) or Uniform Circular Array (UCA).

The entries of matrix $\mathbf{T}$ can be in terms of self and mutual admittances rather than self and mutual impedances. This can be implemented by referring to the Norton equivalent circuit shown in Figure 2.9b from which another version of (2.41) can be written as:

$$i_p = I_p - v_{L,p}Y_{pp} + v_{L,1}Y_{p1} + \cdots + v_{L,q}Y_{pq} + \ldots + v_{L,N}Y_{pN}, \quad p = 1,\ldots,N \qquad (2.55)$$

Replacing $v_{L,q}$, $q = 1,2,\ldots,N$, by their corresponding equivalent terms $i_q/Y_{L,q}$ and following the same procedure used to formulate (2.53) yields another matrix that relates the coupled currents to the uncoupled currents in a receiving antenna array:

$$\begin{bmatrix} I_1 \\ I_2 \\ \vdots \\ I_N \end{bmatrix} = \begin{bmatrix} 1+\dfrac{Y_{11}}{Y_{L,1}} & \dfrac{-Y_{12}}{Y_{L,2}} & \cdots & \dfrac{-Y_{1N}}{Y_{L,N}} \\ \dfrac{-Y_{21}}{Y_{L,1}} & 1+\dfrac{Y_{22}}{Y_{L,2}} & \cdots & \dfrac{-Y_{2N}}{Y_{L,N}} \\ \vdots & \vdots & \ddots & \vdots \\ \dfrac{-Y_{N1}}{Y_{L,1}} & \dfrac{-Y_{N2}}{Y_{22}} & \cdots & 1+\dfrac{Y_{NN}}{Y_{L,N}} \end{bmatrix} \begin{bmatrix} i_1 \\ i_2 \\ \vdots \\ i_N \end{bmatrix} \qquad (2.56)$$

or

$$\mathbf{I} = \mathbf{W}\mathbf{i} \qquad (2.57)$$

and the system (2.55) becomes:

$$\mathbf{v_L} = \left(\mathbf{D} + \mathbf{S}\mathbf{W}^{-1}\right)\mathbf{I} \qquad (2.58)$$

where $\mathbf{W}$ is defined in (2.56). However, when analysing SASPA arrays using Norton equivalent circuit, the load current of any parasitic element in the array should be the current that flows in the self-admittance of each of the parasites because $Y_{L,p} \to \infty$ for parasites. Also, $v_{L,q}$, $q = 1,2,\ldots,N$ with $q \neq p$ and p is the active element, will

be given by $v_{L,q} = i_q/Y_{qq}$, i.e. the coupled current of the corresponding parasitic element divided by the self-admittance and not by the load admittance as in the case of the all-active antenna array shown in (2.55). Thus, for an N-element SASPA array with element #1 active and the other $N-1$ elements parasites, the system in (2.55) will be:

$$i_1 = I_1 - v_{L,1}Y_{11} + v_{L,2}Y_{12} + \cdots + v_{L,q}Y_{1q} + \cdots + v_{L,N}Y_{1N}$$
$$i_2 = I_2 + v_{L,1}Y_{21} + v_{L,3}Y_{23} + \cdots + v_{L,q}Y_{2q} + \cdots + v_{L,N}Y_{2N}$$
$$\vdots$$
$$i_N = I_N + v_{L,1}Y_{N1} + v_{L,2}Y_{N2} + \cdots + v_{L,q}Y_{Nq} + \cdots + v_{L,(N-1)}Y_{N(N-1)}$$

(2.59)

Note that in (2.59) there is no $v_{L,p}Y_{pp}$ term in the equations for the currents i_p, $p = 2,3,\ldots,N$. Replacing $v_{L,1}$ by $i_1/Y_{L,1}$ and $v_{L,p}$, $p = 2,3,\ldots,N$, by i_p/Y_{pp}, after rearranging terms, the system of equations in (2.59) becomes:

$$
\begin{bmatrix} I_1 \\ I_2 \\ . \\ . \\ I_N \end{bmatrix}
=
\begin{bmatrix}
1 + \dfrac{Y_{11}}{Y_{L,1}} & \dfrac{-Y_{12}}{Y_{22}} & \dfrac{-Y_{13}}{Y_{33}} & \cdots & \dfrac{-Y_{1N}}{Y_{NN}} \\
\dfrac{-Y_{21}}{Y_{L,1}} & 1 & \dfrac{-Y_{23}}{Y_{33}} & \cdots & \dfrac{-Y_{2N}}{Y_{NN}} \\
\vdots & \vdots & \vdots & & \vdots \\
\dfrac{-Y_{N1}}{Y_{L,1}} & \dfrac{-Y_{N2}}{Y_{22}} & \dfrac{-Y_{N3}}{Y_{33}} & \cdots & 1
\end{bmatrix}
\begin{bmatrix} i_1 \\ i_2 \\ . \\ . \\ i_N \end{bmatrix}
$$

(2.60)

i.e.

$$\mathbf{I} = \tilde{\mathbf{W}}\mathbf{i}$$

(2.61)

Thus, the coupling matrix $\tilde{\mathbf{W}}$ is based on self and mutual admittances. The formulae for these admittances can be found in [53][54]. In [53], the solution for the current distribution on a dipole is first calculated to find the self-admittance using an integral equation like (2.8) with another kernel function to describe additional boundaries. In calculating the mutual admittance, the authors in [53] used mutual kernel functions between the elements of a ULA to determine the current distributions on these elements. In contrast, in [54] the induced EMF method was used to find the self and

mutual admittances by inserting the magnetic current rather than electric current in the integrand along with the azimuth component of the intensity field.

2.5   Summary

In this Chapter, the concept of mutual coupling between the antenna elements in an antenna array is reviewed from the perspective of antenna theory. This inherent array characteristic is due to the exchange of energy between the antenna elements if they are close together. The presence of mutual coupling is often considered to have an adverse effect on the performance of transmitting and receiving antenna arrays since the response of each element in the array is contaminated by another effect. However, there are antenna arrays such as SASPA arrays that depend closely on the action of mutual coupling for them to work properly.

To start the review on mutual coupling, some of the important aspects of antenna element and antenna array must be first studied. The current distribution, the radiation intensity of a transmitting antenna, and the induced voltage of a receiving antenna are reviewed. The self-impedance of an antenna element and the mutual impedance between two diploe elements are also studied. The formulae given for the self and mutual impedances are based on the induced EMF theory and the concept of reciprocity. These impedances are the main entries of the Mutual Coupling Matrix (MCM) which expresses the mutual coupling effect. The available mutual coupling models in the literature such as OCV, RMIM, and others have been postulated based on different views of the energy exchange between the array elements. However, most of them did not capture all of the physical phenomena associated with mutual coupling, particularly for receiving arrays. In addition, the existing models were derived for all-active arrays where all the antenna elements are either driven (in transmit mode) or loaded (in receive mode). In other words, the existing models cannot be used to develop algorithms for SASPA arrays. As a result, a new model, called Coupled Voltages to Uncoupled Currents (CVUC), is proposed in this chapter.

The derivation of CVUC is based on electromagnetic theory and microwave network theory. The efficacy of this model in SASPA arrays will be shown in the remaining chapters of this thesis.

Chapter 3

SWITCHED ACTIVE SWITCHED PARASITIC ANTENNA (SASPA) ARRAYS

3.1   Introduction

In this chapter, the principle and the effectiveness of using Switched Parasitic Antennas (SPA) in antenna arrays will be explored. The Switched Active Switched Parasitic Antenna (SASPA) as a special case of (SPA) is then analysed.

In general, an SPA array consists of one antenna element which is connected to the RF signal source when the array acts as a transmitter, or to a load when the array is acting as a receiver. This element is called the "active element". The other antenna elements are called "parasitic elements" and their terminations are either short circuited (ON state) or left open circuited (OFF state). In the case of SASPA arrays, one element is active, and the other elements are short circuited parasites. Using PIN diodes, the parasites in SPA arrays can be switched between ON and OFF states. In contrast, in SASPA arrays, the PIN diodes are used to switch one (and only one) element to the active state while keeping the other elements in the parasitic ON state. The role of active element in an SASPA array is then passed to another element after a certain time period, and by rapidly and sequentially switching the elements of the array to the active state and back, the radiation pattern of the SASPA array can be easily and effectively steered to different directions.

A key feature of SPA and SASPA arrays is that they rely on mutual coupling for them to work. This is in contrast to conventional antenna arrays which treat mutual coupling as a nuisance. It will be shown in this chapter that, unlike the mutual coupling models that are available in the literature, the CVUC model proposed in the previous chapter can yield suitable mutual coupling matrices for SASPA arrays. As such, this chapter aims to develop the mathematical basis for the derivation of the

algorithms presented in later chapters that allow SASPA arrays to act as DF arrays.

3.2 Switched Parasitic Antenna (SPA) Arrays

The use of antenna arrays involving passive elements goes back to 1930 when two Japanese scientists, Yagi and Uda, constructed an array of wire antennas arranged in a side by side configuration [55]. This array is called Yagi-Uda after their names and is used for TV signal reception. The array consists of a single half-wave dipole as an active radio receiver connected to the TV set and short-circuited dipole antennas with different lengths acting as parasites. The array is designed so that the induced currents on the parasites together with the current induced on the active element due to the received signal produce a radiation pattern with a narrow directive main lobe in one direction and almost null radiation in other directions. The length of the parasites and the spacing between them have great effects on the resultant radiation pattern since they determine the mutual coupling between the active element and the parasites. However, the Yagi-Uda antenna needs to be steered mechanically to the direction of the required signal to have optimum reception. In other words, the Yagi-Uda array is a Fixed Active Fixed Parasitic Antenna (FAFPA) array.

To electronically steer the radiation pattern, a collection of parasitic antennas can be placed in the vicinity of a single radio receiver and by making use of the mutual coupling between them. Antenna arrays with such a facility are called Switched Parasitic Antenna (SPA) arrays. The parasites in the array can be switched between the "ON" and "OFF" states using PIN diodes which can operate with very short switching times. In the literature of smart antennas, the benefits of SPA arrays in cellular communications have been investigated. In [56], the effectiveness of using SPA arrays to provide a variety of switched beam patterns that are beneficial in mobile communications is studied. It is shown that SPA arrays produce almost orthogonal or uncorrelated patterns. Also, it is shown that the envelope correlation coefficient between the received signals by SPA arrays decreases significantly as the

inter-element spacing decreases. Furthermore, the directivity increases as the number of parasites increases. However, the concept of mutual coupling has not been well investigated in [56].

Antenna diversity by implementing SPA arrays with the active element at the centre of a circular geometry of parasitic elements is studied in [57]. Using only four parasites in the circular geometry with three different terminations, it is possible to have symmetrical radiation patterns directed to the main fundamental directions with a low correlation coefficient. The circular array has been chosen because of symmetry and constant mutual impedance. Also, it is shown in [58] that SPA arrays are beneficial in increasing the capacity of SDMA for packet switching networks in which several simultaneous antenna beams are required. The SPA array as a special class of smart antennas, its potential practical applications, and its advantages in controlling and fabrication antenna arrays over the phased arrays have been discussed in detail in [15]. In addition to being easy in steering its directive radiation pattern, consuming less power, and being comparatively small in size, the SPA array also shows a very low scattering factor S_{11} and almost fixed input impedance [15]. However, 2-D scanning cannot be carried out by the SPA array as in phased arrays [15]. As DF arrays, the capability of SPA for DOA estimation have been discussed in [16] and [17]. "It was found that the SPA array offers high-resolution direction-finding performance using only a single radio receiver" [16].

SPA array example

If two arrays that are like a Yagi-Uda array but sharing the same active element are used [56], see Figure 3.1, the *H*-plane directive radiation pattern can be steered towards two different directions if the termination of the two sets of parasitic elements are changed [15][56]. In this geometry, dipoles #2 and #4 are shorter in length than the active element #1 while dipoles #3 and #5 are longer than the active element #1, and the spacing is not optimized. If the terminals of dipole #2 and dipole

#3 are short circuited, i.e., switching them to the parasitic mode, while leaving the terminals of dipole #4 and dipole #5 open circuited, i.e., effectively disconnected from the array, the *H*-plane radiation pattern will be 130° spatially apart from the *H*-plane radiation pattern of the same geometry if dipoles #4 and #5 are now switched to the parasitic mode , i.e., ON state, and dipoles #2 and #3 are open circuited, i.e., OFF state. Switching a parasite between the ON and OFF state can be implemented by a PIN diode which operates at very fast speed, see Figure 3.2a. Figure 3.3b shows how a dipole can be changed between the parasitic and active states by using a PIN diode. This type of SPA arrays in which one element is fixed to the active state while the parasites are changed between ON and OFF states is called a Fixed Active Switched Parasitic Antenna (FASPA) array. Another type of array, called Switched Active Switched Parasitic Antenna (SASPA) array, is the main topic of this research and will be explained in Section 3.4. These two types of SPA arrays were first proposed by Thiel and Smith, see [15].

3.3   PIN Diodes as RF Switches

PIN diodes are used in SPA and SASPA arrays for the purpose of changing each element of the arrays to the "ON" or "OFF" state for the parasites in SPA arrays, or between "active" and "parasitic" in SASPA arrays. The switching speed of PIN diodes is very high making them very useful as RF switches [59-61]. The ohmic resistance of typical PIN diodes, which are current controlled, varies between 1Ω (forward biasing) to $10K\Omega$ (reverse biasing) making them advantageous in networks operating at UHF and microwave frequencies [59]. PIN diodes are distinctive from other electronic switches with the uniquely characteristic of requiring small DC levels to control large RF signals [61]. In Figure 3.2, typical circuit diagrams of PIN diodes for switching action in SPA and SASPA arrays are illustrated. Figure 3.2a shows the circuit diagram for a Single Pole Single Throw (SPST) switch. This circuit can be used to switch the parasitic element in an SPA array between ON and OFF

states by connecting the element terminals to RF_{IN} and RF_{OUT} terminals respectively. Forward biasing the PIN diode switches the element to ON state. While the OFF state is obtained when reverse biasing the PIN diode.
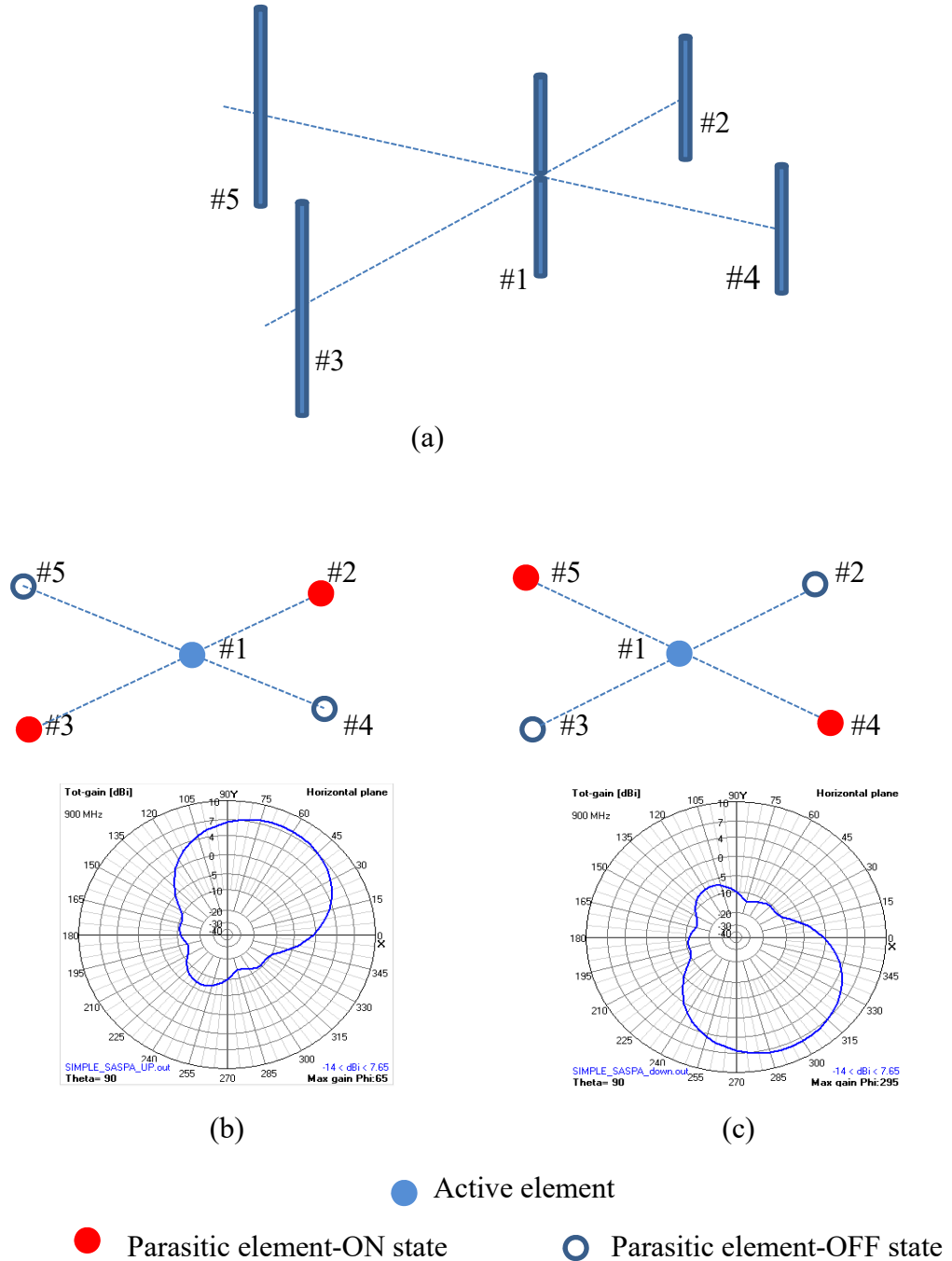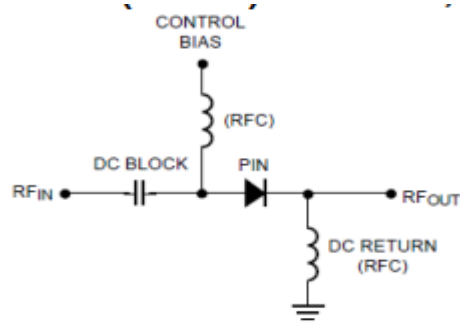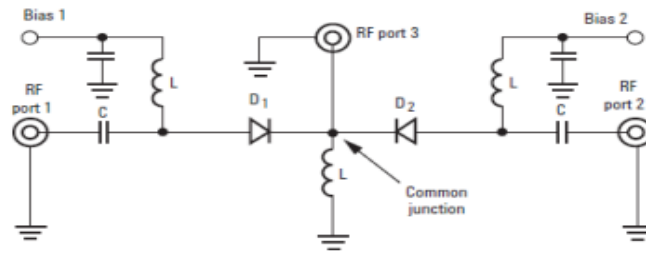

(a)

(b)

(c)

● Active element

● Parasitic element-ON state   ○ Parasitic element-OFF state

Figure 3.1[5]: A simple SPA array acting in transmit mode. (a) The geometry; (b) and (c) Radiation patterns.

[5] The software 4NEC2 is used for plotting figures 3.1(b) and (c). The official web site for 4NEC2 is:
https://www.qsl.net/4nec2/

(a)

(b)

Figure 3.2: Circuit diagrams of RF switches using PIN diode. (a) SPST; (b) SPDT.

In case of SASPA array, the circuit in Figure 3.2a is connected across the load of the corresponding element. When the PIN diode is reverse biased, the element is in the active state. When the PIN diode is forward biased, the element is switched to the parasitic state. In Figure 3.2b, the Single Pole Double Throw (SPDT) switch is shown. The antenna terminals can be connected to RF port 1 and RF port 2 and the load connected between RF port 3 and RF port 2. When D1 and D2 are forward biased, the antenna is in the parasitic state. When D1 is forward biased and D2 is reverse biased, the antenna is in the active state.

3.4   Switched Active Switched Parasitic Antenna (SASPA) Arrays

A special case of SPA arrays is the Switched Active Switched Parasitic Antenna (SASPA) array in which each element can be switched to active state, i.e., at a

certain time only one element is active while the rest of the elements are parasitic. And at a later time, another element which was parasitic is switched to the active state and the previously active element is switched back to the parasitic state. To the knowledge of the author, no previous work in the literature has been reported on the use of SASPA arrays as DF arrays except for [62]. In [62], a digital word consisting of a multiple of ones and zeros controls the terminations of the antenna elements in an array. The ones in the digital word activate the corresponding elements while the zeros parasitize the other elements. Different digital words are chosen so that the azimuth is scanned by the corresponding directive radiation patterns generated by a UCA geometry. This facility is used to estimate the DOA of two signals by measuring the received powers of the signals for all of the chosen digital words in conjunction with the Genetic Algorithm. A drawback of the method is that there should be prior knowledge of the DOAs so that the selected digital words will result in optimum directive radiation patterns.

A simple geometry of an SASPA array consisting of two half-wave dipoles one of which is active and the other is parasitic is shown in Figure 3.3a [15]. The active element is designated as "C" while the parasitic as "P", and they are aligned in a side by side configuration with an inter-element spacing of $d = \lambda/8$. Here, by the active element it is meant that element is driven by a RF voltage or current signal source and hence, the array is in transmit mode. If the array is in receive mode, the active element will be connected to a load. In both modes, the terminal of the parasitic element is short circuited.

Suppose the array is operating in the transmit mode. Because of mutual coupling, a current will be induced on P due to the energizing element C. If the spacing between the two elements is small, the current i_P will be almost equal to but out of phase to i_C, i.e. $i_P \approx -i_C$ [15]. This means that part of the radiation pattern to the left of the array will be reflected by the parasite back to the opposite side, i.e., to the right side of the array, and contributes to producing a directive radiation pattern in

the *H*-plane, as shown in Figure 3.3b. If the situation is reversed, i.e., element *C* becomes parasitic and element *P* becomes active, the *H*-plane radiation pattern is now directed to the left side as shown in Figure 3.3d. Figure 3.4 depicts the effect of the spacing between the elements on the directivity of the array in the *H*-plane. As can be seen, the smaller is the spacing between the array elements the more directivity is produced.
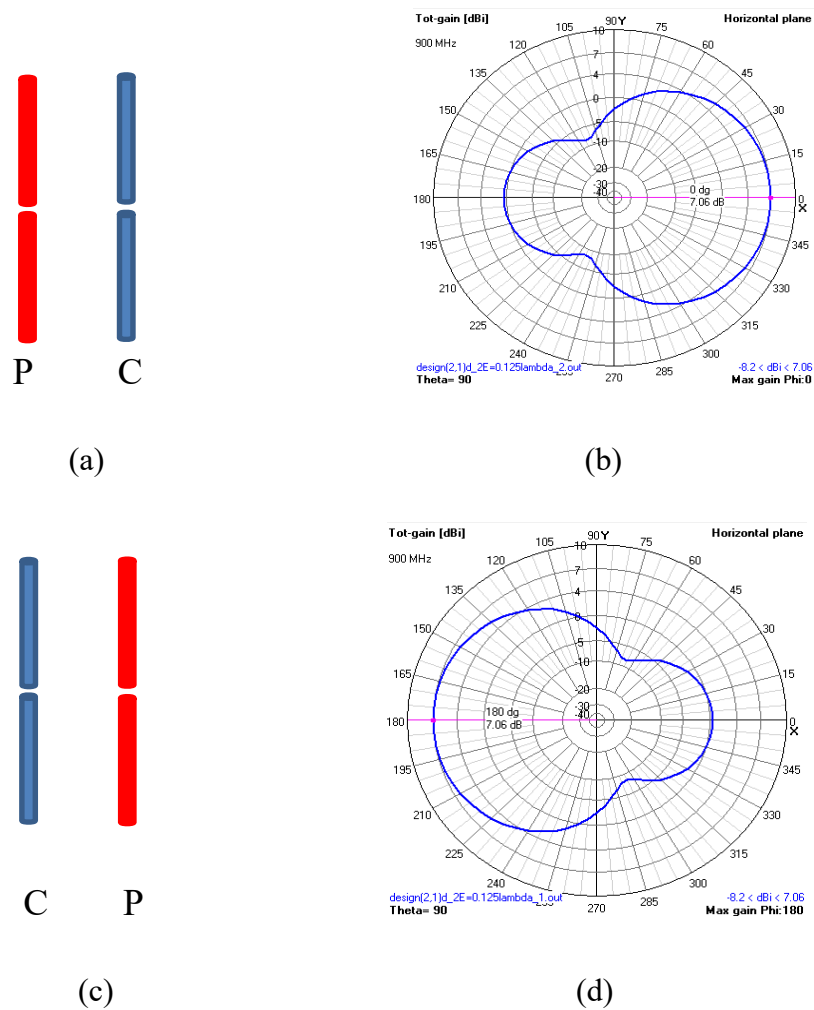

(a)

(b)

(c)

(d)

Figure 3.3[6]: Illustration of the effect of interchanging active and parasitic states between two dipoles of a transmitting SASPA array on the direction of the overall radiation pattern of the array.

---

[6] The software 4NEC2 is used for plotting figures 3.3(b) and (d). The official web site for 4NEC2 is:
https://www.qsl.net/4nec2/
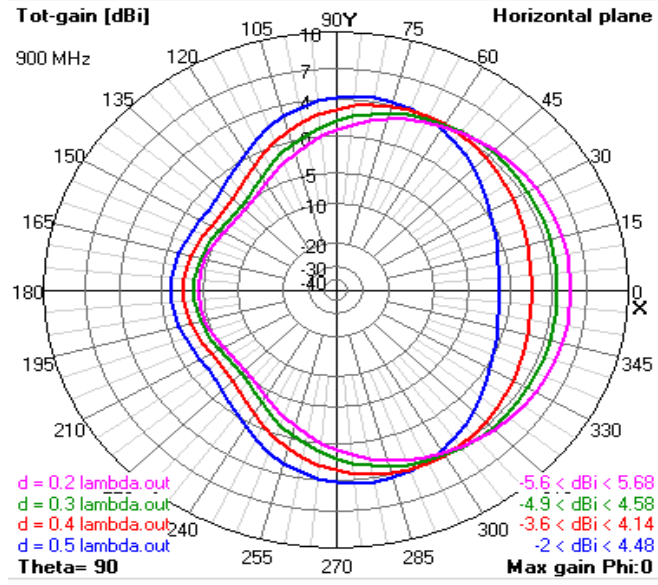
Figure 3.4[7]: The effect of the spacing d on the directivity of the radiation pattern produced by the SASPA array shown in Figure 3.3a.

— $d = 0.2\lambda$ — $d = 0.3\lambda$ — $d = 0.4\lambda$ — $d = 0.5\lambda$

3.5 Far Field Radiation Pattern and Mutual Coupling of SASPA Arrays in Transmit Mode

3.5.1 Far Field Radiation Pattern

For the simple ULA-SASPA array consisting of two dipoles shown in Figure 3.3a, Thiel and Smith [15] have calculated the total H-plane far-electric field when one of the elements is active and the other one is parasitic with the active element as a reference element, i.e., positioned at the origin:

$$E_{tot1}(r,\theta,\phi) = \frac{j\omega\mu}{2\pi kr} \left[\frac{\cos\left(\frac{\pi}{2}\cos\theta\right)}{\sin\theta} \right] \left(i_P e^{-jkd\cos\phi} + i_C \right) \tag{3.1}$$

where (r,θ,ϕ) is the spherical coordinates of the observation point, d is the spacing between the elements, and i_C, i_P are the active and parasitic currents respectively. Thus, E_{tot} of the array in the H-plane will be determined mainly by the amplitude

---

[7] The software 4NEC2 is used for plotting Figure 3.4. The official web site for 4NEC2 is: https://www.qsl.net/4nec2/

and phase of the elements' current and the spacing between them as shown in Figure 3.3b. Equation (3.1) can be rewritten in vector form as:

$$E_{tot1}(r,\theta,\phi) = \alpha(\theta)[i_P \quad i_C]\left[e^{-jkd\cos\phi} \quad 1\right]^T \tag{3.2}$$

where $\alpha(\theta) = \left(\left(\frac{\pi}{2}\right)\cos\theta / \sin\theta\right)$ and $[\cdot]^T$ is the transpose of a vector.

If the element C is switched to the parasitic state and the element P to active, E_{tot1} now becomes:

$$E_{tot2}(r,\theta,\phi) = \frac{j\omega\mu}{2\pi kr}\left[\frac{\cos\left(\frac{\pi}{2}\cos\theta\right)}{\sin\theta}\right]\left(i_C\, e^{-jkd\cos\phi} + i_P\right)$$
$$= \alpha(\theta)[i_C \quad i_P]\left[e^{-jkd\cos\phi} \quad 1\right]^T \tag{3.3}$$

and the *H*-plane radiation pattern is now rotated through 180°, see Figure 3.3d. Note that the phase of the parasitic current in (3.3) is positive with respect to the phase of the current in the active element, i.e. it is out of phase with respect to the current of the parasitic element in (3.1) due to the swapping of the active and parasitic states between the elements (see Appendix A). Equations (3.2) and (3.3) can be generalized for an *N*-element ULA-SASPA array as follows, with the active element the reference element:

$$E_{tot}^{(n)}(r,\theta,\phi) = \alpha(\theta)\left(i_C^{(n)} + \sum_{\substack{q=1 \\ q\neq n}}^{N} i_{P_q}^{(n)}e^{+j(q-n)kd\cos\phi}\right)$$
$$= \alpha(\theta)\left[i_{P_1}^{(n)} \quad \cdots \quad i_C^{(n)} \quad \cdots \quad i_{P_N}^{(n)}\right]\cdot$$
$$\left[e^{j(1-n)kd\cos\phi} \quad \cdots \quad 1 \quad \cdots \quad e^{j(N-n)kd\cos\phi}\right]^T$$
$$= \alpha(\theta)\left(\mathbf{i}^{(n)}\right)^T \mathbf{a}^{(n)}(\phi) \tag{3.4}$$

where $\mathbf{i}^{(n)}$ is the vector of the coupled currents of the array and $\mathbf{a}^{(n)}(\theta)$ is the array factor or the steering vector. The index n refers to the position of the active element. Due to the presence the array factor $\mathbf{a}^{(n)}(\theta)$ which is produced when the elements of the SASPA array are successively switched between active and parasitic states, the SASPA array could be considered as a self-beamforming array.

SASPA array example

Figure 3.5 depicts the radiation fields produced by a four-element ULA-SASPA array when each element is successively switched to active starting from element #1 and assuming this element is positioned at the origin. The inter-element spacing is $d = \lambda/8$. When element #1 is active and the rest of the elements are parasites, the *H*-plane radiation pattern will have a single main lobe directed to the left with $\phi_{\max} = 180°$, see Figure 3.5a. When element #2 is switched to active and the previous active element (element #1) switched to parasitic, a new shape of the radiation pattern will be produced because of the array factor is now different from the one in (3.4) which will be:

$$\mathbf{a}^{(2)}(\phi) = \begin{bmatrix} e^{-jkd\cos\phi} & 1 & e^{+jkd\cos\phi} & \cdots & e^{+j(N-2)kd\cos\phi} \end{bmatrix}^{T} \tag{3.5}$$

and the current vector becomes:

$$\mathbf{i}^{(2)} = \begin{bmatrix} i_{P_1}^{(2)} & i_C^{(2)} & i_{P_3}^{(2)} & \cdots & i_{P_N}^{(2)} \end{bmatrix}^{T} \tag{3.6}$$

Notice the symmetry that occurs between the radiation patterns produced by the active elements #1 and #4 and between elements #2 and #3. As a comparison between Figure 3.5b and Figure 3.3d, the maximum gain for the two-element ULA-SASPA array is 7.06 dB at $\phi_{\max} = 180°$, the Front-to-Back ratio (F/B) is 7 dB, and the 3 dB beamwidth HPBW is 120° while the corresponding values for the four-element ULA-SASPA array are 10.83 dB, 6 dB, and 60° respectively. Notice that the radiation patterns produced by active elements #1 and #2 in Figure 3.5 are asymmetrical and have different F/B ratios. However, the radiation patterns produced by active elements #1 and #4 are symmetrical. This demonstrates the asymmetrical and centro-symmetric properties of ULA arrays. In addition, the second and the third radiation patterns in Figure 3.5 have additional large lobes in contrast with the first and last ones in which a unique $|\phi_{\max}|$ is defined. This unwanted phenomenon may cause the array to be ambiguous in DOA estimation.
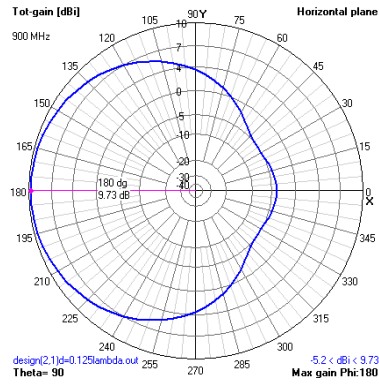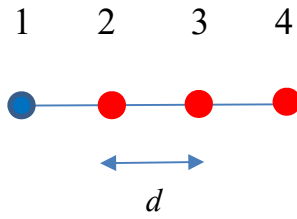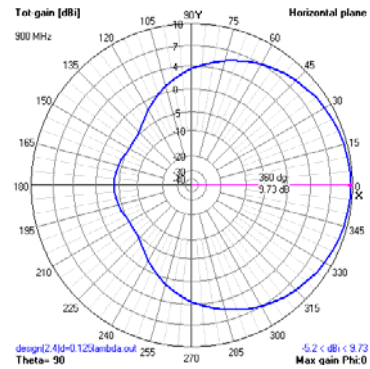
(a)
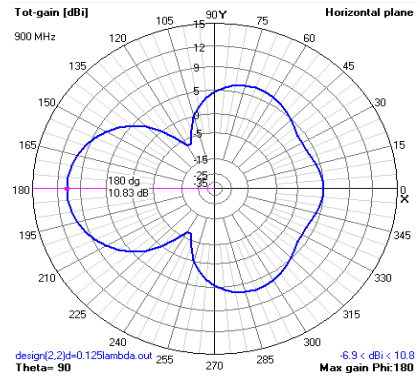
(b)
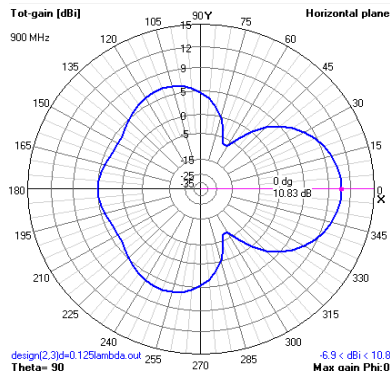
(c) $d = \lambda/8$ (d)

● Active element   ● Parasitic element

Figure 3.5[8]: A four-element ULA-SASPA array acting in transmit mode.

---

[8] The software 4NEC2 is used for plotting the radiation patterns in Figure 3.5. The official web site for 4NEC2 is:
https://www.qsl.net/4nec2/

$$R = \lambda/8$$
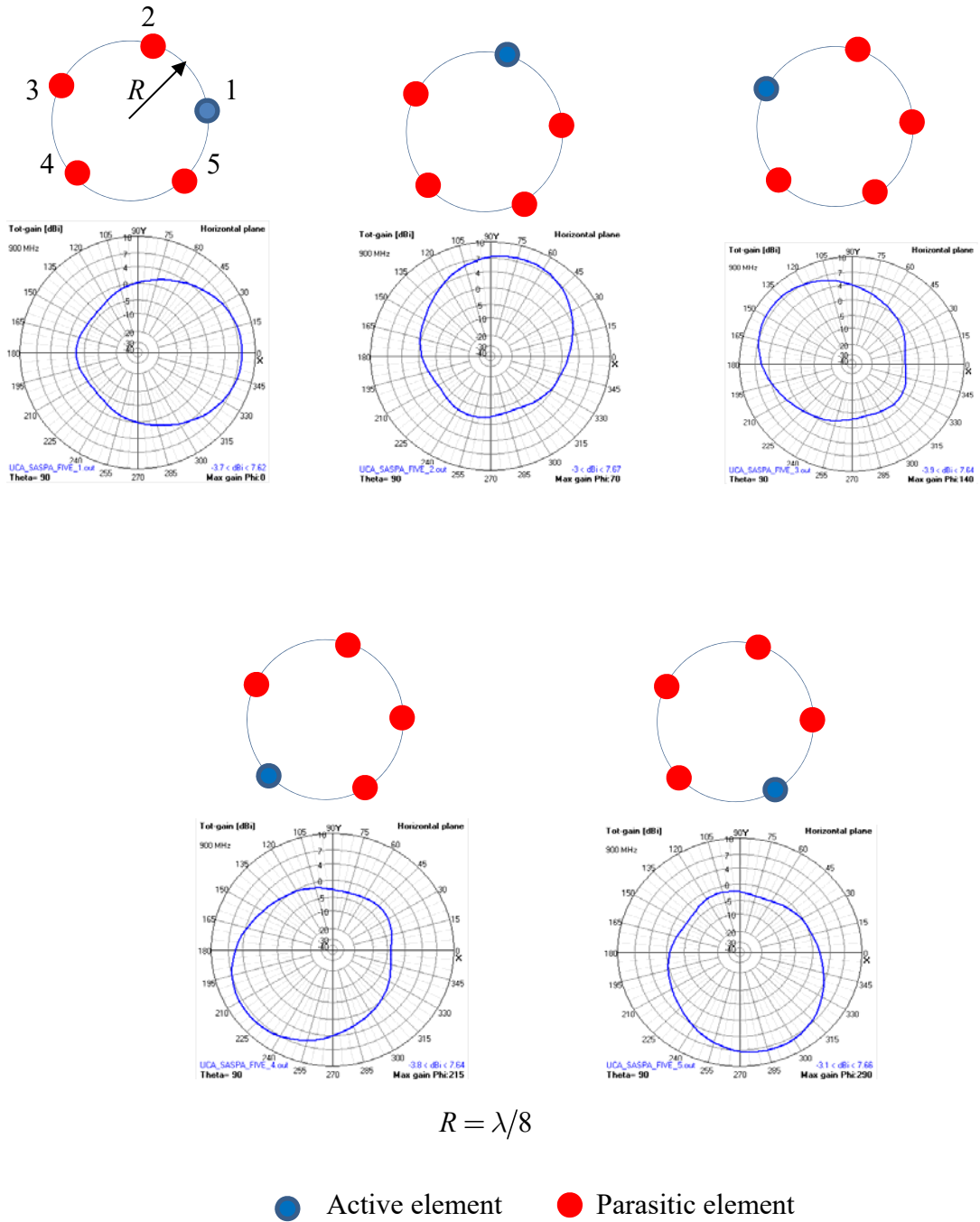
● Active element   ● Parasitic element

Figure 3.6[9]: A five-element UCA-SASPA array acting in transmit mode.

To produce symmetrical radiation patterns with the same gain, F/B and 3 dB BW, the UCA-SASPA array can meet such requirements. Figure 3.6 shows a five-element

---

[9] The software 4NEC2 is used for plotting the radiation patterns in Figure 3.6. The official web site for 4NEC2 is: https://www.qsl.net/4nec2/

UCA-SASPA array with the elements equally placed on the perimeter of a circle with radius $R = \lambda/8$. Each one of the five radiation patterns formed by this geometry has maximum gain of 7.65 dB, F/B ratio of 10.4 dB, and 3 dB BW of 95°. Successively switching each element to active while keeping the rest of the elements parasitic sweeps $\phi_{\max}$ over the entire azimuth plane with each $\phi_{\max}$ at the angular position of the element n [62]:

$$\phi_{\max} = \frac{n-1}{N} 2\pi, \quad n = 1, 2, \dots, N \tag{3.7}$$

Thus, the array factor $\mathbf{a}^{(n)}(\theta)$ in (3.4) for a UCA-SASPA array takes the form [63, pp. 15-16]:

$$\mathbf{a}^{(1)}(\phi) = e^{-jkR\cos\phi} \left[e^{jkR\cos\phi} \quad e^{jkR\cos\left(\phi - 2\pi\frac{1}{N}\right)} \quad \dots \quad e^{jkR\cos\left(\phi - 2\pi\frac{N-1}{N}\right)} \right]^T \tag{3.8}$$

$$\mathbf{a}^{(2)}(\phi) = e^{-jkR\cos\left(\phi - \frac{2\pi}{N}\right)} \left[e^{jkR\cos\phi} \quad e^{jkR\cos\left(\phi - 2\pi\frac{1}{N}\right)} \quad \dots \quad e^{jkR\cos\left(\phi - 2\pi\frac{N-1}{N}\right)} \right]^T \tag{3.9}$$

3.5.2 Mutual Coupling in Transmit SASPA Array

Mutual impedance plays an important role in determining the resultant radiation pattern of an SPA array which in turn depends mainly on the current of each element in the array. The amplitude and phase of the current i_C induced in the active element of a transmitting SASPA array entails two components: the first one is the uncoupled component I_C that is due to energizing the active element by a RF voltage or current source, and the other component is mutually coupled from the short circuit currents of the parasites which are induced by the active element. Thus, $E_{tot}^{(n)}(r,\theta,\phi)$ in (3.1) and (3.2) can be defined in terms of the uncoupled currents rather than the coupled currents. To do so, the Thévenin equivalent circuit in Figure 2.5 for an array can be used, provided the effect of mutual coupling is included, see Figure 3.7.
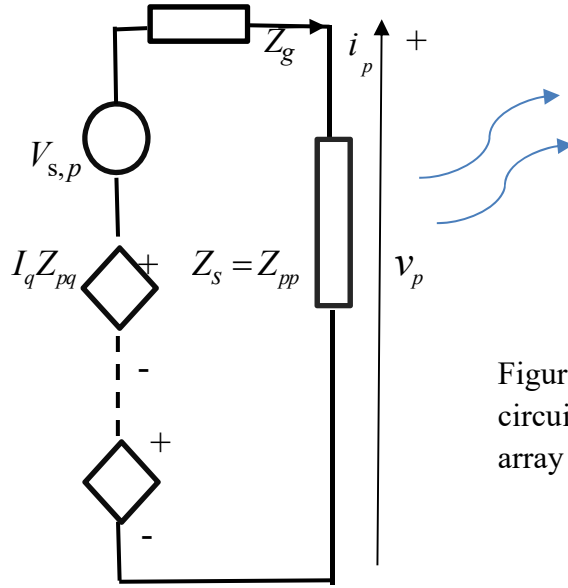
Figure 3.7: Thévenin equivalent circuit for a dipole in an antenna array acting in transmit mode.

Using the superposition theorem for an N-element ULA array and assuming that each element is supplied by an RF voltage source V_s with identical internal impedance Z_g, the model expressing the voltage across the self-impedance of each antenna element including the effect of mutual coupling is:

$$v_1 = i_1 Z_{11} = I_1 Z_{11} + I_1 Z_{12} \frac{Z_{11}}{Z_{11} + Z_g} + \cdots + I_N Z_{1N} \frac{Z_{11}}{Z_{11} + Z_g}$$

$$v_2 = i_2 Z_{22} = I_1 Z_{21} \frac{Z_{22}}{Z_{22} + Z_g} + I_2 Z_{22} + \cdots + I_N Z_{2N} \frac{Z_{22}}{Z_{22} + Z_g} \qquad (3.10)$$

$$\vdots$$

$$v_N = i_N Z_{NN} = I_1 Z_{N1} \frac{Z_{NN}}{Z_{NN} + Z_g} + I_1 Z_{N2} \frac{Z_{NN}}{Z_{NN} + Z_g} + \cdots + I_N Z_{NN}$$

Each $V_{s,p}$ drives the uncoupled current I_p into the self-impedance Z_{pp} of the corresponding element which in turn radiates the near and far fields as if the element is acting alone. The mutual coupling effect of the neighbour elements on the element p is represented by the dependent voltage sources $I_q Z_{pq}$, $q = 1, 2, \ldots, N$, $q \neq p$ which are summed up with $V_{s,p}$ to produce the coupled current $i_p = v_p / Z_{pp}$. In the case of an SASPA array with element #1 active, (3.10) becomes:

$$v_1 = i_1 Z_{11} = I_1 Z_{11} + I_{sc,2} \frac{Z_{12} Z_{11}}{Z_{11} + Z_g} + \cdots + I_{sc,N} \frac{Z_{1N} Z_{11}}{Z_{11} + Z_g}$$

$$v_2 = i_{sc,2} Z_{22} = I_1 \frac{Z_{21} Z_{22}}{Z_{22} + Z_g} + 0 + \cdots + I_{sc,N} \frac{Z_{2N} Z_{22}}{Z_{22} + Z_g} \qquad (3.11)$$

$$\vdots$$

$$v_N = i_{sc,N} Z_{NN} = I_1 \frac{Z_{N1} Z_{NN}}{Z_{NN} + Z_g} + I_{sc,2} \frac{Z_{N2} Z_{NN}}{Z_{NN} + Z_g} + \cdots + 0$$

where $I_{sc,p}$, $p = 2,3,\ldots,N$ are the currents induced on the parasites due to the uncoupled current I_1, and $i_{sc,p}$ is the coupled current on parasitic element p due to I_1 and $I_{sc,p}$. Note $I_p = 0$ because the parasitic elements are not energized by an external voltage or current source.

The system of equations (3.11) can be rewritten as:

$$i_1 = I_1 + I_{sc,2} \frac{Z_{12}}{Z_{11} + Z_g} + \cdots + I_{sc,N} \frac{Z_{1N}}{Z_{11} + Z_g}$$

$$i_{sc,2} = I_1 \frac{Z_{21}}{Z_{22} + Z_g} + 0 + \cdots + I_{sc,N} \frac{Z_{2N}}{Z_{22} + Z_g} \qquad (3.12)$$

$$\vdots$$

$$i_{sc,N} = I_1 \frac{Z_{N1}}{Z_{NN} + Z_g} + I_{sc,2} \frac{Z_{N2}}{Z_{NN} + Z_g} + \cdots + 0$$

which can be expressed in matrix-vector form as:

$$\begin{bmatrix} i_1 \\ i_{sc,2} \\ \vdots \\ i_{sc,N} \end{bmatrix} = \begin{bmatrix} 1 & \dfrac{Z_{12}}{Z_{11} + Z_g} & \dfrac{Z_{12}}{Z_{11} + Z_g} & \cdots & \dfrac{Z_{1N}}{Z_{11} + Z_g} \\ \dfrac{Z_{21}}{Z_{22} + Z_g} & 0 & \dfrac{Z_{23}}{Z_{22} + Z_g} & \cdots & \dfrac{Z_{2N}}{Z_{22} + Z_g} \\ \vdots & \vdots & \vdots & \vdots & \vdots \\ \dfrac{Z_{N1}}{Z_{NN} + Z_g} & \dfrac{Z_{N2}}{Z_{NN} + Z_g} & \dfrac{Z_{N3}}{Z_{NN} + Z_g} & \cdots & 0 \end{bmatrix} \begin{bmatrix} I_1 \\ I_{sc,2} \\ \vdots \\ I_{sc,N} \end{bmatrix} \qquad (3.13)$$

or

$$\mathbf{i}^{(1)} = \mathbf{B}^{(1)} \mathbf{I}^{(1)} \qquad (3.14)$$

The superscripts in (3.14) refer to the active element. Plugging (3.14) into (3.4), the electric far field of an SASPA array when element #1 is active becomes:

$$E_{tot}^{(1)} = \alpha(\theta) \mathbf{I}^{(1)^T} \mathbf{B}^{(1)^T} \mathbf{a}^{(1)}(\theta) \qquad (3.15)$$

The above analysis can be applied to SASPA arrays of both types, ULA and UCA.

3.6 Induced Voltages and Mutual Coupling of SASPA Arrays in Receive Mode

In the previous section, it was shown that the total radiation pattern emanating from a transmitting SASPA array is the result of the uncoupled currents induced on the elements, the array factor, and the mutual coupling between the elements. According to the reciprocity theorem, the same factors which determine the total radiation pattern of an antenna array when transmitting also determine the response of the antenna array when receiving signals. Thus, the previous section paved the way to study the response of an SASPA array to the received signals. However, the mutual coupling in receiving SASPA arrays is different from that in transmitting SASPA arrays since the mechanisms of coupled currents in transmit and receive modes are different [18]. Specifically, in a transmitting SASPA array, <u>only one</u> element is energised by the RF source, while in a receiving SASPA array, <u>all</u> elements are energised by the incident signal. Accordingly, some of the characteristics particular to a receiving SASPA arrays should also be considered since a comprehensive knowledge about these parameters will provide a basis for performing direction-finding using SASPA arrays. The important parameters to be studied in this section are the induced voltages and the receiving mutual coupling models.

3.6.1 Induced Voltages in Receiving SASPA Arrays

In Section 2.2.1.2, the voltage induced at the terminal of an unloaded half-wave dipole that is intercepting an electric field has been derived by solving Hallen's equation (2.10) by considering certain boundaries or by means of the induced EMF method (2.9) which is repeated below for ready reference:

$$V_{ind} = \frac{\lambda E_o}{\pi \sin\left(\frac{kl}{2}\right)} \left| \frac{\cos\left(\frac{kl}{2}\cos\theta\right) - \cos\left(\frac{kl}{2}\right)}{\sin\theta} \right| = \beta(\theta)E_o \quad (3.16)$$

where

$$\beta(\theta) = \frac{\lambda}{\pi \sin\left(\frac{kl}{2}\right)} \left| \frac{\cos\left(\frac{kl}{2}\cos\theta\right) - \cos\left(\frac{kl}{2}\right)}{\sin\theta} \right|$$

In (3.16), E_o is a complex value representing the strength of the electric field of a received signal. In DOA estimation, this value is represented by the notation $s(t)$. For a collection of identical half-wave dipoles arranged in an arbitrary 3-D geometry and receiving a signal, see Figure 3.8, the same induced voltage in (3.16) will be developed at the terminal of each dipole. However, due to the spatial position of each element which is referred to a reference point, usually the origin, each V_{ind_n} would experience a spatial phase shift equal to $e^{-j(-\vec{\mathbf{k}})\cdot\vec{\mathbf{r}}_n} = e^{j\vec{\mathbf{k}}\cdot\vec{\mathbf{r}}_n}$ relative to the origin. In general, each element response V_{ind_n} experiences a phase shift accompanied with a gain. However, the gain of a half-wave dipole equals 1. The vector $\vec{\mathbf{r}}_n$ is the distance vector between element n and the origin of the Cartesian coordinate system [8]:

$$\vec{\mathbf{r}}_n = \begin{bmatrix} d_{x_n} & d_{y_n} & d_{z_n} \end{bmatrix}^T \quad (3.17)$$

and $\vec{\mathbf{k}}$ is a vector containing the spatial wave number of the received signal:

$$\vec{\mathbf{k}} = k\begin{bmatrix} \sin\theta\cos\phi & \sin\theta\sin\phi & \cos\theta \end{bmatrix}^T, \qquad k = 2\pi/\lambda \quad (3.18)$$

The spatial phase shift is due to the delay in time the signal experiences when travelling across the array [8][64]. Thus, the induced voltages at the open-circuited terminals of the elements in an antenna array can be written as the vector:

$$\begin{aligned} \mathbf{v}_{ind} &= \beta(\theta)s(t)\begin{bmatrix} e^{j\vec{\mathbf{k}}\cdot\vec{\mathbf{r}}_1} & e^{j\vec{\mathbf{k}}\cdot\vec{\mathbf{r}}_2} & \cdots & e^{j\vec{\mathbf{k}}\cdot\vec{\mathbf{r}}_N} \end{bmatrix}^T \\ &= \beta(\theta)s(t)\begin{bmatrix} e^{j\vec{\mathbf{k}}^T\vec{\mathbf{r}}_1} & e^{j\vec{\mathbf{k}}^T\vec{\mathbf{r}}_2} & \cdots & e^{j\vec{\mathbf{k}}^T\vec{\mathbf{r}}_N} \end{bmatrix} \end{aligned} \quad (3.19)$$
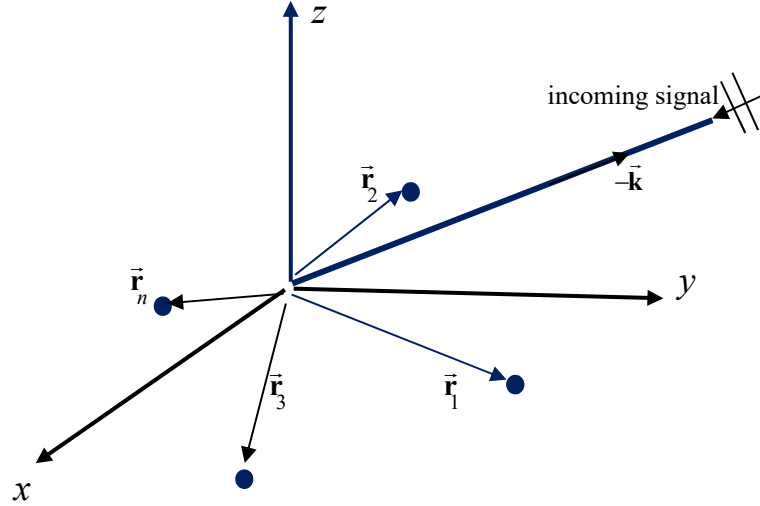
Figure 3.8: An arbitrary 3-D geometry of identical antennas receiving a signal.

If the antenna geometry is a ULA with the elements distributed uniformly with a spacing d on one axis, say the x-axis, see Figure 3.9a, the term $\vec{\mathbf{k}}^T \vec{\mathbf{r}}_n$ for a signal in the x-y plane will be:

$$\vec{\mathbf{k}}^T \vec{\mathbf{r}}_n = k\begin{bmatrix} (n-1)d_x & 0 & 0 \end{bmatrix}\begin{bmatrix} \cos\phi \\ \sin\phi \\ 0 \end{bmatrix}$$

$$= (n-1)kd\cos\phi \tag{3.20}$$

The vector $\vec{\mathbf{k}}$ will have azimuth dependence only because $\theta = \pi/2$. If element #1 is positioned at the origin, then the measurement in (3.19) becomes:

$$\mathbf{v}_{ind} = \kappa s(t)\begin{bmatrix} 1 & e^{jkd\cos\phi} & e^{j2kd\cos\phi} & \cdots & e^{j(N-1)kd\cos\phi} \end{bmatrix}^T$$

$$= \kappa \mathbf{a}_{ULA}(\phi)s(t) \tag{3.21}$$

where

$$\kappa = \beta(\theta) = \text{constant}$$

Similarly, for a UCA with radius R and element #1 located at $(x,y,z) = (R,0,0)$, (3.20) and (3.21) become, respectively:

$$\vec{\mathbf{k}}^T \vec{\mathbf{r}}_n = k \left[R \cos\left(2\pi \frac{n-1}{N}\right) \quad R \sin\left(2\pi \frac{n-1}{N}\right) \quad 0 \right] \left[\cos\phi \quad \sin\phi \quad 0 \right]^T$$

$$= kR \left\{ \cos\phi \cos\left(2\pi \frac{n-1}{N}\right) + \sin\phi \sin\left(2\pi \frac{n-1}{N}\right) \right\} \tag{3.22}$$

$$= kR \cos\left(\phi - 2\pi \frac{n-1}{N}\right)$$

$$\mathbf{v}_{ind} = \kappa s(t) \left[e^{jkR\cos\phi} \quad e^{jkR\cos\left(\phi - 2\pi\frac{1}{N}\right)} \quad \cdots \quad e^{jkR\cos\left(\phi - 2\pi\frac{N-1}{N}\right)} \right]^T \tag{3.23}$$

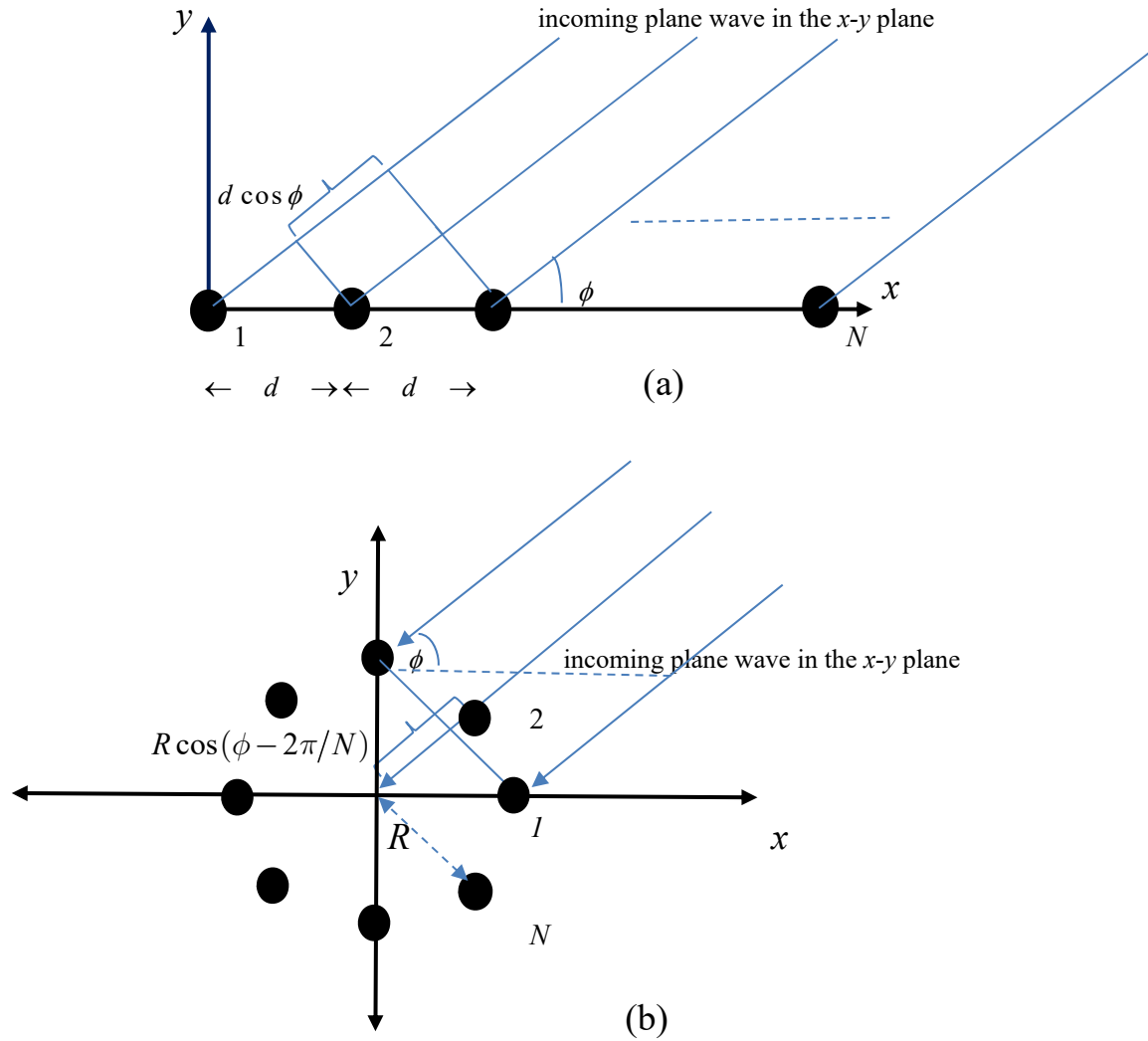$$= \kappa \mathbf{a}_{UCA}(\phi) s(t)$$

Figure 3.9: Antenna array receiving a signal in the *x-y* plane (a) ULA; (b) UCA.

Note that the phase of each element in the UCA geometry of Figure 3.9b has been referred to the origin where no element exists. Each vector of the induced voltages in (3.21) and in (3.23) is related to the vector of load voltages in an all-active receiving antenna array as in (2.38). In the case of SASPA arrays, the variable $s(t)$ represents the response to the uncoupled current on the elements of the array. This is because the load voltage at the terminal of the active element is determined by the induced current on that element and by the short circuit currents induced on the parasites which are then mutually coupled to the active element. In [19, Chapter 24] the induced current on a short-circuited dipole antenna is related to E_o or to $s(t)$. Thus, after pre-multiplying (3.21) or (3.23) by the CVUC model of (2.54) and inserting the Beam Space (BS) term (which will be explained in detail in Chapter 5), the final expression for the load voltage at the terminal of the active element can be obtained.

3.6.2 Mutual Coupling in Receiving SASPA Arrays

In the previous chapter, the CVUC model was formulated to give the coupling matrix of a receiving antenna array. In this section, it will be shown that CVUC matches the operation of an SASPA array. This can be shown when the resultant vector of load voltages is the zero vector except for one non-zero entry which corresponds to the active element. This occurs when substituting $Z_{L,p} = 0$ into the entries of the CVUC model where p corresponds to a parasitic element. For simplicity, let an SASPA array consists of two elements with one of them active (element #1) and the other parasitic (element #2). The vector of the load voltages for this array will be a vector of one non-zero entry which corresponds to the active element and a zero-voltage corresponding to the parasitic element. To show this, the matrix $\left(\mathbf{D}+\mathbf{S T}^{-1}\right)$ in (2.54) for this scenario can be rewritten as:

$$\mathbf{D}+\mathbf{S T}^{-1} = \begin{bmatrix} Z_{11}+Z_{L,1} & 0 \\ 0 & Z_{22}+Z_{L,2} \end{bmatrix} + \begin{bmatrix} -Z_{11} & Z_{12} \\ Z_{21} & -Z_{22} \end{bmatrix} \begin{bmatrix} 1 & \dfrac{-Z_{12}}{Z_{11}+Z_{L,1}} \\ \dfrac{-Z_{21}}{Z_{22}+Z_{L,2}} & 1 \end{bmatrix}^{-1} \quad (3.24)$$

The matrix $\mathbf{T}^{-1}$ can be rewritten as:

$$\mathbf{T}^{-1} = \begin{bmatrix} 1 & \dfrac{-Z_{12}}{Z_{11} + Z_{L,1}} \\[3mm] \dfrac{-Z_{21}}{Z_{22} + Z_{L,2}} & 1 \end{bmatrix}^{-1} = \Delta \begin{bmatrix} 1 & \dfrac{Z_{12}}{Z_{11} + Z_{L,1}} \\[3mm] \dfrac{Z_{21}}{Z_{22} + Z_{L,2}} & 1 \end{bmatrix} \tag{3.25}$$

where

$$\Delta = \frac{(Z_{11} + Z_{L,1})(Z_{22} + Z_{L,2})}{(Z_{11} + Z_{L,1})(Z_{22} + Z_{L,2}) - Z_{12}Z_{21}} \tag{3.26}$$

Pre-multiplying the matrix in (3.25) by the matrix $\mathbf{S}$ and making some simplifications yields:

$$\mathbf{ST}^{-1}$$

$$= \begin{bmatrix} -Z_{11} & Z_{12} \\ Z_{21} & -Z_{22} \end{bmatrix} \cdot \Delta \begin{bmatrix} 1 & \dfrac{Z_{12}}{Z_{11} + Z_{L,1}} \\[3mm] \dfrac{Z_{21}}{Z_{22} + Z_{L,2}} & 1 \end{bmatrix}$$

$$= \frac{(Z_{11} + Z_{L,1})(Z_{22} + Z_{L,2})}{(Z_{11} + Z_{L,1})(Z_{22} + Z_{L,2}) - Z_{12}Z_{21}} \begin{bmatrix} -Z_{11} + \dfrac{Z_{12}Z_{21}}{Z_{22} + Z_{L,2}} & \dfrac{-Z_{11}Z_{12}}{Z_{11} + Z_{L,1}} + Z_{12} \\[3mm] Z_{21} - \dfrac{Z_{22}Z_{21}}{Z_{22} + Z_{L,2}} & \dfrac{-Z_{12}Z_{21}}{Z_{11} + Z_{L,1}} - Z_{22} \end{bmatrix}$$

$$= \begin{bmatrix} \dfrac{(Z_{11} + Z_{L,1})[Z_{12}Z_{21} - Z_{11}(Z_{22} + Z_{L,2})]}{(Z_{11} + Z_{L,1})(Z_{22} + Z_{L,2}) - Z_{12}Z_{21}} & \dfrac{(Z_{22} + Z_{L,2})Z_{12}Z_{L,1}}{(Z_{11} + Z_{L,1})(Z_{22} + Z_{L,2}) - Z_{12}Z_{21}} \\[5mm] \dfrac{(Z_{11} + Z_{L,1})Z_{21}Z_{L,2}}{(Z_{11} + Z_{L,1})(Z_{22} + Z_{L,2}) - Z_{12}Z_{21}} & \dfrac{(Z_{22} + Z_{L,2})[-Z_{12}Z_{21} - Z_{22}(Z_{11} + Z_{L,1})]}{(Z_{11} + Z_{L,1})(Z_{22} + Z_{L,2}) - Z_{12}Z_{21}} \end{bmatrix} \tag{3.27}$$

Finally adding the matrix $\mathbf{D}$ to the result and putting $Z_{L,2} = 0$ produces:

$$\mathbf{D} + \mathbf{ST}^{-1} = \begin{bmatrix} Z_{11} + Z_{L,1} & 0 \\ 0 & Z_{22} \end{bmatrix}$$

$$+ \begin{bmatrix} \dfrac{(Z_{11} + Z_{L,1})[Z_{12}Z_{21} - Z_{11}Z_{22}]}{(Z_{11} + Z_{L,1})Z_{22} - Z_{12}Z_{21}} & \dfrac{Z_{22}Z_{12}Z_{L,1}}{(Z_{11} + Z_{L,1})Z_{22} - Z_{12}Z_{21}} \\[5mm] 0 & \dfrac{Z_{22}[-Z_{12}Z_{21} - Z_{22}(Z_{11} + Z_{L,1})]}{(Z_{11} + Z_{L,1})Z_{22} - Z_{12}Z_{21}} \end{bmatrix}$$

$$= \begin{bmatrix} \dfrac{(Z_{11}+Z_{L,1})Z_{L,1}Z_{22}}{(Z_{11}+Z_{L,1})Z_{22}-Z_{12}Z_{21}} & \dfrac{Z_{22}Z_{12}Z_{L,1}}{(Z_{11}+Z_{L,1})Z_{22}-Z_{12}Z_{21}} \\ 0 & 0 \end{bmatrix} \qquad (3.28)$$

As can be seen, the second row of the resultant CVUC mutual coupling matrix for this case has zero entries. Clearly, the second row corresponds to the parasitic element. If the matrix (3.28) is post-multiplied by the vector of uncoupled currents of the array elements, the result is the voltage vector:

$$\mathbf{v}_L^{(1)} = \begin{bmatrix} v_{L,1} & 0 \end{bmatrix}^T \qquad (3.29)$$

Similarly, if element #1 is converted to parasitic and element #2 is turned to active, the matrix (3.28) will be:

$$\mathbf{D}+\mathbf{ST}^{-1} = \begin{bmatrix} 0 & 0 \\ \dfrac{Z_{11}Z_{21}Z_{L,2}}{(Z_{22}+Z_{L,2})Z_{11}-Z_{12}Z_{21}} & \dfrac{(Z_{22}+Z_{L,2})Z_{L,2}Z_{11}}{(Z_{22}+Z_{L,2})Z_{11}-Z_{12}Z_{21}} \end{bmatrix} \qquad (3.30)$$

The procedure described above can be generalized to N-element SASPA arrays. The results (3.28) and (3.30) show that applying the CVUC model to the couple-free currents (the couple-free load current in the active element and the couple-free short-circuited currents in the parasites) will couple the energy to the active element. This result cannot be obtained if a load impedance of zero is substituted into the OCV model of (2.39) or the RMIM model of (2.40) since some of their entries will be singular.

Figures 3.10 and 3.11 show respectively the radiation patterns of five-dipole ULA-SASPA and six-dipole UCA-SASPA receiving arrays. The mutual coupling between the elements is assumed to be the CVUC. The interelement spacing between the elements of the ULA-SASPA array is $d = 0.15\lambda$. The radius of the UCA-SASPA array is $R = \lambda/4$.

The beam patterns in these plots are the result of the response of the array factor

squared $|AF|^2$ at the active elements in each of the N sub-snapshots which are spread over one snapshot of the measurement. That is, for the ULA-SASPA array:

$$\left|AF_{ULA}^{(n)}\right|^2 = \left|x^{(n)}(\phi)\right|^2 = \left|\left(\mathbf{c}^{(n)}\right)^T \mathbf{a}_{ULA}(\phi)\right|^2 \tag{3.31}$$

and for UCA-SASPA array:

$$\left|AF_{UCA}^{(n)}\right|^2 = \left|x^{(n)}(\phi)\right|^2 = \left|\left(\mathbf{c}^{(n)}\right)^T \mathbf{a}_{UCA}(\phi)\right|^2 \tag{3.32}$$

where $\mathbf{a}_{ULA}(\phi)$ and $\mathbf{a}_{UCA}(\phi)$ are defined in (3.21) and (3.23) respectively and $\left(\mathbf{c}^{(n)}\right)^T$ is the row of the CVUC mutual coupling model which corresponds to the active element n. It can be seen from Figure 3.10 that the beam patterns produced in the ULA-SASPA array are symmetrical around the element in the middle, while in the UCA-SASPA array, all the produced beam patterns are symmetrical. This shows that the ULA-SASPA array suffers from the ambiguity property.

3.7   Summary

The principle of SPA and SASPA antenna arrays has been explored in this chapter. These arrays have a flexible and fast mean to direct and steer their overall radiation pattern to different directions by simply changing the load termination of their omnidirectional elements. Changing the load condition at the termination of each element can be implemented with PIN diodes. These diodes have very short switching times and are eminently suitable to act as RF switches. Steering the overall radiation pattern of SPA and SASPA arrays to different directions has been established through varying the spatial phase shift of the steering vectors by successively altering the termination of the elements. This outweighs conventional antenna arrays when considering beamforming since a weight vector needs to be applied to the latter to achieve a certain beam pattern.
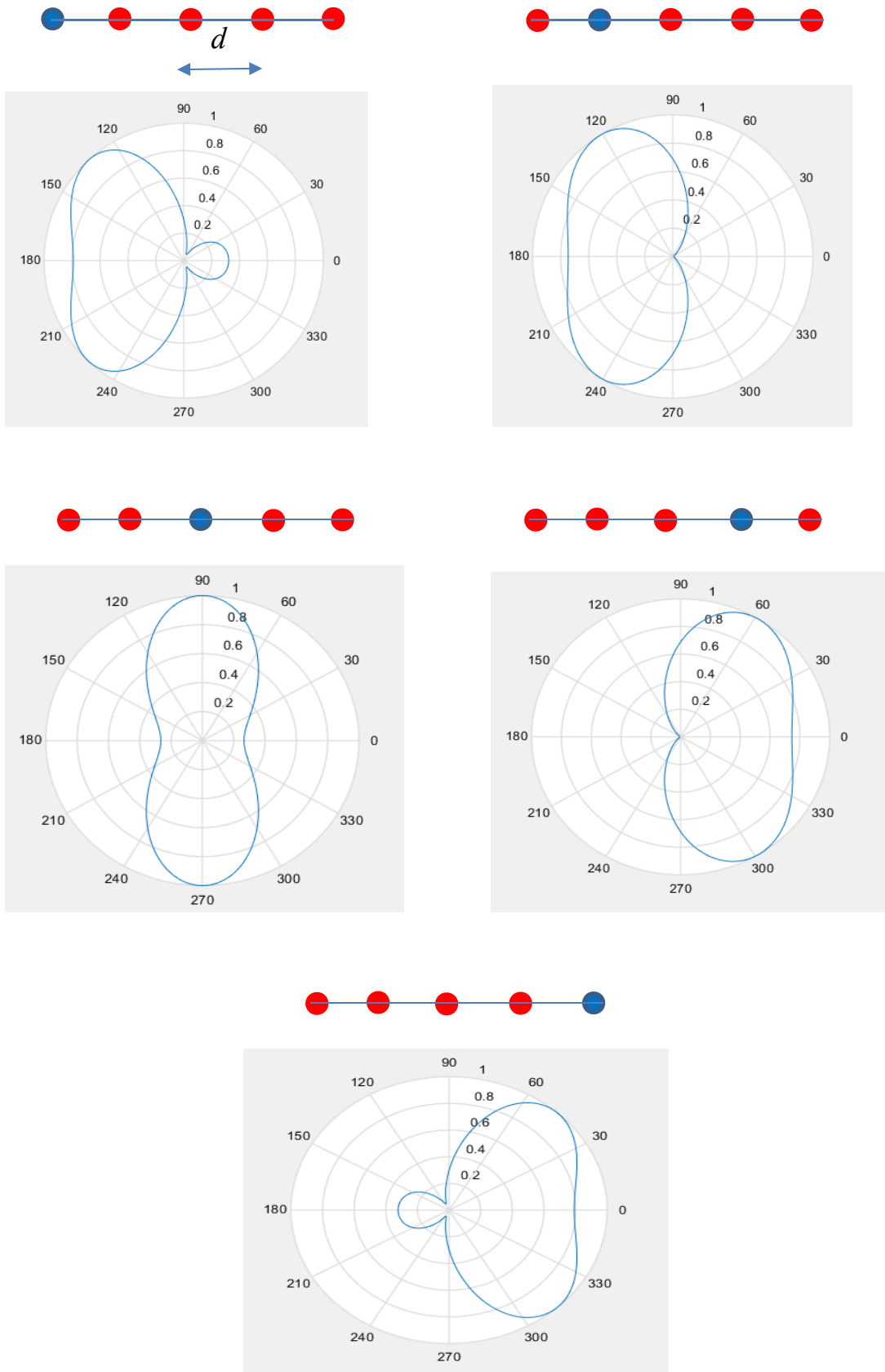
Figure 3.10: Radiation patterns of five-dipole ULA-SASPA receiving array with the CVUC model as the mutual coupling. The interelement spacing is $d = 0.15\lambda$.

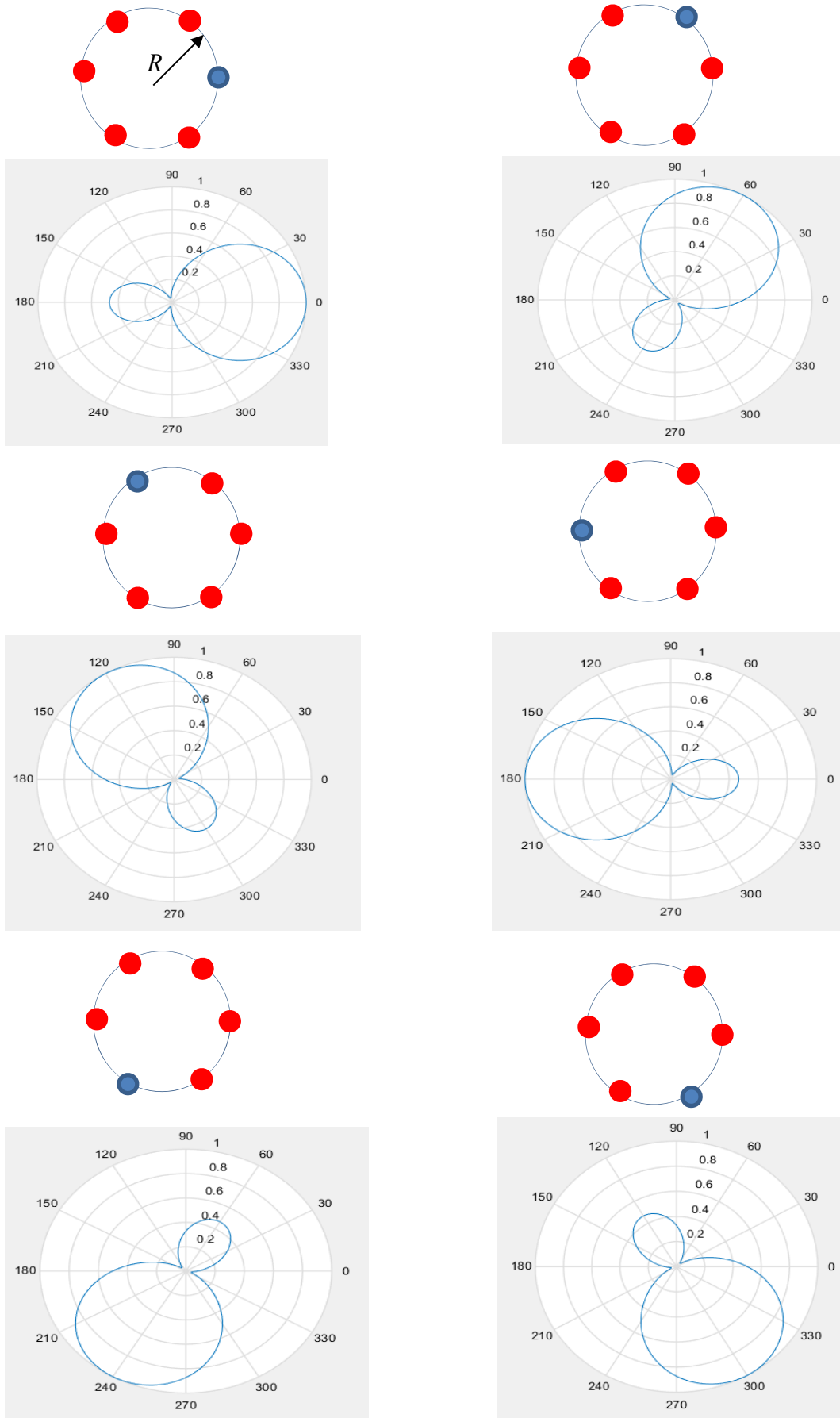🔵 Active element   🔴 Parasitic element

Figure 3.11: Radiation patterns of six-dipole UCA-SASPA receiving array with the CVUC model as the mutual coupling. The radius of the array is $R = \lambda/4$.

One of the important characteristics of SPA and SASPA arrays is mutual coupling. This characteristic, which may be considered to be an adverse effect in conventional antenna arrays, is found to be advantageous in determining the resultant radiation pattern and directivity of an SPA or SASPA array in conjunction with the self-beamforming procedure described above, the number of elements, and the array geometry. The mutual coupling and the total radiation pattern of SASPA arrays in transmit mode have been analysed so that a closer understanding of the response of an SASPA array in receive mode can be gained. It is found that UCA-SASPA arrays produce symmetrical and more directional switched patterns. In contrast, ULA-SASPA arrays produce unsymmetrical and less directional radiation patterns. Also, more than one main lobe can be produced when some of the elements of a ULA-SASPA array are switched to the active state. Thus, UCA-SASPA arrays outperform ULA-SASPA arrays in both transmit and receive modes.

The CVUC model which was postulated in the previous chapter has been shown to give an accurate representation of mutual coupling in SASPA arrays since this model maps the free-coupled currents induced on the array elements due to the received signals only to an appropriate vector of load voltages. The resultant load voltages will be the zero vector except for the entry corresponding to the active element. This result cannot be obtained when other mutual coupling models such as the OCV and RMIM models are used as the mutual coupling model for SASPA arrays.

Chapter 4

DIRECTION OF ARRIVAL ALGORITHM

4.1   Introduction

In conventional antenna arrays, all elements are terminated by a load. Hence the elements are all active at the instant of measurement. Consequently, these arrays are called ***all-active arrays***. This chapter is devoted to explaining one of the many different algorithms that have been proposed to estimate the DOA of signals impinging on a conventional all-active antenna array. The algorithm is MUSIC (MUltiple SIgnal Classification). This DOA algorithm depends mainly on the spectral analysis of the covariance matrix of the measurements.

The data model which reflects the measurements of an all-active array involves the response of the array elements to the received signals plus the effect of noise. The covariance matrix of the measurements which entail the spatial-temporal correlation between the array elements is obtained from the data model. To build up a correct data model, further information about the array's parameters such as the array geometry, antenna characteristic, etc. should be available [8]. Eigendecomposition of the measurement covariance matrix is then performed to determine the signal and noise subspaces. These subspaces are then processed by MUSIC to estimate the underlying DOAs.

In practice, the covariance matrix of the measurements is obtained from a large number of snapshots. This requirement ensures the obtained "covariance matrix and its eigendecomposition are maximum likelihood estimates of the corresponding exact quantities" [8] and unbiased estimation can be achieved. A typical spectral identification of these algorithms is the peaks in the pseudospectrum of the algorithm, such as in MUSIC [8]. The peaks are located near the DOA of the received signals. The most important criteria of the DOA algorithms are the bias and

variance of the DOA estimates, and the resolution of the algorithm, i.e. the ability to resolve closely spaced signal sources [8].

4.2   Review of DOA Estimation with All-Active Antenna Arrays

4.2.1   The Data Model

The data model describes the response of the array elements to the received signals and is central to the derivation of algorithms to estimate some of the spatial-temporal parameters such as DOA, polarization, temporal signal frequency etc. [8]. The array response appears as an induced voltage or current at the terminal impedance of each element of the antenna array. In addition to these responses to the incident signals, the observations or measurements include also noise which are normally assumed to be additive. In practice, data models represent a compromise between the need to model closely the real world [65] and the need to keep them mathematically simple [8]. As such, assumptions are often made when constructing a data model. In the case of antenna array processing, these assumptions are:

1. *Linear transmission in an isotropic and non-dispersive medium*: This assumption implies that several traveling waves can propagate in this media simultaneously [8] and in a straight line [14][65], i.e., the media is invariant with respect to direction and is non-scattering.

2. *Far field:* The received signal is assumed to be in the far field. This means that what is received by the antenna array is a *plane wave,* i.e., the wave is flat and having constant phase [8] provided the distance between the signal sources and the array is large enough so that the wavefront of the spherical waves emanating from the source is approximately a plane wave at the array [8][14][65].

3. *The number of received signals M is less than the number of the array elements, i.e., $M < N$*. It is assumed that the number of signals is known a priori, or it can

be estimated by algorithms such as MDL and Akaike's AIC [8]. It is also assumed that the signals arrive from *M* distinct directions.

4. *Narrow band:* The *m*th received signal, $m = 1, \ldots, M$, can be expressed as:

$$s_m(t) = \mathrm{Re}\left\{\alpha_m(t)e^{j(2\pi f_c t + \beta_m(t))}\right\} = \alpha_m(t)\cos(2\pi f_c t + \beta_m(t)) \tag{4.1}$$

The signal $s_m(t)$ is said to be narrow band as long as the envelope $\alpha_m(t)$ and phase $\beta_m(t)$ are slowly time-varying functions with respect to τ [14][65], where τ is the smallest propagation delay from element to element in the array, i.e.,

$$\alpha_m(t - \tau) \approx \alpha_m(t) \quad \text{and} \quad \beta_m(t - \tau) \approx \beta_m(t)$$

Thus, $s_m(t)$ experiences a phase shift only due to that delay, i.e.,

$$s_m(t - \tau) \approx s_m(t)e^{-j2\pi f_c \tau}$$

In addition, the received signals are assumed to be stochastic with zero mean normal distribution and variance of σ_s^2, i.e. $s_m(t) \sim N(0, \sigma_s^2)$. The response of each element, which is the measured terminal voltage or current, to the delayed version of the *M* received signals will be [14]:

$$x_p(t) = \sum_{m=1}^{M} G_p(\phi_m) s_m(t) e^{-j2\pi f_c \tau_p(\phi_m)}, \quad 1 \le p \le N \tag{4.2}$$

where $G_p(\phi_m)$ is the complex gain and phase of the response of element *p*, and $\tau_p(\phi_m)$ is the delay between element *p* and a reference location. Thus, the response of element *p* is a linear combination of the *M* received signals [66]. Note the *M* received signals are assumed to have the same carrier frequency [14]. Thus, (4.2) can be written in vector-matrix notation as:

$$\mathbf{x}(t) = \sum_{m=1}^{M} \mathbf{a}(\phi_m) s_m(t) = \mathbf{A}(\phi)\mathbf{s}(t) \tag{4.3}$$

where $\mathbf{a}(\phi_m) = \left[G_1(\phi_m)e^{-j2\pi f_c \tau_1(\phi_m)} \quad \cdots \quad G_N(\phi_m)e^{-j2\pi f_c \tau_N(\phi_m)}\right]^T \in \mathbb{C}^{N \times 1}$ is the *steering vector,* $\phi = \{\phi_1, \ldots, \phi_M\}$, and $\mathbf{A}(\phi) = [\mathbf{a}(\phi_1) \quad \cdots \quad \mathbf{a}(\phi_M)] \in \mathbb{C}^{N \times M}$ is the *steering matrix.*

$\mathbf{A}(\phi)$ is full rank since ϕ_m, $m=1,\ldots,M$, are assumed to be distinct, i.e., $\operatorname{rank}(\mathbf{A}(\phi))=M$ [14][65]. Note that the range of the columns of $\mathbf{A}(\phi)$ is confined to the noiseless measurement of the array or specifically to an M-dimensional signal subspace of the N-dimensional space of the output of the antenna array [8][13].

5. *Noise:* The noise $n_p(t)$, which is contained in the measurements at the terminal of each element, is assumed to be a complex circularly Additive White Gaussian Noise (AWGN) [24][65] random-process with mean zero and variance σ_n^2, i.e. $n_p(t) \sim N(0,\sigma_n^2)$. Also, it is assumed that the noise is uncorrelated with the received signals [14][24][65]. Including noise, the observations in (4.3) becomes:

$$\mathbf{x}(t)=\mathbf{A}(\phi)\mathbf{s}(t)+\mathbf{n}(t) \tag{4.4}$$

where $\mathbf{n}(t)\in\mathbb{C}^{N\times1}$ is the noise vector. The regression model in (4.4) is spatial-temporal and forms the foundation of most DOA algorithms.

The structure of the matrix $\mathbf{A}(\phi)$ depends on the array geometry. In ULAs, the delay time τ_p is (see Figure 3.9a):

$$\tau_p(\phi)=-\frac{(p-1)d\cos\phi}{c}=-\frac{(p-1)d\cos\phi}{\lambda f_c} \tag{4.5}$$

Since the antennas used in this work are half-wave dipoles with omnidirectional characteristic, then $a_p(\phi_m)=1$ in (4.2) while the spatial phase shift of each element with respect to the reference element is:

$$e^{-j2\pi f_c\tau_p(\phi)}=e^{j2\pi f_c\frac{(p-1)d\cos\phi}{\lambda f_c}}=e^{j2\pi\frac{(p-1)d\cos\phi}{\lambda}}=e^{j(p-1)kd\cos\phi}$$

The steering matrix for *M* signals received by an *N*-element ULA omnidirectional antenna array will be:

$$\mathbf{A}_{ULA}(\phi) = \begin{bmatrix} 1 & 1 & \cdots & 1 \\ e^{jkd\cos\phi_1} & e^{jkd\cos\phi_2} & \cdots & e^{jkd\cos\phi_M} \\ e^{j2kd\cos\phi_1} & e^{j2kd\cos\phi_2} & \cdots & e^{j2kd\cos\phi_M} \\ \vdots & \vdots & \ddots & \vdots \\ e^{j(N-1)kd\cos\phi_1} & e^{j(N-1)kd\cos\phi_2} & \cdots & e^{j(N-1)kd\cos\phi_M} \end{bmatrix} \qquad (4.6)$$

The matrix in (4.6) has Vandermonde structure [8]. Similarly, for UCAs, the spatial phase shift of each element with respect to the origin (see Figure 3.9b) is found in (3.22) and the corresponding steering matrix will be:

$$\mathbf{A}_{UCA}(\phi) = \begin{bmatrix} e^{jkR\cos\phi_1} & e^{jkRr\cos\phi_2} & \cdots & e^{jkR\cos\phi_M} \\ e^{jkR\cos\left(\phi_1-\frac{2\pi}{N}\right)} & e^{jkRr\cos\left(\phi_2-\frac{2\pi}{N}\right)} & \cdots & e^{jkR\cos\left(\phi_M-\frac{2\pi}{N}\right)} \\ e^{jkR\cos\left(\phi_1-\frac{4\pi}{N}\right)} & e^{jkR\cos\left(\phi_2-\frac{4\pi}{N}\right)} & \cdots & e^{-jkR\cos\left(\phi_M-\frac{4\pi}{N}\right)} \\ \vdots & \vdots & \ddots & \vdots \\ e^{jkR\cos\left(\phi_1-\frac{2\pi(N-1)}{N}\right)} & e^{jkR\cos\left(\phi_2-\frac{2\pi(N-1)}{N}\right)} & \cdots & e^{jkR\cos\left(\phi_M-\frac{2\pi(N-1)}{N}\right)} \end{bmatrix}$$
$$(4.7)$$

4.2.2 Eigenstructure of the Spatial Covariance Matrix

To estimate spatial information, such as the DOAs, from the measurements $\mathbf{x}(t)$, the second order statistics of the output $\mathbf{x}(t_i)$ which is sampled at times $i = 1, 2, \ldots,$ should be calculated, i.e. estimating DOAs from the covariance information among the array elements [8]. If the independent variables in (4.4) are dropped, the covariance matrix for the measurements is:

$$\begin{aligned} \mathbf{R}_\mathbf{x} = \mathbb{E}\{\mathbf{x}\mathbf{x}^H\} &= \mathbb{E}\{(\mathbf{A}\mathbf{s}+\mathbf{n})(\mathbf{A}\mathbf{s}+\mathbf{n})^H\} \\ &= \mathbf{A}\mathbb{E}\{\mathbf{s}\mathbf{s}^H\}\mathbf{A}^H + \mathbf{A}\mathbb{E}\{\mathbf{s}\mathbf{n}^H\} + \mathbb{E}\{\mathbf{n}\mathbf{s}^H\}\mathbf{A}^H + \mathbb{E}\{\mathbf{n}\mathbf{n}^H\} \\ &= \mathbf{A}\mathbb{E}\{\mathbf{s}\mathbf{s}^H\}\mathbf{A}^H + \mathbb{E}\{\mathbf{n}\mathbf{n}^H\} \end{aligned} \qquad (4.8)$$

where $\mathbb{E}\{\cdot\}$ is statistical expectation and $(\cdot)^H$ is the conjugate transpose operation. The cross terms in (4.8) vanish due to the assumption that the incident

signals are random processes, they are uncorrelated with noise, and the signals and noise all have mean zero. Let $\mathbb{E}\{\mathbf{ss}^H\} = \mathbf{S}$ and $\mathbb{E}\{\mathbf{nn}^H\} = \sigma_n^2 \mathbf{I}_N$ denote the statistical expectation of the covariance matrix of the received signals and of noise, respectively. Then:

$$\mathbf{R_x} = \mathbf{ASA}^H + \sigma_n^2 \mathbf{I}_N \qquad (4.9)$$

The signal covariance matrix $\mathbf{S}$ represents the degree of correlation occurring between the received signals. Therefore, when the received signals are totally uncorrelated, $\mathbf{S}$ will be diagonal with the signals' power on the main diagonal [13][66]. However, $\mathbf{S}$ could be singular for totally coherent signals [13][66]. Accordingly, each entry on the main diagonal of $\mathbf{R_x}$ represents the sum of the powers of the received signals absorbed by the corresponding array element plus the noise power at that element. Note that $\mathbf{R_x} \in \mathbb{C}^{N \times N}$ is Hermitian (not Toeplitz), i.e., $\mathbf{R_x}^H = \mathbf{R_x}$. In addition, $\mathbf{R_x}$ is positive definite (pd) and all its eigenvalues are real [8][64]. Therefore, $\mathbf{R_x}$ can be defined in terms of its orthonormal set of eigenvectors scaled by their corresponding real eigenvalues. This can be done by decomposing $\mathbf{R_x}$ as

$$\mathbf{R_x} = \mathbf{E\Lambda E}^H \qquad (4.10)$$

In (4.10), $\mathbf{E} = \begin{bmatrix} \mathbf{e}_1 & \mathbf{e}_2 & \cdots & \mathbf{e}_N \end{bmatrix} \in \mathbb{C}^{N \times N}$ contains the distinct eigenvectors of the covariance matrix $\mathbf{R_x}$ and is unitary, i.e. $\mathbf{E}^H = \mathbf{E}^{-1}$, since its columns are orthonormal. The matrix $\mathbf{\Lambda} = \mathrm{diag}(\Lambda_1, \Lambda_2, \ldots, \Lambda_N)$ is diagonal with entries the real eigenvalues of $\mathbf{R_x}$ ordered such that $\Lambda_1 \geq \Lambda_2 \geq \cdots \geq \Lambda_N$ [8], i.e.

$$\mathbf{\Lambda} = \begin{bmatrix} \Lambda_1 & 0 & \cdots & 0 & 0 \\ 0 & \Lambda_2 & \cdots & 0 & 0 \\ \vdots & \vdots & \ddots & \vdots & \vdots \\ 0 & 0 & \cdots & \Lambda_{N-1} & 0 \\ 0 & 0 & \cdots & 0 & \Lambda_N \end{bmatrix} \qquad (4.11)$$

The decomposition in (4.10) is called Eigen Value Decomposition (EVD) or spectral

factorization. Another expression equivalent to (4.10) can be written in terms of a linear combination of rank one matrices as:

$$\mathbf{R_x} = \sum_{n=1}^{N} \Lambda_n \mathbf{e}_n \mathbf{e}_n^H \tag{4.12}$$

The outer product of each eigenvector by its complex conjugate leads to a rank one matrix which is then scaled by the corresponding eigenvalue.

In practice, the covariance matrix of the data $\mathbf{x}(t)$ is measured over only a limited time. As a result, the estimated covariance matrix $\hat{\mathbf{R}}_x$ may not provide the same eigenvectors and corresponding eigenvalues as those in (4.12) [8]. Therefore, the practical averaged sample of $\mathbf{R_x}$ should be measured for a large number of snapshots Q [8][65], i.e.:

$$\hat{\mathbf{R}}_x = \frac{1}{Q} \sum_{i=1}^{Q} \mathbf{x}(t_i) \mathbf{x}^H(t_i) = \hat{\mathbf{E}} \hat{\mathbf{\Lambda}} \hat{\mathbf{E}}^H \tag{4.13}$$

where the sign $\hat{\cdot}$ denotes estimated value. In addition, the calculation in (4.13) will provide unbiased estimates of the parameters extracted from $\hat{\mathbf{R}}_x$ such as DOAs [8][13][14][68] if Q is large. Thus, (4.4), (4.10), (4.11), and (4.13) are the foundation for describing the methods used in different high-resolution DOA algorithms.

4.2.3   High Resolution DOA Algorithm

In the literature of signal processing, the algorithms that are commonly used to estimate DOAs have been classified into two main categories [8]:

1. Parametric methods

2. Spectral-Based Algorithms.

The spectral-based algorithms are further classified into:

a. Beamforming Techniques

b. Subspace-Based methods.

In this work, the focus will be on subspace-based methods. The most well-known algorithms of this class are MUltiple SIgnal Classification (MUSIC) [66] and Estimation of Signal Parameters via Rotaional Invariance Techniques (ESPRIT) [71]. However, only MUSIC is considered since the purpose of this thesis is to explore the possibility of high resolution direction funding with SASPA arrays.

MUSIC is based on based on partitioning the orthonormal subspace $\hat{\mathbf{E}}$ in (4.13) into two orthogonal subspaces, the signal subspace $\hat{\mathbf{E}}_s$ and the noise subspace $\hat{\mathbf{E}}_n$, and the fact that $\hat{\mathbf{E}}_n$ is orthogonal to the column space of the steering matrix [13][66]. Therefore, the covariance matrix in (4.10) is first partitioned into two subspaces as:

$$\mathbf{R}_\mathbf{x} = \mathbf{E}\boldsymbol{\Lambda}\mathbf{E}^H = \mathbf{E}_s\boldsymbol{\Lambda}_s\mathbf{E}_s^H + \mathbf{E}_n\boldsymbol{\Lambda}_n\mathbf{E}_n^H \tag{4.14}$$

The partitioning in (4.14) follows from the fact that the column range of the steering matrix $\mathbf{A}$ is confined to the measurements therefore it should be confined to the M-dimensional subspace of $\mathbf{E}$, i.e. $\mathbf{E}_s \in \mathbb{C}^{N \times M}$, while the $N - M$ columns of $\mathbf{E}$ form the noise subspace $\mathbf{E}_n \in \mathbb{C}^{N \times (N-M)}$ [14][63]-[65]. Accordingly, the M eigenvalues $\Lambda_1 \geq \Lambda_2 \geq \cdots \geq \Lambda_M > 0$ are the elements of the diagonal matrix $\boldsymbol{\Lambda}_s$ while $\Lambda_{M+1} = \Lambda_{M+2} = \cdots = \Lambda_N = \sigma_n^2$ are the elements of the diagonal matrix $\boldsymbol{\Lambda}_n$ with $\Lambda_{M+1} < \Lambda_M$.

4.2.3.1 The MUSIC Algorithm

The **MU**ltiple **SI**gnal **C**lassification algorithm was found by R. O. Schmidt in his PhD dissertation in 1982 [66]. The basic idea behind this algorithm is that the noise subspace, which is estimated along with the signal subspace from the measurements as in (4.14), is also orthogonal to the subspace spanned by the columns of the steering matrix [66], i.e.

$$\{\mathcal{R}(\mathbf{A}) = \mathcal{R}(\mathbf{E}_s)\} \perp \mathcal{R}(\mathbf{E}_n) \tag{4.15}$$

where $\mathcal{R}(\mathbf{A})$ is the range space of the matrix $\mathbf{A}$.

Let $\mathbf{e}_{n_i}$, $i = M+1,\dots,N$ be the set of the noise subspace vectors. Then one vector of this set is an eigenvector of the covariance matrix $\mathbf{R_x}$ with an associated eigenvalue of σ_n^2. Now, for any square matrix $\mathbf{A}$, it is well-known that if $(\mathbf{v}, \lambda)$ is a solution of $\mathbf{Av} = \Lambda\mathbf{v}$, then $\mathbf{v}$ is an eigenvector of $\mathbf{A}$ and Λ is the associated eigenvalue. It then follows that:

$$\mathbf{R_x}\mathbf{e}_{n_i} = \sigma_n^2\mathbf{e}_{n_i}$$

or   (4.16)

$$\mathbf{R_x}\mathbf{e}_{n_i} - \sigma_n^2\mathbf{e}_{n_i} = \mathbf{0}_{N\times 1}$$

Therefore, post multiplying (4.9) by $\mathbf{e}_{n_i}$ yields:

$$\mathbf{R_x}\mathbf{e}_{n_i} = \mathbf{ASA}^H\mathbf{e}_{n_i} + \sigma_n^2\mathbf{e}_{n_i}$$

Rearranging and using (4.16), the above equation is reduced to

$$\mathbf{ASA}^H\mathbf{e}_{n_i} = \mathbf{0}_{N\times 1} \qquad (4.17)$$

Assuming $\mathbf{A}$ is full rank, and $\mathbf{S}$ is positive definite and non-singular, then:

$$\mathbf{A}^H\mathbf{e}_{n_i} = \mathbf{0}_{M\times 1}$$

or   (4.18)

$$\mathbf{A}^H\mathbf{E}_n = \mathbf{0}_{M\times N}$$

This means the noise subspace is orthogonal to the columns of $\mathbf{A}$ [13][66], i.e. every noise eigenvector is in the null space of $\mathbf{A}^H$. Schmidt has exploited the result in (4.18) to estimate the DOA of the received signals by searching for the peaks that occur when the squared distance between the search vector $\mathbf{a}(\phi)$ for all possible $\phi \in \{-\pi, \pi\}$ ($\phi \in \{0, \pi\}$ in the case of ULAs because of ambiguity) and the signal subspace is minimum. Alternatively, the goal is to search for the peaks when the projection of the search vector $\mathbf{a}(\phi)$ onto the noise subspace is minimum [66], i.e. by searching for the peaks in the MUSIC spectrum

$$P_{MUSIC}(\phi) = \frac{1}{\mathbf{a}^H(\phi)\hat{\mathbf{E}}_n\hat{\mathbf{E}}_n^H\mathbf{a}(\phi)} = \frac{1}{\left\|\hat{\mathbf{E}}_n^H\mathbf{a}(\phi)\right\|_2^2} \tag{4.19}$$

In estimating the signal subspace from the covariance matrix of the measurements, there should be prior knowledge about the number of incident signal impinging so that $\hat{\mathbf{E}}$ can be consistently partitioned into two subspaces. Schmidt has pointed out [66] that for an array of N antenna elements receiving M signals, the number of signals that can be estimated is:

$$\hat{M} = N - \hat{F} \tag{4.20}$$

where $\hat{F}$ is the estimated multiplicity of the minimum eigenvalue $\Lambda_{\min} = \sigma_n^2$ of $\hat{\mathbf{R}}_\mathbf{x}$. This is because the noiseless measurements, $\mathbf{ASA}^H \in \mathbb{C}^{N \times N}$ has minimum eigenvalue $\Lambda_{\min} = 0$ with multiplicity F. This means $\mathbf{ASA}^H$ is singular, i.e., it is rank deficient ($\mathrm{rank}\left(\mathbf{ASA}^H\right) = M < N$) [13]. Accordingly, the dimension of the null space of $\mathbf{ASA}^H$ is F. Adding $\sigma_n^2\mathbf{I}_N$ to $\mathbf{ASA}^H$ will make the latter invertible with $\hat{F}$ minimum eigenvalues equal to σ_n^2. The last method is called "diagonal loading" [67]. Practically, the equality sign in (4.18) may be replaced by an almost-equal sign, i.e., $\mathbf{A}^H\mathbf{e}_{n_i} \approx \mathbf{0}_{M \times 1}$ because the estimated noise eigenvalues will differ slightly from σ_n^2. The result is merging some portion of the signal subspace into the noise subspace. This occurs when the value of some of the eigenvalues of the signal subspace are close to the value of the eigenvalues of the noise subspace. To avoid such a case and to have an exact value of $\hat{F}$, the following conditions are desirable when implementing the MUSIC algorithm [66] [68]:

1. The number of snapshots Q should be large.
2. The SNR ratio of the received signal should be high.
3. The number of the elements in the array should be large.
4. The array aperture should be large.

As a result, sharper peaks near the true DOAs will be seen in the MUSIC spectrum [68]. The following simulations illustrate the influence of the above four parameters

on the performance of MUSIC. Figure 4.1 shows the normalized MUSIC spectrum for two signals incident from $\phi_1 = 60°$ and $\phi_2 = 20°$, both with SNR $= 10$ dB. The two signals are impinging on a ULA array consisting of eight identical antenna elements with inter-element spacing $d = 0.5\lambda$. A measurement sample of five runs with 1000 snapshots for each run is used. Figure 4.2 shows the MUSIC spectrum for the same scenario but with SNR $= 2$ dB, $d = 0.25\lambda$ and 100 snapshots for each of the five runs. In Figure 4.3, two closely spaced signals $\phi_1 = 20°$ and $\phi_2 = 30°$ with SNR $= 10$ dB are incident on an antenna array of four identical elements with inter element spacing $d = 0.2\lambda$ and 1000 snapshots for each of the five runs. In this case, the array aperture is very small. It is clear from Figure 4.2 that the performance of MUSIC degrades when the desirable conditions stated above are partially not valid. Also, Figure 4.3 shows that MUSIC fails to estimate the DOAs when the array aperture is very small, and the signals are closely spaced.

The MUSIC cost function in (4.19) can be rewritten in terms of the signal subspace as follows. Since the matrix $\mathbf{E}$ in (4.14) consists of a signal subspace and a noise subspace, then it can be written as:

$$\mathbf{E} = \begin{bmatrix} \mathbf{E}_s & \mathbf{E}_n \end{bmatrix} \tag{4.21}$$

and because of $\mathbf{E}$ is unitary, then:

$$\mathbf{E}\mathbf{E}^H = \begin{bmatrix} \mathbf{E}_s & \mathbf{E}_n \end{bmatrix} \begin{bmatrix} \mathbf{E}_s^H \\ \mathbf{E}_n^H \end{bmatrix} = \mathbf{I}_N$$

or $\tag{4.22}$

$$\mathbf{E}_s\mathbf{E}_s^H + \mathbf{E}_n\mathbf{E}_n^H = \mathbf{P}_s + \mathbf{P}_n = \mathbf{P}_s + \mathbf{P}_s^\perp = \mathbf{I}_N$$

The matrix $\mathbf{P}_s = \mathbf{E}_s\mathbf{E}_s^H \in \mathbb{C}^{N \times N}$ is the orthogonal projection matrix on the signal subspace and $\mathbf{P}_n = \mathbf{P}_s^\perp = \mathbf{E}_n\mathbf{E}_n^H \in \mathbb{C}^{N \times N}$, which is orthogonal to $\mathbf{P}_s$, is the orthogonal projection matrix on the noise subspace [8]. Any square matrix $\mathbf{P}$ is said to be an orthogonal projection matrix if it satisfies the following conditions $\mathbf{P}^2 = \mathbf{P}$ and $\mathbf{P}^H = \mathbf{P}$ [60]. Substituting (4.22) into (4.19), we get:

$$P_{MUSIC}(\phi) = \frac{1}{\mathbf{a}^H(\phi)\left(\mathbf{I}_N - \hat{\mathbf{E}}_s\hat{\mathbf{E}}_s^H\right)\mathbf{a}(\phi)} = \frac{1}{\mathbf{a}^H(\phi)\mathbf{a}(\phi) - \mathbf{a}^H(\phi)\hat{\mathbf{E}}_s\hat{\mathbf{E}}_s^H\mathbf{a}(\phi)}$$

$$= \frac{1}{N - \left\|\hat{\mathbf{E}}_s^H\mathbf{a}(\phi)\right\|_2^2}$$

(4.23)

where $\mathbf{a}^H(\phi)\mathbf{a}(\phi) = N$. That is, the peaks at the DOAs occur when the norm-2 (the Euclidian norm) squared of the projection of the steering vectors onto the signal subspace is approximately equals to N; the number of array elements. Eq (4.23) will be next used in Chapter 5.
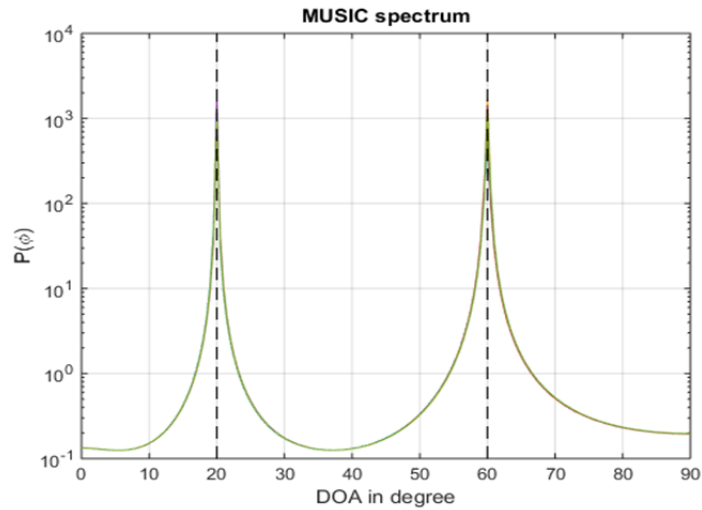
Figure 4.1: MUSIC spectrum for two signals coming from $\phi_1 = 60°$ and $\phi_2 = 20°$ with SNR $= 10$ dB impinging on an 8-element dipole ULA array with inter-element spacing $d = 0.5\lambda$. Five runs with 1000 snapshots for each run are used for this simulation.
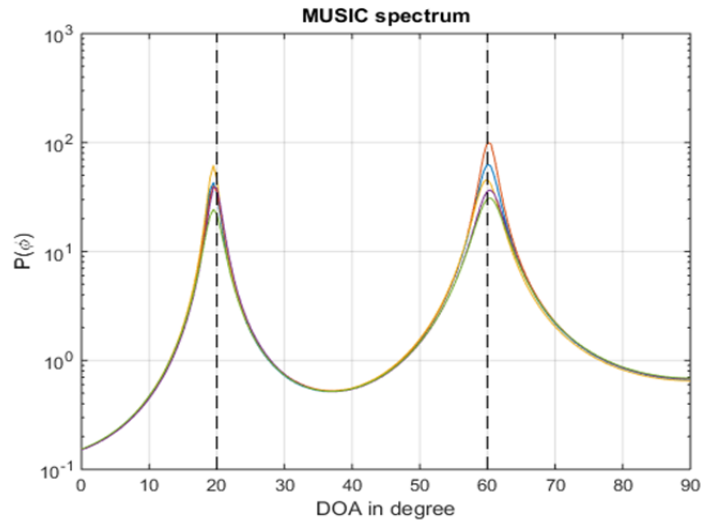
Figure 4.2: MUSIC spectrum for the same scenario of Figure 4.1 but with $\mathrm{SNR} = 2$ dB, $d = 0.25\lambda$.
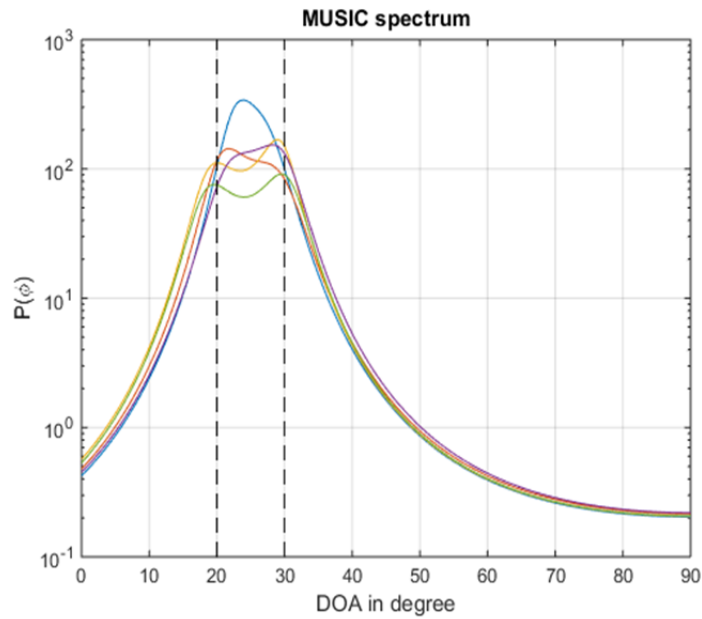
Figure 4.3: MUSIC spectrum for two signals coming from directions $\phi_1 = 20°$ and $\phi_2 = 30°$ and incident on an antenna array of four elements with $d = 0.2\lambda$.

4.3 Data Models with Mutual Coupling Present

MUSIC has been proposed to estimate DOAs but the mutual coupling effect between the array elements is often not considered. In the real world, this phenomenon always exists as a result the performance of these DOA algorithms will be degraded because

the data collected from the antenna elements will be contaminated by additional information that are related to the energy exchange between the array elements. In other words, the DOA algorithms described in the previous section rely on the uncoupled voltages or currents that are induced on the array elements due to the received signals only. Thus, the real data model (4.4) should reflect the contribution of mutual coupling on the measurements along with the response of the array to the incident signals. A square matrix $\mathbf{C}(\theta,\phi,d) \in \mathbb{C}^{N \times N}$ that represents the mutual coupling can be inserted into (4.4) as:

$$\breve{\mathbf{x}}(t) = \mathbf{C}(\theta,\phi,d) \cdot \left(\mathbf{A}(\phi)\mathbf{s}(t) + \mathbf{n}(t) \right) \tag{4.24}$$

where $\breve{\mathbf{x}}(t)$ is now the measurement that includes mutual coupling effects. Note that $\mathbf{C}(\theta,\phi,d)$ depends on azimuth, elevation angles of arrival, and the inter-element spacing [23]. However, in this thesis, it is assumed the received signals are incident in the plane perpendicular to the array, for example, the *x-y* plane if the dipole elements are aligned parallel to the *z*-axis. Moreover, the antenna elements used in the arrays are assumed to be omnidirectional. Therefore, mutual coupling in this work will be a function of the inter-element spacing only. For simplicity $\mathbf{C}(\theta,\phi,d)$ will be represented by $\mathbf{C}$ only. The structure of $\mathbf{C}$ depends on the geometry of the array, and in general, for an arbitrary geometry of antenna elements $\mathbf{C}$ will have the following structure:

$$\mathbf{C} = \begin{bmatrix} c_{11} & c_{12} & c_{13} & \cdots & c_{1N} \\ c_{21} & c_{22} & c_{23} & \cdots & c_{2N} \\ c_{31} & c_{32} & c_{33} & \cdots & c_{3N} \\ \vdots & \vdots & \vdots & \ddots & \vdots \\ c_{N1} & c_{N2} & c_{N3} & \cdots & c_{NN} \end{bmatrix} \tag{4.25}$$

Each entry c_{ij}, $i,j = 1,2,\ldots,N$ denotes the mutual coupling between elements i and j. Note that, if the spacing between the elements is large, then $c_{ij} \approx 0$ and $\mathbf{C}$ is a banded matrix. In addition, in geometries that consist of identical elements, the mutual coupling between any two elements is reciprocal, i.e. $c_{ij} = c_{ji}$. Therefore, $\mathbf{C}$

is symmetric.

When the inter-element spacing between the elements is uniform, such as in a ULA, then $\mathbf{C}$ will have a Toeplitz structure, i.e. $c_{ij} = c_{(i+1)(j+1)}$ [70][72]. This means that $\mathbf{C}_{ULA}$ is symmetric Toeplitz, i.e.:

$$\mathbf{C}_{ULA} = \begin{bmatrix} c_{11} & c_{12} & c_{13} & \cdots & c_{1(N-1)} & c_{1N} \\ c_{12} & c_{11} & c_{12} & c_{13} & \cdots & c_{1(N-1)} \\ c_{13} & c_{12} & c_{11} & c_{12} & \ddots & \vdots \\ \vdots & c_{13} & c_{12} & \ddots & \ddots & c_{13} \\ c_{1(N-1)} & \vdots & \ddots & \ddots & c_{11} & c_{12} \\ c_{1N} & c_{1(N-1)} & \cdots & c_{13} & c_{12} & c_{11} \end{bmatrix} \tag{4.26}$$

Note that $\mathbf{C}_{ULA}$ in (4.26) can be defined by its first row, or first column, only.

If the array is UCA, then the structure of $\mathbf{C}_{UCA}$ will be circulant which is a special case of Toeplitz matrices. In a circulant matrix, each row is the same as the preceding row except for a rotation of one element to the right [73]. However, since the UCA is symmetric around one fundamental Cartesian axis (if N is odd) or is symmetric around the two fundamental axes (if N is even), then the additional condition $c_{ij} = c_{(N-i)j}$ also applies [73]. Thus

$$\mathbf{C}_{UCA} = \begin{bmatrix} c_{11} & c_{12} & c_{13} & \cdots & c_{13} & c_{12} \\ c_{12} & c_{11} & c_{12} & c_{13} & \cdots & c_{13} \\ c_{13} & c_{12} & c_{11} & c_{12} & \ddots & \vdots \\ \vdots & c_{13} & c_{12} & \ddots & \ddots & c_{13} \\ c_{13} & \vdots & \ddots & \ddots & c_{11} & c_{12} \\ c_{12} & c_{13} & \cdots & c_{13} & c_{12} & c_{11} \end{bmatrix} \tag{4.27}$$

i.e., $\mathbf{C}_{UCA}$ is symmetric circulant. In contrast to $\mathbf{C}_{ULA}$, $\mathbf{C}_{UCA}$ is defined either by the first $(N/2)+1$ terms in its first row or column if N is even or by the first $(N+1)/2$ terms in the first row or column if N is odd. Obviously, being defined by fewer elements, $\mathbf{C}_{UCA}$ is more beneficial than $\mathbf{C}_{ULA}$ since the latter needs more computations in calibration or decoupling scenarios. The entries of $\mathbf{C}$, whether it is

for ULA or UCA, can be calculated from Sections 2.3.3 and 2.4.1.

Now, returning to (4.24) which can be written in a simpler form as:

$$\breve{\mathbf{x}}(t) = \mathbf{C} \cdot \Big(\mathbf{A}(\phi)\mathbf{s}(t) + \mathbf{n}(t) \Big) \tag{4.28}$$

the effect of $\mathbf{C}$ on the noise $\mathbf{n}(t)$ depends on the source of the noise [24]. The voltage induced on the antenna due to environmental noise such as cosmic and solar noise can be exchanged between the array elements via mutual coupling [24]. For this scenario, the model (4.28) is valid and the coupling effect represented by $\mathbf{C}$ can be easily counteracted by pre-multiplying (4.28) by $\mathbf{C}^{-1}$ (assuming $\mathbf{C}$ is non-singular) to retrieve the model in (4.4) which is the model for measurements with no mutual coupling. The matrix $\mathbf{C}^{-1}$ can be one of the MCMs mentioned in Section 2.4. Thus, after removing mutual coupling from (4.28), the procedure described in Section 4.2.3.1 can be followed to estimate the underlying DOAs.

On the other hand, mutual coupling may have no effect on the noise if the dominant noise source is due to the hardware of the receiver, such as thermal noise [24]. The model (4.28) then reduces to:

$$\hat{\mathbf{x}}(t) = \mathbf{C}\mathbf{A}(\phi)\mathbf{s}(t) + \mathbf{n}(t) \tag{4.29}$$

Obviously, the method used to counteract mutual coupling in (4.28) is not valid for (4.29). A method that has been proposed in the literature to estimate DOAs in the presence of mutual coupling that does not affect noise will be discussed in the next section.

It should be emphasized here that the discussion thus far in this Chapter relates to all-active arrays only. In the case of SASPA arrays, the assumptions used to derive (4.28) and (4.29) will be used in Chapter 5 and Chapter 6 respectively to develop the corresponding data models for SASPA arrays. Applying each of these data models on SASPA arrays in some situations will result in improvements in DOA estimation.

Reverting back to all-active arrays, obviously the eigenstructure of the covariance matrix obtained from (4.29) will differ from the eigenstructure of the covariance matrix obtained from (4.4) and the actual information about the signal parameters will be disturbed. As a result, the DOA algorithms may fail to find the true DOAs [50]. In the next section, a method to counteract such a phenomenon when implementing DOA algorithms (on all-active arrays) is discussed.

4.4   MUSIC Algorithm with Coupled Received Signals and Uncoupled Noise

The covariance matrix for the data model of (4.29) is:

$$
\begin{aligned}
\widehat{\mathbf{R}}_{\mathbf{x}} = \mathbb{E}\left\{\widehat{\mathbf{x}}\widehat{\mathbf{x}}^{H}\right\} &= \mathbf{CA}\mathbb{E}\left\{\mathbf{ss}^{H}\right\}\mathbf{A}^{H}\mathbf{C}^{H} + \mathbb{E}\left\{\mathbf{nn}^{H}\right\} \\
&= \mathbf{CASA}^{H}\mathbf{C}^{H} + \sigma_{n}^{2}\mathbf{I}_{N}
\end{aligned}
\tag{4.30}
$$

With a method similar to (4.14), $\widehat{\mathbf{R}}_{\mathbf{x}}$ can be eigendecomposed as $\widehat{\mathbf{E}}\widehat{\mathbf{\Lambda}}\widehat{\mathbf{E}}^{H}$. Also, the matrix $\widehat{\mathbf{E}}$ can be partitioned into two orthogonal subspaces, a signal subspace $\widehat{\mathbf{E}}_{s}$, and a noise subspace $\widehat{\mathbf{E}}_{n}$. However, the column range of the signal subspace $\widehat{\mathbf{E}}_{s}$ is now confined to the column range of the matrix $\mathbf{CA}$ when mutual coupling is present [24], i.e.:

$$
\mathcal{R}\left(\widehat{\mathbf{E}}_{s}\right) \subseteq \mathcal{R}(\mathbf{CA})
\tag{4.31}
$$

This means that the subspace spanned by the columns of $\mathbf{CA}$ is orthogonal to the noise subspace $\widehat{\mathbf{E}}_{n}$, i.e., $\mathcal{R}(\mathbf{CA}) \perp \mathcal{R}\left(\widehat{\mathbf{E}}_{n}\right)$. This result can be used to update the cost function of MUSIC by searching for peaks in the MUSIC spectrum at the DOAs where the search vector $\mathbf{Ca}(\phi)$, $\phi \in [-\pi, \pi]$ is orthogonal to $\widehat{\mathbf{E}}_{n}$ [50], i.e. (4.19) becomes:

$$
P_{MUSIC}(\phi) = \frac{1}{\mathbf{a}^{H}(\phi)\mathbf{C}^{H}\widehat{\mathbf{E}}_{n}\widehat{\mathbf{E}}_{n}^{H}\mathbf{Ca}(\phi)} = \frac{1}{\left\|\widehat{\mathbf{E}}_{n}^{H}\mathbf{Ca}(\phi)\right\|_{2}^{2}}
\tag{4.32}
$$

4.5   MUSIC Algorithm in Conjunction with CVUC

In Section 2.4.3, CVUC as a mutual coupling model is formulated. The salient feature of this model is that it can be applied to all-active and SASPA arrays, and the **C** matrix obtained from the model can be used in the direction finding algorithm of (4.32). Also, as was shown in Section 3.6.2, for SASPA arrays, pre-multiplying the vector of uncoupled currents of a receiving array by the CVUC model will result in a vector of the load voltages, and this vector will contain zeros if the load impedances corresponding to parasites in the CVUC model are set to zero.

In the next section, the effectiveness of CVUC in conjunction with (4.32) to perform DOA estimation using all-active antenna arrays will be investigated through simulations. In addition, the fulfilment of the condition $M < N$ for a successful DOA estimation will also be examined. Specifically, this condition will be verified by considering SASPA arrays with a certain number of fixed active elements. That is, if the number of active elements is g, then the number of signals that can be detected by that SASPA array should be $M < g$ since no measurements will be made at the terminals of the parasites. For such a case, the $N \times N$ covariance matrix will contain rows and columns that are all-zeros. As a result, three subspaces which are orthogonal to each other will be obtained from the eigendecomposition of the covariance matrix. . The first subspace is the *signal subspace* $\mathbf{E}_s \in \mathbb{C}^{N \times M}$, the second subspace is the *noise subspace* $\mathbf{E}_n \in \mathbb{C}^{N \times (g-M)}$, and the last subspace is the *parasitic subspace* $\mathbf{E}_p \in \mathbb{C}^{N \times (N-g)}$ whose corresponding eigenvalues are all zeros. Since the eigenvalues of the estimated subspace $\hat{\mathbf{E}}_p$ are all "solid" zeros (just like the eigenvalues of the theoretical $\mathbf{E}_p$) compared to the almost constant, but never all constant, eigenvalues of $\hat{\mathbf{E}}_n$, this means $\hat{\mathbf{E}}_p$ will be more efficient than $\hat{\mathbf{E}}_n$ in estimating the underlying DOAs when used in (4.32).

4.6   Simulation Study

This section is devoted to show the performance of using MUSIC in conjunction with the CVUC model to estimate the DOAs of impinging signals on a non-switching ULA-SASPA array. As pointed out in Section 3.6.2, setting the load impedances of the parasites to zero in the CVUC model results in a vector of load voltages with zero entries except for the entries corresponding to the active elements. The measurements obtained from such a system under the data model (4.29) is then used to calculate the covariance matrix which in turn is used to obtain the corresponding signal, noise, and parasitic subspaces. The underlying DOAs are then estimated from (4.32) with the $\mathbf{C}$ matrix found from the CVUC model of (2.54).

In the following simulations, a seven-element ULA-SASPA array is used to estimate the DOAs of three signals impinging on the array using (4.32). The inter-element spacing is $d = 0.35\lambda$. The received signals are coming from azimuth directions $\phi_1 = 60°$, $\phi_2 = 62°$ and $\phi_3 = 75°$ with $\text{SNR} = 20\,\text{dB}$ for each signal. The simulations are conducted with different number of active elements g to emphasize the validity of the condition that the number of active elements in a receiving array should be greater than the number of received signals, i.e. $M < g$ for DOA estimation to be successful. In addition, the use of the theoretical covariance matrix calculated in (4.30) is compared against the use of the covariance matrix obtained from the simulated measurements in (4.13).

In Figure 4.4, the MUSIC spectrums for DOA estimation using the theoretical covariance matrix in (4.30) are plotted against the number of active elements in the array. The plots show clearly that the three signals can be detected by the ULA-SASPA array under the condition $M < g$ with high resolution, same as the all-active array with the same number of elements. On the same figure, a plot showing the failure to detect the DOAs when the condition $M < g$ has been violated is also shown.
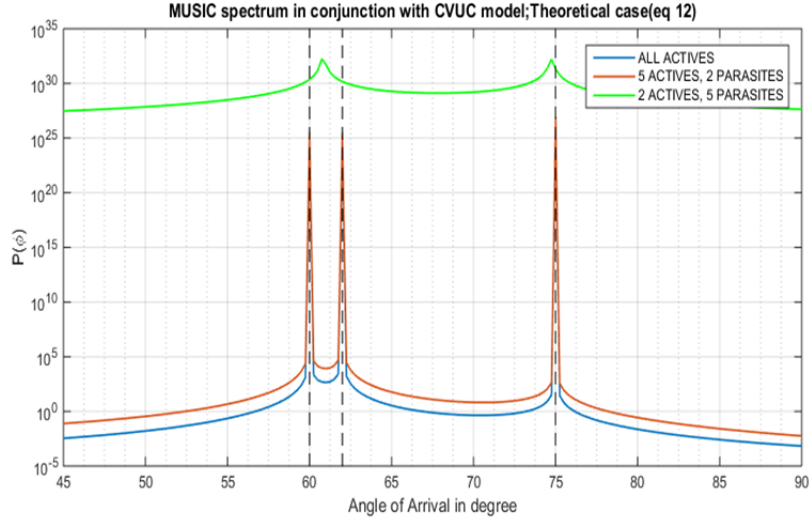
Figure 4.4: MUSIC spectrums for DOA estimation from the covariance matrix of (4.30) in conjunction with the CVUC model. The array is a 7-element ULA all-active and ULA-SASPA array with $d = 0.35\lambda$. Each array is receiving three signals emanated from the directions $\phi_1 = 60°$, $\phi_2 = 62°$ and $\phi_3 = 75°$.

Figure 4.5 shows the simulation for DOA estimation carried out for the measurements obtained from (4.13). The same ULA all-active and ULA-SASPA arrays are used. Also, the same signal scenario is used. Each simulation is conducted over five runs with 1000 snapshots for each run. The first plot is for the all-active array; the second plot is for the ULA-SASPA array with 5 active and 2 parasitic elements. The last plot is for the ULA-SASPA array with 2 active and 5 parasitic elements.

In Figure 4.6, the effectiveness of the parasitic subspace over the noise subspace when used in (4.32) is depicted. The array is a 7-element ULA-SASPA array with inter-element spacing $d = 0.25\lambda$ and receiving three signals with the same scenario as in Figures 4.4 and 4.5. However, only 750 snapshots are used for each of the five runs. Figure 4.6a shows the MUSIC spectrum when projecting the search vector in (4.32) onto the parasitic subspace. Figure 4.6b shows the MUSIC spectrum when projecting the search vector onto the noise subspace. The simulations in Figures 4.4 and 4.5 show that the MUSIC algorithm of (4.32) with the CVUC model succeeded in estimating the underlying DOAs with very high resolution provided the number of active elements in the array exceeds the number of received signals.

It is clear from Figure 4.6 that the resolution for the underlying DOAs obtained from using the parasitic subspace in (4.32) is much better than the resolution attained when using the noise subspace. This shows that using the parasitic subspace in (4.32) can overcome the problem of subspace leakage into the noise subspace. The latter may occur when some of the signal eigenvalues are almost equal to the noise power.
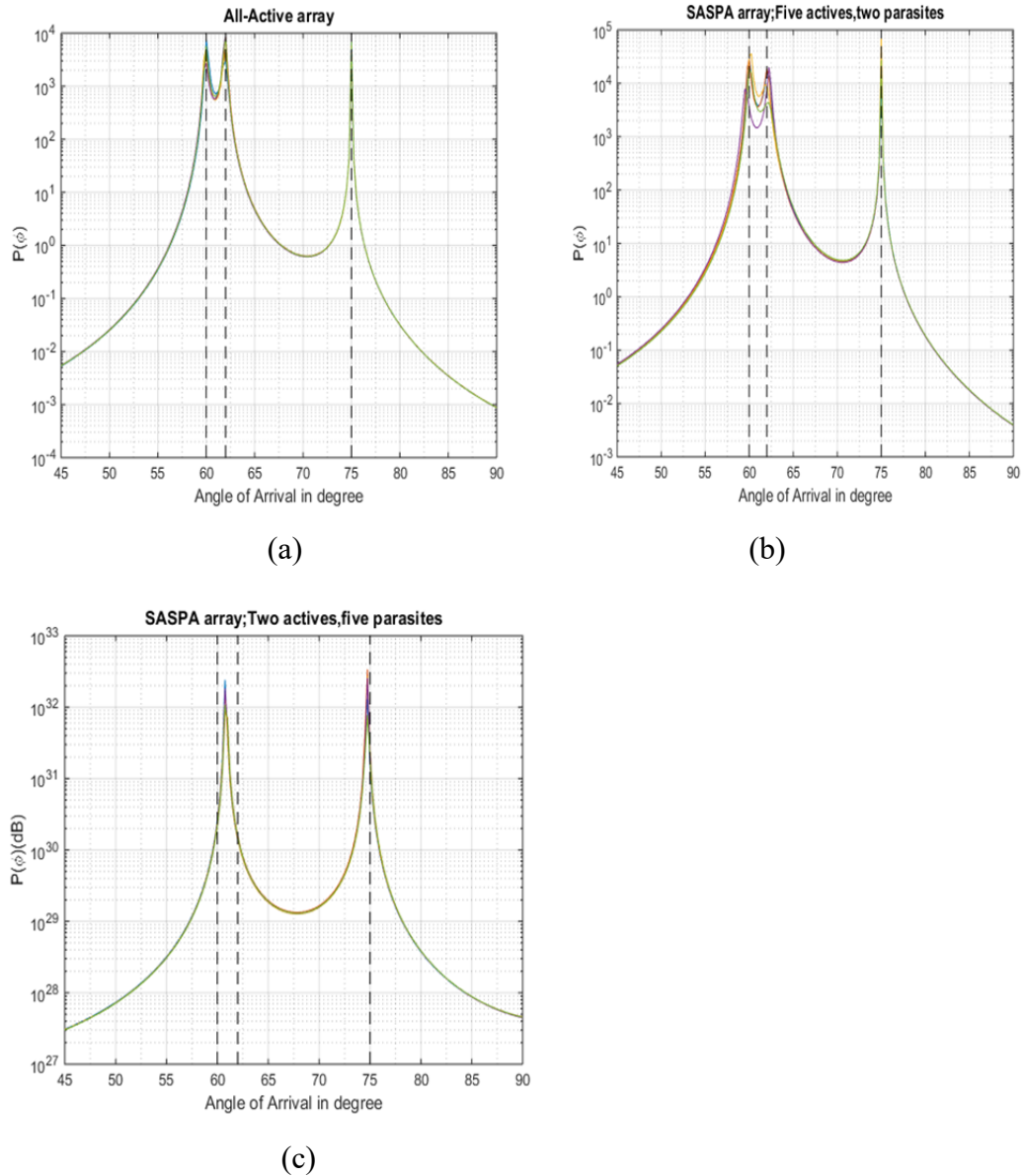

(a)

(b)

(c)

Figure 4.5: Three simulations for DOA estimation from the covariance matrix (4.13) for the same scenario used in plotting Figure 4.4. Each simulation is executed with five runs with 1000 snapshots for each run. The signals are received with $SNR = 20$ dB. (a) ULA all-active array; (b) ULA-SASPA array with five actives and two parasites; (c) ULA-SASPA array with two actives and five parasites.
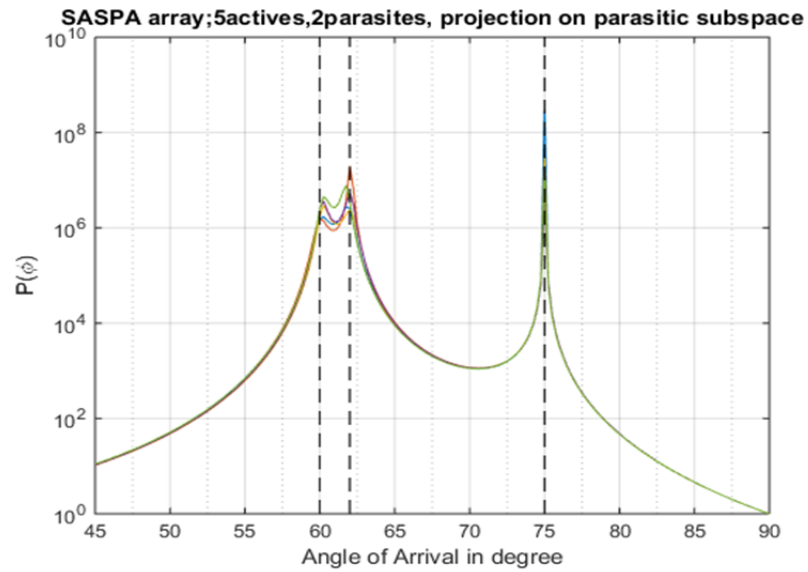
(a)
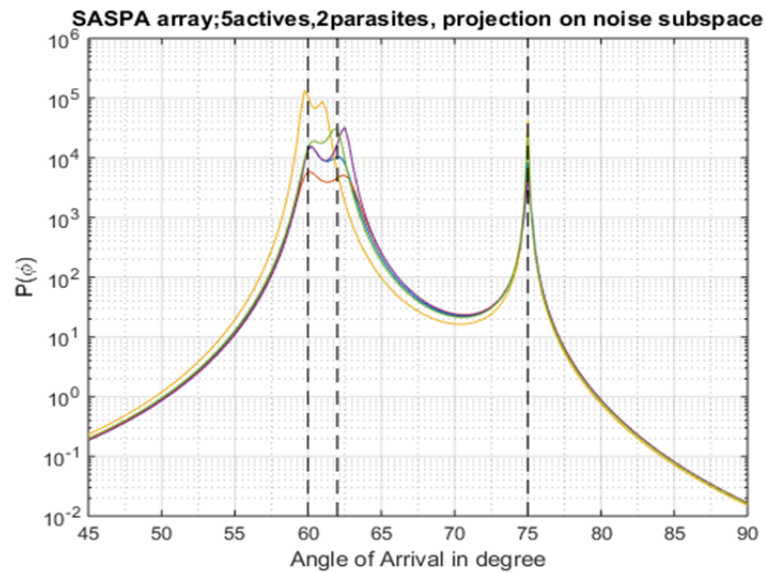
(b)

Figure 4.6: Comparison between the effectiveness of the parasitic subspace and noise subspace when each one of them is used in (4.32) to estimate three signals $\phi_1 = 60°$, $\phi_2 = 62°$ and $\phi_3 = 75°$ with $SNR = 20$ db impinging on a 7-element ULA-SASPA array with $d = 0.25\lambda$. Five runs with 750 snapshots for each run are used. (a) MUSIC spectrum when the parasitic subspace is used; (b) MUSIC spectrum when the noise subspace is used.

4.7   Summary

This chapter explores the well-known and effective algorithm for DOA estimation: MUSIC. The MUSIC algorithm will be used in the next two chapters to investigate the ability of SASPA arrays to produce DOA estimation that is superior to that of conventional all-active arrays. These concepts will be helpful to understand some of the key characteristics provided by SASPA arrays. Mutual coupling is one of the characteristics by which SASPA arrays determine their response to the received signals.

The CVUC model which is found to be an appropriate mutual coupling model for SASPA arrays is used in conjunction with MUSIC to estimate the underlying DOAs. It is shown the mandatory condition that the number of received signals should be less than the number of array elements for a successful DOA estimation can be verified by changing the number of active elements in an SASPA array. This procedure can be executed by varying the number of parasites in an SASPA by setting to zero the load impedances corresponding to the parasites. The result is that DOAs can be detected with very high resolution when the number of active elements exceeds the number of received signals. Eigendecomposing an SASPA array's covariance matrix will result in three orthogonal subspaces: signal, noise and parasitic. It is found by simulation that using the parasitic subspace will lead to better resolution for DOA estimation compared to the noise subspace.

Chapter 5

DOA ESTIMATION USING SASPA ARRAYS WITH KNOWN MUTUAL COUPLING AND COUPLED NOISE

5.1 Introduction

In this chapter and the next chapter, the ability of N-element SASPA arrays to estimate the DOAs of a set of impinging signals with high resolution is explored. The study assumes mutual coupling between the elements of the SASPA array affects both the array elements' response and noise. Thus, the data model that applies is akin to (4.28) which assumes noise is pre-dominantly background noise.

The procedure to obtain a snapshot of measurements from an SASPA array is to leave all antenna elements in the parasitic state while sequentially switch one element from the parasitic state to the active state and back. In other words, a single snapshot consists of a frame of N sub-snapshots. In practice, the aforesaid measurement procedure can be implemented using very high-speed PIN diodes to switch the antenna elements between the active and parasitic state during each sub-snapshot. It is obvious that a fundamental requirement of the measurement procedure is that the bandwidth of the impinging signals must be narrow enough to allow one to assume the N sub-snapshots taken to form one snapshot are taken almost instantaneously.

The mutual coupling model that is used in the study reported in this chapter is the CVUC model derived in Chapter 2, since it was shown in Chapter 3 that this model accommodates the operational mode of SASPA arrays, that is, in each sub-snapshot, only one antenna element is active (its terminals connected by a load impedance) and the remaining ones are parasitic (their terminals shorted together). It shall be assumed the CVUC model is known a priori so that couple-free measurements can be

obtained after decoupling mutual coupling from the measurements. As a result, *N* versions of the underlying steering matrix will be produced. Thus, the signal covariance matrix of SASPA array acting under the CSCN condition will be more accurate compared with the all-active antenna receiving array having the same geometry. In this chapter, the potential enhancement in performance of MUSIC in conjunction with switching SASPA arrays, relative to all-active arrays, is investigated. To ensure the comparison is fair, in the simulation study reported in this chapter, each all-active array will have the same geometry as the SASPA array studied, i.e., same number of elements and same inter-element spacing. Also, mutual coupling that would normally exist in the measurements of the all-active array, is fully compensated.

As a side remark, Sections 4.5 and 4.6 of the previous chapter, which examined the performance of non-switching SASPA arrays with more than one active elements, provides a bridge from all-active arrays to the study of switching SASPA arrays having only one active element in each sub-snapshot.

5.2   Array Data Models

The data model that expresses the response of an SASPA array to the received signals shall be formulated first. This model should depict the spatial-temporal dependence since the observations generated by the antenna array is a function of time and space. In the case of SASPA arrays, the data model should accommodate the fast switching, within a sub-snapshot, of the elements from active to parasitic state or vice versa. This fast switching can be modelled as sub-sampling of one snapshot. Accordingly, a model that includes a representation of the unavoidable time skew of the sub-snapshots is reqruied. In the following, the all-active array data model is derived first in a more general setting, mainly to establish notations and some concepts. The SASPA array data model is then derived.

5.2.1   All-Active Array Data Model

Consider an all-active antenna array (i.e., a conventional antenna array) with N antenna elements where the nth array element, $n = 1, \ldots, N$, has directional gain $G_n(\theta, \phi)$ and is located at $\mathbf{r}_n = [x_n \; y_n \; z_n]^T$. Suppose the array is operating in an isotropic, homogeneous, and non-dispersive medium. The response of the array to a plane wave with wavelength λ (or frequency ω) arriving from direction $\mathbf{u}(\theta, \phi)$

$$\mathbf{u}(\theta, \phi) = \begin{bmatrix} \sin\theta\cos\phi \\ \sin\theta\sin\phi \\ \cos\theta \end{bmatrix} \tag{5.1}$$

is given by the *array response vector*

$$\mathbf{b}(\theta, \phi) = \mathbf{C}_{AA}(\theta, \phi) \begin{bmatrix} G_1(\theta, \phi) e^{jk\mathbf{r}_1^T \mathbf{u}(\theta, \phi)} \\ \vdots \\ G_N(\theta, \phi) e^{jk\mathbf{r}_N^T \mathbf{u}(\theta, \phi)} \end{bmatrix} \tag{5.2}$$

where $\mathbf{C}_{AA}(\theta, \phi) \in \mathbb{C}^{N \times N}$ is the all-active mutual coupling matrix, and k is the wavenumber

$$k = \frac{2\pi}{\lambda} \tag{5.3}$$

Figure 5.1 shows the spatial coordinate system.
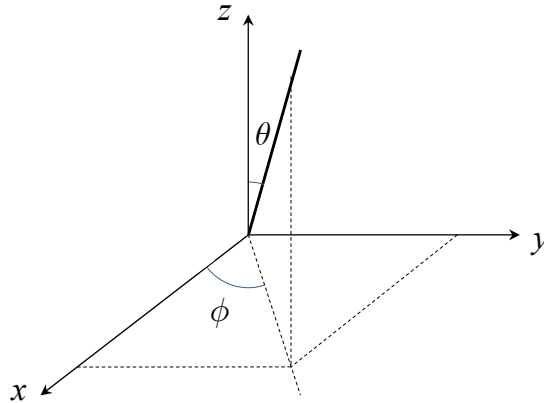
Figure 5.1: The spatial coordinate system

In the literature, the *array manifold vector* is also defined. It is given by

$$
\mathbf{a}(\theta, \phi) = \begin{bmatrix} e^{jk\mathbf{r}_1^T \mathbf{u}(\theta, \phi)} \\ \vdots \\ e^{jk\mathbf{r}_N^T \mathbf{u}(\theta, \phi)} \end{bmatrix}
\tag{5.4}
$$

That is, $\mathbf{a}(\theta, \phi)$ gives, for a signal arriving from $\mathbf{u}(\theta, \phi)$, the phase delays of the signal at the array elements.

In the general case where M signals $s_m(t)$, $m = 1, \ldots, M$, each arriving from $\mathbf{u}(\theta_m, \phi_m)$, are impinging on the array, the output of the array elements, as captured in one snapshot, is given by

$$
\mathbf{x}_{AA}(t) = \begin{bmatrix} \mathbf{b}(\theta_1, \phi_1) & \cdots & \mathbf{b}(\theta_M, \phi_M) \end{bmatrix} \begin{bmatrix} s_1(t) \\ \vdots \\ s_M(t) \end{bmatrix} + \overline{\mathbf{C}}_{AA} \begin{bmatrix} n_{\mathrm{amb},1}(t) \\ \vdots \\ n_{\mathrm{amb},N}(t) \end{bmatrix} + \begin{bmatrix} n_{\mathrm{self},1}(t) \\ \vdots \\ n_{\mathrm{self},N}(t) \end{bmatrix}
\tag{5.5}
$$

where $n_{\mathrm{amb},n}(t)$ is the ambient noise sensed by the nth array element, $n_{\mathrm{self},n}(t)$ is the self or internal noise due to the electronic circuitry of the nth array element, and $\overline{\mathbf{C}}_{AA}$ is the non-directional all-active average mutual coupling matrix

$$
\overline{\mathbf{C}}_{AA} = \frac{1}{4\pi} \int_0^\pi \int_{-\pi}^\pi \mathbf{C}_{AA}(\theta, \phi) \sin\theta \, d\phi \, d\theta
\tag{5.6}
$$

Now, suppose the mutual coupling matrix $\mathbf{C}_{AA}(\theta, \phi)$ is independent of direction, and the element gains $G_n(\theta, \phi)$ are omnidirectional. Equation (5.5) can then be written in the more familiar form

$$
\mathbf{x}_{AA}(t) = \mathbf{C}_{AA} \{ \mathbf{A}(\boldsymbol{\theta}, \boldsymbol{\phi}) \mathbf{s}(t) + \mathbf{n}_{\mathrm{amb}}(t) \} + \mathbf{n}_{\mathrm{self}}(t)
\tag{5.7}
$$

where

$$
\mathbf{A}(\boldsymbol{\theta}, \boldsymbol{\phi}) = \begin{bmatrix} e^{jk\mathbf{r}_1^T \mathbf{u}(\theta_1, \phi_1)} & \cdots & e^{jk\mathbf{r}_1^T \mathbf{u}(\theta_M, \phi_M)} \\ \vdots & & \vdots \\ e^{jk\mathbf{r}_N^T \mathbf{u}(\theta_1, \phi_1)} & \cdots & e^{jk\mathbf{r}_N^T \mathbf{u}(\theta_M, \phi_M)} \end{bmatrix}
\tag{5.8}
$$

$$
\mathbf{s}(t) = \begin{bmatrix} s_1(t) \\ \vdots \\ s_M(t) \end{bmatrix}
\tag{5.9}
$$

$$\mathbf{n}_{\mathrm{amb}}(t) = \begin{bmatrix} n_{\mathrm{amb},1}(t) \\ \vdots \\ n_{\mathrm{amb},N}(t) \end{bmatrix} \tag{5.10}$$

$$\mathbf{n}_{\mathrm{self}}(t) = \begin{bmatrix} n_{\mathrm{self},1}(t) \\ \vdots \\ n_{\mathrm{self},N}(t) \end{bmatrix} \tag{5.11}$$

and

$$\mathbf{C}_{AA} = \mathbf{C}_{AA}(\theta, \phi) = \bar{\mathbf{C}}_{AA} \tag{5.12}$$

Suppose next that the array is planar in the *xy*-plane, and the incident signals are also in the *xy*-plane. In the case of a Uniform Linear Array (ULA) with element #1 at the origin and the other elements distributed uniformly along the +*x* axis, spaced *d* apart, (5.8) then becomes

$$\mathbf{A}_{ULA}(\phi) = \begin{bmatrix} 1 & \cdots & 1 \\ e^{jkd\cos\phi_1} & \cdots & e^{jkd\cos\phi_M} \\ \vdots & & \vdots \\ e^{jkd(N-1)\cos\phi_1} & \cdots & e^{jkd(N-1)\cos\phi_M} \end{bmatrix} \tag{5.13}$$

And in the case of a Uniform Circular Array (UCA) array with radius *R*, centred at the origin, and element #1 located at $\mathbf{r}_1 = [R \ \ 0 \ \ 0]^T$, (5.8) becomes

$$\mathbf{A}_{UCA}(\phi) = \begin{bmatrix} e^{jkR\cos\phi_1} & \cdots & e^{jkR\cos\phi_M} \\ e^{jkR\cos\left(\phi_1 - 2\pi\frac{1}{N}\right)} & \cdots & e^{jkR\cos\left(\phi_M - 2\pi\frac{1}{N}\right)} \\ \vdots & & \vdots \\ e^{jkR\cos\left(\phi_1 - 2\pi\frac{N-1}{N}\right)} & \cdots & e^{jkR\cos\left(\phi_M - 2\pi\frac{N-1}{N}\right)} \end{bmatrix} \tag{5.14}$$

5.2.2 SASPA Array Data Model

For an *N*-element SASPA array, a snapshot is spread over *N* sub-sampling periods. Suppose, with no loss of generality, that element #1 is sampled first, followed by element #2, then by element #3, etc. Let T_s be the sub-sampling period, and $x^{(n)}(t)$

be the output from element n, the active element. A snapshot of an SASPA array is then formed by

$$\mathbf{x}_{SASPA}(t) = \begin{bmatrix} x^{(1)}(t) \\ x^{(2)}(t+T_{\mathrm{s}}) \\ \vdots \\ x^{(N)}(t+(N-1)T_{\mathrm{s}}) \end{bmatrix} = \begin{bmatrix} x^{(1)}(t_1) \\ x^{(2)}(t_2) \\ \vdots \\ x^{(N)}(t_N) \end{bmatrix} \tag{5.15}$$

where, for $n = 1, \ldots, N$,

$$t_n = t + (n-1)T_s \tag{5.16}$$

$$x^{(n)}(t_n) = \begin{bmatrix} b^{(n)}(\theta_1, \phi_1) & \cdots & b^{(n)}(\theta_M, \phi_M) \end{bmatrix} \begin{bmatrix} s_1(t_n) \\ \vdots \\ s_M(t_n) \end{bmatrix}$$

$$+ \left(\overline{\mathbf{c}}^{(n)}_{SASPA}\right)^T \begin{bmatrix} n^{(n)}_{\mathrm{amb},1}(t_n) \\ \vdots \\ n^{(n)}_{\mathrm{amb},N}(t_n) \end{bmatrix} + n_{\mathrm{self},n}(t_n) \tag{5.17}$$

$$b^{(n)}(\theta_m, \phi_m) = \left(\mathbf{c}^{(n)}_{SASPA}(\theta_m, \phi_m)\right)^T \begin{bmatrix} G_1(\theta_m, \phi_m) e^{jk\mathbf{r}_1^T \mathbf{u}(\theta_m, \phi_m)} \\ \vdots \\ G_N(\theta_m, \phi_m) e^{jk\mathbf{r}_N^T \mathbf{u}(\theta_m, \phi_m)} \end{bmatrix} e^{j\omega(n-1)T_s} \tag{5.18}$$

and where $\mathbf{c}^{(n)}_{SASPA}(\theta, \phi)$ and $\overline{\mathbf{c}}^{(n)}_{SASPA}$ are the nth column of the SASPA (CVUC) mutual coupling matrices $\mathbf{C}_{SASPA}(\theta, \phi)$ and $\overline{\mathbf{C}}_{SASPA}$, respectively.

$$\overline{\mathbf{C}}_{SASPA} = \frac{1}{4\pi} \int_0^\pi \int_{-\pi}^\pi \mathbf{C}_{SASPA}(\theta, \phi) \sin\theta \, d\phi d\theta \tag{5.19}$$

Suppose that, relative to T_s, the bandwidths of the incident signals are sufficiently narrow such that

$$s_m(t) \approx s_m(t+(N-1)T_s), \quad m = 1, \ldots, M \tag{5.20}$$

Accordingly, the time-skew due to sub-sampling can be compensated by simply scaling the measurement from the nth array element by $e^{-j\omega(n-1)T_s}$. That is,

$$x_{comp}^{(n)}(t) = e^{-j\omega(n-1)T_s} \cdot x^{(n)}(t_n)$$

$$= \left[b_{comp}^{(n)}(\theta_1, \phi_1) \quad \cdots \quad b_{comp}^{(n)}(\theta_M, \phi_M) \right] \begin{bmatrix} s_1(t) \\ \vdots \\ s_M(t) \end{bmatrix} \tag{5.21}$$

$$+ e^{-j\omega(n-1)T_s} \left\{ \left(\overline{\mathbf{c}}_{SASPA}^{(n)} \right)^T \begin{bmatrix} n_{\text{amb},1}^{(n)}(t_n) \\ \vdots \\ n_{\text{amb},N}^{(n)}(t_n) \end{bmatrix} + n_{\text{self},n}(t_n) \right\}$$

where

$$b_{comp}^{(n)}(\theta_m, \phi_m) = e^{-j\omega(n-1)T_s} \cdot \left(\mathbf{c}_{SASPA}^{(n)}(\theta_m, \phi_m) \right)^T \begin{bmatrix} G_1(\theta_m, \phi_m) e^{jk\mathbf{r}_1^T \mathbf{u}(\theta_m, \phi_m)} \\ \vdots \\ G_N(\theta_m, \phi_m) e^{jk\mathbf{r}_N^T \mathbf{u}(\theta_m, \phi_m)} \end{bmatrix} e^{j\omega(n-1)T_s}$$

$$= \left(\mathbf{c}_{SASPA}^{(n)}(\theta_m, \phi_m) \right)^T \begin{bmatrix} G_1(\theta_m, \phi_m) e^{jk\mathbf{r}_1^T \mathbf{u}(\theta_m, \phi_m)} \\ \vdots \\ G_N(\theta_m, \phi_m) e^{jk\mathbf{r}_N^T \mathbf{u}(\theta_m, \phi_m)} \end{bmatrix} \tag{5.22}$$

If the ambient noise and self-noise terms in (5.21) are circularly complex and mutually independent, then the effect of the time-realignment term $e^{-j\omega(n-1)T_s}$ is simply to rotate them with no effect on their statistical properties. As such, the time-realignment term can be removed from them to yield the following ***time-aligned SASPA array data model***.

$$\mathbf{x}_{comp}(t) = \begin{bmatrix} x_{comp}^{(1)}(t) \\ x_{comp}^{(2)}(t) \\ \vdots \\ x_{comp}^{(N)}(t) \end{bmatrix} = \begin{bmatrix} x^{(1)}(t_1) \\ e^{-j\omega T_s} x^{(2)}(t_2) \\ \vdots \\ e^{-j\omega(N-1)T_s} x^{(N)}(t_N) \end{bmatrix} \tag{5.23}$$

where

$$x_{comp}^{(n)}(t) = \left[b_{comp}^{(n)}(\theta_1, \phi_1) \quad \cdots \quad b_{comp}^{(n)}(\theta_M, \phi_M) \right] \begin{bmatrix} s_1(t) \\ \vdots \\ s_M(t) \end{bmatrix} + \left(\overline{\mathbf{c}}_{SASPA}^{(n)} \right)^T \begin{bmatrix} n_{\text{amb},1}^{(n)}(t_n) \\ \vdots \\ n_{\text{amb},N}^{(n)}(t_n) \end{bmatrix}$$
$$+ n_{\text{self},n}(t_n) \tag{5.24}$$

and $b_{comp}^{(n)}(\theta_m, \phi_m)$ is given by (5.22).

Finally, for the simplified signal scenario often studied in the literature where it is assumed that

(a) the array is operating in the *xy*-plane,

(b) the mutual coupling matrix is independent of the direction of arrival of the impinging signal such that $\mathbf{C}_{SASPA}(\theta, \phi) = \overline{\mathbf{C}}_{SASPA}$

(c) the gain of the array elements is omnidirectional (at least in the *xy*-plane) such that, with no loss of generality, the gain can be set equal to 1,

it follows the sub-sampling time-skew compensated sub-snapshot $x_{comp}^{(n)}(t)$, (5.24), can be simplified to:

$$x_{comp}^{(n)}(t) = \left(\mathbf{c}^{(n)}\right)^T \left\{\mathbf{A}(\phi)\mathbf{s}(t) + \mathbf{n}_{amb}^{(n)}(t_n)\right\} + n_{self,n}(t_n) \tag{5.25}$$

where $\mathbf{A}(\phi)$ is defined by (5.8) with $\theta_1 = \cdots = \theta_M = 90°$, $\mathbf{s}(t)$ is defined by (5.9),

$$\mathbf{n}_{amb}^{(n)}(t_n) = \begin{bmatrix} n_{amb,1}^{(n)}(t_n) \\ \vdots \\ n_{amb,N}^{(n)}(t_n) \end{bmatrix} \tag{5.26}$$

and $\mathbf{c}^{(n)}$ is the *n*th column of the directionless mutual coupling matrix $\mathbf{C}$ where

$$\mathbf{C} = \mathbf{C}_{SASPA}(\theta, \phi) = \overline{\mathbf{C}}_{SASPA} = \begin{bmatrix} \mathbf{c}^{(1)} & \cdots & \mathbf{c}^{(N)} \end{bmatrix} \tag{5.27}$$

Substituting (5.25) into (5.23) yields the reduced ***time-aligned SASPA array data model***

$$\mathbf{x}_{comp}(t) = \mathbf{C}\mathbf{A}(\phi)\mathbf{s}(t) + \begin{bmatrix} \left(\mathbf{c}^{(1)}\right)^T \mathbf{n}_{amb}^{(1)}(t_1) \\ \vdots \\ \left(\mathbf{c}^{(N)}\right)^T \mathbf{n}_{amb}^{(N)}(t_N) \end{bmatrix} + \mathbf{n}_{self}(t) \tag{5.28}$$

where

$$\mathbf{n}_{self}(t) = \begin{bmatrix} n_{self,1}(t_1) \\ \vdots \\ n_{self,N}(t_N) \end{bmatrix} \tag{5.29}$$

5.3 The SASPA Coupled-Signals-Coupled-Noise Model

5.3.1 Direct Model

If ambient noise is the dominant noise source, then the reduced time-aligned SASPA array data model (5.28) can be simplified to the following Coupled-Signals-Coupled-Noise (CSCN) model.

$$\mathbf{f}(t) = \begin{bmatrix} f^{(1)}(t) \\ \vdots \\ f^{(N)}(t) \end{bmatrix} = \mathbf{CA}(\phi)\mathbf{s}(t) + \begin{bmatrix} \left(\mathbf{c}^{(1)}\right)^T \mathbf{n}_{\mathrm{amb}}^{(1)}(t_1) \\ \vdots \\ \left(\mathbf{c}^{(N)}\right)^T \mathbf{n}_{\mathrm{amb}}^{(N)}(t_N) \end{bmatrix} \tag{5.30}$$

The covariance matrix of the time-aligned snapshot $\mathbf{f}(t)$ is given by

$$\mathbf{R_f} = \mathbb{E}\left\{\mathbf{f}(t)\mathbf{f}(t)^H\right\} = \mathbf{R_{fs}} + \mathbf{R_{f}}_n \tag{5.31}$$

where $\mathbf{R_{fs}}$ is the *signal covariance matrix*

$$\begin{aligned}\mathbf{R_{fs}} &= \mathbb{E}\left\{\mathbf{CA}(\phi)\mathbf{s}(t)\mathbf{s}(t)^H \mathbf{A}(\phi)^H \mathbf{C}^H\right\} \\ &= \mathbf{CA}(\phi)\mathbf{S}\mathbf{A}(\phi)^H \mathbf{C}^H \end{aligned} \tag{5.32}$$

$$\mathbf{S} = \mathbb{E}\left\{\mathbf{s}(t)\mathbf{s}(t)^H\right\} \tag{5.33}$$

and $\mathbf{R_{f}}_n$ is the *noise covariance matrix* (see (5.26))

$$\mathbf{R_{f}}_n = \mathbb{E}\left\{ \begin{bmatrix} \left(\mathbf{c}^{(1)}\right)^T \begin{bmatrix} n_{\mathrm{amb},1}^{(1)}(t_1) \\ \vdots \\ n_{\mathrm{amb},N}^{(1)}(t_1) \end{bmatrix} \\ \vdots \\ \left(\mathbf{c}^{(N)}\right)^T \begin{bmatrix} n_{\mathrm{amb},1}^{(N)}(t_N) \\ \vdots \\ n_{\mathrm{amb},N}^{(N)}(t_N) \end{bmatrix} \end{bmatrix} \begin{bmatrix} \begin{bmatrix} n_{\mathrm{amb},1}^{(1)}(t_1) \\ \vdots \\ n_{\mathrm{amb},N}^{(1)}(t_1) \end{bmatrix}^H \left(\mathbf{c}^{(1)}\right)^* & \cdots & \begin{bmatrix} n_{\mathrm{amb},1}^{(N)}(t_N) \\ \vdots \\ n_{\mathrm{amb},N}^{(N)}(t_N) \end{bmatrix}^H \left(\mathbf{c}^{(N)}\right)^* \end{bmatrix} \right\}$$

$$
= \begin{bmatrix} \left(\mathbf{c}^{(1)}\right)^{T} \cdot \sigma_n^2 \mathbf{I} \cdot \left(\mathbf{c}^{(1)}\right)^{*} & \cdots & 0 \\ \vdots & \ddots & \vdots \\ 0 & \cdots & \left(\mathbf{c}^{(N)}\right)^{T} \cdot \sigma_n^2 \mathbf{I} \cdot \left(\mathbf{c}^{(N)}\right)^{*} \end{bmatrix} \tag{5.34}
$$

$$
= \sigma_n^2 \, \mathrm{diag}\left(\left\|\mathbf{c}^{(1)}\right\|_2^2, \ldots, \left\|\mathbf{c}^{(N)}\right\|_2^2\right)
$$

The second equality of (5.34) follows from the assumption that the noise terms are identically distributed, circularly complex Gaussian, and mutually independent. That is, for $n_1, n_2, n_3, n_4 = 1, \ldots, N$

$$
\mathbb{E}\left\{n_{n_1}\left(t_{n_2}\right) n_{n_3}^{*}\left(t_{n_4}\right)\right\} = \begin{cases} \sigma_n^2, & n_1 = n_3 \text{ and } n_1 = n_3 \\ 0, & \text{otherwise} \end{cases} \tag{5.35}
$$

Observe that the noise covariance matrix $\mathbf{R}_{\mathbf{f}n}$ is not a scaled identity matrix. This implies the MUSIC algorithm derived from the direct model will require a generalised eigendecomposition on the estimated data covariance matrix $\mathbf{R}_{\mathbf{f}}$.

5.3.2 Decoupled Model

The reduced CSCN model (5.30) can also be expressed in the decoupled form. It follows from (5.30) that:

$$
\mathbf{f}(t) = \begin{bmatrix} f^{(1)}(t) \\ \vdots \\ f^{(N)}(t) \end{bmatrix} = \begin{bmatrix} \left(\mathbf{c}^{(1)}\right)^{T} & & 0 \\ & \ddots & \\ 0 & & \left(\mathbf{c}^{(N)}\right)^{T} \end{bmatrix} \begin{bmatrix} \mathbf{A}(\phi)\mathbf{s}(t) + \mathbf{n}_{\mathrm{amb}}^{(1)}(t_n) \\ \vdots \\ \mathbf{A}(\phi)\mathbf{s}(t) + \mathbf{n}_{\mathrm{amb}}^{(N)}(t_n) \end{bmatrix}
$$

$$
= \mathbf{\Omega} \begin{bmatrix} \mathbf{A}(\phi)\mathbf{s}(t) + \mathbf{n}_{\mathrm{amb}}^{(1)}(t_n) \\ \vdots \\ \mathbf{A}(\phi)\mathbf{s}(t) + \mathbf{n}_{\mathrm{amb}}^{(N)}(t_n) \end{bmatrix} \tag{5.36}
$$

$$
= \mathbf{\Omega}\,\boldsymbol{\alpha}(t)
$$

where each zero entry in the block diagonal matrix $\mathbf{\Omega} \in \mathbb{C}^{N \times N^2}$ is a $1 \times N$ zero row vector, and $\boldsymbol{\alpha}(t)$ represents the couple-free measurements:

$$\boldsymbol{\alpha}(t) = \begin{bmatrix} \mathbf{A}(\phi)\mathbf{s}(t) + \mathbf{n}_{amb}^{(1)}(t_n) \\ \vdots \\ \mathbf{A}(\phi)\mathbf{s}(t) + \mathbf{n}_{amb}^{(N)}(t_n) \end{bmatrix} \in \mathbb{C}^{N^2 \times 1} \tag{5.37}$$

The system (5.36) consists of N equations in N^2 unknowns (the elements of $\boldsymbol{\alpha}(t)$).
Therefore, it is underdetermined. The Least Square (LS) method can be used to find
the smallest solution for such a system, which is:

$$\boldsymbol{\alpha}(t) = \boldsymbol{\Omega}^H \left(\boldsymbol{\Omega}\boldsymbol{\Omega}^H \right)^{-1} \mathbf{f}(t) = \boldsymbol{\Omega}^\dagger \mathbf{f}(t) \tag{5.38}$$

where $\boldsymbol{\Omega}^\dagger$ is the right pseudo-inverse of $\boldsymbol{\Omega}$ [76]. Note that $\boldsymbol{\Omega}$ has full row rank, i.e.,
$\operatorname{rank}(\boldsymbol{\Omega}) = N$.

The couple-free measurement vector $\boldsymbol{\alpha}(t)$ can be decomposed as:

$$\boldsymbol{\alpha}(t) = \begin{bmatrix} \boldsymbol{\alpha}^{(1)}(t) \\ \vdots \\ \boldsymbol{\alpha}^{(N)}(t) \end{bmatrix} \tag{5.39}$$

where

$$\boldsymbol{\alpha}^{(n)}(t) = \mathbf{A}(\phi)\mathbf{s}(t) + \mathbf{n}_{amb}^{(n)}(t_n) \tag{5.40}$$

is the estimated couple-free measurement when element n is active. Averaging these
measurements yields:

$$\boldsymbol{\gamma}(t) = \frac{1}{N}\sum_{n=1}^{N} \boldsymbol{\alpha}^{(n)}(t) = \mathbf{A}(\phi)\mathbf{s}(t) + \frac{1}{N}\sum_{n=1}^{N} \mathbf{n}_{amb}^{(n)}(t) \tag{5.41}$$

The covariance matrix of $\boldsymbol{\gamma}(t)$ is then:

$$\mathbf{R}_{\gamma} = \mathbb{E}\left\{ \boldsymbol{\gamma}(t)\boldsymbol{\gamma}(t)^H \right\} = \mathbf{R}_{\gamma s} + \mathbf{R}_{\gamma n} \tag{5.42}$$

where the *signal covariance matrix* is given by

$$\begin{aligned} \mathbf{R}_{\gamma s} &= \mathbb{E}\left\{ \mathbf{A}(\phi)\mathbf{s}(t)\mathbf{s}(t)^H \mathbf{A}(\phi)^H \right\} \\ &= \mathbf{A}(\phi)\mathbf{S}\mathbf{A}(\phi)^H \end{aligned} \tag{5.43}$$

and the *noise covariance matrix* is given by (see (5.26))

$$
\mathbf{R}_{\gamma n} = \mathbb{E}\left\{ \frac{1}{N^2}\left(\sum_{n=1}^{N}\mathbf{n}_{\text{amb}}^{(n)}(t)\right)\left(\sum_{n=1}^{N}\mathbf{n}_{\text{amb}}^{(n)}(t)\right)^{H}\right\}
$$

$$
= \frac{1}{N^2}\mathbb{E}\left\{\begin{bmatrix} \sum_{n=1}^{N} n_{\text{amb},1}^{(n)}(t_n) \\ \vdots \\ \sum_{n=1}^{N} n_{\text{amb},N}^{(n)}(t_n) \end{bmatrix}\begin{bmatrix} \sum_{n=1}^{N} n_{\text{amb},1}^{(n)}(t_n)^{*} & \cdots & \sum_{n=1}^{N} n_{\text{amb},N}^{(n)}(t_n)^{*} \end{bmatrix}\right\}
$$

$$
= \frac{1}{N^2}\begin{bmatrix} N\sigma_n^2 & & 0 \\ & \ddots & \\ 0 & & N\sigma_n^2 \end{bmatrix}
$$

$$
= \frac{1}{N}\sigma_n^2\mathbf{I}_N \tag{5.44}
$$

Comparing (5.43) and (5.44) with (5.32) and (5.34), it can be seen that the decoupled model of SASPA arrays improves the SNR of the received signals, implying its data covariance matrix is more accurate. In [77], it is shown that by increasing the SNR, the amount of leakage of the signal subspace into the noise subspace can be reduced. Moreover, in [78], it is shown that by increasing the SNR, the eigenvalues of the signal subspace become larger and, hence, the merging of the signal subspace into the noise subspace is significantly avoided. Therefore, when using $\hat{\mathbf{E}}_S$ in the MUSIC cost function (4.23), more accurate DOA estimates can be obtained since these subspaces are closer, in some sense, to the (unknown) theoretical signal subspaces.

The next two sections point out the enhanced performance of the MUSIC algorithm when ULA-SASPA and UCA-SASPA arrays with small inter-element spacing are used, compared with the performance of the corresponding all-active arrays.

5.4   Simulation Study

To illustrate the benefits of ULA-SASPA and UCA-SASPA arrays and their improved MUSIC performance even when the inter-element spacing is very small, the following simulation study was conducted. The enhancements will be demonstrated by comparing the performance of an array when it is SASPA and when it is all-active. The simulations are carried out for *couple-free* measurements assuming the mutual coupling effect has been first removed.

Figure 5.2 shows the MUSIC spectrum for two signals coming from $\phi_1 = 70°$ and $\phi_2 = 80°$, i.e., they are emanating from a direction close to a ULA array's broadside. The ULA array consists of six identical elements with inter-element spacing of $d = 0.15\lambda$. The SNR of each signal is 15 dB and five runs with 1000 simulation snapshots for each run are shown. Figure 5.3 shows a high-resolution DOA estimation for two signals emanating from $\phi_1 = 80°$ and $\phi_2 = 85°$, and both with $SNR = 30\,dB$, as received by the same ULA-SASPA array. And as before, the simulation was conducted over five runs with 1000 snapshots per run.

The ULA-SASPA array with closely spaced elements has also the capability to improve DOA estimation for signals coming from directions close to the array's end fire, as can be seen from the simulation plots shown in Figure 5.4. The two signals arrive from $\phi_1 = 20°$ and $\phi_2 = 30°$. Their SNRs are both 30 dB. The ULA-SASPA array is the same as that used in the simulation plots shown in Figure 5.2 except $d = 0.12\lambda$. The simulation condition is five runs with 3000 snapshots per run.

Observe that, in spite of the elements of the array being very close to each other, and the DOA of the received signals also being very close, the ULA-SASPA array was able to estimate the DOAs with high resolution due to the effect of multiplying the signal covariance matrix by N relative to the noise covariance matrix, as in (5.43) and (5.44). In contrast, the all-active ULA with the same inter-element spacing failed to find the DOAs of the received signals.

Figure 5.5 shows the DOA estimation by a UCA-SASPA array of two signals with $SNR = 25 \, dB$ coming from directions $\phi_1 = 70°$ and $\phi_2 = 80°$. The array has a radius $R = 0.2\lambda$ and consists of six identical half-wave dipoles. The figure also shows the estimation of the same signals received by a six dipole UCA all-active antenna array with the same radius. Clearly, the UCA-SASPA array succeeded in estimating the signals' DOAs with high resolution despite its very small geometry. In contrast, the UCA all-active array is not able to resolve the received signals.

In Figure 5.6, the same scenario as in the previous simulation is used except the received signals are now coming from $\phi_1 = 20°$ and $\phi_2 = 30°$. Figures 5.5 and 5.6 confirm that a UCA-SASPA array with a small radius has the capability to estimate signals coming from different directions with the same SNR and same number of snapshots. The reason for that is the noise eigenvalues of the data covariance matrix of the UCA-SASPA $\mathbf{R}_\gamma$ are scaled by $1/N$.

ULA-SASPA array

(a)
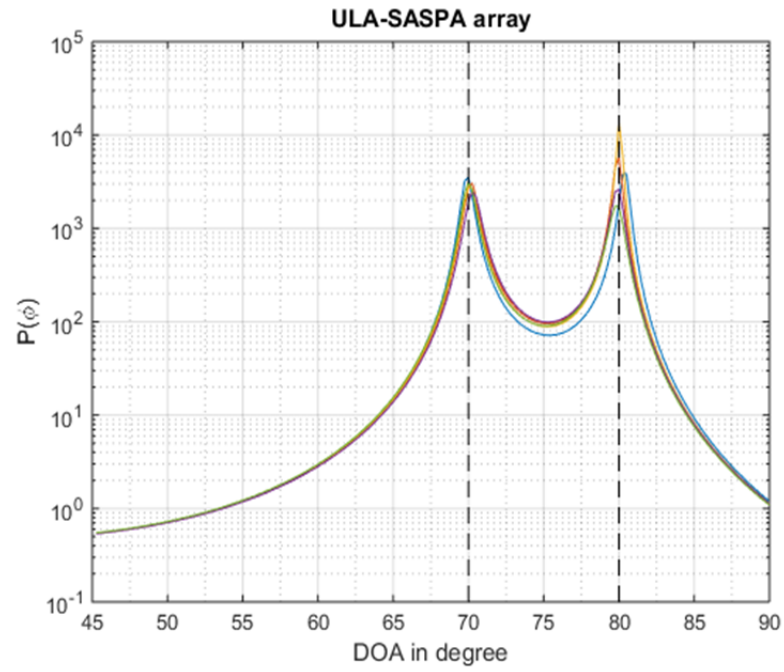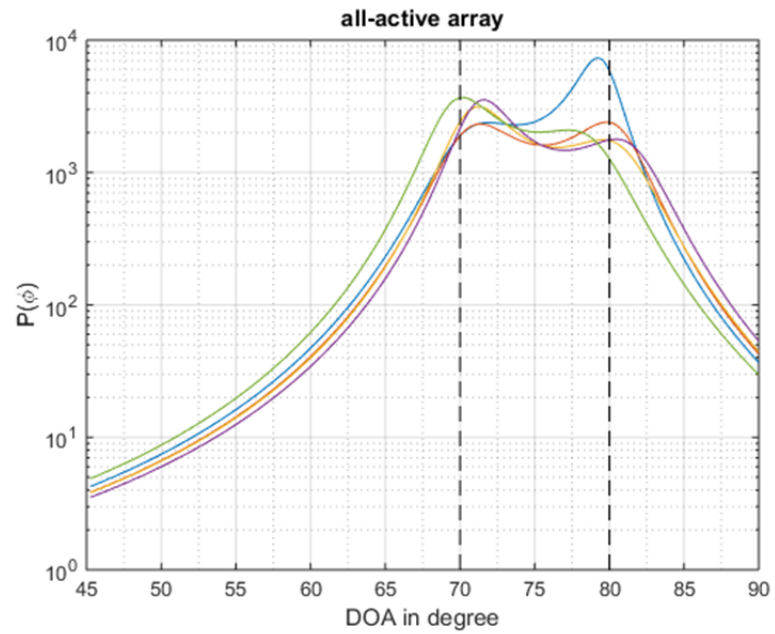
all-active array

(b)

Figure 5.2: MUSIC spectrums for two signals with SNR 15 dB coming from $\phi_1 = 70°$ and $\phi_2 = 80°$. ULA has 6 identical dipoles with inter-element spacing $d = 0.15\lambda$. 5 runs with 1000 simulation snapshots per run are used. (a) ULA-SASPA array; (b) ULA all-active array.
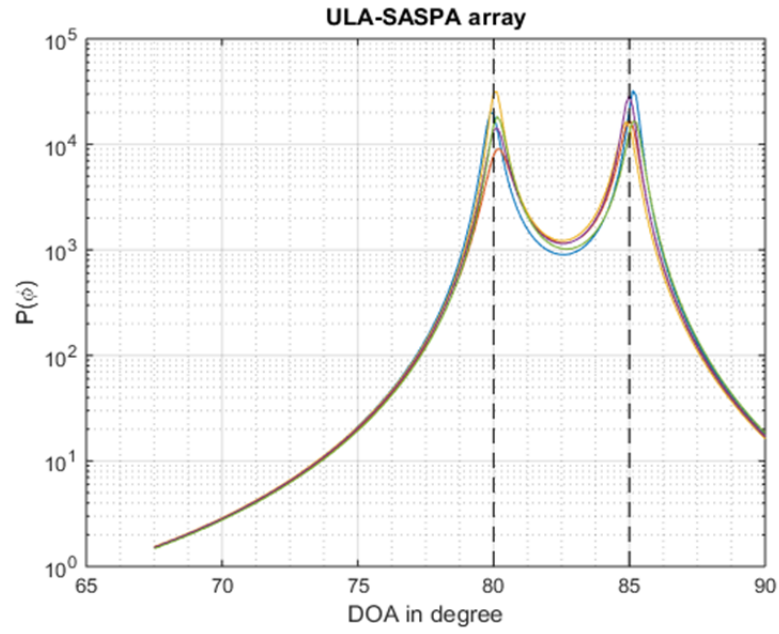
(a)
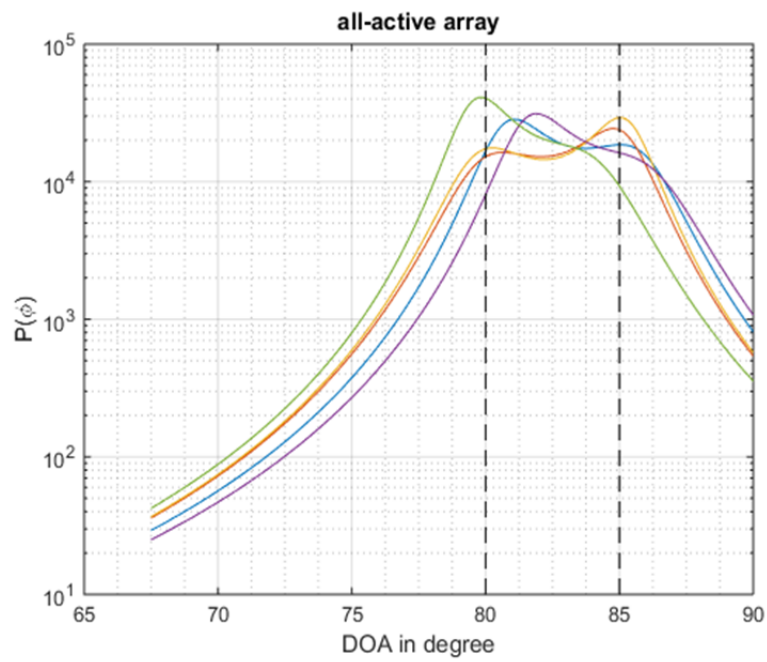
(b)

Figure 5.3: MUSIC spectrum for two closely signals with SNR 30 dB coming from $\phi_1 = 80°$ and $\phi_2 = 85°$. Array and simulation conditions same as in Figure 5.2. (a) ULA-SASPA array; (b) ULA all-active array.
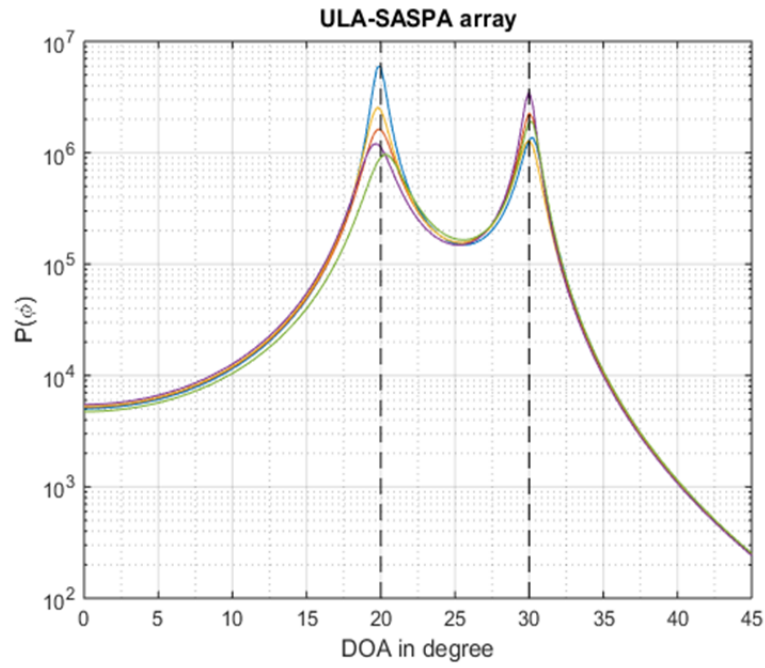
(a)
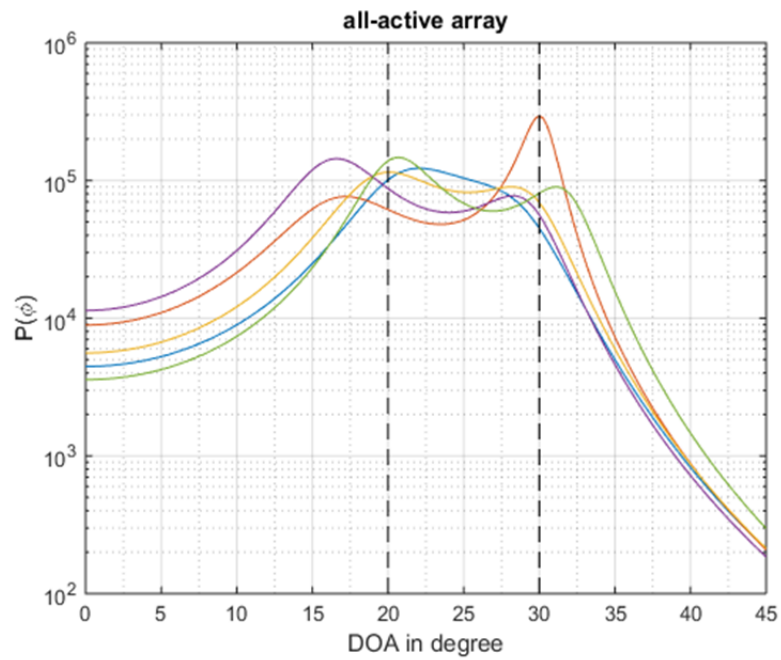
(b)

Figure 5.4: MUSIC spectrum for two signals with SNR 35 dB coming from $\phi_1 = 20°$ and $\phi_2 = 30°$. Array same as in Figures 5.2 and 5.3 except $d = 0.12\lambda$. Simulation conducted over 5 runs and 3000 snapshots per run. (a) ULA-SASPA array; (b) ULA all-active array.
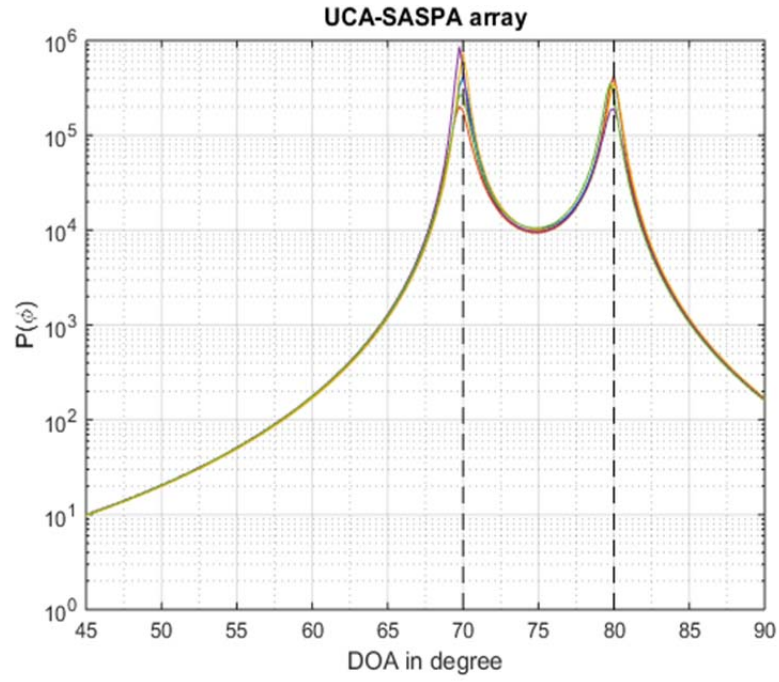
(a)
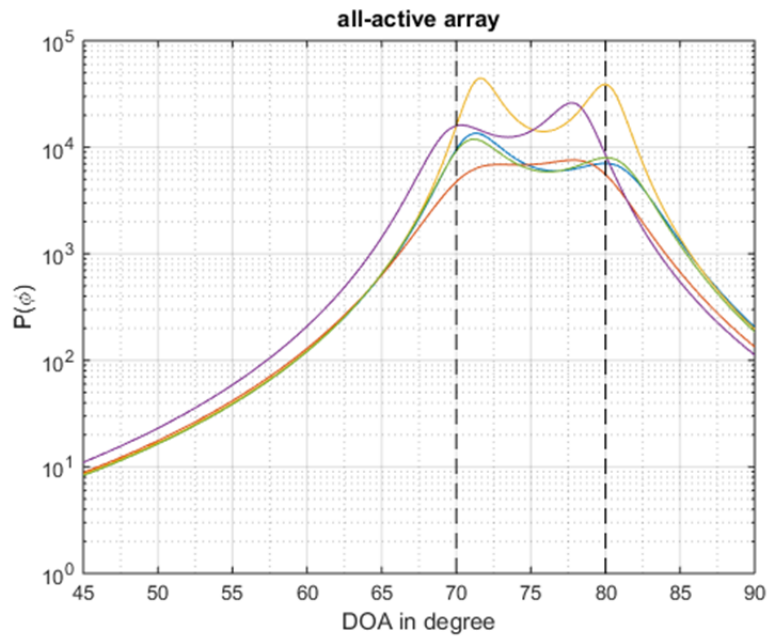
(b)

Figure 5.5: Comparison between the estimation of two signals coming from direction $\phi_1 = 70°$ and $\phi_2 = 80°$ with $\text{SNR} = 25$ dB and incident on (a) UCA-SASPA array with six identical half wave dipoles and radius $R = 0.2\lambda$; (b) similar UCA all-active array.
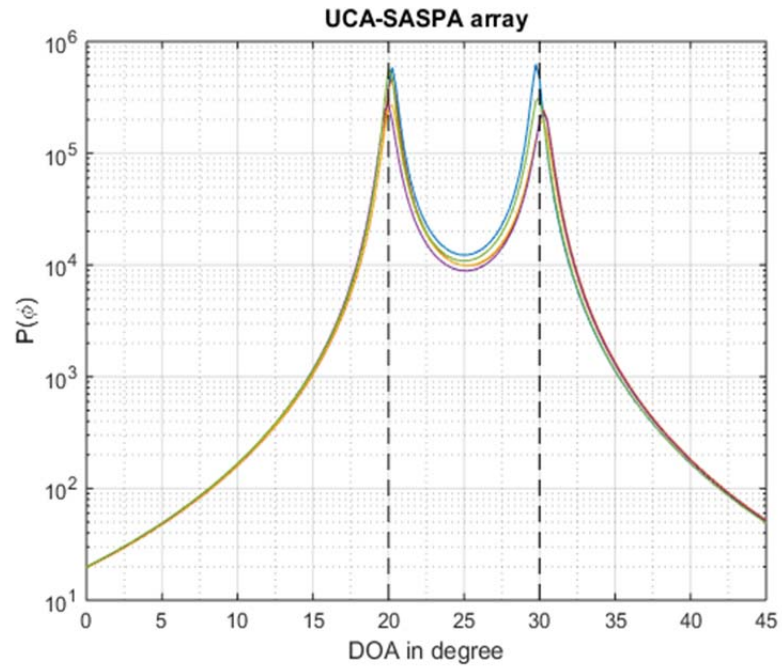
(a)
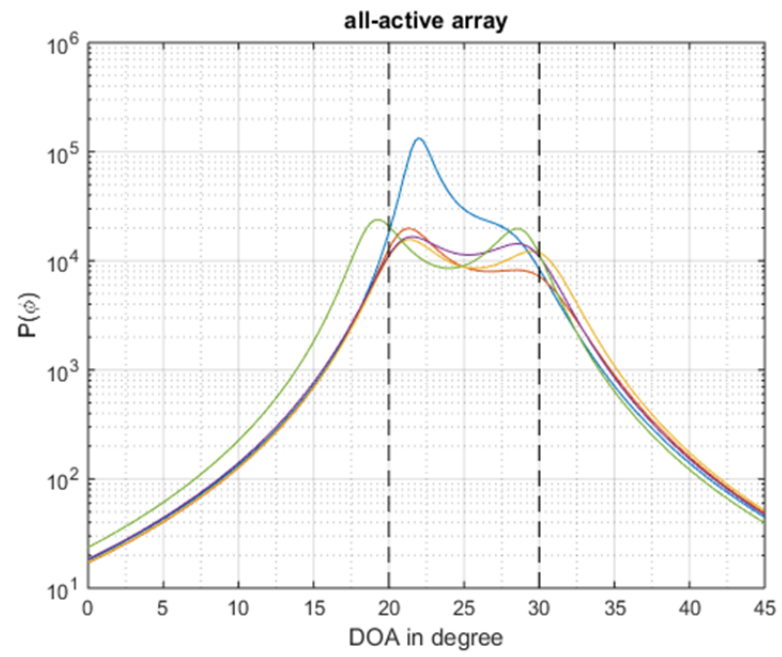
(b)

Figure 5.6: DOA estimation for the same scenario as in Figure 5.5 but for the signals coming from directions $\phi_1 = 20°$ and $\phi_2 = 30°$.

5.5   RMSE Simulations

To confirm the improvement provided by ULA-SASPA arrays in DOA estimation over the corresponding all-active arrays, the criteria Root Mean Square Error (RMSE) which is defined as:

$$\text{RMSE} = \sqrt{\frac{\sum_{i=1}^{L}\left(\hat{\phi}_i - \phi_1\right)^2}{L}} \qquad (5.45)$$

will be considered in the following simulation study where $\hat{\phi}_i$ is the estimated value of the DOA calculated from ith simulation run and ϕ_1 is the actual or true value of the DOA.

Figure 5.7a shows the variation of RMSE against the SNR of a received signal coming from $\phi_1 = 80°$, i.e., from a direction close to the broadside of a ULA-SASPA array. The array consists of four identical dipole elements with $d = 0.15\lambda$. The simulation was conducted for 100 runs with 100 snapshots for each run. The simulation is compared with a ULA all-active array with the same structure. Another comparison is shown in Figure 5.7b which was carried out for the same arrays, but with the signal arriving from $\phi_1 = 20°$, which is close to the end fire direction. It is clear from Figure 5.7 that the ULA-SASPA array has lowered the RMSE of the all-active array.

Figure 5.8 illustrates how a UCA-SASPA array performs over a range of SNR through investigating the RMSE criterion of (5.45). Figure 5.8a shows the variation of RMSE against SNR for a signal emanating from $\phi_1 = 80°$, and impinging on a six-element UCA-SASPA array with $R = 0.2\lambda$. 100 simulation runs with 50 snapshots for each run were conducted to establish this plot. Figure 5.8b is a plot of RMSE versus SNR for a received signal from $\phi_1 = 20°$ impinging on the same array. The simulations show that the UCA-SASPA array has also lowered its RMSE with respect to the all-active array irrespective of the direction of the received signals.
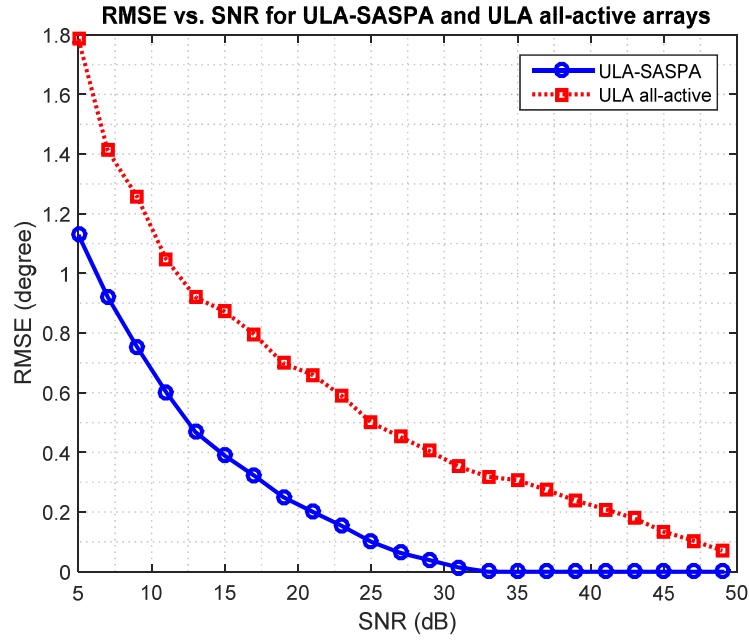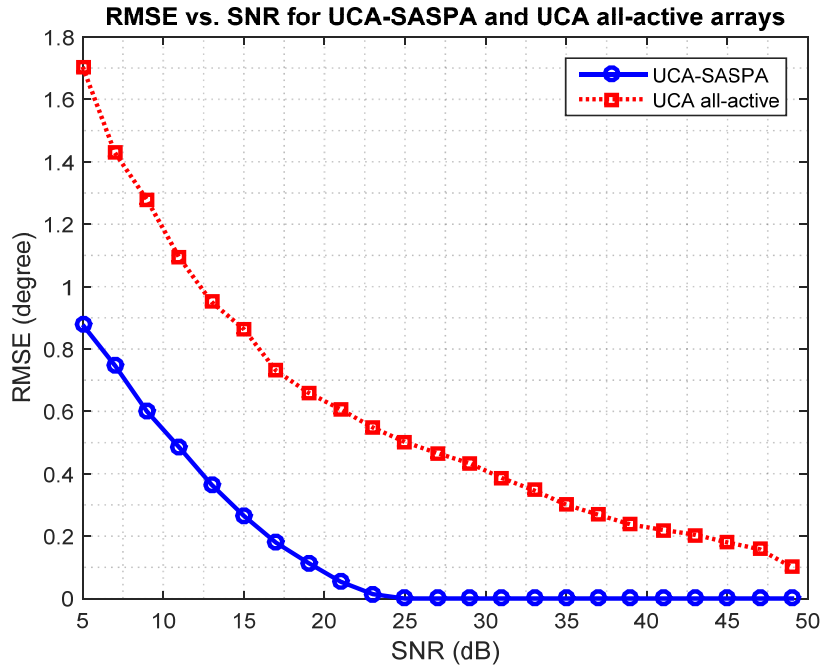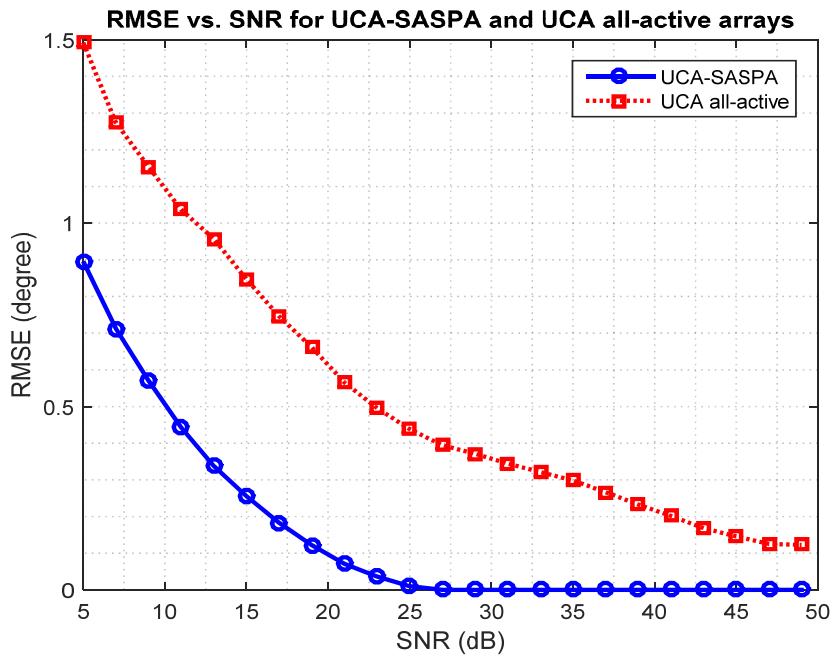
(a)
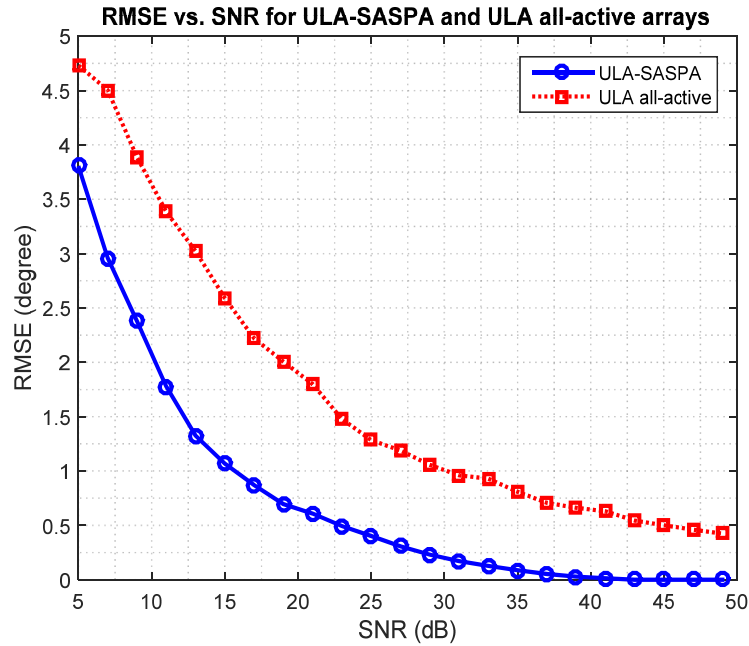
(b)

Figure 5.7: Two simulations illustrating the variation of RMSE of the estimated DOA of a single signal against its SNR. The signal is received by a ULA-SASPA array consisting of four identical antenna elements with $d = 0.15\lambda$. 100 runs with 100 snapshots for every run are used. The signal direction is (a) $\phi_l = 80°$; (b) $\phi_l = 20°$.

RMSE vs. SNR for UCA-SASPA and UCA all-active arrays

(a)

RMSE vs. SNR for UCA-SASPA and UCA all-active arrays

(b)

Figure 5.8: Two simulations to illustrate the variation of RMSE of the estimated DOA of a single signal against its SNR. The signal is received by a UCA-SASPA array consisting of four identical antenna elements with $R = 0.2\lambda$. 100 runs with 50 snapshots for every run are used. The signal direction is is (a) $\phi_1 = 80°$; (b) $\phi_1 = 20°$.

5.6 Summary

The data model for an *N*-element SASPA array of arbitrary geometry is developed in this chapter. This model includes both coupled noise and self noise. The consequence of assembling a data snapshot from the sequentially measured sub-snapshots is also included in the model. It is shown that the time misalignment resulting from the delays in acquiring the sub-snapshots can be compensated easily by applying an appropriate phase rotation to each measured sub-snapshot.

This chapter illustrates the performance of ULA-SASPA and UCA-SASPA arrays as direction finding arrays in conjunction with the MUSIC algorithm assuming mutual coupling is known, and the noise developed at the array elements are coupled between them. Decoupling the mutual coupling results in N^2 measurements from which a scaled steering matrix is obtained. The scaling matrix represents a gain provided by SASPA arrays to the received signals despite the elements of the arrays being close together. This benefit improves the performance of SASPA arrays as direction finding arrays compared to all-active antenna arrays with the same geometrical structure. The reason behind this improvement is the decrease in the distance measure between the signal subspace and the related steering matrix, thereby reducing the leakage of the signal subspace into the noise subspace.

Computer simulations have been carried out to gain a good view about the enhancement provided by SASPA arrays over all-active arrays when acting as DF arrays and to support the theoretical conclusion mentioned above. Also, RMSE plots show that SASPA arrays have lower RMSE than all-active antenna arrays. This benefit can be exploited when the DOAs of signals with low SNR are required to be estimated.

In the next chapter, high resolution direction finding with SASPA arrays operating with uncoupled noise is explored.

Chapter 6

DOA ESTIMATION USING ULA-SASPA ARRAYS WITH KNOWN MUTUAL COUPLING AND UNCOUPLED NOISE

6.1   Introduction

In this chapter, it is assumed that receiver self-noise is the dominant noise. This noise is not exchanged between the array elements through mutual coupling [17][24]. Assuming the SASPA array is operating under the simplified signal scenario described in Section 5.2.2, it follows from the reduced time-aligned SASPA array data model (5.28) that the Coupled-Signals-Uncoupled-Noise (CSUN) model is given by:

$$\mathbf{g}(t) = \begin{bmatrix} g^{(1)}(t) \\ \vdots \\ g^{(N)}(t) \end{bmatrix} = \mathbf{CA}(\phi)\mathbf{s}(t) + \mathbf{n}_{\text{self}}(t) \tag{6.1}$$

where from (5.29)

$$\mathbf{n}_{\text{self}}(t) = \begin{bmatrix} n_{\text{self},1}(t_1) \\ \vdots \\ n_{\text{self},N}(t_N) \end{bmatrix} \tag{6.2}$$

As can be readily shown, the covariance matrix of $\mathbf{g}(t)$ is given by

$$\mathbf{R_g} = \mathbb{E}\left\{\mathbf{g}(t)\mathbf{g}(t)^H\right\} = \mathbf{R}_{\mathbf{g}s} + \mathbf{R}_{\mathbf{g}n} \tag{6.3}$$

where, as with (5.32), the *signal covariance matrix* is

$$\mathbf{R}_{\mathbf{g}s} = \mathbf{CA}(\phi)\mathbf{SA}(\phi)^H \mathbf{C}^H \tag{6.4}$$

and the *noise covariance matrix* is

$$\mathbf{R}_{\mathbf{g}n} = \sigma_n^2 \mathbf{I}_N \tag{6.5}$$

6.2 Coupled-Signals-Uncoupled-Noise: the $\mathbf{z}(t)$ Model for ULA-SASPA Arrays

Consider now an *N*-element **ULA-SASPA** array consisting of half-wave dipoles with inter-element spacing *d* and operating in the *xy*-plane, and whose dominant noise source is internal self-noise. Suppose *N* is even. The $\mathbf{z}(t)$ model of a ULA-SASPA array operating under the CSUN condition is defined by:

$$
\mathbf{z}(t) = \begin{vmatrix} \frac{1}{2}\left(g^{(1)}(t) + g^{(N)}(t)\right) \\ \frac{1}{2}\left(g^{(2)}(t) + g^{(N-1)}(t)\right) \\ \vdots \\ \frac{1}{2}\left(g^{(N/2)}(t) + g^{(N/2+1)}(t)\right) \\ \frac{1}{2j}\left(g^{(1)}(t) - g^{(N)}(t)\right) \\ \frac{1}{2j}\left(g^{(2)}(t) - g^{(N-1)}(t)\right) \\ \vdots \\ \frac{1}{2j}\left(g^{(N/2)}(t) - g^{(N/2+1)}(t)\right) \end{vmatrix} = \frac{1}{2}\begin{bmatrix} \mathbf{I}_{N/2} & \mathbf{J}_{N/2} \\ -j\mathbf{I}_{N/2} & j\mathbf{J}_{N/2} \end{bmatrix}\mathbf{g}(t) \tag{6.6}
$$

where $\mathbf{I}_k$ and $\mathbf{J}_k$ are, respectively, the $k \times k$ identity matrix and the $k \times k$ exchange matrix.

The ***noise covariance matrix*** can be found as follows:

$$
\mathbf{R_{zn}} = \mathbb{E}\left\{ \frac{1}{2}\begin{bmatrix} \mathbf{I}_{N/2} & \mathbf{J}_{N/2} \\ -j\mathbf{I}_{N/2} & j\mathbf{J}_{N/2} \end{bmatrix} \mathbf{n}_{\text{self}}(t)\mathbf{n}_{\text{self}}(t)^H \begin{bmatrix} \mathbf{I}_{N/2} & j\mathbf{I}_{N/2} \\ \mathbf{J}_{N/2} & -j\mathbf{J}_{N/2} \end{bmatrix} \frac{1}{2} \right\}
$$

$$
= \frac{1}{4}\begin{bmatrix} \mathbf{I}_{N/2} & \mathbf{J}_{N/2} \\ -j\mathbf{I}_{N/2} & j\mathbf{J}_{N/2} \end{bmatrix} \cdot \sigma_n^2 \mathbf{I}_N \cdot \begin{bmatrix} \mathbf{I}_{N/2} & j\mathbf{I}_{N/2} \\ \mathbf{J}_{N/2} & -j\mathbf{J}_{N/2} \end{bmatrix} \tag{6.7}
$$

$$
= \frac{1}{2}\sigma_n^2 \mathbf{I}_N
$$

To find the signal covariance matrix, suppose, with no loss of generality, that the array geometry is as shown in Figure 6.1. As can be readily shown, the array

manifold vector is given by

$$\mathbf{a}_{ULA}(\phi) = \left[e^{-jk\left(\frac{N-1}{2}\right)d\cos\phi} \quad e^{-jk\left(\frac{N-3}{2}\right)d\cos\phi} \quad \cdots \quad e^{+jk\left(\frac{N-1}{2}\right)d\cos\phi} \right]^T \tag{6.8}$$

whereupon the steering matrix for signals arriving from $\phi_1, \ldots, \phi_M$ is given by

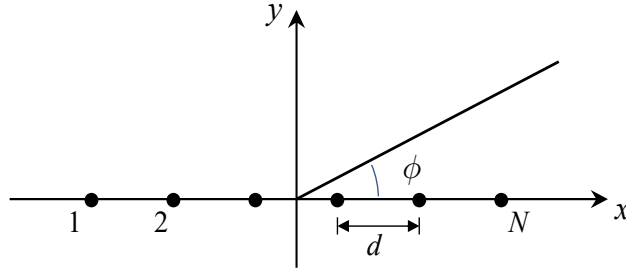$$\mathbf{A}_{ULA}(\Phi) = \left[\mathbf{a}_{ULA}(\phi_1) \quad \cdots \quad \mathbf{a}_{ULA}(\phi_M) \right] \tag{6.9}$$

Figure 6.1: A ULA-SASPA antenna array with even number of elements and located symmetrically about the y-axis.

Now, from (6.1), (6.6) and (6.9)

$$\mathbf{z}(t) = \frac{1}{2} \begin{bmatrix} \mathbf{I}_{N/2} & \mathbf{J}_{N/2} \\ -j\mathbf{I}_{N/2} & j\mathbf{J}_{N/2} \end{bmatrix} \mathbf{g}(t) = \mathbf{T}\left(\mathbf{C}\mathbf{A}_{ULA}(\Phi)\mathbf{s}(t) + \mathbf{n}_{\text{self}}(t) \right) \tag{6.10}$$

where

$$\mathbf{T} = \frac{1}{2} \begin{bmatrix} \mathbf{I}_{N/2} & \mathbf{J}_{N/2} \\ -j\mathbf{I}_{N/2} & j\mathbf{J}_{N/2} \end{bmatrix} \tag{6.11}$$

The *signal covariance matrix* under the $\mathbf{z}(t)$ model is then given by

$$\mathbf{R}_{\mathbf{z}s} = \mathbf{T}\mathbf{C}\mathbf{A}_{ULA}(\Phi)\mathbf{S}\mathbf{A}_{ULA}(\Phi)^H \mathbf{C}^H\mathbf{T}^H \tag{6.12}$$

An alternative expression for the signal covariance matrix can be derived as follows. As can be readily verified, (6.8) has the property that

$$\mathbf{a}_{ULA}(\phi) = \mathbf{J}_N \mathbf{a}_{ULA}^*(\phi) \tag{6.13}$$

Therefore

$$\mathbf{A}_{ULA}(\phi) = \mathbf{J}_N \mathbf{A}_{ULA}(\phi)^* \tag{6.14}$$

Also, since the mutual coupling matrix is symmetrical and Toeplitz,

$$\mathbf{c}^{(N+1-n)} = \mathbf{J}_N \mathbf{c}^{(n)} \tag{6.15}$$

Accordingly

$$
\begin{aligned}
\left(\mathbf{c}^{(n)}\right)^T & \mathbf{A}_{ULA}(\phi) + \left(\mathbf{c}^{(N+1-n)}\right)^T \mathbf{A}_{ULA}(\phi) \\
&= \left(\mathbf{c}^{(n)}\right)^T \mathbf{A}_{ULA}(\phi) + \left(\mathbf{c}^{(n)}\right)^T \mathbf{J}_N \cdot \mathbf{J}_N \mathbf{A}_{ULA}(\phi)^* \\
&= \left(\mathbf{c}^{(n)}\right)^T \mathbf{A}_{ULA}(\phi) + \left(\mathbf{c}^{(n)}\right)^T \mathbf{A}_{ULA}(\phi)^* \\
&= 2\left(\mathbf{c}^{(n)}\right)^T \mathrm{Re}\left(\mathbf{A}_{ULA}(\phi)\right)
\end{aligned}
\tag{6.16}
$$

Likewise

$$-j\left(\mathbf{c}^{(n)}\right)^T \mathbf{A}_{ALU}(\phi) + j\left(\mathbf{c}^{(N+1-n)}\right)^T \mathbf{A}_{ALU}(\phi) = 2\left(\mathbf{c}^{(n)}\right)^T \mathrm{Im}\left(\mathbf{A}_{ALU}(\phi)\right) \tag{6.17}$$

In other words, the $\mathbf{z}(t)$ model can be expressed as

$$\mathbf{z}(t) = \mathbf{M}(\phi)\mathbf{s}(t) + \mathbf{Tn}_{\mathrm{self}}(t) \tag{6.18}$$

where

$$\mathbf{z}(t) = \begin{bmatrix} \mathbf{z}_1(t) \\ \mathbf{z}_2(t) \end{bmatrix} \in \mathbb{C}^{N \times 1} \tag{6.19}$$

$$\mathbf{z}_1(t) = \begin{bmatrix} \frac{1}{2}\left(g^{(1)}(t) + g^{(N)}(t)\right) \\ \vdots \\ \frac{1}{2}\left(g^{(N/2)}(t) + g^{(N/2+1)}(t)\right) \end{bmatrix} \in \mathbb{C}^{\frac{N}{2} \times 1} \tag{6.20}$$

$$\mathbf{z}_2(t) = \begin{bmatrix} \frac{1}{2j}\left(g^{(1)}(t) - g^{(N)}(t)\right) \\ \vdots \\ \frac{1}{2j}\left(g^{(N/2)}(t) - g^{(N/2+1)}(t)\right) \end{bmatrix} \in \mathbb{C}^{\frac{N}{2} \times 1} \tag{6.21}$$

$$\mathbf{M}(\phi) = \begin{bmatrix} \mathbf{M}_1(\phi) \\ \mathbf{M}_2(\phi) \end{bmatrix} \in \mathbb{R}^{N \times M} \tag{6.22}$$

$$\mathbf{M}_1(\phi) = \frac{1}{2} \begin{bmatrix} \left(\mathbf{c}^{(1)}\right)^T \\ \vdots \\ \left(\mathbf{c}^{(N/2)}\right)^T \end{bmatrix} \left(\mathbf{A}_{ULA}(\phi) + \mathbf{A}_{ULA}(\phi)^*\right) = \mathbf{C}'^T \operatorname{Re}\left(\mathbf{A}_{ULA}(\phi)\right) \in \mathbb{C}^{\frac{N}{2} \times M} \tag{6.23}$$

$$\mathbf{M}_2(\phi) = \frac{1}{2j} \begin{bmatrix} \left(\mathbf{c}^{(1)}\right)^T \\ \vdots \\ \left(\mathbf{c}^{(N/2)}\right)^T \end{bmatrix} \left(\mathbf{A}_{ULA}(\phi) - \mathbf{A}_{ULA}(\phi)^*\right) = \mathbf{C}'^T \operatorname{Im}\left(\mathbf{A}_{ULA}(\phi)\right) \in \mathbb{C}^{\frac{N}{2} \times M} \tag{6.24}$$

and

$$\mathbf{C}' = \begin{bmatrix} \mathbf{c}^{(1)} & \cdots & \mathbf{c}^{(N/2)} \end{bmatrix} \in \mathbb{C}^{N \times \frac{N}{2}} \tag{6.25}$$

i.e., $\mathbf{C}'$ consists of the first $N/2$ columns of the mutual coupling matrix $\mathbf{C}$

$$\mathbf{C}' = \begin{bmatrix} c_{11} & c_{12} & c_{13} & \cdots & c_{1\left(\frac{N}{2}\right)} \\ c_{12} & c_{11} & c_{12} & \cdots & c_{1\left(\frac{N}{2}-1\right)} \\ c_{13} & c_{12} & c_{11} & \cdots & c_{1\left(\frac{N}{2}-2\right)} \\ c_{14} & c_{13} & c_{12} & \cdots & c_{1\left(\frac{N}{2}-3\right)} \\ \vdots & \vdots & \vdots & & \vdots \\ c_{1N} & c_{1(N-1)} & c_{1(N-2)} & \cdots & c_{1\left(\frac{N}{2}+1\right)} \end{bmatrix} \tag{6.26}$$

Now, from (6.8) and (6.9)

$$\operatorname{Re}\left(\mathbf{A}_{ULA}(\phi)\right) = \begin{bmatrix} \operatorname{Re}\left(\mathbf{a}_{ULA}(\phi_1)\right) & \cdots & \operatorname{Re}\left(\mathbf{a}_{ULA}(\phi_M)\right) \end{bmatrix} \in \mathbb{R}^{N \times M} \tag{6.27}$$

and

$$\operatorname{Im}\left(\mathbf{A}_{ULA}(\phi)\right) = \begin{bmatrix} \operatorname{Im}\left(\mathbf{a}_{ULA}(\phi_1)\right) & \cdots & \operatorname{Im}\left(\mathbf{a}_{ULA}(\phi_M)\right) \end{bmatrix} \in \mathbb{R}^{N \times M} \tag{6.28}$$

where

$$\operatorname{Re}\left(\mathbf{a}_{ULA}(\phi_m)\right) = \begin{bmatrix} \cos\left(\frac{1-N}{2}\right)\psi_m & \cos\left(\frac{3-N}{2}\right)\psi_m & \cdots & \cos\left(\frac{N-1}{2}\right)\psi_m \end{bmatrix}^T \tag{6.29}$$

$$\mathrm{Im}\left(\mathbf{a}_{ULA}(\phi_m)\right)=\left[\sin\left(\frac{1-N}{2}\right)\psi_m \quad \sin\left(\frac{3-N}{2}\right)\psi_m \quad \cdots \quad \sin\left(\frac{N-1}{2}\right)\psi_m\right]^T \tag{6.30}$$

and

$$\psi_m = kd\cos\phi_m \tag{6.31}$$

As can be seen, (6.29) and (6.30) exhibit the following symmetries.

$$\mathrm{Re}\left(\mathbf{a}_{ULA}(\phi_m)\right)=\mathbf{J}_N\,\mathrm{Re}\left(\mathbf{a}_{ULA}(\phi_m)\right) \tag{6.32}$$

and

$$\mathrm{Im}\left(\mathbf{a}_{ULA}(\phi_m)\right)=-\mathbf{J}_N\,\mathrm{Im}\left(\mathbf{a}_{ULA}(\phi_m)\right) \tag{6.33}$$

Therefore, partitioning $\mathbf{C}'$ as follows

$$\mathbf{C}'=\begin{bmatrix}\mathbf{C}'_1\\ \mathbf{C}'_2\end{bmatrix} \tag{6.34}$$

where $\mathbf{C}'_1 \in \mathbb{C}^{\frac{N}{2}\times\frac{N}{2}}$ and $\mathbf{C}'_2 \in \mathbb{C}^{\frac{N}{2}\times\frac{N}{2}}$, and defining

$$\mathbf{a}_{ULA,\cos}(\phi_m)=\left[\cos\left(\frac{N-1}{2}\right)\psi_m \quad \cos\left(\frac{N-3}{2}\right)\psi_m \quad \cdots \quad \cos\left(\frac{1}{2}\right)\psi_m\right]^T \in \mathbb{R}^{\frac{N}{2}\times 1} \tag{6.35}$$

$$\mathbf{a}_{ULA,\sin}(\phi_m)=\left[\sin\left(\frac{N-1}{2}\right)\psi_m \quad \sin\left(\frac{N-3}{2}\right)\psi_m \quad \cdots \quad \sin\left(\frac{1}{2}\right)\psi_m\right]^T \in \mathbb{R}^{\frac{N}{2}\times 1} \tag{6.36}$$

$$\mathbf{C}''_{\cos}=\left(\mathbf{C}'_1+\mathbf{J}_{N/2}\mathbf{C}'_2\right)\in\mathbb{C}^{\frac{N}{2}\times\frac{N}{2}} \tag{6.37}$$

and

$$\mathbf{C}''_{\sin}=\left(-\mathbf{C}'_1+\mathbf{J}_{N/2}\mathbf{C}'_2\right)\in\mathbb{C}^{\frac{N}{2}\times\frac{N}{2}} \tag{6.38}$$

It can be verified that (6.23) and (6.24) can be written as

$$\mathbf{M}_1(\phi)=\left(\mathbf{C}''_{\cos}\right)^T\mathbf{A}_{ULA,\cos}(\phi) \tag{6.39}$$

$$\mathbf{M}_2(\phi)=\left(\mathbf{C}''_{\sin}\right)^T\mathbf{A}_{ULA,\sin}(\phi) \tag{6.40}$$

where

$$A_{ULA,\cos}(\phi) = \begin{bmatrix} a_{ULA,\cos}(\phi_1) & \cdots & a_{ULA,\cos}(\phi_M) \end{bmatrix} \in \mathbb{R}^{\frac{N}{2} \times M} \tag{6.41}$$

and

$$A_{ULA,\sin}(\phi) = \begin{bmatrix} a_{ULA,\sin}(\phi_1) & \cdots & a_{ULA,\sin}(\phi_M) \end{bmatrix} \in \mathbb{R}^{\frac{N}{2} \times M} \tag{6.42}$$

The *signal covariance matrix* of $z(t)$ is also given, therefore, by

$$R_{zs} = \mathbb{E}\left[M(\phi)s(t)s(t)^H M(\phi)^H \right] = M(\phi)SM(\phi)^H \tag{6.43}$$

where

$$M(\phi) = \begin{bmatrix} (C''_{\cos})^T A_{ULA,\cos}(\phi) \\ (C''_{\sin})^T A_{ULA,\sin}(\phi) \end{bmatrix} \tag{6.44}$$

Remarks

(a) It is worthwhile to comment here that, from (6.10), (6.22)-(6.24), and (6.44), $M(\phi)$ has the following equivalent expressions:

$$M(\phi) = TCA_{ULA}(\phi) = \begin{bmatrix} C'^T \operatorname{Re}(A_{ULA}(\phi)) \\ C'^T \operatorname{Im}(A_{ULA}(\phi)) \end{bmatrix} = \begin{bmatrix} (C''_{\cos})^T A_{ULA,\cos}(\phi) \\ (C''_{\sin})^T A_{ULA,\sin}(\phi) \end{bmatrix} \tag{6.45}$$

Another expression involving only the first column of the mutual coupling matrix C will be presented in the next section.

(b) A significant feature of the $z(t)$ model of (6.18) is that, compared to the direct measurement model of (6.1), the noise covariance matrix of $z(t)$ is halved, see (6.5) and (6.7). More accurate estimates of the true data covariance matrix can thus be achieved with the $z(t)$ model, leading to more accurate estimates of the incident signals' DOA.

(c) Another important feature of the $z(t)$ model is that $A_{ULA,\cos}(\phi)$ and $A_{ULA,\sin}(\phi)$ in (6.44) are real-valued matrices. This can result in a reduction in the computational load when simulating a ULA-SASPA array operating under

the coupled-signals-uncoupled-noise model of (6.1) [65][74][85][86]. It may also lead to a reduction in the computational load if the search vector of the MUSIC algorithm derived from the $\mathbf{z}(t)$ model is to be calculated on-line. This issue will be discussed further in Section 6.4.

(d) It is interesting at this juncture to compare the above development with the work reported in [74]. In [74], a complex-valued unitary transformation matrix is applied to the measurements (or the estimated covariance matrix) of an all-active array such that the steering matrix is real-valued. This leads to the development of an ESPRIT algorithm that requires less computation. The requirements of the method discussed in [74] are that the array structure is centrosymmetric, for example, ULA, and that no mutual coupling is present. In contrast, the method described in this chapter, which leads to the real-valued matrices $\mathbf{A}_{ULA,\cos}(\phi)$ and $\mathbf{A}_{ULA,\sin}(\phi)$, (i) requires the array to be ULA, (ii) still requires a complex-valued transformation matrix to be applied to the measurements, except it is sparse since it involves only simple additions and subtractions of the measured sub-snapshots, (iii) does not require the absence of mutual coupling., and (iv) is able to take advantage of the self-beamforming feature of the array due to the switching of the active element (see Figure 3.5) to provide more accurate DOA estimates relative to the array's all-active counterpart if certain conditions are met [9][101].

6.3   MUSIC Algorithm in Conjunction with ULA-SASPA Array

Recall the coupled-signals-uncoupled-noise $\mathbf{z}(t)$ model of (6.18).

$$\mathbf{z}(t) = \mathbf{M}(\phi)\mathbf{s}(t) + \mathbf{T}\mathbf{n}_{\text{self}}(t) \tag{6.18}$$

Using a derivation similar to that shown in the seminal MUSIC paper [13], it can be seen the MUSIC spectrum of $\mathbf{z}(t)$ is given by:

$$P_{\mathbf{z},MUSIC}(\phi) = \frac{1}{\left\| \mathbf{E}_{\mathbf{z}n}^{H} \mathbf{m}(\phi) \right\|_{2}^{2}} \tag{6.46}$$

where $\mathbf{m}(\phi)$ is given by:

$$\mathbf{m}(\phi) = \begin{bmatrix} \left(\mathbf{C}_{\cos}''\right)^{T} \mathbf{a}_{ULA,\cos}(\phi) \\ \left(\mathbf{C}_{\sin}''\right)^{T} \mathbf{a}_{ULA,\sin}(\phi) \end{bmatrix} \tag{6.47}$$

and $\mathbf{E}_{\mathbf{z}n}$ is the noise subspace estimated from the eigendecomposition of $\mathbf{R}_{\mathbf{z}}$.

6.4   Steering Matrix of ULA-SASPA Arrays in term of $\mathbf{c}^{(1)}$

Mutual coupling matrices are symmetric Toeplitz. Therefore, they are characterised fully by their first row, or first column, i.e., $\mathbf{c}^{(1)}$. This notion of being able to represent a mutual coupling matrix as a vector can be useful, for example, in situations where the mutual coupling matrix is unknown and is to be estimated from the measurements, as will be discussed in Chapter 7.

Here, an alternative expression for the MUSIC search vector $\mathbf{m}(\phi)$, (6.47), is derived. Unlike the expression given in (6.47) which involves $\mathbf{c}^{(1)},\ldots,\mathbf{c}^{(N/2)}$, the new expression involves only $\mathbf{c}^{(1)}$.

Observe firstly from (6.23), (6.24), (6.27) and (6.28) that, with

$$\mathbf{M}(\phi) = \begin{bmatrix} \mathbf{m}(\phi_1) & \cdots & \mathbf{m}(\phi_M) \end{bmatrix} = \begin{bmatrix} \mathbf{m}_1(\phi_1) & \cdots & \mathbf{m}_1(\phi_M) \\ \mathbf{m}_2(\phi_1) & \cdots & \mathbf{m}_2(\phi_M) \end{bmatrix} \tag{6.48}$$

where $\mathbf{m}(\phi_m) \in \mathbb{C}^{N \times 1}$, $\mathbf{m}_1(\phi_m) \in \mathbb{C}^{\frac{N}{2} \times 1}$ and $\mathbf{m}_2(\phi_m) \in \mathbb{C}^{\frac{N}{2} \times 1}$, one obtains:

$$\mathbf{m}(\phi_m) = \left[\frac{\mathbf{m}_1(\phi_m)}{\mathbf{m}_2(\phi_m)} \right] = \left[\begin{array}{c} \left(\mathbf{c}^{(1)}\right)^T \mathrm{Re}\left(\mathbf{a}_{ULA}(\phi_m)\right) \\ \left(\mathbf{c}^{(2)}\right)^T \mathrm{Re}\left(\mathbf{a}_{ULA}(\phi_m)\right) \\ \vdots \\ \left(\mathbf{c}^{(N/2)}\right)^T \mathrm{Re}\left(\mathbf{a}_{ULA}(\phi_m)\right) \\ \hline \left(\mathbf{c}^{(1)}\right)^T \mathrm{Im}\left(\mathbf{a}_{ULA}(\phi_m)\right) \\ \left(\mathbf{c}^{(2)}\right)^T \mathrm{Im}\left(\mathbf{a}_{ULA}(\phi_m)\right) \\ \vdots \\ \left(\mathbf{c}^{(N/2)}\right)^T \mathrm{Im}\left(\mathbf{a}_{ULA}(\phi_m)\right) \end{array} \right] = \left[\begin{array}{c} \mathrm{Re}\left(\mathbf{a}_{ULA}(\phi_m)\right)^T \mathbf{c}^{(1)} \\ \mathrm{Re}\left(\mathbf{a}_{ULA}(\phi_m)\right)^T \mathbf{c}^{(2)} \\ \vdots \\ \mathrm{Re}\left(\mathbf{a}_{ULA}(\phi_m)\right)^T \mathbf{c}^{(N/2)} \\ \hline \mathrm{Im}\left(\mathbf{a}_{ULA}(\phi_m)\right)^T \mathbf{c}^{(1)} \\ \mathrm{Im}\left(\mathbf{a}_{ULA}(\phi_m)\right)^T \mathbf{c}^{(2)} \\ \vdots \\ \mathrm{Im}\left(\mathbf{a}_{ULA}(\phi_m)\right)^T \mathbf{c}^{(N/2)} \end{array} \right] \quad (6.49)$$

where $\mathrm{Re}\left(\mathbf{a}_{ULA}(\phi_m)\right)$ and $\mathrm{Im}\left(\mathbf{a}_{ULA}(\phi_m)\right)$ are defined, respectively, by (6.29) and (6.30).

Re-writing the matrices $\mathbf{m}_1(\phi_m)$ and $\mathbf{m}_2(\phi_m)$ in (6.49) as follows:

$$\mathbf{m}_1(\phi_m) = \mathbf{F}_1(\phi_m)\mathbf{c}^{(1)} = \left[\mathbf{F}_1'(\phi_m) + \mathbf{F}_1''(\phi_m)\right]\mathbf{c}^{(1)} \quad (6.50)$$

$$\mathbf{m}_2(\phi_m) = \mathbf{F}_2(\phi_m)\mathbf{c}^{(1)} = \left[\mathbf{F}_2'(\phi_m) - \mathbf{F}_2''(\phi_m)\right]\mathbf{c}^{(1)} \quad (6.51)$$

or

$$\mathbf{m}(\phi_m) = \left[\begin{array}{c} \mathbf{m}_1(\phi_m) \\ \mathbf{m}_2(\phi_m) \end{array} \right] = \left[\begin{array}{c} \mathbf{F}_1(\phi_m) \\ \mathbf{F}_2(\phi_m) \end{array} \right] \mathbf{c}^{(1)} = \mathbf{F}(\phi_m)\mathbf{c}^{(1)} \quad (6.52)$$

with:

$$\mathbf{F}_1'(\phi_m) = \left[\begin{array}{c} \left(\mathrm{Re}\left(\mathbf{a}_{ULA}(\phi_m)\right)\right)^T \\ \left(\mathrm{Re}\left(\mathbf{a}_{ULA}(\phi_m)\right)\right)^T \mathbf{I}_N' \\ \left(\mathrm{Re}\left(\mathbf{a}_{ULA}(\phi_m)\right)\right)^T \mathbf{I}_N'^2 \\ \vdots \\ \left(\mathrm{Re}\left(\mathbf{a}_{ULA}(\phi_m)\right)\right)^T \mathbf{I}_N'^{N/2-1} \end{array} \right] \in \mathbb{R}^{N/2 \times N} \quad (6.53)$$

and $\mathbf{I}_N'$ is an $N \times N$ identity matrix but with the first column becoming the last

column, i.e.:

$$\mathbf{I}'_N = \begin{bmatrix} 0 & 0 & 0 & \cdots & 1 \\ 1 & 0 & 0 & \cdots & 0 \\ 0 & 1 & 0 & \cdots & 0 \\ \vdots & \vdots & \ddots & & \vdots \\ 0 & 0 & 0 & 1 & 0 \end{bmatrix} = \begin{bmatrix} \mathbf{0}_{1\times(N-1)} & 1 \\ \mathbf{I}_{N-1} & \mathbf{0}_{(N-1)\times 1} \end{bmatrix} \tag{6.54}$$

and more generally

$$\mathbf{I}'_N{}^n = \mathbf{I}'_N \cdot (n \text{ times}) \cdot \mathbf{I}'_N = \begin{bmatrix} \mathbf{0}_{n\times(N-1)} & \mathbf{I}_n \\ \mathbf{I}_{N-n} & \mathbf{0}_{(N-n)\times n} \end{bmatrix} \tag{6.55}$$

$$\mathbf{F}''_1(\phi_m) = \begin{bmatrix} \mathbf{0}_{1\times N} \\ \left(\mathrm{Re}\left(\mathbf{a}_{ULA}(\phi_m)\right)\right)^T \mathbf{K}^{(1)} \\ \left(\mathrm{Re}\left(\mathbf{a}_{ULA}(\phi_m)\right)\right)^T \mathbf{K}^{(2)} \\ \vdots \\ \left(\mathrm{Re}\left(\mathbf{a}_{ULA}(\phi_m)\right)\right)^T \mathbf{K}^{(N/2-1)} \end{bmatrix} \in \mathbb{R}^{N/2\times N} \tag{6.56}$$

where $\mathbf{K}^{(n)}$, $n = 1,\ldots,(N/2-1)$, is an $N \times N$ matrix with the following structure:

$$\mathbf{K}^{(1)} = \begin{bmatrix} 0 & 1 & 0 & \cdots & 0 & -1 \\ 0 & 0 & 0 & \cdots & 0 & 0 \\ 0 & 0 & 0 & \cdots & 0 & 0 \\ \vdots & \vdots & \vdots & & \vdots & \vdots \\ 0 & 0 & 0 & \cdots & 0 & 0 \end{bmatrix} \tag{6.57}$$

$$\mathbf{K}^{(2)} = \begin{bmatrix} 0 & 0 & 1 & \cdots & -1 & 0 \\ 0 & 1 & 0 & \cdots & 0 & -1 \\ 0 & 0 & 0 & \cdots & 0 & 0 \\ \vdots & \vdots & \vdots & & \vdots & \vdots \\ 0 & 0 & 0 & \cdots & 0 & 0 \end{bmatrix}, \quad \text{etc.} \tag{6.58}$$

or more generally,

$$\mathbf{K}^{(n)} = \left[\begin{array}{c} \begin{matrix} \mathbf{0}_{n\times 1} & \mathbf{J}_n & \mathbf{0}_{n\times(N-2n-1)} & -\mathbf{I}_n \end{matrix} \\ \hline \mathbf{0}_{(N-n)\times N} \end{array} \right] \tag{6.59}$$

Likewise,

$$\mathbf{F}_2'(\phi_m) = \begin{bmatrix} \left(\mathrm{Im}\left(\mathbf{a}_{ULA}(\phi_m)\right)\right)^T \\ \left(\mathrm{Im}\left(\mathbf{a}_{ULA}(\phi_m)\right)\right)^T \mathbf{I}_N' \\ \left(\mathrm{Im}\left(\mathbf{a}_{ULA}(\phi_m)\right)\right)^T {\mathbf{I}_N'}^2 \\ \vdots \\ \left(\mathrm{Im}\left(\mathbf{a}_{ULA}(\phi_m)\right)\right)^T {\mathbf{I}_N'}^{N/2-1} \end{bmatrix} \in \mathbb{R}^{N/2 \times N} \tag{6.60}$$

$$\mathbf{F}_2''(\phi_m) = \begin{bmatrix} \mathbf{0}_{1 \times N} \\ \left(\mathrm{Im}\left(\mathbf{a}_{ULA}(\phi_m)\right)\right)^T \mathbf{K}^{(1)} \\ \left(\mathrm{Im}\left(\mathbf{a}_{ULA}(\phi_m)\right)\right)^T \mathbf{K}^{(2)} \\ \vdots \\ \left(\mathrm{Im}\left(\mathbf{a}_{ULA}(\phi_m)\right)\right)^T \mathbf{K}^{(N/2-1)} \end{bmatrix} \in \mathbb{R}^{N/2 \times N} \tag{6.61}$$

As an example, $\mathbf{F}(\phi_m)$ for a six-element ULA-SASPA will have the structure:

$$\mathbf{F}(\phi_m) = \begin{bmatrix} \mathbf{F}_1(\phi_m) \\ \mathbf{F}_2(\phi_m) \end{bmatrix} = \begin{bmatrix} \mathbf{F}_1'(\phi_m) + \mathbf{F}_1''(\phi_m) \\ \mathbf{F}_1'(\phi_m) - \mathbf{F}_1''(\phi_m) \end{bmatrix}$$

$$= \begin{bmatrix} \cos\left(\frac{5}{2}\right)\psi_m & \cos\left(\frac{3}{2}\right)\psi_m & \cos\left(\frac{1}{2}\right)\psi_m & \cos\left(\frac{1}{2}\right)\psi_m & \cos\left(\frac{3}{2}\right)\psi_m & \cos\left(\frac{5}{2}\right)\psi_m \\ \cos\left(\frac{3}{2}\right)\psi_m & \cos\left(\frac{1}{2}\right)\psi_m + \cos\left(\frac{5}{2}\right)\psi_m & \cos\left(\frac{1}{2}\right)\psi_m & \cos\left(\frac{3}{2}\right)\psi_m & \cos\left(\frac{5}{2}\right)\psi_m & 0 \\ \cos\left(\frac{1}{2}\right)\psi_m & \cos\left(\frac{1}{2}\right)\psi_m + \cos\left(\frac{3}{2}\right)\psi_m & \cos\left(\frac{3}{2}\right)\psi_m + \cos\left(\frac{5}{2}\right)\psi_m & \cos\left(\frac{5}{2}\right)\psi_m & 0 & 0 \\ -\sin\left(\frac{5}{2}\right)\psi_m & -\sin\left(\frac{3}{2}\right)\psi_m & -\sin\left(\frac{1}{2}\right)\psi_m & \sin\left(\frac{1}{2}\right)\psi_m & \sin\left(\frac{3}{2}\right)\psi_m & \sin\left(\frac{5}{2}\right)\psi_m \\ -\sin\left(\frac{3}{2}\right)\psi_m & -\sin\left(\frac{1}{2}\right)\psi_m - \sin\left(\frac{5}{2}\right)\psi_m & \sin\left(\frac{1}{2}\right)\psi_m & \sin\left(\frac{3}{2}\right)\psi_m & \sin\left(\frac{5}{2}\right)\psi_m & 0 \\ -\sin\left(\frac{1}{2}\right)\psi_m & \sin\left(\frac{1}{2}\right)\psi_m - \sin\left(\frac{3}{2}\right)\psi_m & \sin\left(\frac{3}{2}\right)\psi_m - \sin\left(\frac{5}{2}\right)\psi_m & \sin\left(\frac{5}{2}\right)\psi_m & 0 & 0 \end{bmatrix} \tag{6.62}$$

Using (6.50) and (6.51), the system $\mathbf{z}(t)$ in (6.18) can be rewritten as:

$$\begin{aligned} \mathbf{z}(t) &= \begin{bmatrix} \mathbf{F}(\phi_1)\mathbf{c}^{(1)} & \mathbf{F}(\phi_2)\mathbf{c}^{(1)} & \cdots & \mathbf{F}(\phi_M)\mathbf{c}^{(1)} \end{bmatrix} \mathbf{s}(t) + \mathbf{T}\mathbf{n}_{\mathrm{self}}(t) \\ &= \mathbf{\Gamma}(\phi)\left(\mathbf{I}_M \otimes \mathbf{c}^{(1)}\right)\mathbf{s}(t) + \mathbf{T}\mathbf{n}_{\mathrm{self}}(t) \end{aligned} \tag{6.63}$$

where $\mathbf{\Gamma}(\phi) \in \mathbb{R}^{N \times NM}$ is defined as:

$$\mathbf{\Gamma}(\phi) = \begin{bmatrix} \mathbf{F}(\phi_1) & \mathbf{F}(\phi_2) & \cdots & \mathbf{F}(\phi_M) \end{bmatrix} \tag{6.64}$$

and $\otimes$ stands for Kronecker product.

The covariance matrix of $\mathbf{z}(t)$ can be derived as follows. First, as can be readily verified:

$$\left(\mathbf{I}_M \otimes \mathbf{c}^{(1)}\right)\mathbf{s}(t) = \mathbf{s}(t) \otimes \mathbf{c}^{(1)} \tag{6.65}$$

Thus:

$$\begin{aligned}
\mathbf{R}_{\mathbf{z}} &= \mathbb{E}\left[\mathbf{z}(t)\mathbf{z}(t)^H\right] \\
&= \mathbb{E}\left[\mathbf{\Gamma}(\phi)\left\{\left(\mathbf{I}_M \otimes \mathbf{c}^{(1)}\right)\mathbf{s}(t)\right\}\left\{\mathbf{s}(t)^H\left(\mathbf{I}_M \otimes \mathbf{c}^{(1)}\right)^H\right\}\mathbf{\Gamma}(\phi)^H\right] + \frac{\sigma_n^2}{2}\mathbf{I}_N \\
&= \mathbf{\Gamma}(\phi)\mathbb{E}\left[\left(\mathbf{s}(t) \otimes \mathbf{c}^{(1)}\right)\left(\mathbf{s}(t) \otimes \mathbf{c}^{(1)}\right)^H\right]\mathbf{\Gamma}(\phi)^H + \frac{\sigma_n^2}{2}\mathbf{I}_N \\
&= \mathbf{\Gamma}(\phi)\mathbb{E}\left[\left(\mathbf{s}(t)\mathbf{s}(t)^H\right) \otimes \left(\mathbf{c}^{(1)}\left(\mathbf{c}^{(1)}\right)^H\right)\right]\mathbf{\Gamma}(\phi)^H + \frac{\sigma_n^2}{2}\mathbf{I}_N \\
&= \mathbf{\Gamma}(\phi)\left(\mathbf{S} \otimes \mathbf{C}^{(1)}\right)\mathbf{\Gamma}(\phi)^H + \frac{\sigma_n^2}{2}\mathbf{I}_N
\end{aligned} \tag{6.66}$$

where

$$\mathbf{S} = \mathbb{E}\left[\mathbf{s}(t)\mathbf{s}(t)^H\right] \tag{6.67}$$

$$\mathbf{C}^{(1)} = \mathbf{c}^{(1)}\left(\mathbf{c}^{(1)}\right)^H \tag{6.68}$$

and the following property of matrix Kronecker product [84] has been invoked to obtain the fourth line:

$$(\mathbf{A} \otimes \mathbf{B})(\mathbf{A} \otimes \mathbf{B})^H = \left(\mathbf{A}\mathbf{A}^H\right) \otimes \left(\mathbf{B}\mathbf{B}^H\right), \text{ for any matrices } \mathbf{A} \text{ and } \mathbf{B}.$$

Note that $\mathbf{S}$, the signal covariance matrix, is diagonal if the received signals are mutually uncorrelated. The powers of the received signals are listed along the diagonal.

The MUSIC spectrum of $\mathbf{z}(t)$ is given by:

$$P_{\mathbf{z},MUSIC} = \frac{1}{\left\|\mathbf{E}_{\mathbf{z}n}^H\mathbf{m}(\phi)\right\|_2^2} = \frac{1}{\left\|\mathbf{E}_{\mathbf{z}n}^H\mathbf{F}(\phi)\mathbf{c}^{(1)}\right\|_2^2} \tag{6.69}$$

where $\mathbf{F}(\phi)\mathbf{c}^{(1)}$ is now the search vector.

Concerning (6.69), it is worthwhile to recall that $\mathbf{F}(\phi)$ is real. Moreover, as can be seen from the example of (6.62), it can be easily constructed once $\cos\left(\frac{N-1}{2}\right)\psi$, $\cos\left(\frac{N-3}{2}\right)\psi$, ..., $\cos\left(\frac{1}{2}\right)\psi$ and $\sin\left(\frac{N-1}{2}\right)\psi$, $\sin\left(\frac{N-3}{2}\right)\psi$, ..., $\sin\left(\frac{1}{2}\right)\psi$ have been computed.

6.5　Simulation Study

The MUSIC cost function (6.46) is used in this section to estimate the DOAs of the signals impinging on a ULA-SASPA array. As remarked in Section 6.2, (6.46) offers enhanced performance in DOA estimation compared to the classical MUSIC cost function of (4.32). This claim will be verified via simulation studies in this section. In the simulations, the classical MUSIC algorithm is implemented on an all-active ULA with the same array geometry as the ULA-SASPA array and operating in the same signal environment as the ULA-SASPA array.

Figure 6.2 shows the MUSIC spectrum for two signals impinging on an 8-element dipole array with inter-element spacing $d = 0.25\lambda$. The signals are incident from $\phi_1 = 60°$ and $\phi_2 = 62°$, and both with $\mathrm{SNR} = 5\,\mathrm{dB}$. The figure shows two sets of plot, one for the ULA-SASPA array and one for the ULA all-active array. Both plots show the results from 5 simulation runs, where 250 snapshots are used for each run.

Figure 6.3 shows the MUSIC spectrum for the same two arrays as in Figure 6.2 but with the impinging signals arriving from $\phi_1 = 20°$ and $\phi_2 = 22°$, and $\mathrm{SNR} = 25\,\mathrm{dB}$. Also, 1000 snapshots per simulation run were used.

In Figure 6.4, the number of antenna elements used in the first two simulations was reduced to 6 but with the same inter-element spacing. The DOAs of the two impinging signals are also the same except now, $\mathrm{SNR} = 10\,\mathrm{dB}$.

In Figure 6.5, the two 6-element arrays of Figure 6.4 were used to detect two signals,

one from $\phi_1 = 20°$ and the other from $\phi_2 = 22°$. The SNR has also been increased to 25 dB, and 1000 snapshots were used for each of the five simulation runs.

As can be seen from Figures 6.2 to 6.5, ULA-SASPA arrays with the $\mathbf{z}(t)$ model outperform their ULA all-active array counterparts in direction finding when the number of the elements is small. Also, ULA-SASPA arrays are capable of estimating the DOAs when the available measurement data set is short, and the power of the received signals is low. The superior performance of the ULA-SASPA arrays can be attributed to their lower noise level as a result of the $\mathbf{z}(t)$ transformation and shown in (6.7).

However, comparing Figure 6.2 with Figure 6.3, and Figure 6.4 with Figure 6.5, it can be seen the unsymmetrical property in the beam pattern of ULAs is still affecting the performance of the ULA-SASPA arrays. In particular, for ULA-SASPA arrays and ULA all-active arrays to be able to detect or resolve signals arriving from near end fire directions (Figures 6.3 and 6.5), (i) the signals are required to have larger SNRs, and/or (ii) more measurement snapshots are required to estimate the data
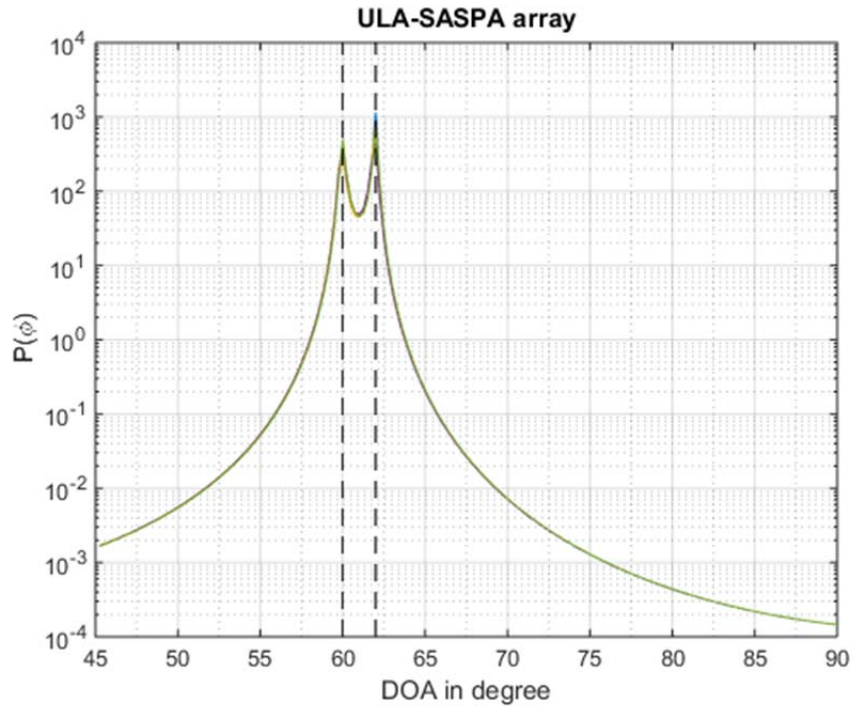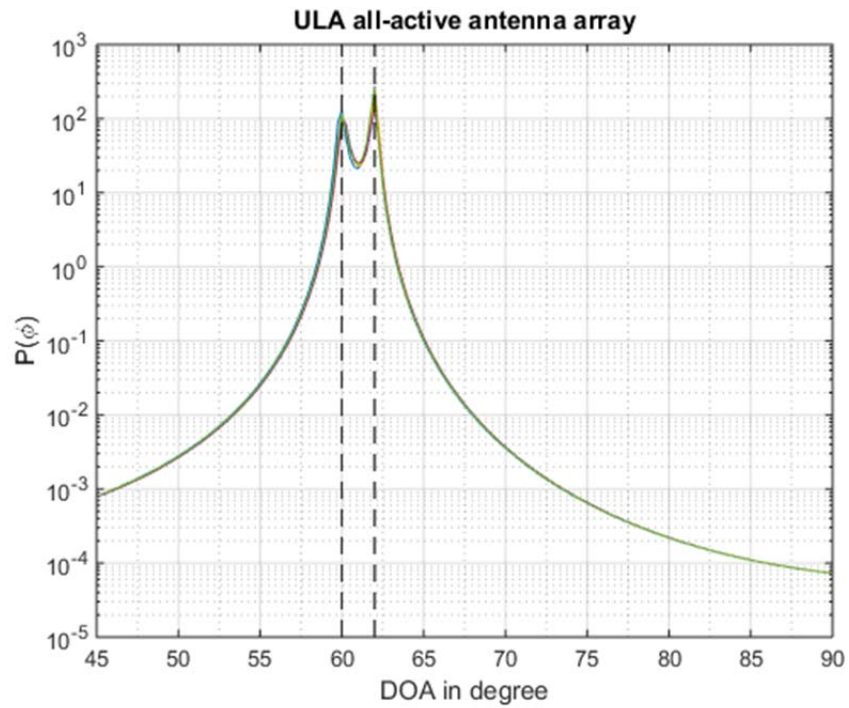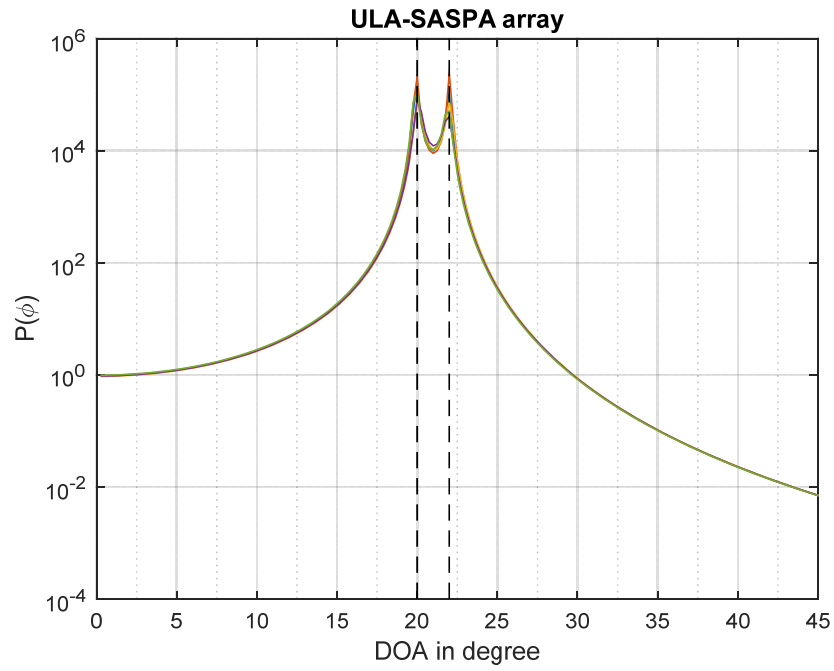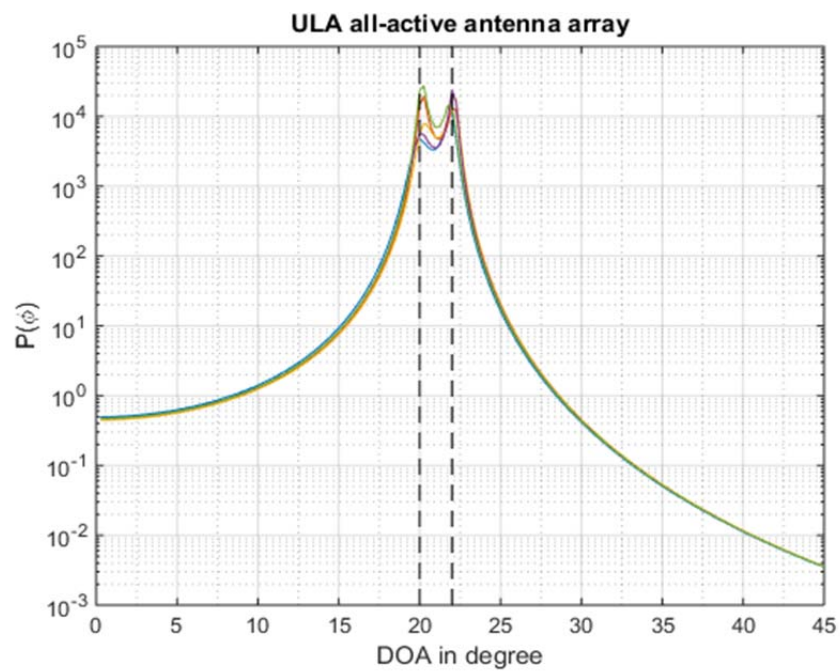
Figure 6.2: MUSIC spectrum for the DOA estimation of two signals impinging on an 8-dipole receiving array with inter-element spacing $d = 0.2\lambda$. The signals are coming from $\phi_1 = 60°$ and $\phi_2 = 62°$ with $SNR = 5\ dB$. Five simulation runs with 250 snapshots for each run are shown. (a) ULA-SASPA array; (b) ULA all-active antenna array.
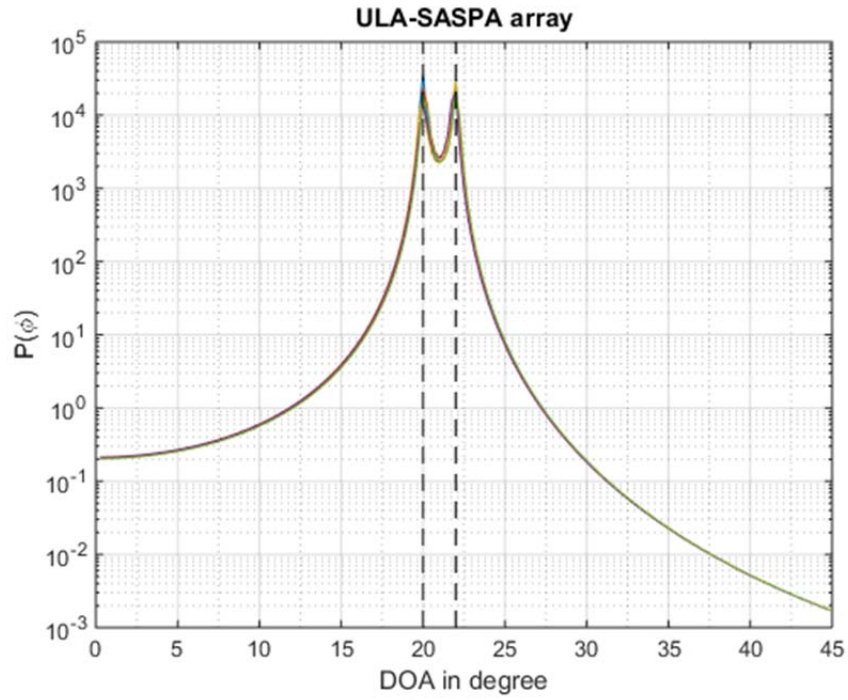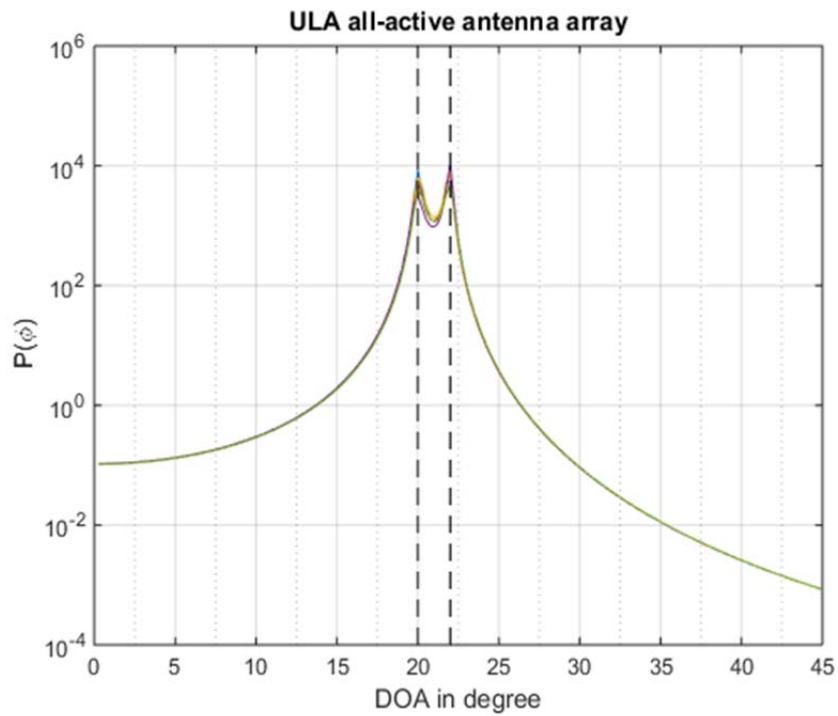
Figure 6.3: MUSIC spectrum for the DOA estimation of two signals impinging on an 8-dipole receiving array with inter-element spacing $d = 0.25\lambda$. The signals are coming from from $\phi_1 = 20°$ and $\phi_2 = 22°$ with $SNR = 20$ dB. Five simulation runs with 1000 snapshots for each run are shown. (a) ULA-SASPA array; (b) ULA all-active antenna array.
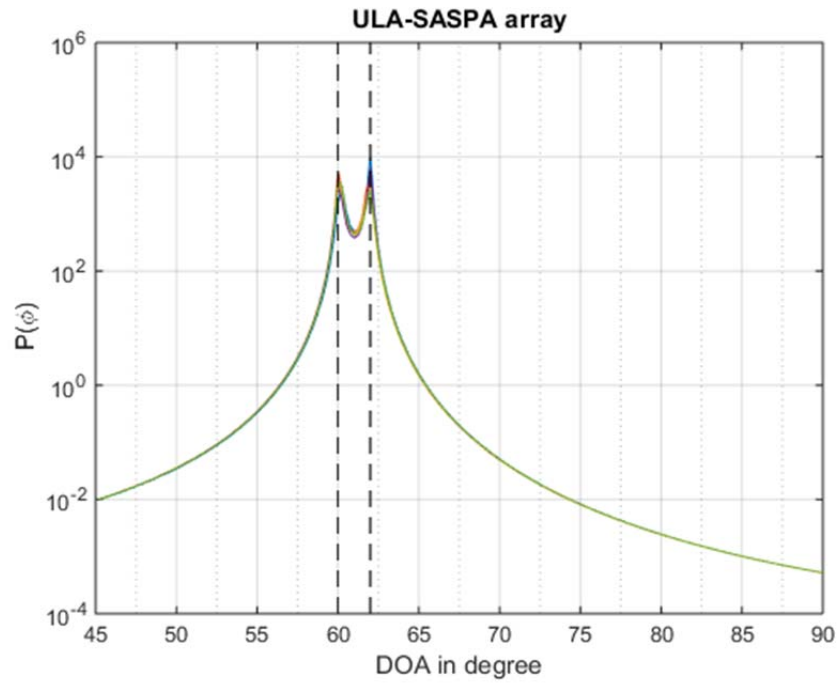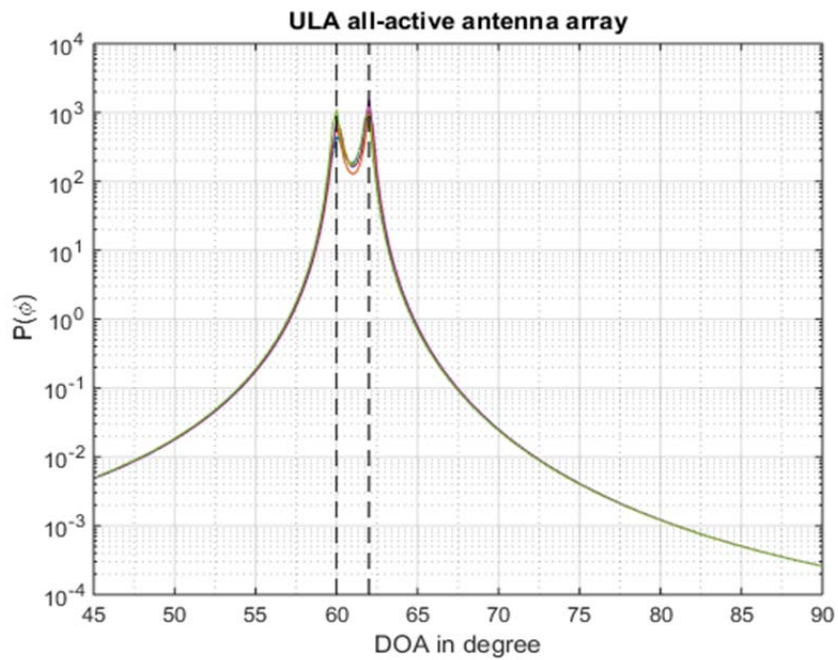
Figure 6.4: MUSIC spectrum for the DOA estimation of two signals impinging on a 6-dipole receiving array with inter-element spacing $d = 0.25\lambda$. The signals are coming from $\phi_1 = 60°$ and $\phi_2 = 62°$ with $SNR = 10$ dB. Five simulation runs with 500 snapshots for each run are shown. (a) ULA-SASPA array; (b) ULA all-active antenna array.

(a)

(b)

Figure 6.5: MUSIC spectrum for the DOA estimation of two signals impinging on a 6-dipole receiving array with inter-element spacing $d = 0.25\lambda$. The signals are coming from $\phi_1 = 20°$ and $\phi_2 = 22°$ with $SNR = 25$ dB. Five simulation runs with 1000 snapshots for each run are shown. (a) ULA-SASPA array; (b) ULA all-active antenna array.

6.6 RMSE Simulations

In this section, the RMSE criterion (5.45) is used to study the performance of ULA-SASPA arrays over a range of SNRs. In the following simulations, mutual coupling is assumed to follow the CVUC model, and the ULA-SASPA arrays are operating under the $\mathbf{z}(t)$ model.

Figures 6.6 plots the RMSE for estimating two broadside signals whose DOAs are separated by $\Delta\phi = \phi_2 - \phi_1 = 82° - 80° = 2°$. The ULA-SASPA array and the ULA all-active array both have six-elements with inter-element spacing $d = 0.2\lambda$. The RMSE is calculated over 100 runs with 100 snapshots for each run.

The plots in Figure 6.7 show the RMSE for estimating two end fire signals whose DOAs are separated by $\Delta\phi = \phi_2 - \phi_1 = 25° - 20° = 5°$, and impinging on the same arrays as in Figure 6.5. In terms of the simulation runs, the plots in Figure 6.6 were similarly obtained from 100 runs except 300 snapshots per run were used.

In Figure 6.8, the plots show the RMSE for one signal coming from the severe DOA of $\phi_1 = 5°$. Both the ULA-SASPA array and ULA all-active array have four elements with inter-element spacing $d = 0.12\lambda$, and the plots are obtained from 100 runs with 50 snapshots for each run.

The superior performance of the ULA-SASPA array is clearly self-evident in the plots of Figures 6.6 and 6.8. It can be seen from these figures that ULA-SASPA arrays have lowered the RMSE of all-active arrays using short data. However, large number of snapshots are required when the received signals are close to the end-fire direction of the array.
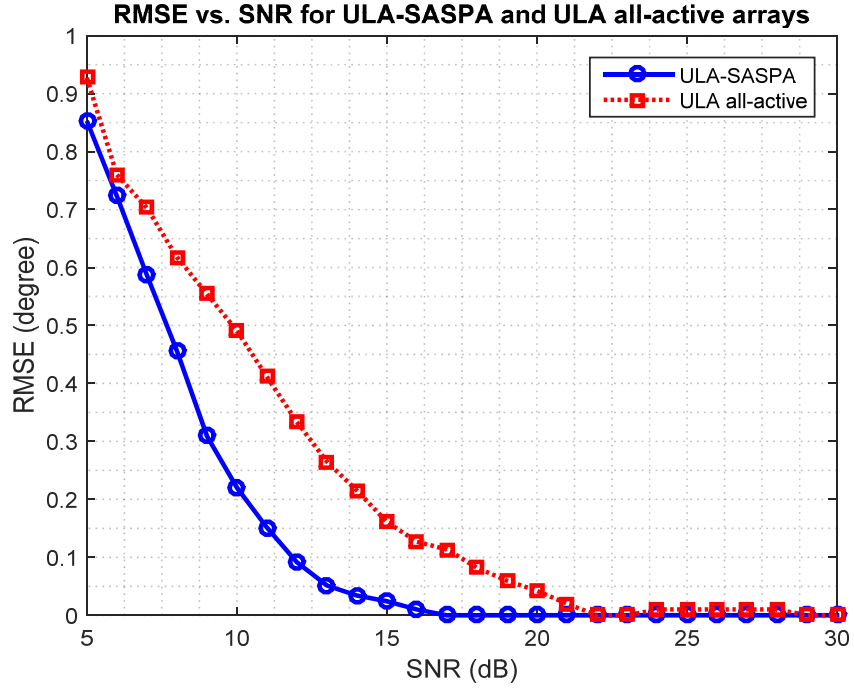
Figure 6.6: RMSE versus SNR for estimating $\Delta\phi$ between two signals coming from $\phi_1 = 80°$ and $\phi_2 = 82°$ and impinging on a ULA-SASPA array and a ULA all-active array. Both arrays consist of 6 dipoles with $d = 0.2\lambda$. 100 runs with 250 snapshots for each run are used.
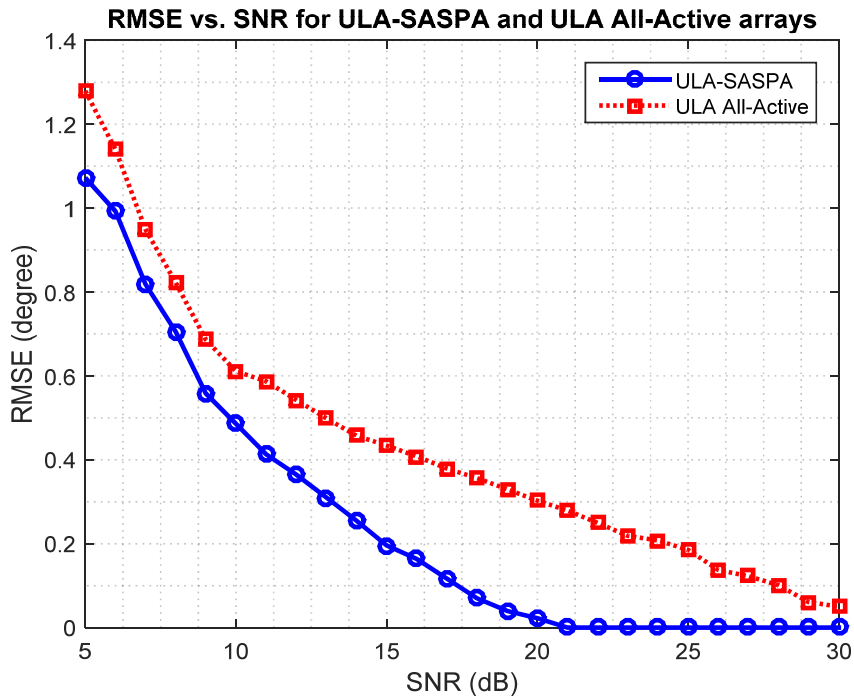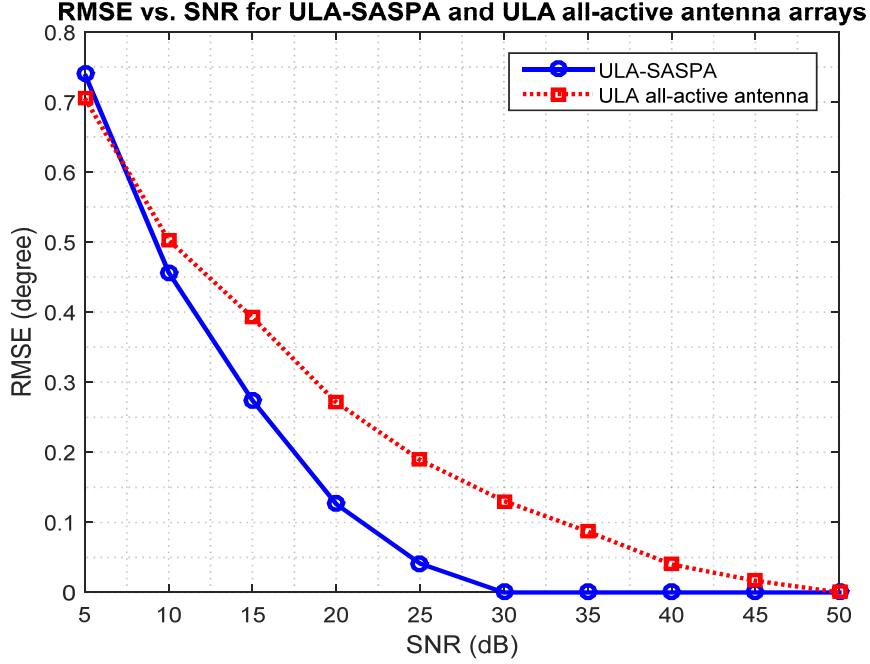

Figure 6.7: RMSE versus SNR for estimating $\Delta\phi$ between two signals coming from $\phi_1 = 20°$ and $\phi_2 = 25°$ and impinging on a ULA-SASPA array and a ULA all-active array. Both arrays consist of 6 dipoles with $d = 0.2\lambda$. 100 runs with 1000 snapshots for each run are used.

Figure 6.8: RMSE versus SNR for estimating the DOA of a signal coming from $\phi = 5°$ and impinging on a ULA-SASPA array and a ULA all-active array. Both arrays consist of 4 dipoles with inter-element spacing $d = 0.12\lambda$. 100 runs with 50 snapshots for each run are used.

6.7 Receiver Block Diagram of a DOA Estimator using an SASPA Array

The block diagram of a DOA estimator operating in conjunction with an N-element SASPA array is shown in Figure 6.9. The RF modulated signal developed at the loaded terminals of the active element n is down-converted to base band via the demodulator. Selection of the output of the active element in a sub-snapshot is implemented in the stage following the antenna elements by controlling the PIN diodes which are part of one of the circuits shown in Figures 3.2a or 3.2b. This can be done by the N size digital word of all zeros except for one logic 1 bit which causes the PIN diode of the corresponding antenna element to be forward-biased. Thus, it is required to generate N different N-size digital words to cover one measurement snapshot.

The base band signal is processed in the stage following the demodulator. The

processing consists of either decoupling the mutual coupling if the array is acting under the CSCN model, or applying the **T** transformation as in (6.6) if the array is acting under the CSUN model. Finally, the DOA estimator collects the processed data taken in one snapshot and over a number of snapshots to estimate the DOA of the underlying received signals.
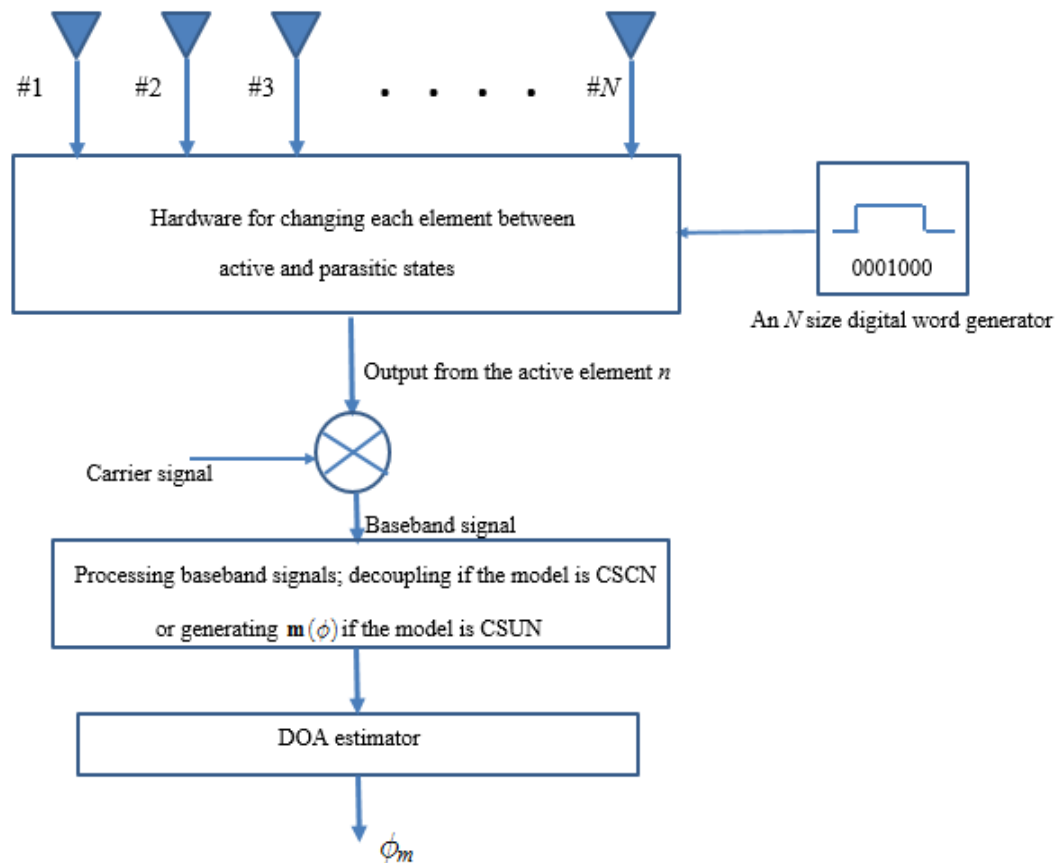

Figure 6.9: Block diagram for DOA estimation using an SASPA array.

6.8   Summary

This chapter investigates the improvements that can be obtained from a ULA-SASPA array with an even number of antenna elements. The noise measurements of the ULA-SASPA array are assumed to be not affected by mutual coupling between the antenna elements.

It is shown that, after applying a simple transformation to the measured data in a snapshot, measurement noise is effectively reduced leading to improved performances in DOA estimations. It is also found that a real-valued DOA dependent steering matrix can be obtained from the transformation which can result in savings in the computational load when either simulating the ULA-SASPA array or calculating the MUSIC search vector on-line. The transformation basically adds and subtracts the second half set of the measurements to the first half set. The aforesaid benefits have been supported by a set of simulation studies. The simulations show that ULA-SASPA arrays acting under the CVUN model can outperform all-active arrays when used as direction finding arrays despite their small size antenna array aperture and the availability of only short data.

Chapter 7

MUTUAL COUPLING ESTIMATION USING ULA-SASPA ARRAY

7.1   Introduction

The enhancement provided by SASPA arrays in DOA estimation has been investigated in Chapters 5 and 6 assuming mutual coupling is known. In practice, knowledge of mutual coupling on-line is often required since it can deviate from the ideal. Mutual coupling in antenna arrays can change for many reasons. The characteristics of the array elements and the associated electronic circuitry are subjected to manufacturing tolerances. They can also change over time due to component ageing and thermal effects [23][81]. Also, nearby metal objects or other environmental effects can be another reason for causing mutual coupling to depart from the ideal. Accordingly, it is desirable to have a technique to estimate the mutual coupling between the array elements. This technique, or algorithm, can be applied prior to or simultaneously with DOA estimation.

In this Chapter, the feasibility of estimating the mutual coupling of a ULA-SASPA array will be examined assuming the data model is CSUN. Another viable achievement that can be attained for this antenna array is estimating the DOA dependent matrix $\mathbf{F}(\phi)$ that is formed in Chapter 6. To accomplish the work addressed in this chapter, a test signal is first used to estimate the fitted subspace of the on-line mutual coupling of an N-element ULA-SASPA array receiving that signal. Thereafter, the estimated mutual coupling is used into (6.69) to estimate the DOAs of the underlying received signals.

7.2 Literature Background on On-Line Mutual Coupling Estimation

Many researches have been reported in the literature to estimate mutual coupling on-line, prior to or along with estimating the DOAs in a receiving antenna array. Most of these methods are based on finding a minimum solution to a cost function which is a likelihood function of all the unknown parameters of the array [8]. In [81], iterative LS solutions for the MUSIC cost function (4.32) are proposed but they require the gain and phase of the array elements to be inserted. In this method, the mutual coupling matrix (MCM) is assumed to be a banded matrix if the array is ULA. This assumption is based on the fact that the mutual coupling is inversely proportional to the distance between two array elements. The procedure is to fix all parameters except one for which the LS solution is to be found in the first set of iterations. Therefore, initial values are first required for the fixed parameters. The solution obtained is then plugged into the cost function to find the solution for the next parameter. In [90], the same technique is used but the cost function is the observations of the array which is a random process.

In [24], another iterative LS method is developed based on the root-MUSIC cost function. The author used this method to avoid divergent solutions due to improper selection of the initial value. The method requires only two steps. The first one is implemented to find the nearest roots to the unit circle on which the roots $\exp(jkd\cos\phi)$ should reside as if mutual coupling is not present. These roots are then inserted into the cost function to estimate the unknown mutual coupling. However, this method is useful for ULA arrays only and the nearest roots might not be found.

Another criterion has been exploited in [39] to search for an LS solution for the unknown mutual coupling after using the rank deficiency of a matrix formed from the orthogonality between the noise subspace and the mutual-coupled steering matrix

to find the LS solution to the underlying DOAs. The estimated DOAs are then plugged into the first cost function to estimate the mutual coupling. Thus, this method requires initial values for the DOAs. To do so, a pre-estimation for certain sectors covered by the proposed beamformed array is first implemented.

Obviously, the aforementioned methods are computationally intensive, and the iterative methods may end up with local minima rather than the global minimum if the initial values are not selected properly, or there will be no solution at all. Furthermore, some of these methods that assume the mutual coupliong matrix is banded did not show how to select the useful bandwidth of the MCM. Instead the bandwidth is selected arbitrarily to simplify the problem, and this assumption may result in errors when determining the true mutual coupling. Also, the banded matrix property cannot be applied on SASPA arrays since the elements are close to each other and mutual coupling between elements far apart cannot be ignored.

7.3   Estimating the Mutual Coupling of a ULA-SASPA

The capability to estimate the mutual coupling of an *N*-element ULA-SASPA array prior to processing the measurements for DOA estimation is examined in this section. The method is based on estimating a fitted vector to the mutual coupling vector of a symmetrical Toeplitz MCM. This fitted vector can be obtained from the null space of a rank deficient matrix. Recall that a symmetrical Toeplitz MCM can be defined by its first row or first column. The rank deficient matrix is formed from left multiplying the real valued DOA independent matrix $\mathbf{F}(\phi)$ found in Chapter 6 by the orthogonal projection on the estimated noise subspace.

In this work, mutual coupling is assumed to be DOA independent. Furthermore, the data model used is the one defined in (6.1), i.e., where noise is not affected by mutual coupling. Using (6.48), (6.63) and (6.64), the steering matrix $\mathbf{M}(\phi)$ for an *N*-element ULA-SASPA array receiving *M* uncorrelated and with an even number

of array elements is:

$$
\begin{aligned}
\mathbf{M}(\phi) &= \left[\mathbf{F}(\phi_1)\mathbf{c}^{(1)} \quad \mathbf{F}(\phi_2)\mathbf{c}^{(1)} \quad \cdots \quad \mathbf{F}(\phi_M)\mathbf{c}^{(1)} \right] \\
&= \boldsymbol{\Gamma}(\phi)\left[\mathbf{I}_M \otimes \mathbf{c}^{(1)} \right] \\
&= \boldsymbol{\Gamma}(\phi)\mathbf{U}
\end{aligned}
\tag{7.1}
$$

where $\boldsymbol{\Gamma}(\phi)$ is defined by (6.64), and

$$
\mathbf{U} = \left(\mathbf{I}_M \otimes \mathbf{c}^{(1)} \right) \in \mathbb{C}^{MN \times M}
\tag{7.2}
$$

The orthogonal projection onto the subspace spanned by the columns of $\mathbf{M}(\phi)$, i.e., onto $\mathcal{R}(\mathbf{M}(\phi))$ [8][14][65][91], is

$$
\begin{aligned}
\mathbf{P}_{\mathbf{M}(\phi)} &= \mathbf{M}(\phi)\mathbf{M}(\phi)^{\dagger} = \mathbf{M}(\phi)\left[\mathbf{M}(\phi)^H \mathbf{M}(\phi) \right]^{-1} \mathbf{M}(\phi)^T \\
&= \boldsymbol{\Gamma}(\phi)\mathbf{U}\left[\mathbf{U}^H \boldsymbol{\Gamma}(\phi)^T \boldsymbol{\Gamma}(\phi)\mathbf{U} \right]^{-1} \mathbf{U}^H \boldsymbol{\Gamma}(\phi)^T
\end{aligned}
\tag{7.3}
$$

Note that $\mathbf{P}_{\mathbf{M}(\phi)} \in \mathbb{C}^{N \times N}$ is an orthogonal projection because it is idempotent, i.e. $\mathbf{P}_{\mathbf{M}(\phi)}^2 = \mathbf{P}_{\mathbf{M}(\phi)}$, and it is Hermitian, i.e., $\mathbf{P}_{\mathbf{M}(\phi)}^H = \mathbf{P}_{\mathbf{M}(\phi)}$ [70][92][93]. Post-multiplying (7.3) by $\boldsymbol{\Gamma}(\phi)$ yields:

$$
\mathbf{P}_{\mathbf{M}(\phi)}\boldsymbol{\Gamma}(\phi) = \boldsymbol{\Gamma}(\phi)\mathbf{U}\left[\mathbf{U}^H \boldsymbol{\Gamma}(\phi)^T \boldsymbol{\Gamma}(\phi)\mathbf{U} \right]^{-1} \mathbf{U}^H \boldsymbol{\Gamma}(\phi)^T \boldsymbol{\Gamma}(\phi)
\tag{7.4}
$$

or

$$
\mathbf{P}_{\mathbf{M}(\phi)}\boldsymbol{\Gamma}(\phi) = \boldsymbol{\Gamma}(\phi)\mathbf{P}_{\mathbf{U}/\mathbf{D}(\phi)}
\tag{7.5}
$$

where

$$
\begin{aligned}
\mathbf{P}_{\mathbf{U}/\mathbf{D}(\phi)} &= \mathbf{U}\left[\mathbf{U}^H \boldsymbol{\Gamma}(\phi)^T \boldsymbol{\Gamma}(\phi)\mathbf{U} \right]^{-1} \mathbf{U}^H \boldsymbol{\Gamma}(\phi)^T \boldsymbol{\Gamma}(\phi) \\
&= \mathbf{U}\left[\mathbf{U}^H \mathbf{D}(\phi)\mathbf{U} \right]^{-1} \mathbf{U}^H \mathbf{D}(\phi)
\end{aligned}
\tag{7.6}
$$

and $\mathbf{D}(\phi)$ is the non-negative definite matrix

$$
\mathbf{D}(\phi) = \boldsymbol{\Gamma}(\phi)^T \boldsymbol{\Gamma}(\phi)
\tag{7.7}
$$

$\mathbf{P}_{\mathbf{U}/\mathbf{D}(\phi)} \in \mathbb{C}^{MN \times MN}$ is an oblique projection onto the subspace spanned by the

columns of the matrix $\mathbf{U} = \left(\mathbf{I}_M \otimes \mathbf{c}^{(1)} \right)$ along the subspace spanned by the columns of $\mathbf{D}(\phi)$ [92]. Also, this projection matrix can be considered as a weighted orthogonal projection onto $\mathcal{R}(\mathbf{U})$. $\mathbf{P}_{\mathbf{U}/\mathbf{D}(\phi)}$ satisfies the condition of idempotency but it is not Hermitian, i.e., $\mathbf{P}_{\mathbf{U}/\mathbf{D}(\phi)}^{H} \neq \mathbf{P}_{\mathbf{U}/\mathbf{D}(\phi)}$.

The equation (7.5) is a homogenous Sylvester matrix equation, i.e., it has the form $\mathbf{AX} - \mathbf{XB} = \mathbf{0}_{N \times NM}$ where $\mathbf{A} \in \mathbb{C}^{N \times N}$, $\mathbf{B} \in \mathbb{C}^{NM \times NM}$ and $\mathbf{X} \in \mathbb{C}^{N \times NM}$ [94]-[96]. Equation (7.5) has a non-zero solution if and only if $\mathbf{P}_{\mathbf{M}(\phi)}$ and $\mathbf{P}_{\mathbf{U}/\mathbf{D}(\phi)}$ have common eigenvalues [96]. Thus (7.5) has a solution, that is, $\mathbf{\Gamma}(\phi)$ exists since the eigenvalues of the projections $\mathbf{P}_{\mathbf{M}(\phi)}$ and $\mathbf{P}_{\mathbf{U}/\mathbf{D}(\phi)}$ is the set $\Lambda_i \in \{0,1\}$.

7.4   Calculation of the Projection Matrices $\mathbf{P}_{\mathbf{M}(\phi)}$ and $\mathbf{P}_{\mathbf{U}/\mathbf{D}(\phi)}$

The matrix $\mathbf{P}_{\mathbf{M}(\phi)}$ can be calculated from the estimated signal subspace as [98]:

$$\mathbf{P}_{\mathbf{M}(\phi)} = \mathbf{M}(\phi) \left[\mathbf{M}(\phi)^{H} \mathbf{M}(\phi) \right]^{-1} \mathbf{M}(\phi)^{T} = \hat{\mathbf{E}}_s \hat{\mathbf{E}}_s^{H} \tag{7.8}$$

provided the steering matrix is full rank. The matrix $\mathbf{P}_{\mathbf{U}/\mathbf{D}(\phi)}$ can be found from the following relationship:

$$\mathbf{P}_{\mathbf{M}(\phi)} \mathbf{\Gamma}(\phi) \mathbf{P}_{\mathbf{U}/\mathbf{D}(\phi)}$$

$$= \mathbf{\Gamma}(\phi) \mathbf{U} \left[\mathbf{U}^{H} \mathbf{\Gamma}(\phi)^{T} \mathbf{\Gamma}(\phi) \mathbf{U} \right]^{-1} \mathbf{U}^{H} \mathbf{\Gamma}(\phi)^{T} \cdot \mathbf{\Gamma}(\phi)$$

$$\qquad \cdot \mathbf{U} \left[\mathbf{U}^{H} \mathbf{\Gamma}(\phi)^{T} \mathbf{\Gamma}(\phi) \mathbf{U} \right]^{-1} \mathbf{U}^{H} \mathbf{\Gamma}(\phi)^{T} \mathbf{\Gamma}(\phi) \tag{7.9}$$

$$= \mathbf{\Gamma}(\phi) \cdot \left[\mathbf{U}^{H} \mathbf{\Gamma}(\phi)^{T} \mathbf{\Gamma}(\phi) \mathbf{U} \right]^{-1} \mathbf{U}^{H} \mathbf{\Gamma}(\phi)^{T} \mathbf{\Gamma}(\phi)$$

$$= \mathbf{\Gamma}(\phi) \mathbf{P}_{\mathbf{U}/\mathbf{D}(\phi)}$$

i.e.,

$$\left[\mathbf{I}_N - \mathbf{P}_{\mathbf{M}(\phi)} \right] \mathbf{\Gamma}(\phi) \mathbf{P}_{\mathbf{U}/\mathbf{D}(\phi)} = \mathbf{P}_{\mathbf{M}(\phi)}^{\perp} \mathbf{\Gamma}(\phi) \mathbf{P}_{\mathbf{U}/\mathbf{D}(\phi)} = \mathbf{0}_{N \times MN} \tag{7.10}$$

or

$$\mathbf{V}(\phi) \mathbf{P}_{\mathbf{U}/\mathbf{D}(\phi)} = \mathbf{0}_{N \times MN} \tag{7.11}$$

where

$$V(\phi) = P_{M(\phi)}^{\perp} \Gamma(\phi) \in \mathbb{C}^{N \times MN} \tag{7.12}$$

and

$$P_{M(\phi)}^{\perp} = \left[I_N - P_{M(\phi)} \right] \in \mathbb{C}^{N \times N} \tag{7.13}$$

is the orthogonal projection on the noise subspace, i.e., $P_{M(\phi)}^{\perp} = \hat{E}_n \hat{E}_n^H$. Note that $\text{rank}\left(P_{M(\phi)}\right) = M$ and $\text{rank}\left(P_{M(\phi)}^{\perp}\right) = N - M$.

Equations (7.10)-(7.12) state that $P_{U/D(\phi)}$ is in the null space of $V(\phi)$. In [99], it has been proved that $P_{U/D(\phi)}$ and P_U are similar where P_U is the orthogonal projection on $\mathcal{R}(U)$, i.e.:

$$P_U = U\left(U^H U\right)^{-1} U = \left(I_M \otimes c^{(1)}\right)\left[\left(I_M \otimes c^{(1)}\right)^H \left(I_M \otimes c^{(1)}\right)\right]^{-1} \left(I_M \otimes c^{(1)}\right)^H \tag{7.14}$$

Therefore, P_U is also in the null space of $V(\phi)$.

7.5 Estimating the Mutual Coupling Vector $c^{(1)}$

As pointed out in the previous section, P_U is in $\mathcal{N}(V(\phi))$. It can be revealed from (7.10) and (7.11) that the rank of $V(\phi)$ is the minimum of the ranks of $P_{M(\phi)}^{\perp}$ and $\Gamma(\phi)$ [102], i.e.:

$$\text{rank}(V(\phi)) \leq \min\left(\text{rank}\left(P_{M(\phi)}^{\perp}\right), \text{rank}(\Gamma(\phi))\right) \tag{7.15}$$

Thus,

$$\text{rank}(V(\phi)) = \min(N - M, N) = N - M \tag{7.16}$$

Now, according to the rank-nullity theorem which states that $\text{rank}(A) + \mathcal{N}(A) = M$ for any given matrix $A \in \mathbb{C}^{N \times M}$ [103], one has the following:

$$\dim(\mathcal{N}(V(\phi))) = MN - \text{rank}(V(\phi)) \tag{7.17}$$

Hence, for a ULA-SASPA array receiving a single signal, i.e., $M = 1$, the dimension of the null space of $\mathbf{V}(\phi)$ from (7.17) will be

$$\dim(\mathcal{N}(\mathbf{V}(\phi))) = MN - (M - N) = 1 \tag{7.18}$$

And according to (7.10) and (7.11), the mutual coupling vector $\mathbf{c}^{(1)}$ of a ULA-SASPA array receiving a test signal from ϕ_{test} can be estimated with:

$$\begin{aligned}
\hat{\mathbf{c}}^{(1)} = \mathcal{N}(\mathbf{V}(\phi)) = \mathcal{N}(\mathbf{V}(\phi_{test})) &= \mathcal{N}\left(\mathbf{P}_{\mathbf{m}(\phi_{test})}^{\perp}\mathbf{\Gamma}(\phi_{test})\right) \\
&= \mathcal{N}\left(\mathbf{P}_{\mathbf{m}(\phi_{test})}^{\perp}\mathbf{F}(\phi_{test})\right)
\end{aligned} \tag{7.19}$$

where $\mathbf{F}(\phi_{test})$ can be formed from (6.50)-(6.61) for a test signal emanating from a known direction, and $\mathbf{P}_{\mathbf{m}(\phi_{test})}^{\perp}$ can be calculated from (7.13). The estimate $\hat{\mathbf{c}}^{(1)}$ can then be used in (6.69) to estimate the DOAs of the underlying signals after estimating the signal subspace $\hat{\mathbf{E}}_n$ from the data covariance matrix of a ULA-SASPA array.

Note that $\hat{\mathbf{c}}^{(1)}$, as calculated in (7.19), is the fitted vector to the actual $\mathbf{c}^{(1)}$. Also, the vector $\hat{\mathbf{c}}^{(1)}$ will be a normalized vector if MATLAB is used to find $\mathcal{N}(\mathbf{V}(\phi_{test}))$. In terms of MUSIC, the scaling of $\hat{\mathbf{c}}^{(1)}$ will only result in a vertical shift of the plotted MUSIC spectrum. There are no changes to the position of the peaks and, concomitant with that, the bias and variance of the estimated DOAs.

7.6   Estimating the DOA Dependent Matrix $\mathbf{F}(\phi)$

The structure of the ULA-SASPA array also allows the matrix $\mathbf{F}(\phi)$, as defined in Section 6.4, to be estimated for a given $\hat{\mathbf{c}}^{(1)}$ or $\mathbf{c}^{(1)}$. As pointed out in Section 6.4, the steering matrix of a ULA-SASPA array receiving a single signal can be found by post-multiplying the matrix $\mathbf{F}(\phi)$ by the mutual coupling vector $\mathbf{c}^{(1)}$. In Section 7.5, the procedure to estimate a vector fitted to $\mathbf{c}^{(1)}$ was shown. Also, in Section 7.3, it was pointed out that $\mathbf{\Gamma}(\phi)$ is the solution to the Sylvester equation (7.5). In [95][97], the solution of (7.5) is found to be:

$$\left[\mathbf{I}_{MN} \otimes \mathbf{P}_{\mathbf{M}(\phi)} - \mathbf{P}_{\mathbf{U}/\mathbf{D}(\phi)}^{T} \otimes \mathbf{I}_N\right] \cdot \text{vec}(\mathbf{\Gamma}(\phi)) = \text{vec}(\mathbf{0}_{N \times MN}) = \mathbf{0}_{(MN^2) \times 1} \tag{7.20}$$

where $\text{vec}(\mathbf{\Gamma}(\phi))$ is the vectorization operator which stacks the columns of $\mathbf{\Gamma}(\phi)$ one on top of another, i.e.:

$$\text{vec}(\mathbf{\Gamma}(\phi)) = \begin{bmatrix} \Gamma_{11} & \Gamma_{21} & \cdots & \Gamma_{N1} & \Gamma_{12} & \Gamma_{22} & \cdots & \Gamma_{N2} & \Gamma_{13} & \Gamma_{23} & \cdots & \Gamma_{MN} \end{bmatrix}^T \in \mathbb{R}^{MN^2 \times 1}$$

(7.21)

If only one signal is incident on the ULA-SASPA array, then $M = 1$ and (7.20) reduces to:

$$\left[\mathbf{I}_N \otimes \mathbf{P}_{\mathbf{m}(\phi)} - \mathbf{P}_{\mathbf{U}/\mathbf{D}(\phi)}^T \otimes \mathbf{I}_N \right] \cdot \text{vec}(\mathbf{F}(\phi)) = \text{vec}(\mathbf{0}_{N \times N}) = \mathbf{0}_{N^2 \times 1}$$

(7.22)

where, see (7.8)

$$\mathbf{P}_{\mathbf{m}(\phi)} = \mathbf{m}(\phi) \left[\mathbf{m}(\phi)^H \mathbf{m}(\phi) \right]^{-1} \mathbf{m}(\phi)^T = \hat{\mathbf{e}}_s \hat{\mathbf{e}}_s^H$$

(7.23)

Note that the signal subspace $\hat{\mathbf{E}}_s = \hat{\mathbf{e}}_s$ consists of only one eigenvector when only one signal is received.

Now, it follows from (6.64), (7.2) and (7.6) that, for a single signal, i.e., $M = 1$,

$$\mathbf{\Gamma}(\phi) = \mathbf{F}(\phi)$$

(7.24)

$$\mathbf{U} = \left(\mathbf{I}_1 \otimes \mathbf{c}^{(1)} \right) = \mathbf{c}^{(1)}$$

(7.25)

$$\mathbf{P}_{\mathbf{U}/\mathbf{D}(\phi)} = \mathbf{U} \left[\mathbf{U}^H \mathbf{\Gamma}(\phi)^T \mathbf{\Gamma}(\phi) \mathbf{U} \right]^{-1} \mathbf{U}^H \mathbf{\Gamma}(\phi)^T \mathbf{\Gamma}(\phi)$$

$$= \mathbf{c}^{(1)} \left[\left(\mathbf{c}^{(1)} \right)^H \mathbf{F}(\phi)^T \mathbf{F}(\phi) \mathbf{c}^{(1)} \right]^{-1} \left(\mathbf{c}^{(1)} \right)^H \mathbf{F}(\phi)^T \mathbf{F}(\phi)$$

(7.26)

The oblique projection matrix $\mathbf{P}_{\mathbf{U}/\mathbf{D}(\phi)}$ for a single signal can thus be replaced by the matrix $\mathbf{G}(\phi)$ which is defined as:

$$\mathbf{G}(\phi) = \mathbf{F}(\phi)^{-1} \mathbf{P}_{\mathbf{m}(\phi)} \mathbf{F}(\phi)$$

(7.27)

because:

$$\mathbf{G}(\phi) = \mathbf{F}(\phi)^{-1} \mathbf{P}_{\mathbf{m}(\phi)} \mathbf{F}(\phi)$$

$$= \mathbf{F}(\phi)^{-1} \left\{ \mathbf{m}(\phi) \left[\mathbf{m}(\phi)^H \mathbf{m}(\phi) \right]^{-1} \mathbf{m}(\phi)^T \right\} \mathbf{F}(\phi)$$

$$= \mathbf{F}(\phi)^{-1} \left\{ \mathbf{F}(\phi)\mathbf{c}^{(1)} \left[\left(\mathbf{c}^{(1)} \right)^H \mathbf{F}(\phi)^T \mathbf{F}(\phi)\mathbf{c}^{(1)} \right]^{-1} \left(\mathbf{c}^{(1)} \right)^H \mathbf{F}(\phi)^T \right\} \mathbf{F}(\phi)$$

$$= \mathbf{c}^{(1)} \left[\left(\mathbf{c}^{(1)} \right)^H \mathbf{F}(\phi)^T \mathbf{F}(\phi)\mathbf{c}^{(1)} \right]^{-1} \left(\mathbf{c}^{(1)} \right)^H \mathbf{F}(\phi)^T \mathbf{F}(\phi) \qquad (7.28)$$

$$= \mathbf{P}_{\mathbf{U}/\mathbf{D}(\phi)}$$

Therefore, (7.22) becomes:

$$\left[\mathbf{I}_N \otimes \mathbf{P}_{\mathbf{m}(\phi)} - \mathbf{G}(\phi)^T \otimes \mathbf{I}_N \right] \cdot \mathrm{vec}\left(\mathbf{F}(\phi) \right) = \mathrm{vec}\left(\mathbf{0}_{N \times N} \right) = \mathbf{0}_{N^2 \times 1} \qquad (7.29)$$

Recall from (7.27) that $\mathbf{G}(\phi) = \mathbf{F}(\phi)^{-1} \mathbf{P}_{\mathbf{m}(\phi)} \mathbf{F}(\phi)$, and it is shown in (7.23) that $\mathbf{P}_{\mathbf{m}(\phi)}$ can be calculated from the estimated signal subspace $\hat{\mathbf{e}}_S$, i.e. from the measurements. Therefore, the matrix $\mathbf{F}(\phi)$ can be found by searching for a ϕ that solves (7.29). The above procedure will be demonstrated in the simulation of Section 7.7.

Now, suppose the received signal is a test signal. Equation (7.29) then becomes

$$\left[\mathbf{I}_N \otimes \mathbf{P}_{\mathbf{m}(\phi_{test})} - \mathbf{G}(\phi_i)^T \otimes \mathbf{I}_N \right] \cdot \mathrm{vec}\left(\hat{\mathbf{F}}(\phi_{test}) \right) = \mathbf{0}_{N^2 \times 1} \qquad (7.30)$$

or

$$\mathbf{B} \cdot \mathrm{vec}\left(\hat{\mathbf{F}}(\phi_{test}) \right) = \mathbf{0}_{N^2 \times 1} \qquad (7.31)$$

where

$$\mathbf{B} = \left[\mathbf{I}_N \otimes \mathbf{P}_{\mathbf{m}(\phi_{test})} - \mathbf{G}(\phi_i)^T \otimes \mathbf{I}_N \right] \qquad (7.32)$$

Equation (7.31) states that the vector $\mathrm{vec}\left(\hat{\mathbf{F}}(\phi_{test}) \right)$ is in the null space of the matrix $\mathbf{B}$, i.e. $\mathrm{vec}\left(\hat{\mathbf{F}}(\phi_{test}) \right) \subseteq \mathcal{N}(\mathbf{B})$. However, the solution to (7.30) or (7.31) involves calculating the matrix $\mathbf{G}(\phi_i)^T$ for the set $\{\phi_i, \ i = 1, 2, \ldots\}$ which includes ϕ_{test}. To find the solution, the following squared Euclidean norm function is minimized to find the global minimum which should occur at $\phi_{i_o} = \phi_{test}$:

$$i_{\circ} = \arg\left\{ \min_i \left\| \mathbf{Y}\left(\hat{\mathbf{F}}(\phi_i) \right) \right\|_2^2 \right\} = \arg\left\{ \min_i \left\| \hat{\mathbf{E}}_{n_{test}}^H \hat{\mathbf{F}}(\phi_i) \hat{\mathbf{c}}^{(1)} \right\|_2^2 \right\} \qquad (7.33)$$

Note that the vector $\hat{\mathbf{c}}^{(1)}$ can be replaced by $\mathbf{c}^{(1)}$ if the latter is available. Once the

null space of **B** is calculated, $\hat{\mathbf{F}}(\phi_{test})$ can be found by reshaping $\text{vec}\left(\hat{\mathbf{F}}(\phi_{test})\right)$.

The aforementioned method for estimating $\hat{\mathbf{F}}(\phi_{test})$ cannot be used, however, when more than one signal is impinging on the ULA-SASPA array. The reason is the inability to form the search matrix $\mathbf{F}(\phi_i)$ when two signals are received unless these signals are close to each other; in which case, the set $\{\phi_i,\ i = 1, 2, \ldots\}$ is chosen with a step equal to the difference between the directions of the two received signals. Also, $\mathbf{F}(\phi_i)^{-1}$ is not defined for two signals since it is not a square matrix anymore.

As pointed out in Section 7.3, the method described above is valid for the CSUN data model of (6.1). In case of the system acting under the CSCN data model of (5.30), the test signal should have a very large SNR in order that the coupled noise among the array elements can be ignored.

7.7   Simulation Study

The following simulations demonstrate the effectiveness of the methods proposed in Section 7.5 to estimate the DOAs of the signals received by a ULA-SASPA array after estimating the mutual coupling. These examples are simulated for array geometries with very small interelement spacings. The mutual coupling is first estimated assuming a test signal with a known direction is incident on the array. The estimated mutual coupling is then used to estimate the DOAs of the underlying signals that are incident on the same array. Also, several simulations will be conducted to show the possibility of estimating $\hat{\mathbf{F}}(\phi_{test})$ from the measurements obtained from a ULA-SASPA array as explained in Section 7.6.

In Figure 7.1, the MUSIC spectra for two signals incident from $\phi_1 = 40°$ and $\phi_2 = 43°$ on a 6-element ULA-SASPA array with interelement spacing $d = 0.3\lambda$ are shown. The SNR of each of the received signals is 15 dB and five runs with 500 simulation snapshots for each run are used. The mutual coupling vector $\mathbf{c}^{(1)}$ is estimated with a test signal from $\phi_{test} = 82°$ and SNR $= 15$ dB. The upper plot is the

result of the simulation for estimating the DOAs along with the estimated mutual coupling vector $\hat{\mathbf{c}}^{(1)}$ using the process explained in Section 7.5. The lower plot is the simulation for estimating the DOAs with the actual mutual coupling vector $\mathbf{c}^{(1)}$. In addition to these plots, Figure 7.1 also shows a plot of the function $\mathbf{Y}\left(\hat{\mathbf{F}}(\phi_i)\right)$ defined in (7.33) versus ϕ_i.

Figure 7.2 shows the simulation results for the same scenario as in Figure 7.1 except the direction of the test signal is $\phi_{test} = 56°$, the received signals have $\text{SNR} = 15$ dB, and $d = 0.2\lambda$. Figure 7.3 shows the same simulation as Figure 7.2 but with $\text{SNR} = 20$ dB, and $\phi_{test} = 24°$.

Figures 7.4 shows the MUSIC spectrum for two signals arriving from $\phi_1 = 20°$ and $\phi_2 = 25°$, both with $\text{SNR} = 30$ dB, on a 6-element ULA-SASPA array with interelement spacing $d = 0.2\lambda$. Five runs with 1000 simulation snapshots for each run are used to obtain the plots. The test signal is from $\phi_{test} = 82°$.

Finally, Figure 7.5 shows the DOA estimation for two signals coming from $\phi_1 = 40°$ and $\phi_2 = 43°$ and impinging on the same array as in Figure 7.4 but with $d = 0.15\lambda$. Compared with the simulation of Figure 7.1, it is necessary to use for Figure 7.5 a higher SNR for the received signals (from 15 dB to 25 dB) and more snapshots (from 500 to 1000) to obtain distinguishable DOAs.

Figures 7.1 to 7.5 show that DOA estimation in conjunction with the estimated mutual coupling vector closely matches the results of DOA estimation in conjunction with the actual mutual coupling vector. This is in spite of the interelement spacing between the array elements is small and/or the signals that are incident on the array are spatially close. The plots for $\mathbf{Y}\left(\hat{\mathbf{F}}(\phi_i)\right)$ also confirm that the proposed method for estimating the DOA dependent steering matrix $\hat{\mathbf{F}}(\phi_{test})$ is effective and gives the exact value of ϕ_{test}.
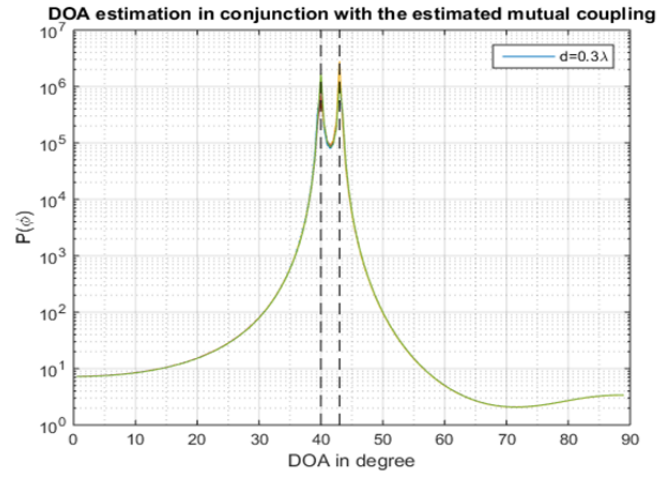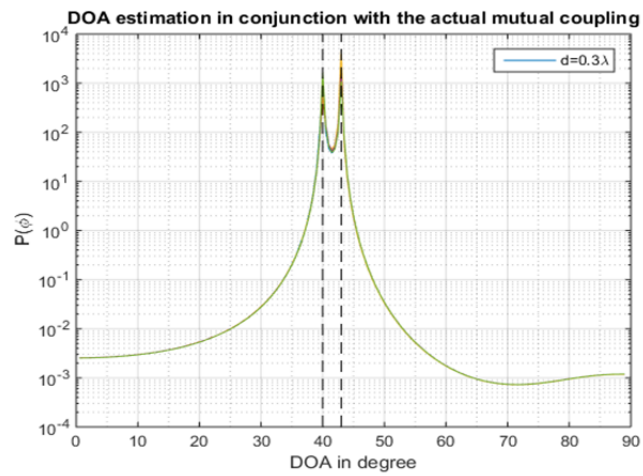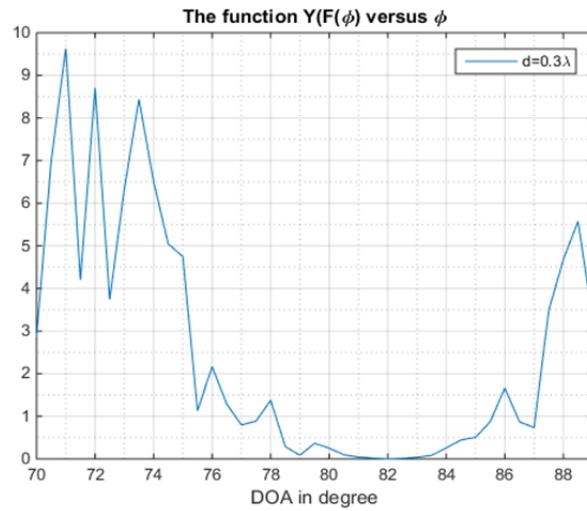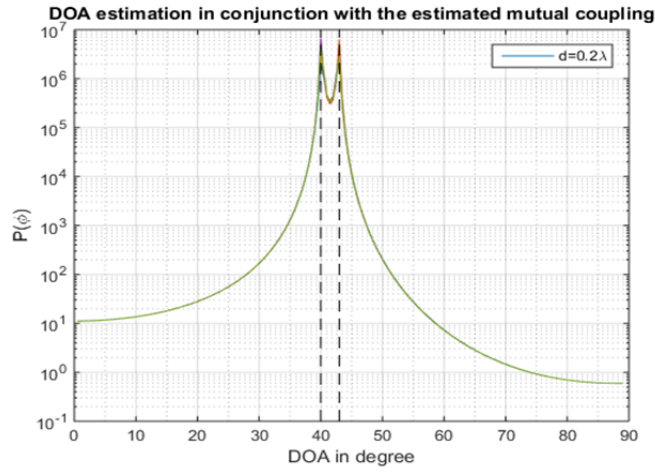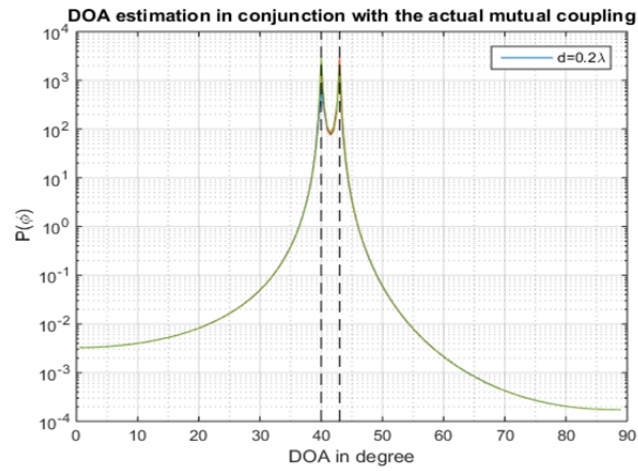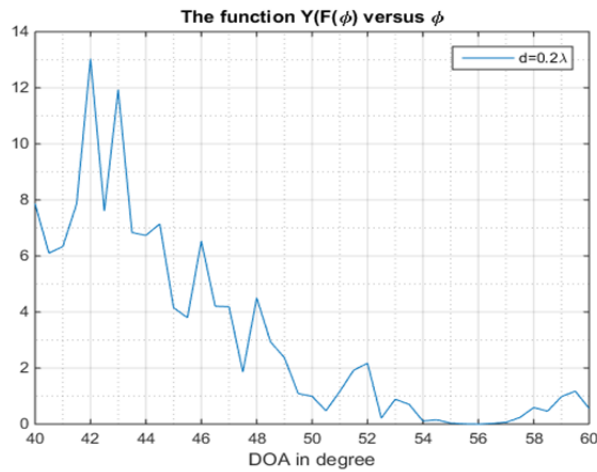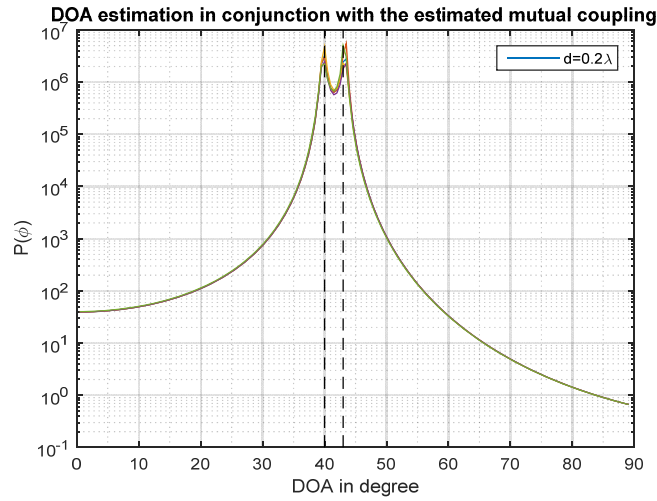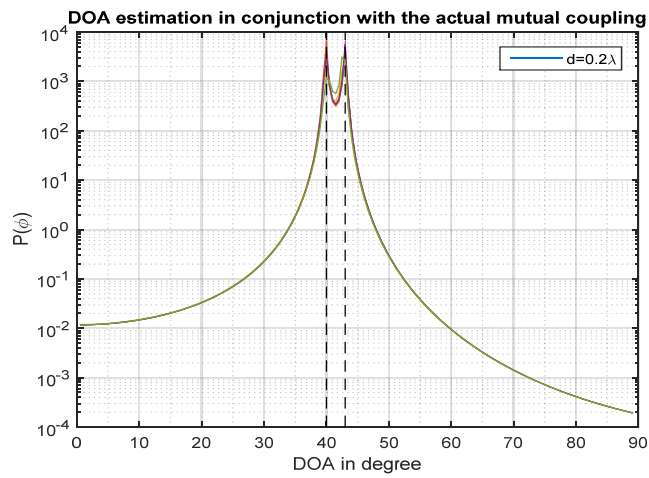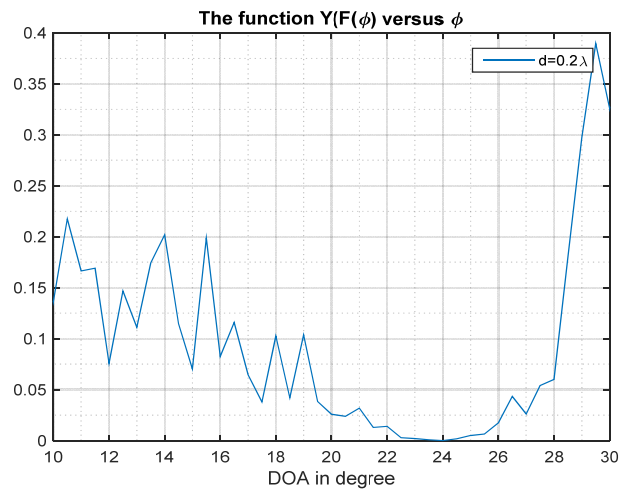
Figure 7.1: MUSIC spectrum for the DOA estimation of two signals impinging on a 6-dipole ULA-SASPA array with $d = 0.3\lambda$. The signals are from $\phi_1 = 40°$ and $\phi_2 = 43°$ with $\text{SNR} = 15 \text{ dB}$. Five simulation runs with 500 snapshots for each run are shown. The test signal has $\phi_{test} = 82°$. (a) In conjunction with the estimated $\hat{\mathbf{c}}^{(1)}$; (b) in conjunction with the actual $\mathbf{c}^{(1)}$; (c) the function $\mathbf{Y}\left(\hat{\mathbf{F}}(\phi_i)\right)$ versus ϕ_i.
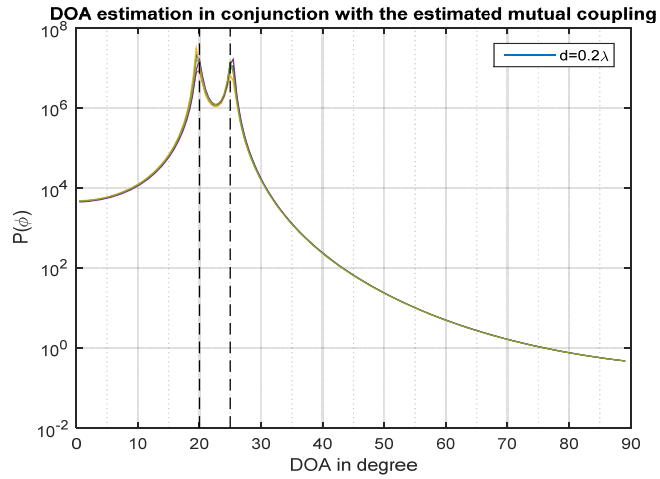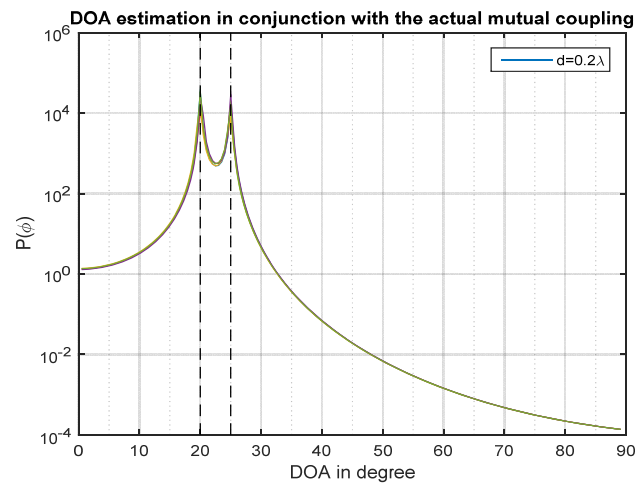
(a)

(b)

(c)

Figure 7.2: MUSIC spectrum for the DOA estimation of two signals impinging on a 6-dipole ULA-SASPA array with $d = 0.2\lambda$. The signals are from $\phi_1 = 40°$ and $\phi_2 = 43°$ with $\text{SNR} = 15$ dB. Five simulation runs with 500 snapshots for each run are shown. The test signal is $\phi_{test} = 56°$. (a) In conjunction with the estimated $\hat{\mathbf{c}}^{(1)}$; (b) in conjunction with the actual $\mathbf{c}^{(1)}$; (c) the function $\mathbf{Y}\left(\hat{\mathbf{F}}(\phi_i)\right)$ versus ϕ_i.
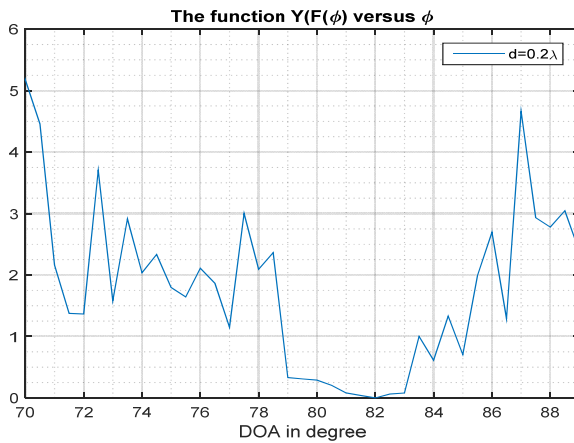
Figure 7.3: MUSIC spectrum for the DOA estimation of two signals impinging on a 6-dipole ULA-SASPA array with $d = 0.2\lambda$. The signals are from $\phi_1 = 40°$ and $\phi_2 = 43°$ with $\text{SNR} = 20\,\text{dB}$.. Five simulation runs with 750 snapshots for each run are shown. The test signal has $\phi_{test} = 24°$. (a) In conjunction with the estimated $\hat{\mathbf{c}}^{(1)}$; (b) in conjunction with the actual $\mathbf{c}^{(1)}$, (c) the function $\mathbf{Y}\left(\hat{\mathbf{F}}(\phi_i)\right)$ versus ϕ_i.
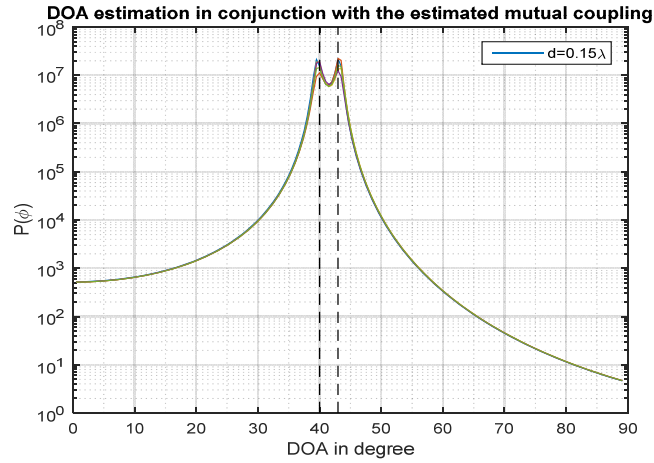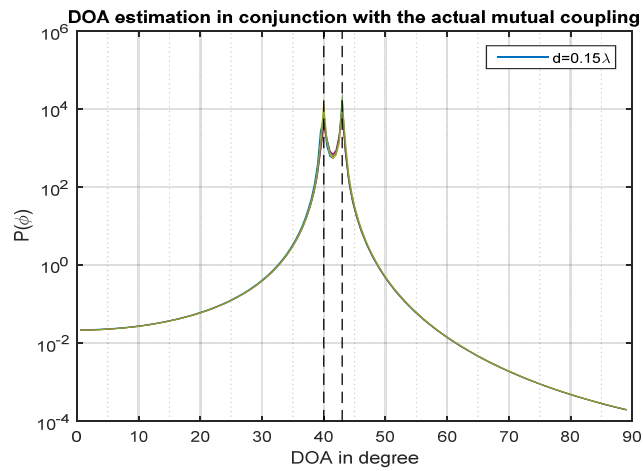
(a)

(b)

(c)

Figure 7.4: MUSIC spectrum for the DOA estimation of two signals impinging on a 6-dipole ULA-SASPA array with $d = 0.2\lambda$. The signals are from $\phi_1 = 20°$ and $\phi_2 = 25°$ with $\text{SNR} = 30$ dB.. Five simulation runs with 1000 snapshots for each run are shown. The test signal has $\phi_{test} = 82°$. (a) In conjunction with the estimated $\hat{\mathbf{c}}^{(1)}$; (b) in conjunction with the actual $\mathbf{c}^{(1)}$, (c) the function $\mathbf{Y}\left(\hat{\mathbf{F}}(\phi_i)\right)$ versus ϕ_i.
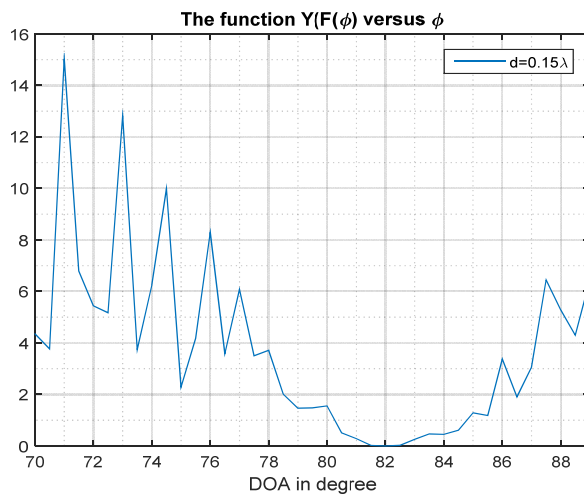
Figure 7.5: MUSIC spectrum for the DOA estimation of two signals impinging on a 6-dipole ULA-SASPA array with $d = 0.15\lambda$. The signals are from $\phi_1 = 40°$ and $\phi_2 = 43°$ with $\text{SNR} = 25\,\text{dB}$.. Five simulation runs with 1000 snapshots for each run are shown. The test signal has $\phi_{test} = 82°$. (a) In conjunction with the estimated $\hat{\mathbf{c}}^{(1)}$; (b) in conjunction with the actual $\mathbf{c}^{(1)}$, (c) the function $\mathbf{Y}\left(\hat{\mathbf{F}}(\phi_i)\right)$ versus ϕ_i.

7.8 RMSE Simulation

The RMSE criterion versus SNR for different for DOA estimation scenarios is examined in this section. Also, $\Delta\theta$, the angle between the estimated mutual coupling vector and the actual mutual coupling vector versus SNR is investigated. The formula (5.45) is used to calculate the RMSE, while the MATLAB built-in function "subspace" is used to find the angle $\Delta\theta$ between the estimated and the actual mutual coupling vectors.

Figure 7.6a shows the plot for the RMSE against SNR for a signal coming from $\phi_1 = 20°$ and incident on a 6-dipole ULA-SASPA array with interelement spacing $d = 0.2\lambda$. The plot is obtained from 50 runs with 10 snapshots for each run. In Figure 7.6b, the variation of the angle $\Delta\theta$ between the estimated and the actual mutual coupling versus SNR for the same scenario is shown. Figure 7.7 shows the variation of the same parameters, i.e., RMSE and the angle $\Delta\theta$, against SNR for the same scenario used for the plots in Figure 7.6 but with the number of the array elements reduced to four.

It can be clearly seen from the plots of Figures 7.6 and 7.7 that the power of the received signals has almost no effect on the performance of ULA-SASPA in estimating the unknown mutual coupling. This outcome is confirmed by the plots for the variation of $\Delta\theta$ for a wide range of SNR. The plots illustrate that the angle between the estimated mutual coupling and the actual mutual coupling vector is very small. This shows these two vectors are almost linearly dependent.
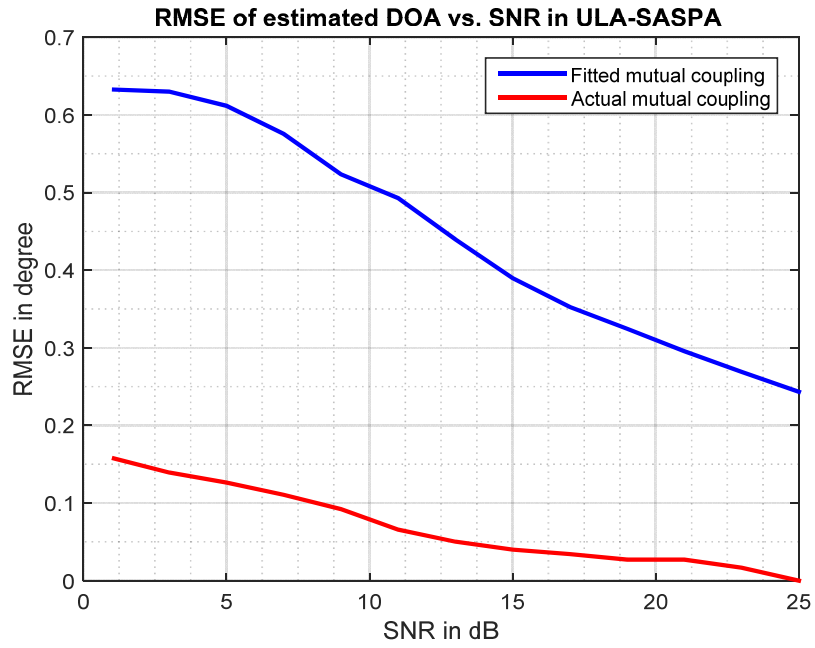
(a)
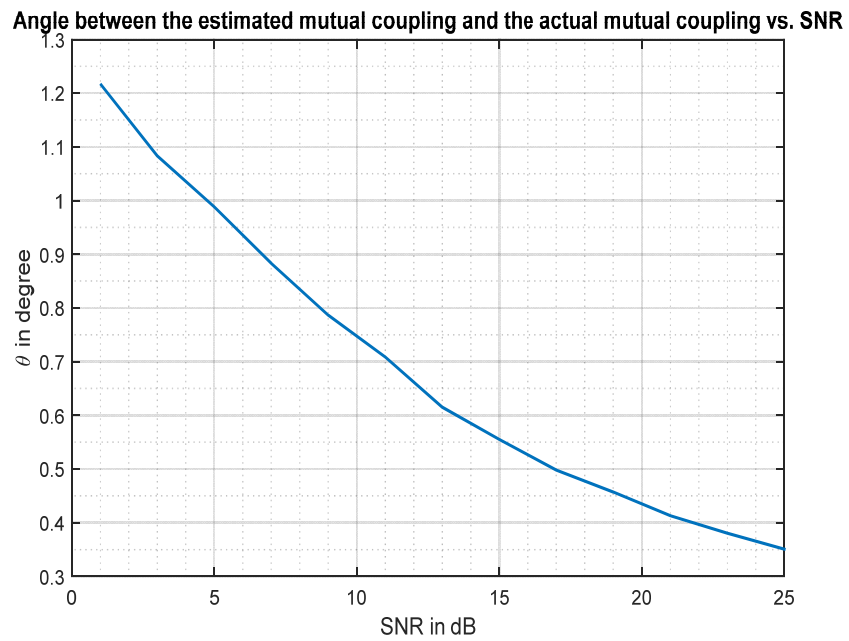
(b)

Figure 7.6: (a) RMSE of a signal coming from $\phi = 20°$ versus SNR. The signal is received by a six-dipole ULA-SASPA array with $d = 0.2\lambda$. The plots are derived from 50 runs with 10 snapshots for each run. (b) The angle between the estimated and the actual coupling vectors versus SNR.

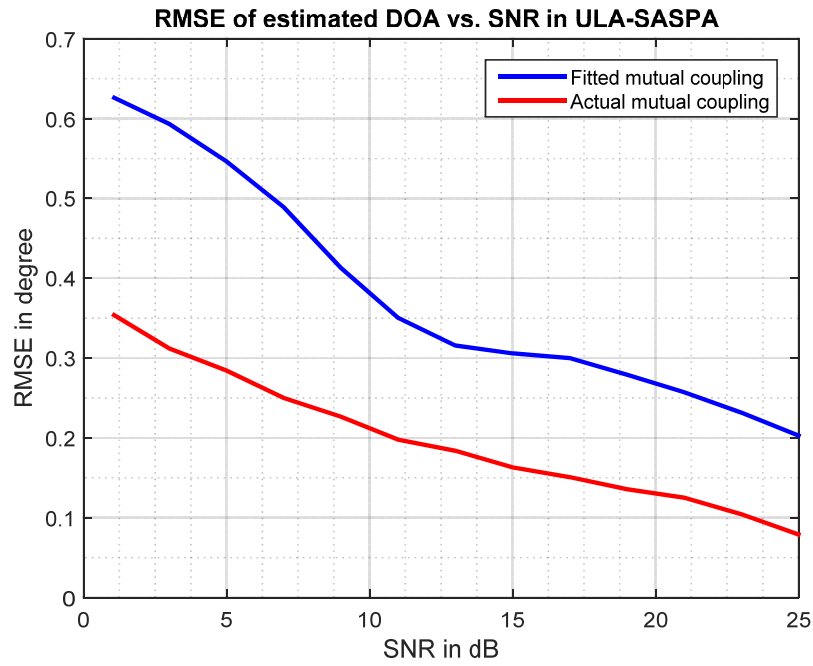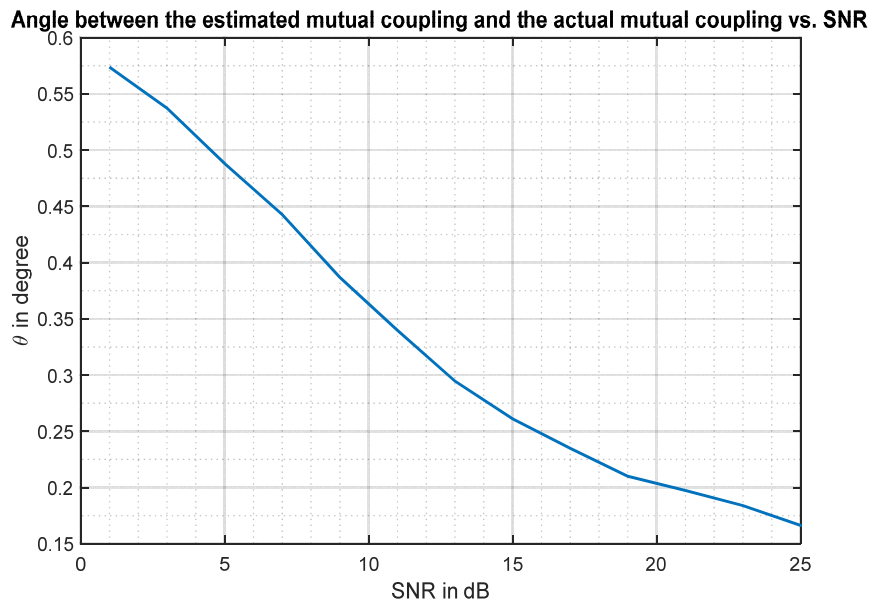(a)

(b)

Figure 7.7: (a) RMSE of a signal coming from $\phi = 20°$ versus SNR. The signal is received by a four-dipole ULA-SASPA array with $d = 0.2\lambda$. The plots are derived from 50 runs with 10 snapshots for each run. (b) The angle between the estimated and the actual coupling vectors versus SNR.

7.9   Summary

This chapter demonstrates the ability of a method proposed in this thesis to estimate the unknown mutual coupling vector of ULA-SASPA arrays. Determining the unknown mutual coupling is required when this inherent array phenomenon is time varying. Antenna arrays are subjected to the influence of different factors that may result in a previously determined mutual coupling to become out-of-date. Changing element behaviour, environmental changes, locating metal objects in the array's vicinity are some of these factors.

Most of the on-line mutual coupling estimation methods that have been proposed in the literature depend on finding, iteratively, the LS solutions to a cost function which involve the MCM together with other parameters. Thus, these methods are computationally intensive, are subjected to the problem of choosing a suitable set of initial values, may have issues with convergence of the iterative method, and are restricted by certain array conditions.

The proposed method in this Chapter exploits the structure of ULA-SASPA arrays from which a new steering matrix can be obtained. By making use of this newly formed steering matrix, the proposed method estimates the mutual coupling vector from the null space of a rank deficient matrix produced from the product of the orthogonal projection on the noise subspace with the real-valued DOA dependent steering matrix of the ULA-SASPA array. It has been proved that this null space has a one-to-one correspondence with the actual mutual coupling vector if only one signal is impinging on the array. Thereafter, the estimated mutual coupling vector can be used in the cost function of a MUSIC algorithm for precise estimation of the DOAs of the received signals.

Another key characteristic that distinguishes ULA-SASPA arrays from other antenna arrays, thus classifying them as an important class of antenna arrays, is the possibility of estimating the real-valued DOA dependent steering matrix $\mathbf{F}(\phi_{test})$. It is found

that $\mathbf{F}(\phi_{test})$ can be estimated from the solution of a Sylvester matrix equation when applied to the measurements of a ULA-SASPA array.

The plots for the MUSIC algorithm, RMSE criterion, and the angle difference between the estimated and the actual mutual coupling vectors, confirm the simplicity, importance and effectiveness of the method explained in this Chapter. It is clearly shown that using the estimated mutual coupling vector in the MUSIC cost function can result in high resolution DOA estimation similar to the DOA resolution when using the actual mutual coupling vector. This conclusion is also valid for small aperture ULA-SASPA arrays and for closely spaced received signals. If the array measurements involve the effect of noise that is coupled by mutual coupling, the proposed method is still valid provided the power of the test signal is high enough so that the coupled noise among the elements can be ignored.

Thus, the method formulated in this Chapter for determining the on-line mutual coupling characteristic in receiving ULA-SASPA arrays is found to be very efficient, easily implemented, and computationally less intensive.

Chapter 8

Conclusions and Future Work

8.1   Conclusions

This dissertation has studied the ability of a special kind of smart antenna arrays, called Switched Active Switched Parasitic Antenna (SASPA) arrays, to estimate the DOA of the received signals. In addition, the improvements due to the key characteristics these arrays provide over all-active antenna arrays are also explored. The main idea behind using such antenna array is the very fast changing between two states; active and parasitic, over the array elements in successive sub-snapshots which form a frame of one snapshot of the measurement. In each one of these sub-snapshots, one element is made active by connecting its terminals to the load and the other are made parasitic by short circuiting their terminals. Thus, N different measurements (N is the number of elements in the SASPA array) will be obtained within one snapshot. The fast switching can be implemented by RF PIN diodes integrated in the hardware that is connected to the terminal of each element of the SASPA array.

The capability and enhancement of SASPA arrays as direction finding arrays have been examined in conjunction with the MUSIC algorithm under different conditions of the data model. Also, the ability to estimate the unknown mutual coupling of a ULA-SASPA array is studied. The following conclusions explain briefly the results that are obtained when using SASPA arrays as direction finding arrays:

1. The main subject that is studied in **Chapter 2** is the mutual coupling between the elements of antenna arrays. This characteristic along with the element response determines the overall response of transmitting and receiving SASPA arrays. The available MCM in the literature are not useful for interpreting mutual coupling in receiving SASPA arrays. As a result, a new mutual coupling model called Coupled

Voltages to Uncoupled Currents (CVUC) has been formulated. This new model is derived from electromagnetic theory and represented by a Thévenin equivalent circuit. The CVUC model accommodates both conventional and SASPA receiving arrays.

2. **Chapter 3** discusses the principle of SASPA arrays and how these arrays operate as transmitting and receiving arrays. The switched radiation patterns produced by Uniform Linear Array SASPA (ULA-SASPA) arrays and Uniform Circular Array SASPA (UCA-SASPA) arrays indicate SASPA arrays have the flexible property of self-beamforming and self-steering their radiation pattern by simple successive changes of the state of each element in the array between active and parasitic states. The self-beamforming and self-steering property result from the coupled currents induced on each element and are accompanied inherently by a specific array factor produced due to the switching of one element to the active state at a given point in time. These beneficial properties avoid the requirement for weight vector that is needed in phased arrays to obtain beamforming and steering the array's radiation pattern.

Also, the mutual coupling matrix in transmitting SASPA arrays is studied so that a formula for the overall radiation pattern of these arrays in terms of the uncoupled currents of the elements is obtained. Therefore, the analysis of the performance of transmitting SASPA arrays provides a good insight to receiving SASPA arrays since these arrays obey the principle of reciprocity. However, receiving mutual coupling in SASPA arrays is different from transmitting SASPA arrays since the contribution of the active element to the overall response of SASPA arrays is different in transmitting and receiving modes.

Also, the validation of the CVUC model formulated in Chapter 2 is examined in this Chapter. It is shown that this model matches the mutual coupling in receiving SASPA arrays. This model has mapped the uncoupled currents on active and

parasitic elements to a vector of load voltages which is specifically the zero vector except for the entry corresponding to the active element. This vector of resultant load voltages is obtained when substituting the corresponding loads of the parasitic elements in the CVUC model by the zero impedance.

3. In **Chapter 4**, the well-known DOA algorithm; MUSIC is reviewed. This algorithm estimates the DOAs of signals received by all-active antenna arrays by exploiting the properties of the signal and noise subspaces obtained from the eigendecomposition of the covariance matrix of the measurements. The data model of the measurements at the terminals of the array elements reflects the response of the array to the received signals and to noise as well. The MUSIC algorithm searches for the orthogonality between the noise subspace and the search vector which defines the response of the array to all possible directions. The spectral decomposition on which MUSIC relies on is efficient and computationally less complex than other direction-finding algorithms. However, certain conditions should be considered to achieve unbiased, successful, and distinguishable DOAs estimation with high resolution when using the MUSIC algorithm. These conditions are large number of measurement snapshots, large array aperture, high SNR of the received signals and the number of array elements should be greater the number of received signals. Violation of one or more of these factors may result in poor resolution or undistiguashable DOAs. Several simulations for DOA estimation using MUSIC have been conducted to show the importance of the aforementioned factors.

The CVUC model is used in this Chapter to illustrate the validity of the constraint on the maximum number of signals received by a receiving FASPA array. It is shown that when the number of active elements in an FASPA array is less than the number of received signals, MUSIC algorithm fails to estimate the desired DOAs despite the actual number of array elements (active plus parasites) is greater than the received signals. Also, it is found in this Chapter that using the CVUC model contributes to producing three subspaces; signal subspace, noise subspace, and parasitic subspace.

These subspaces are mutually orthogonal to each other. However, using the parasitic subspace in the cost function of MUSIC gives DOA spectrum that is superior to the spectrum obtained with the noise subspace. The reason is that the eigenvalues accompanied with the parasitic subspace all have "solid" zero values. Accordingly, the merging of a portion of the signal subspace into the parasitic subspace will not occur even when some of the eigenvalues of the signal subspace are small.

4. **Chapter 5** is dedicated to investigating the capability of and the enhancement offered by SASPA arrays in DOA estimation. In this chapter, the scenario *coupled-signals-coupled-noise* is assumed for the data model of SASPA arrays. This means that the energy excited by the received signals and the noise are coupled among the array elements. The noise which is affected by mutual coupling is the background noise picked up by all the array elements. Processing the measurements of a receiving SASPA array under the *coupled-signals-coupled-noise* model results in the steering matrix being scaled by factor of *N*. This outcome is noteworthy since a directive gain to the underlying received signals will be attained. Accordingly, the estimated signal subspace of SASPA arrays will be accompanied with eigenvalues larger than the eigenvalues of the signal subspace obtained from an all-active antenna array.

It is found by conducting several simulations of DOA estimation using the MUSIC algorithm that SASPA arrays (ULA-SASPA and UCA-SASPA) structured in small size apertures provide significant improvements in DOA estimation as compared with the analogous all-active antenna arrays. Also, the plots for the criterion RMSE for signals coming from different directions and received by SASPA arrays demonstrate the efficiency of these arrays since these plots show almost constant performance over a wide range of SNRs.

5. In **Chapter 6**, the data model of a ULA-SASPA array is assumed to follow the *coupled-signals-uncoupled-noise* model. The main sources of noise are those made

by the electronic circuitry and they are not affected by mutual coupling. The structure of ULA-SASPA arrays under such conditions offers two advantages. Firstly, the power of the noise will be reduced by half. Secondly, a new steering matrix that is different from the steering matrix of ULA all-active arrays can be obtained. The new steering matrix is a product of a real-valued matrix and a matrix. The second matrix represents the mutual coupling but its number of columns is half the number of columns of the original MCM. The real-valued matrix contains the DOA information. The new steering matrix reduces the computational complexity of calculating the steering matrix and the covariance matrix of the measurements. Also, the estimated signal subspace will be accompanied by larger real eigenvalues, and the round-off error will be reduced. Generation of the real-valued steering matrix in ULA-SASPA array needs no transformation matrices that are used in other works in the literature such as the method used in [74]. As a result, ULA-SASPA arrays provide high resolution DOA estimation that is superior to ULA all-active antenna arrays.

Several simulations conducted for estimating the DOAs of received signals using MUSIC in conjunction with ULA-SASPA arrays has asserted this superiority. The simulations show clearly that spatially close signals have been distinguishably detected when incident on small aperture ULA-SASPA arrays. The effectiveness of ULA-SASPA arrays is also noticed when the RMSE criterion is used to study the performance of MUSIC for received signals that are emanated from different directions.

6. It can be concluded from the work of **Chapter 7** that ULA-SASPA array can be used effectively for estimating the unknown mutual coupling before estimating the DOAs of signals impinging on this array. A test signal incident on the underlying ULA-SASPA array is first used to estimate the vector of the mutual coupling. The null space of a rank deficient matrix determines the fitted vector to the actual mutual coupling vector. The rank deficient matrix is produced from the product of the

orthogonal projection on the noise subspace of the covariance matrix of the measurement of the test signal by the real-valued DOA dependent steering matrix of the test signal.

The proposed method is clearly very simple and require small amount of computations compared with other methods proposed in the literature which most of them depend on iterative LS solutions such as the methods used in [24] and [81].

Simulations for DOA estimation using MUSIC show that the fitted vector greatly matches the actual mutual coupling vector since the MUSIC spectrums obtained in conjunction with these two vectors are very similar. Also, the plots for RMSE for the received signal versus SNR show that the performance of a ULA-SASPA array as an estimator for mutual coupling and DOA is almost SNR independent. The plots for the angle difference between the estimated and actual mutual coupling vectors show obvious linear dependency between them.

Finally, the following is a list of the advantages provided by SASPA arrays in brief:

1. Capability of DOA estimation with very high resolution as compared with all-active antenna arrays.

2. Estimation of the unknown mutual coupling of the array.

3. Self-beamforming and self-steering of the overall radiation pattern of the array.

4. Providing parasitic subspace that is orthogonal to the signal subspace and having eigenvalues with zero value.

5. Reduction in the computation complexity for calculating the steering matrix and the covariance matrix.

6. Operation at low SNR and with short data measurements.

7. Possible physically fitting into compact devices.

8.2   Suggested Future Work

To the best of the author's knowledge, the subject of using SASPA arrays in high resolution DOA estimation and the enhancement that these arrays provide was rarely investigated in the literature. Thus, many and different future work can be conducted on this type of antenna arrays through considering several parameters which may give further attention to SASPA arrays since these arrays are beneficial when mounted in a user's compact sets.

1. The consecutive switching of each element to the active state in SASPA arrays results in steering matrices associated with the array's key characteristics. These characteristics allocate advantages to SASPA array as receiving antenna arrays when used in the field of DOA estimation. The case of switching one element to the active state within one sub-snapshot period and leaving the other elements in the parasitic state has been dealt with in this work. It will be useful to study the advantages and improvements of these arrays when several elements are enabled to be active during one sub-snapshot. The mutual coupling model for such a scenario is required to be updated over the mutual coupling model of the SASPA arrays formed in this work. In addition, the structure of the steering matrix for both conditions; known and unknown mutual coupling can also be investigated.

2. The DOA dependent matrix in (6.64), $\mathbf{\Gamma}(\phi)$, can be estimated from the equation (7.5) which represents the homogenous Sylvester equation $\mathbf{AX} - \mathbf{BX} = \mathbf{0}$. It is useful to estimate the matrix $\mathbf{P}_{\mathbf{U}/\mathbf{D}(\phi)}$ from the array's measurement of the received signals. Thus, estimation of $\mathbf{\Gamma}(\phi)$ may lead to estimating the DOAs directly with accurate values without using the MUSIC cost function or other DOA algorithms. Hence, new algorithms based on ULA-SASPA arrays may be formulated.

3. In Chapter 6, the number of the elements in a ULA-SASPA array is assumed to be even. The new measurements $\mathbf{z}_1(t)$ and $\mathbf{z}_2(t)$ can be obtained either from

adding the first $N/2+1$ measurements to the remaining flipped upside-down $N/2+1$ measurements and subtracting the last flipped upside-down $N/2$ measurements from the first $N/2$ measurement or vice versa. A further analysis for these new measurements can be studied to investigate the advantages that might be obtained when using ULA-SASPA arrays with odd N.

4. In this work, the received signals are assumed to be uncorrelated. It is advantageous to study the performance of SASPA arrays when receiving correlated signals. Under such a case, the signal covariance matrix $\mathbf{S} = \mathbb{E}\left\{\mathbf{s}(t)\mathbf{s}(t)^H\right\}$ will no-longer be diagonal. This could be investigated for both the data models assumed in Chapters 5 and 6.

5. To work on UCA-SASPA arrays with unknown mutual coupling and to follow the same procedure of obtaining the steering matrix as was carried out in Chapter 7. It is well known that UCA arrays are more beneficial than ULA because of their symmetrical and unambiguous characteristics. Therefore, processing the measurements of UCA-SASPA array with unknown mutual coupling could lead to a new data model and in turn to estimated subspaces from which DOA and coupling matrix determination can be achieved more accurately.

Appendix A – Figure 3.3

To show how exchanging the state of the elements in Figure 3.3 between active and parasitic states results in (3.3), the following diagrams illustrate the idea. To start with, the geometry of the antenna array corresponding to (3.2) is as follows:

🔵   active element
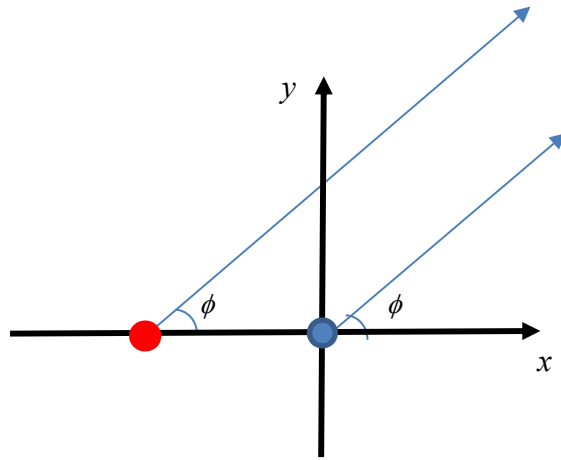
🔴   parasitic element

Figure A1

The expression for the total *H*-plane electric field in Figure A1 is given by (3.2) and is rewritten below for ready reference [15]:

$$E_{tot1}(r,\theta,\phi) = \alpha(\theta)[i_P \quad i_C]\left[e^{-jkd\cos\phi} \quad 1\right]^T \tag{3.2}$$

When the active and parasitic states are swapped between the two elements in Figure A1, the geometry of the antenna array becomes as shown in Figure A2.

The new expression for the total *H*-plane electric field as a result of the antenna array shown in Figure A2 is:

$$E_{tot2}(r,\theta,\phi) = \alpha(\theta)[i_C \quad i_P]\left[e^{-jkd\cos\phi} \quad 1\right]^T \tag{3.3}$$
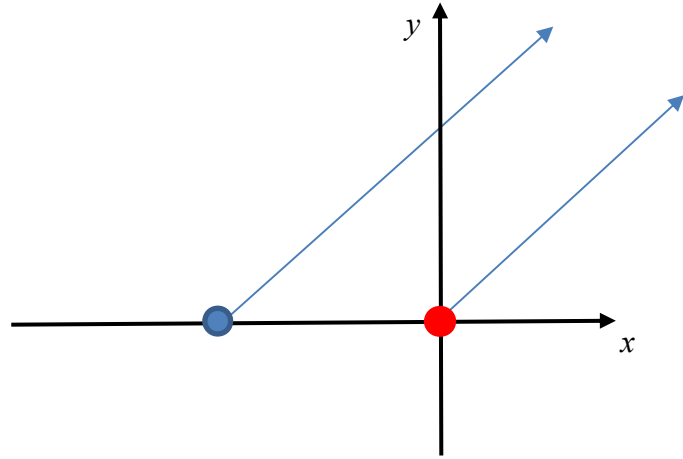
Figure A2

Figure A2 can be updated by shifting the *y*-axis to the left so that the active element is positioned at the origin. This can be implemented if (3.3) is multiplied by the factor $e^{+jkd\cos\phi}$. Thus, Figure A2 becomes:as shown in Figure A3.
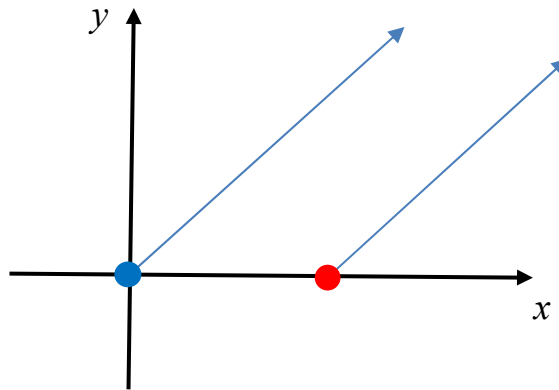

Figure A3

The resultant total electric field can now be expressed as:

$$E_{tot2}(r,\theta,\phi)=\alpha(\theta)[i_C \quad i_P]e^{+jkd\cos\phi}\left[e^{-jkd\cos\phi} \quad 1\right]^T$$
$$=\alpha(\theta)[i_C \quad i_P]\left[1 \quad e^{+jkd\cos\phi}\right]^T \tag{A1}$$

But

$$e^{+jkd\cos\phi}=e^{-jkd(-\cos\phi)}=e^{-jkd\cos(\phi+\pi)} \tag{A2}$$

Therefore,

$$E_{tot2}(r,\theta,\phi)=\alpha(\theta)\begin{bmatrix} i_C & i_P \end{bmatrix}\begin{bmatrix} 1 & e^{-jkd\cos(\phi+\pi)} \end{bmatrix}^T$$

$$=\alpha(\theta)\begin{bmatrix} i_P & i_C \end{bmatrix}\begin{bmatrix} e^{-jkd\cos(\phi+\pi)} & 1 \end{bmatrix}^T \qquad \text{(A3)}$$

which when compared with (3.2), it can be seen that the radiation pattern will be the same as the one produced by (3.2) except it is rotated around the *y*-axis by $180°$.

References

[1] *IEEE Trans. Antennas and Propagation*, Special Issue on Adaptive Antennas, vol. 24, no. 5, September 1976.

[2] R. A. Monzingo and T. W. Miller, *Introduction to Adaptive Arrays*, Wiley, 1980.

[3] S. Haykin (ed.), J. H. Justice, N. L. Owsley, J. L. Yen and A. C. Kak, *Array Signal Processing*, Prentice-Hall, 1985.

[4] *IEEE Trans. Antennas and Propagation*, Special Issue on Adaptive Processing Antenna Systems, vol. 34, no. 3, March 1986.

[5] B. D. Van Veen and K. M. Buckley, "Beamforming: A Versatile Approach to Spatial Filtering," *IEEE ASSP Magazine*, vol. 5, no. 2, pp. 4-24, April 1988.

[6] S. U. Pillai, *Array Signal Processing*, Springer-Verlag, 1989.

[7] D. H. Johnson and D. E. Dudgeon, *Array Signal Processing: Concepts and Techniques*, Prentice-Hall, 1993.

[8] H. Krim and M. Viberg, "Two Decades of Array Signal Processing Approach, The Parametric Approach," *IEEE Signal Processing Magazine*, vol. 13, no. 4, pp. 67- 94, July 1996.

[9] H. L. Van Trees, *Optimum Array Processing*, Wiley, 2002.

[10] J. Benesty, J. Chen and Y. Huang, *Microphone Array Signal Processing*, Springer-Verlag, 2008.

[11] P. S. Naidu, *Sensor Array Signal Processing*, 2nd ed., CRC Press, 2009.

[12] B. Völcker, M. Bengtsson and B. Ottersten, "Spatially Spread Sources in Antenna Array Processing," in S. Chandran (ed.), *Adaptive Antenna Arrays: Trends and Applications*, Springer-Verlag, 2004.

[13] R. O. Schmidt, "Multiple Emitter Location and Signal Parameter estimation," *IEEE Trans. Antennas and Propagation*, vol. 34, no. 3, pp. 276-280, March 1986.

[14] R. Roy and T. Kailath, "ESPRIT – Estimation of Signal Parameters Via Rotational Invariance Techniques," *IEEE Trans. Acoustics, Speech, and Signal Processing*, vol. 37, no. 7, pp. 984-995, July 1989.

[15] D. V. Thiel and S. Smith, *Switched Parasitic Antennas for Cellular Communications*, Artech House, 2002.

[16] T. Svantesson and M. Wennstrom, "High-resolution direction finding using a switched parasitic antenna," in *Proc. 11th IEEE Signal Processing Workshop on Statistical Signal Processing,* Singapore, August 2001, pp. 508–511.

[17] T. Svantesson, *Antennas and Propagation from a Signal Processing Perspective*, PhD Thesis, Chalmers University of Technology, Sweden, 2001.

[18] C. A. Balanis, *Antenna theory: Analysis and design*, 4th ed., John Wiley & Sons, 2016.

[19] S. J. Orfanidis, *Electromagnetic Waves and Antennas*, Rutgers University. Available at www.ece.rutgers.edu/~orfanidi/ewa.

[20] J. D. Kraus, *Antennas*. McGraw Hill. New York. 1988.

[21] E. C. Jordan and K. G. Balmain, *Electromagnetic waves and radiating systems*. 2nd ed. Prentice Hall, New Jersey, 1968.

[22] K. Kishore, *Antenna and wave propagation*. I.K. International Publishing House. Pvt. Ltd, New Delhi, 2009.

[23] H. Singh, H. L. Sneha, and R. M. Jha, "Mutual coupling in phased arrays: A Review", *International Journal of Antennas and Propagation*, vol. 2013, Article ID 348123, 23 pages.

[24] T. Svantesson, *Direction Finding in the Presence of Mutual Coupling*. Thesis for the degree of Licentiate of Engineering. Department of Signals and Systems. School of Electrical and Computer Engineering. Chalmers University of Technology. Sweden 1991.

[25] P. Kildal, "Equivalent Circuits of Receive Antennas in Signal Processing Arrays", *Microwave and Optical Technology Letters*, vol. 21, no. 4, pp. 244-246, May 1999.

[26] A. W. Love, "Comments on "Limitations of the Thévenin and Norton Equivalent Circuits for a Receiving Antenna", *IEEE Antennas and Propagation Magazine*, vol. 45, no. 4, August 2003.

[27] D. Pozar, "Scattered and Absorbed Powers in Receiving Antennas", *IEEE Antennas and Propagation Magazine*, vol. 46, no. 1, February 2004.

[28] S. R. Best and B. C. Kaanta, "A Tutorial on the Receiving and Scattering Properties of Antennas", *IEEE Antennas and Propagation Magazine*, vol. 51, no. 5, October 2009.

[29] P. Papakanellos, "Study of Scattering and Receiving Dipole Antennas on the Basis of the Method of Auxiliary Sources", *Electromagnetics,* vol. 23, no. 6, pp. 525-537, January 2003. doi: 10.1080/02726340390222053

[30] R. P. Meys, "A Summary of the Transmitting and Receiving Properties of Antennas", *IEEE Antennas and Propagation Magazine*, vol. 42, no. 3, June 2000.

[31] J. V. Bladel, "On the Equivalent Circuit of a Receiving Antenna", *IEEE Antennas and Propagation Magazine*, vol. 44, no. 1, February 2002.

[32] R. E. Collin, "Limitations of the Thévenin and Norton Equivalent Circuits for a Receiving Antenna", *IEEE Antennas and Propagation Magazine*, vol. 45, no. 2, April 2003.

[33] A. W. Love, "Comment: On the Equivalent Circuits of a Receiving Antenna", *IEEE Antennas and Propagation Magazine*, vol. 44, no. 5, October 2002.

[34] J. L. Allen and B. L. Diamond, "Mutual Coupling in Antenna arrays", *Technical Report*, Lincoln Laboratories, Massachusetts Institute of Technology, 1966.

[35] C. Craeye and D. González-Ovejero, "A review on array mutual coupling analysis", *Radio Sci.*, vol. 46, no.2, April 2011. doi: 10.1029/2010RS004518.

[36] T. Su and H. Ling, "On modelling mutual coupling in antenna arrays using the coupling matrix", *Microwave and Optical Technology Letters*, vol. 28, no. 4, pp. 231-237, 2001.

[37] I. J. Gupta and A. A. Ksienski, "Effect of Mutual Coupling on the Performance of Adaptive Arrays", *IEEE Transactions on Antennas and Propagation*, vol. AP-31, no.5, September 1983.

[38] E. BouDaher *et al.,* "DOA Estimation with Co-Prime Arrays in the Presence of Mutual Coupling", *23rd European Signal Processing Conference (EUSIPCO)*, pp. 2880-2884, 2015.

[39] Z. Liu, *et al.*, "DOA estimation with uniform linear arrays in the presence of mutual coupling via blind calibration", *Signal Processing* 89, pp. 1446-1456, July 2009. doi: 10.1016/j.sigpro.2009.01.017

[40] H. E. King, "Mutual Impedance of Unequal Length Antennas in Echelon", *IRE Transactions on Antennas and Propagation*, vol. AP-5, pp. 306-313, 1957.

[41] H. Yamada, Y. Ogawa, and Y. Yamagucji, "Mutual Coupling Compensation in Array Antenna for High-Resolution DOA Estimation", *Proceedings of ISAP2005*, Korea, 2005.

[42] T. Sato and R. Kohno, "New Calibration Matric Calculation Method for Removing the Effect of Mutual Coupling for Uniform Linear Arrays", *IEEE 63rd Vehicular Technology Conference*, vol. 6, pp. 2686-2690, 2006.

[43] H. T. Hui, "A New Definition of Mutual Impedance for Application in Dipole Receiving Antenna Arrays", *IEEE Antennas and Wireless Propagation Letters*, vol. 3, pp. 364-367, 2004.

[44] H. T. Hui and S. Lu, "Receiving Mutual Impedance between Two Parallel Dipole Antennas", *IEEE Region 10 Conference*, pp. 1-4, 2006.

[45] H. Lui, H. T. Hui, and M. S. Leong "A note on the Mutual-Coupling Problems in Transmitting and Receiving Antenna Arrays", *IEEE Antennas and Propagation Magazine*, vol. 51, no. 5, pp. 171-176, 2009.

[46] Y. Yu and H. T. Hui, "Design of Mutual Compensation Network for a Small Receiving Monopole Array", *IEEE Transactions on Microwave Theory and Techniques,* vol. 59, no. 9, pp. 2241-2245, 2011

[47] H. S. Lui and H. T. Hui, "Mutual Coupling Compensation for Direction-of-Arrival Estimations Using the Receiving-Mutual-Impedance Method", *International Journal of Antennas and Propagation,* vol. 2010, Article ID 373061, 7 pages, 2010.

[48] S. Henault and Y. M. M. Antar, "Comparison of Various Mutual Coupling Compensation Methods in Receiving Antenna Arrays", *IEEE Antennas and Propagation Society International Symposium,* pp. 1-4, June 2009.

[49] N. Parhizgar *et al.,* "A Modified Decoupling Scheme for Receiving Antenna Arrays with Application to DOA Estimation", *International Journal of RF and Computer-Aided Engineering,* vol. 23, no. 2, pp. 246-259, 2013.

[50] C. Yeh, M. Leou, and D. R. Ucci, "Bearing Estimation with Mutual Coupling Present", *IEEE Transactions on Antennas and Propagation*, vol. 37, no. 10, October 1989.

[51] R. G. Vaughan and J. B. Andersen, "Antenna Diversity in Mobile Communications", *IEEE Transactions on Vehicular Technology*, vol. VT-36, no. 10, November 1987.

[52] C. W. Harrison, "Calculation of the Impedance Properties of Parasitic Antenna Arrays Involving Elements of Finite Radius", *Wiley Online Library,* May 2009. doi:10.1111/j.1559-3584. 1945.tb01663.x

[53] R. W. P. King, G. J. Fikioris, and R. B. Mack*, Cylindrical Antenna and Arrays*, Cambridge University Press 2002.

[54] T. A. Milligan, *Modern Antenna Design*, 2nd ed., A John Wiley & Sons, INC., Publications, 2005.

[55] Yagi-Uda Antenna, From Wikipedia, the free encyclopedia, https://en.wikipedia.org/wiki/Yagi%E2%80%93Uda_antenna

[56] R. G. Vaughan, "Switched Parasitic Elements for Antenna Diversity" *IEEE Transactions on Antennas and Propagation*, vol. 47, no. 2, pp. 399-405, February 1999.

[57] N. L. Scott, M. O. Leonard-Taylor and R. G. Vaughan, "Diversity Gain from a Single-Port Adaptive Antenna Using Switched Parasitic Elements Illustrated with a Wire and Monopole Prototype", *IEEE Transactions on Antennas and Propagation*, vol. 47, no. 6, pp. 1066-1070, June 1999.

[58] A. A. Almhdie, V. Kezys, and T. D. Todd, "Improved Capacity TDMA/SDMA using Switched Parasitic Antennas", *IEEE international symposium on personal, indoor and mobile communications*, vol. 1, pp. 363-367, London, September 2000.

[59] Microsemi-Watertown, *THE PIN DIODE CIRCUIT DESIGNERS' HANDBOOK*, Microsemi Corporation, 1998.

[60] PIN diode, From Wikipedia, the free encyclopedia, https://en.wikipedia.org/wiki/PIN_diode

[61] Iulian Rosu, YO3DAC/VA3IUL, *RF Switches*, https://www.qsl.net/va3iul/RF_Switches/RF_Switches.pdf

[62] P. K. Varlamos and C. N. Capsalis, "Direction-of-Arrival Estimation (DOA) Using Switched Parasitic Planar Arrays and the Method of Genetic Algorithms", *Wireless Personal Communications*, vol. 28(1), pp. 59-75, 2004.

[63] S. Chandran (ed.), *Advances in Direction-of-Arrival Estimation*, ARTECH HOUSE, INC. 2006.

[64] J. Foutz, A. Spanias, and M. K. Banavar, *Narrowband Direction of Arrival Estimation for Antenna Arrays*, Morgan & Claypool Publishers 2008.

[65] Z. Chen, G. Gokeda, and Y. Yu, *Introduction to Direction-of-Arrival Estimation*, Artech house, 2010.

[66] R. O. Schmidt, *A signal subspace approach to multiple emitter location and spectral estimation*, Ph.D. dissertation, Stanford University, Palo Alto, CA, 1982.

[67] B. D. Carlson, "Covariance Matrix Estimation Errors and Diagonal Loading in Adaptive Arrays", *IEEE Transactions on Aerospace and Electronics Systems*, vol 24. no. 4 July 1988.

[68] P. Stocia and A. Nehorai, "MUSIC, Maximum Likelihood, and Cramer-Rao Bound", *IEEE Transactions on Acoustics, Speech, and Signal Processing*, vol. 37, no. 5, pp. 720-741, May1989.

[69] M. S. Vijay and U. L. Bombale, "An Overview of Smart Antenna and a Survey on Direction of Arrival Estimation Algorithms for Smart Antenna", *IOSR Journal of Electronics and Communication Engineering (IOSR-JECE) ISSN: 2278-2834 ISBN: 2278-8735* pp. 01-06.

[70] G. H. Golub and C. F. Van Loan, *Matrix Computation*, 4th ed., The Johns Hopkins University Press, 2013.

[71] R. H. Roy. *ESPRIT: Estimation of signal parameters via rotational invariance techniques*, Ph.D. dissertation, Stanford University, 1987.

[72] Toeplitz matrix, From Wikipedia, the free encyclopedia, https://en.wikipedia.org/wiki/Toeplitz_matrix

[73] Circulant matrix, From Wikipedia, the free encyclopedia, https://en.wikipedia.org/wiki/Circulant_matrix

[74] M. Haardt, *Efficient One-, Two-, and Multidimensional High-Resolution Array Signal Processing*, Shaker Verlag, Aachen 1997.

[75] H. Lee, and M. Wengrovitz, "Resolution threshold of beam space MUSIC for two closely spaced emitters", *IEEE Transactions on Acoustics, Speech, and Signal Processing*, vol. 38, no. 9, pp. 1545-1559, September 1990.

[76] Moore-Penrose pseudoinverse, From Wikipedia, the free encyclopedia, https://en.wikipedia.org/wiki/Moore%E2%80%93Penrose_inverse

[77] M. Shaghaghi and S. A. Vorobyov, "Subspace Leakage Analysis and Improved DOA Estimation With Small Sample Size", *IEEE Transactions on Signal Processing,* vol. 63, no. 12, June 2015.

[78] M. L. McCloud and L. L. Scharf, "A New Subspace Identification Algorithm for High-Resolution DOA Estimation", *IEEE Transactions on Antennas and Propagation*, vol. 50, no. 10, pp. 1382-1390, October 2002.

[79] Singular Value Decomposition, From Wikipedia, the free encyclopedia https://en.wikipedia.org/wiki/Singular_value_decomposition

[80] B. R. Jackson *et al.*, "Direction of Arrival Estimation using Directive Antennas in Uniform Circular Arrays", *IEEE Transactions on Antennas and Propagation*, vol. 63, no. 2, pp. 736-747, February 2015.

[81] B. Friedlander and A. J. Weiss, "Direction Finding in the Presence of Mutual Coupling", *IEEE Transactions on Antennas and Propagation*, vol. 39, no. 3, pp. 273-284, March 1991.

[82] Normal Distribution, From Wikipedia, the free encyclopedia, https://en.wikipedia.org/wiki/Normal_distribution

[83] Hadamard products (matrices), From Wikipedia, the free encyclopedia, https://en.wikipedia.org/wiki/Hadamard_product_(matrices)

[84] W.-H. Steeb and Y. Hardy, *Matrix calculus and Kronecker product: a practical approach to linear and multilinear algebra*, 2nd ed., World Scientific Publishing Co. Pte Ltd, Singapore, 2011.

[85] K.-C. Huarng and C.-C. Yeh, "A Unitary Transformation Method for Angle-of-Arrival Estimation", *IEEE Transactions on Signal Processing,* vol. 39, no. 4, April 1991.

[86] J. Dai, W. Xu, and D. Zhao, "Real-Valued DOA estimation for uniform linear array with unknown mutual coupling", *Signal Processing 92*, pp 2056-2065, 2012. doi: 10.1016/j.sigpro.2012.01.017

[87] Z. Ye, J. Dai, X. Xu and X. Wu, "DOA Estimation for Uniform Linear Array with Mutual Coupling", *IEEE Transactions on Aerospace and Electronic Systems*, Vol. 45, No.1 January 2009.

[88] I. Selesnik, "Least Squares with Examples in Signal Processing", NYU-Poly, March 2013. https://www.semanticscholar.org/paper/Least-Squares-with-Examples-in-Signal-Processing-1-Selesnick/7164db0fa52a1a7e1be91586dd02695394c34925

[89] Band matrix, From Wikipedia, the free encyclopedia, https://en.wikipedia.org/wiki/Band_matrix

[90] Q. Bao and W. Zhi, "DOA Estimation under Unknown Mutual Coupling and Multipath", *IEEE Transactions on Aerospace and Electronic Systems*, vol. 41, no. 2, April 2005

[91] Projection (Linear Algebra), From Wikipedia, the free encyclopedia, https://en.wikipedia.org/wiki/Projection_(linear_algebra)

[92] R. T. Behrens and L. L. Scharf, "Signal Processing Applications of Oblique Projection Operators", *IEEE Transactions on Signal Processing,* vol. 42, no. 6, June 1994.

[93] R. A. Horn and C. R. Johnson, *Matrix Analysis*, Second Edition, Cambridge University Press, New York, USA.

[94] W.-H. Steeb, *Matrix Calculus and Kronecker Product with Applications and C++ programs*, World Scientific Publishing Co. Pte. Ltd., 1997.

[95] A. J. Laub, *Matrix Analysis for Scientists & Engineers*, Siam, 2005.

[96] S. K. Godunov, *Modern Aspects of Linear Algebra*, Translations of Mathematical Monographs, Vol. 175, American Mathematical Society, 1998.

[97] A. Graham, *Kronecker Products and Matrix Calculus: with Applications*, Ellis Horwood Ltd., 1981.

[98] X. Zhang, *Matrix Analysis and Applications*, Cambridge University Press, 2017.

[99] S. N. Afriat, "Orthogonal and Oblique Projections and the Characteristics of Pairs of Vector Spaces", *Mathematical Proceedings of the Cambridge Philosophical Society,* vol. 53(4), pp. 800-816, 1957

[100] C. A. Balanis, *Advanced Engineeriing Electromagnetics*, 2nd ed., John Wiley & Sons, Inc., 2012.

[101] P. Stoica and A. Nehorai, "Comparative performance study of element-space and beam-space MUSIC estimators", *Circuits, Systems and Signal Processing*, vol. 10, no. 3, pp. 285-292, September 1991.

[102] Rank (linear algebra), From Wikipedia, the free encyclopedia, https://en.wikipedia.org/wiki/Rank_(linear_algebra)

[103] Rank-nullity theorem, From Wikipedia, the free encyclopedia, https://en.wikipedia.org/wiki/Rank%E2%80%93nullity_theorem